
Università degli Studi di Napoli Federico II
Facoltà di Ingegneria



Vincenzo Macillo

**SPECIAL JOINT SYSTEMS FOR
ALUMINIUM STRUCTURES:
EXPERIMENTAL TESTS AND
NUMERICAL MODELS**

*Tesi di Dottorato
XXV ciclo*

*Il Coordinatore
Prof. Ing. Luciano ROSATI*

Dottorato di Ricerca in Ingegneria delle Costruzioni

Vincenzo Macillo

SPECIAL JOINT SYSTEMS FOR ALUMINIUM STRUCTURES: EXPERIMENTAL TESTS
AND NUMERICAL MODELS

Copyright © 2013 Università degli Studi di Napoli Federico II - P.le Tecchio 80, 80136 Napoli,
Italy - web: www.unina.it

Proprietà letteraria, tutti i diritti riservati. La struttura ed il contenuto del presente volume non possono essere riprodotti, neppure parzialmente, salvo espressa autorizzazione. Non ne è altresì consentita la memorizzazione su qualsiasi supporto (magnetico, magnetico-ottico, ottico, cartaceo, etc.).

Benché l'autore abbia curato con la massima attenzione la preparazione del presente volume, Egli declina ogni responsabilità per possibili errori ed omissioni, nonché per eventuali danni dall'uso delle informazione ivi contenute.

Finito di stampare il 02/04/2013

To Anna Rachele

ACKNOWLEDGMENT

At the end of this three years long journey, I feel to thank all the people I met that made this experience unforgettable.

I would to express my deep gratitude to prof. Federico M. Mazzolani, who introduced me to the fascinating and innovative world of aluminium structures. He guided me during my activity transmitting me his passion and enthusiasm in the research activity.

I am very grateful to prof. Raffaele Landolfo, who demonstrated to believe in me and who always gave me new chances of growth.

I think this work was not possible without the support of dr. Luigi Fiorino. I am very thankful to him for the precious suggestions and the encouragement to bring out the best in me.

I would like to thank dr. Beatrice Faggiano and dr. Antonio Formisano who made me feel part of this important research team.

I cannot forget to thank eng. Tony De Lucia who shared with me these three years and he has always been helpful without any hesitation. I found a very good friend.

Another person I cannot forget is arch. Maria Teresa Terracciano who always gave a touch of cheerfulness to our “engineeristic” room.

A special thanks also to dr. Carmine Castaldo, for our discussions on steel structures, and to arch. Roberta Fonti for her kindly “architectural” point of view.

And how to forget eng. Tayyab Naqash, I miss our interesting conversations and I will always be thankful for his ABAQUS suggestions.

I would also like to thank dr. Ornella Iuorio and my dear colleagues of XXV cycle eng. Giusy Terracciano, eng. Giuseppe Lucibello and eng. Maurizio Toreno.

I would respectfully express my gratitude to METRA S.p.A that financially supported this research and my scholarship and, in particular, to eng. Ernesto Carretta for his availability and suggestions. I would also like to thank TECFI S.p.A. that furnished all the screws used in experimental campaign. A special thanks to eng. Giuseppe Campanella for his competence and technical support during the experimental activity.

I wish to thank my family that always believed in me supporting and encouraging my choice specially in difficult moments.

A felt thanks to Salvatore and Carmela for their affection and kindness.

The last, but not the least, I wish to thank Anna Rachele who is always by my side with her love and patience. All this would not be possible without her support and encouragement.

TABLE OF CONTENTS

TABLE OF CONTENTS	i
LIST OF FIGURES	v
LIST OF TABLES	xi

Chapter 1

GENERAL OVERVIEW ON STRUCTURAL USE OF ALUMINIUM AND ITS ALLOYS	5
1.1 EARLY HISTORY OF ALUMINIUM	5
1.2 STRUCTURAL APPLICATION OF ALUMINIUM	7
1.3 FABRICATION PROCESSES	15
1.3.1 From ore to semi-fabricated products	15
1.3.2 Extrusion process	18
1.4 CLASSIFICATION OF ALLOYS	23
1.4.1 Alloy designations	23
1.4.2 Fabrication stage designation.....	26
1.5 STRUCTURAL PROPERTIES OF ALUMINIUM	28
1.5.1 Physical and mechanical properties	28
1.5.2 Models for stress-strain law	31

Chapter 2

DEFINITION AND PROPERTIES OF SPECIAL JOINTS	37
2.1 JOINING TECHNIQUES FOR ALUMINIUM STRUCTURES.....	37
2.1.1 General.....	37
2.1.2 Traditional joints.....	38

2.1.3	Innovative joints	42
2.2	SPECIAL JOINTS	46
2.2.1	General information.....	46
2.2.2	Screw port joints.....	47
2.2.3	Bolt-channel joints.....	50
2.2.4	Main applications	51
2.3	REVIEW OF THE EXISTING LITERATURE ON SPECIAL JOINTS	55
2.3.1	STATE OF THE ART	55
2.3.2	Hellgren (1996).....	56
2.3.3	Menzemer et al. (2008).....	57
2.4	CODE SPECIFICATIONS AND DESIGN MANUALS	57
2.5	FORMULATION FOR STRENGTH PREDICTION	59

Chapter 3

CHAPTER 3 EXPERIMENTAL CHARACTERIZATION OF THE STRUCTURAL BEHAVIOUR OF SPECIAL JOINTS..... 67

3.1	DEFINITION OF EXPERIMENTAL CAMPAIGN.....	67
3.2	TESTS ON MATERIALS	69
3.2.1	Tests on aluminium alloys.....	69
3.2.1	Tests on screw material	72
3.3	TESTS ON SCREWED JOINTS.....	74
3.3.1	Test specimen and program.....	74
3.3.2	Test set-up and instrumentation.....	78
3.3.3	Test Results.....	81
3.3.4	Failure mechanism considerations.....	88
3.3.5	Experimental vs. predicted strength	89
3.4	TESTS ON BOLT-CHANNEL JOINTS.....	91
3.4.1	Test specimen and program.....	91
3.4.2	Slip tests.....	94
3.4.2.1	<i>Test set-up and instrumentation.....</i>	<i>94</i>
3.4.2.2	<i>Test results</i>	<i>96</i>
3.4.1	Shear tests	99
3.4.1.1	<i>Test set-up and instrumentation.....</i>	<i>99</i>
3.4.1.2	<i>Test results</i>	<i>101</i>

3.4.2	Pull-out tests	105
3.4.2.1	<i>Test set-up and instrumentation</i>	105
3.4.2.2	<i>Test results</i>	107
3.4.3	Experimental vs. predicted strength.....	110
 <i>Chapter 4</i>		
CHAPTER 4 NUMERICAL MODEL CALIBRATION OF SPECIAL JOINTS		113
4.1	GENERALITIES ON FINITE ELEMENT ANALYSIS	113
4.2	SCREWED JOINT MODELS	116
4.2.1	Axisymmetric model.....	116
4.2.2	Model description	118
4.2.3	Mesh sensitivity analysis	122
4.2.4	Numerical vs. experimental results.....	125
4.3	BOLT-CHANNEL MODELS	134
4.3.1	General assumption.....	134
4.3.2	Shear model	136
4.3.2.1	<i>Model description</i>	136
4.3.2.2	<i>Mesh sensitivity analysis</i>	138
4.3.2.3	<i>Numerical vs. experimental results</i>	141
4.3.3	Pull-out model.....	143
4.3.3.1	<i>Model description</i>	143
4.3.3.2	<i>Mesh sensitivity analysis</i>	146
4.3.3.3	<i>Numerical vs. experimental results</i>	149
 CONCLUSIONS.....		153
REFERENCES		157
 <i>Appendix A</i>		
TESTS ON MATERIALS		163
<i>Appendix B</i>		
TESTS ON SCREWED JOINTS.....		175
<i>Appendix C</i>		
TESTS ON BOLT-CHANNEL JOINTS.....		225

LIST OF FIGURES

FIGURE 1.1: FIRST APPLICATIONS OF ALUMINIUM: THE STATUE OF EROS IN PICCADILLY CIRCUS; ROOFING OF THE DOME OF THE SAN GIOACCHINO CHURCH IN ROME.....	7
FIGURE 1.2: TYPICAL SHAPES OF EXTRUDED PROFILES.....	8
FIGURE 1.3: RETICULAR SPACE STRUCTURES: THE INTERNATIONAL CONGRESS CENTRE OF RIO DE JANEIRO AND THE INTERAMERICAN EXHIBITION CENTER OF SAO PAULO (MAZZOLANI, 2003).....	10
FIGURE 1.4: ONE OF TWO TWIN DOMES WITHIN OF THE THERMAL POWER PLANT OF ENEL IN NORTH TORREVALDALIGA NEAR CIVITAVECCHIA (MAZZOLANI, 2010).....	10
FIGURE 1.5: ERECTION OF A FULLY PREFABRICATED HELIDECK (HTTP://ALUMINIUM.MATTER.ORG.UK).....	10
FIGURE 1.6: RIEKERHAVEN BRIDGE IN AMSTERDAM (HTTP://ALUMINIUM.MATTER.ORG.UK).....	11
FIGURE 1.7: THE SEWAGE PLANT POOL OF PO-SANGONE IN TURIN (MAZZOLANI, 2006).....	11
FIGURE 1.8: OFFSHORE STRUCTURES IN THE NORTH SEA (DWIGHT, 1999).....	12
FIGURE 1.9: A LIGHTING TOWER AND A MOTORWAY SIGN SUPPORT (MAZZOLANI, 2012).....	12
FIGURE 1.10: EXAMPLES OF EXTRUDED SHAPES USED FOR SPECIAL JOINT SYSTEMS.....	13
FIGURE 1.11: THE BAYER PROCESS (BUDD, 1999).....	15
FIGURE 1.12: HALL-HÉROULT PROCESS (BUDD, 1999).....	17
FIGURE 1.13: THE EXTRUSION PROCESS (DWIGHT, 1999).....	19
FIGURE 1.14: EXTRUSION PHASES - A) BILLET PREHEATING, B) DIE PREHEATING, C) EXTRUSION, D) COOLING, E) STRAIGHTENING, F) ARTIFICIAL AGING (CARRETTA AND MACILLO, 2012).....	20
FIGURE 1.15: A) DIE FOR SOLID PROFILES; B) DIE FOR HOLLOW PROFILES (HYDRO, 2009).....	21

FIGURE 1.16: TYPICAL LIMITS OF DIAMETER OF THE CIRCUMSCRIBING CIRCLE (HTTP://WWW.ALUMINIUMDESIGN.NET).....	22
FIGURE 1.17: TYPICAL STRESS-STRAIN DIAGRAM OF ALUMINIUM.....	29
FIGURE 1.18: EFFECTS OF TEMPERATURE ON MECHANICAL PROPERTIES OF ALUMINIUM ALLOYS (SHARP, 1993).....	30
FIGURE 1.19: PIECEWISE LINEAR MODELS – A) BI-LINEAR, B) THREE-LINEAR	31
FIGURE 1.20: INFLUENCE OF EXPONENT N OF RAMBERG-OSGOOD LAW (MAZZOLANI, 1995)	33
FIGURE 1.21: CHOICE OF REFERENCE POINT FOR RAMBERG-OSGOOD LAW.....	35
FIGURE 2.1: BOLTED CONNECTION (BUDDE, 1999)	38
FIGURE 2.2: A) MIG, B) TIG WELDING PROCEDURE	39
FIGURE 2.3: A) SOLID RIVET, B) HUCKBOLT, C) BLIND RIVET (BUDDE, 1999).....	41
FIGURE 2.4: SELF-TAPPING AND SELF-DRILLING SCREWS (HÖGLUND, 1999).....	41
FIGURE 2.5: ADHESIVE BONDED JOINTS (SOETENS AND VAN HOVE, 2003).....	43
FIGURE 2.6: FRICTION STIR WELDING (HTTP://WWW.ALUMINIUMDESIGN.NET)	44
FIGURE 2.7: CLINCHING (BUDDE, 1999)	44
FIGURE 2.8: FOLDING PROCESS (BUDDE, 1999)	45
FIGURE 2.9: POSSIBLE FEATURE FOR JOINING ALUMINIUM PROFILES (AEC, 2013)	47
FIGURE 2.10: SNAP-FIT JOINT (HÖGLUND, 1999)	47
FIGURE 2.11: SCREW PORT CONFIGURATION.....	48
FIGURE 2.12: SCREW-BOSS SYSTEM (SAPA, 2009).....	49
FIGURE 2.13: SCREW PORT JOINT APPLICATION (SAPA, 2009)	49
FIGURE 2.14: BOLT-CHANNEL JOINT (SAPA, 2009).....	50
FIGURE 2.15: APPLICATION OF BOLT-CHANNEL JOINTS (SAPA, 2009) ...	51
FIGURE 2.16: MODULSYSTEM BY METRA (2012).....	52
FIGURE 2.17: ROXROTH ALUMINUM STRUCTURAL FRAMING (HTTP://WWW.BOSCHREXROTH.COM).....	52
FIGURE 2.18: SCREW-BOSS JOINT IN CURTAIN WALLS (METRA, 2011A) 53	
FIGURE 2.19: SCREW-BOSS JOINT IN SOLAR PANEL STRUCTURES (METRA, 2011B).....	53
FIGURE 2.20: ALUSCALAE STAIRCASE SYSTEM (HTTP://WWW.ALUSCALAE.IT)	54
FIGURE 2.21: SAPA INDUSTRIAL STAIRWAY SYSTEMS (SAPA, 2012).....	54
FIGURE 2.22: MAKEABRIDGE® SYSTEM (MAADI, 2011)	55
FIGURE 2.23: ASSUMED SYMBOLS FOR SCREW-GROOVE JOINTS	60
FIGURE 2.24: ASSUMED SYMBOLS FOR BOLT-CHANNEL JOINTS.....	63

FIGURE 3.1: EXTRUDED PROFILES USED IN SCREW JOINT TESTS	68
FIGURE 3.2: EXTRUDED PROFILES USED IN BOLT-CHANNEL TESTS	68
FIGURE 3.3: TEST COUPONS FOR DIFFERENT TESTED ALUMINIUM ALLOYS	70
FIGURE 3.4: EXPERIMENTAL STRESS-STRAIN CURVES FOR AW 6082-T6	72
FIGURE 3.5: TESTED ALUMINIUM COUPONS	72
FIGURE 3.6: TENSILE TEST ON SCREW MATERIAL.....	73
FIGURE 3.7: EXPERIMENTAL STRESS-STRAIN CURVE FOR SCREW MATERIAL	74
FIGURE 3.8: NOMINAL VS. EFFECTIVE EMBEDMENT LENGTH	75
FIGURE 3.9: SCREW-GROOVE SPECIMENS.....	76
FIGURE 3.10: SCREW-TUBE SPECIMENS.....	77
FIGURE 3.11: SCREW-BOSS SPECIMEN	77
FIGURE 3.12: SET-UP FOR SCREWED JOINT TESTS	79
FIGURE 3.13: SCREW-TUBE SPECIMEN	80
FIGURE 3.14: SCREW-BOSS SPECIMEN	80
FIGURE 3.15: PULL-OUT FAILURE OF SCREW-GROOVE JOINTS	82
FIGURE 3.16: BENDING DEFORMATION OF SCREW SLOT.....	82
FIGURE 3.17: EXPERIMENTAL CURVES OF SCREW-GROOVE JOINTS	83
FIGURE 3.18: FAILURE MECHANISM OF SB-6.3-15.....	83
FIGURE 3.19: EXPERIMENTAL CURVES OF SCREW-BOSS JOINTS.....	84
FIGURE 3.20: FAILURE MECHANISM IN SCREW-TUBE JOINTS: A) SCREW PULL-OUT; B) SCREW FAILURE; C) ALUMINIUM FAILURE.....	84
FIGURE 3.21: EXPERIMENTAL CURVES OF SCREW-TUBE JOINTS (SG-5.5)	85
FIGURE 3.22: EXPERIMENTAL CURVES OF SCREW-TUBE JOINTS (SG-6.3)	86
FIGURE 3.23: EXPERIMENTAL CURVES OF SCREW-TUBE JOINTS (SG-M6)	87
FIGURE 3.24: FAILURE MECHANISM CHART FOR SCREW JOINTS	88
FIGURE 3.25: EXPERIMENTAL BASED FAILURE CHART	89
FIGURE 3.26: BOLT-CHANNEL SPECIMENS.....	92
FIGURE 3.27: STEEL PLATE NUTS	93
FIGURE 3.28: ALUMINIUM CHANNELS FOR SLIP TESTS.....	94
FIGURE 3.29: DIMENSION OF SLIP TESTS SET-UP	95
FIGURE 3.30: SET-UP AND INSTRUMENTATION FOR SLIP TESTS.....	96
FIGURE 3.31: DEFORMED CONFIGURATION OF SLIP TEST SPECIMENS .	97
FIGURE 3.32: EXPERIMENTAL CURVES OF SLIP TESTS ON BOLT- CHANNEL JOINTS	98
FIGURE 3.33: MATERIAL REMOVAL IN SLIP TEST SPECIMEN	98
FIGURE 3.34: ALUMINIUM CHANNELS FOR SHEAR TESTS.....	99
FIGURE 3.35: SHEAR TESTS SET-UP	100
FIGURE 3.36: SET-UP AND INSTRUMENTATION FOR SHEAR TESTS.....	101
FIGURE 3.37: LDVTS FOR OVERSIZED CONNECTIONS MEASUREMENT	101

FIGURE 3.38: FAILURE MECHANISM IN BC-SH-10 SERIES.....	102
FIGURE 3.39: FAILURE MECHANISM IN BC-SH-18 SERIES.....	103
FIGURE 3.40: EXPERIMENTAL CURVES OF SHEAR TESTS ON BOLT- CHANNEL JOINTS	104
FIGURE 3.41: DEFORMED CONFIGURATION OF BC-SH-10.....	104
FIGURE 3.42: DEFORMED CONFIGURATION OF BC-SH-18.....	104
FIGURE 3.43: ALUMINIUM CHANNELS FOR PULL-OUT TESTS.....	105
FIGURE 3.44: PULL-OUT TESTS SET-UP	106
FIGURE 3.45: SPECIMEN TO SET-UP CONNECTION.....	106
FIGURE 3.46: SET-UP AND INSTRUMENTATION FOR PULL-OUT TESTS	107
FIGURE 3.47: FAILURE MECHANISM IN BC-PO-10 SERIES.....	108
FIGURE 3.48: FAILURE MECHANISM IN BC-PO-18 SERIES.....	109
FIGURE 3.49: EXPERIMENTAL CURVES OF PULL-OUT TESTS ON BOLT- CHANNEL JOINTS	110
FIGURE 4.1: GEOMETRY OF FEM MODEL.....	119
FIGURE 4.2: THREADED PROFILE FOR SELF-TAPPING SCREW(A) AND METRIC BOLT (B)	119
FIGURE 4.3: ENGINEERING VS. TRUE STRESS-STRAIN CURVE FOR AW 6082-T6	121
FIGURE 4.4: INTERACTION CONTACT DEFINITION	122
FIGURE 4.5: MODEL LOAD AND BOUNDARY CONDITIONS.....	122
FIGURE 4.6: ASSUMED MESH SIZE (A) COARSE , (B) INTERMEDIATE, (C) FINE	124
FIGURE 4.7: MESH SENSITIVITY ANALYSIS RESULTS	124
FIGURE 4.8: NUMERICAL VS. EXPERIMENTAL RESULTS FOR ST-55-10	127
FIGURE 4.9: FAILURE MECHANISM FOR ST-55-10	127
FIGURE 4.10: NUMERICAL VS. EXPERIMENTAL RESULTS FOR ST-55-15	128
FIGURE 4.11: FAILURE MECHANISM FOR ST-55-15	128
FIGURE 4.12: NUMERICAL VS. EXPERIMENTAL RESULTS FOR ST-63-10	129
FIGURE 4.13: FAILURE MECHANISM FOR ST-63-10	129
FIGURE 4.14: NUMERICAL VS. EXPERIMENTAL RESULTS FOR ST-63-15	130
FIGURE 4.15: FAILURE MECHANISM FOR ST-63-15	130
FIGURE 4.16: NUMERICAL VS. EXPERIMENTAL RESULTS FOR ST-M6-10	131
FIGURE 4.17: FAILURE MECHANISM FOR ST-M6-10.....	131
FIGURE 4.18: NUMERICAL VS. EXPERIMENTAL RESULTS FOR ST-M6-15	132
FIGURE 4.19: FAILURE MECHANISM FOR ST-M6-15.....	132
FIGURE 4.20: NUMERICAL VS. EXPERIMENTAL RESULTS FOR ST-M6H-15	133

FIGURE 4.21: NUMERICAL VS. EXPERIMENTAL RESULTS FOR ST-M6H-15	133
FIGURE 4.22: ENGINEERING VS. TRUE STRESS-STRAIN CURVE FOR AW 6005A-T6	135
FIGURE 4.23: IMPLEMENTED MODEL PARTS	136
FIGURE 4.24: MODEL LOAD AND BOUNDARY CONDITIONS	137
FIGURE 4.25: BOUNDARY CONDITION AT CHANNEL ENDS	138
FIGURE 4.26: ASSUMED MESH SIZE (A) COARSE , (B) INTERMEDIATE, (C) FINE	139
FIGURE 4.27: MESH SENSITIVITY ANALYSIS RESULTS	140
FIGURE 4.28: COMPARISON BETWEEN NUMERICAL AND EXPERIMENTAL RESPONSE CURVES	142
FIGURE 4.29: DEFORMED CONFIGURATION AT FAILURE – FRONTAL VIEW	142
FIGURE 4.30: DEFORMED CONFIGURATION AT MIDDLE SECTION	143
FIGURE 4.31: DEFORMED CONFIGURATION OF ALUMINIUM CHANNEL END (EXPERIMENTAL VS. NUMERICAL)	143
FIGURE 4.32: IMPLEMENTED MODEL PARTS	144
FIGURE 4.33: MODEL LOAD AND BOUNDARY CONDITIONS	145
FIGURE 4.34: BOUNDARY CONDITION AT THE CONNECTION WITH SET- UP	145
FIGURE 4.35: MODEL IMPERFECTION CALIBRATION	146
FIGURE 4.36: ASSUMED MESH SIZE (A) COARSE , (B) INTERMEDIATE, (C) FINE	147
FIGURE 4.37: MESH SENSITIVITY ANALYSIS RESULTS	148
FIGURE 4.38: COMPARISON BETWEEN NUMERICAL AND EXPERIMENTAL RESPONSE CURVES	149
FIGURE 4.39: DEFORMED CONFIGURATION FOR THE ASSUMED IMPERFECTIONS	150
FIGURE 4.40: DEFORMED CONFIGURATION – FRONTAL VIEW	151
FIGURE 4.41: DEFORMED CONFIGURATION AT MIDDLE SECTION	152
FIGURE 4.42: DEFORMED CONFIGURATION – LATERAL VIEW	152

LIST OF TABLES

TABLE 1.1: THE MAIN STRUCTURAL APPLICATIONS OF ALUMINIUM ALLOYS (MAZZOLANI, 2003)	14
TABLE 1.2: NUMERICAL DESIGNATION FOR WROUGHT ALLOYS	26
TABLE 1.3: PHYSICAL PROPERTIES OF ALUMINIUM AND STEEL.....	28
TABLE 2.1: RANGE OF VALIDITY OF SCREW-GROOVE JOINT	60
TABLE 2.2: RANGE OF VALIDITY OF BOLT-CHANNEL JOINT	63
TABLE 3.1: RESULTS OF TEST ON ALUMINIUM ALLOYS	71
TABLE 3.2: RESULTS OF TEST ON SCREW MATERIAL	74
TABLE 3.3: TEST PROGRAM FOR SCREWED JOINTS.....	78
TABLE 3.4: EXPERIMENTAL RESULTS OF SCREWED JOINTS TESTS	81
TABLE 3.5: COMPARISON BETWEEN PREDICTED AND EXPERIMENTAL STRENGTH FOR SCREW-GROOVE JOINTS.....	90
TABLE 3.6: COMPARISON BETWEEN PREDICTED AND EXPERIMENTAL STRENGTH FOR SCREW-TUBE JOINTS.....	91
TABLE 3.7: TEST PROGRAM FOR SCREWED JOINTS.....	94
TABLE 3.8: EXPERIMENTAL RESULTS OF SLIP TEST ON BOLT-CHANNEL JOINTS.....	96
TABLE 3.9: EXPERIMENTAL RESULTS OF SHEAR TEST ON BOLT-CHANNEL JOINTS.....	102
TABLE 3.10: EXPERIMENTAL RESULTS OF PULL-OUT TESTS ON BOLT-CHANNEL JOINTS.....	107
TABLE 3.11: COMPARISON BETWEEN PREDICTED AND EXPERIMENTAL SLIP STRENGTH FOR BOLT-CHANNEL JOINTS	111
TABLE 3.12: COMPARISON BETWEEN PREDICTED AND EXPERIMENTAL SHEAR STRENGTH FOR BOLT-CHANNEL JOINTS.....	111
TABLE 3.13: COMPARISON BETWEEN PREDICTED AND EXPERIMENTAL PULL-OUT STRENGTH FOR BOLT-CHANNEL JOINTS	112

TABLE 4.1: ASSUMED DIMENSION FOR ALUMINIUM SLOTS	7
TABLE 4.2: ASSUMED SCREWS MATERIAL PROPERTIES	9
TABLE 4.3: MESH PARAMETERS	11
TABLE 4.4: COMPARISON BETWEEN NUMERICAL AND EXPERIMENTAL RESULTS	14
TABLE 4.5: ASSUMED MATERIAL PROPERTIES	23
TABLE 4.6: MESH PARAMETERS	28
TABLE 4.7: COMPARISON BETWEEN NUMERICAL AND EXPERIMENTAL RESULTS	29
TABLE 4.8: MESH PARAMETERS	36
TABLE 4.9: COMPARISON BETWEEN NUMERICAL AND EXPERIMENTAL RESULTS	39

INTRODUCTION

The wide choice of cross-sectional shapes obtainable by means of extrusion process represents one of the main advantages for aluminium alloys structures. The extrusion process allows to customize the cross-section shapes with ribs, bulbs, slots in order to optimize the structural efficiency. These features can be also exploited to conceive in a more rational way the connections between the different parts of the structures. Therefore, it is possible to obtain by specific extrusion cross-sections with semi-hollow parts, namely slot or track, in which mechanical fasteners can be located, such as bolts or screws. Extruded shapes with specific projections can be also used in self-locking joining systems without any type of fasteners. These systems are generally known as “special joints” or “non-conventional joints” for aluminium extrusions.

Special joints are very competitive with respect to conventional joining solutions thank to the possibility of easy and rapid execution, treatments and machining reduction. The main advantage of using these joint typologies lies in the optimization of the parent material with a reduced need of additional joint elements, such as angles and gusset plates. These features entail a significant reduction in fabrication and execution costs.

These joint typologies are commonly used in several applications, both structural and non. The fields of application of special joint systems are very wide. In effect, the applications are not only limited to building and civil engineering but also the automotive, railways and aerospace industry. Special joints are mainly employed in applications

under middle-low loads like complementary building structures, such as façades, structures for solar panels, doors and windows fixture. But, in the last years, other structural applications like staircases, floors, pedestrian bridge, industrial furniture and shelves have been developed involving special joints.

Although the special joints are widely used in structural applications, few literature about this topic is available and no clear design rules are provided by the main aluminium structures codes. The available formulations for strength prediction are generally limited to specific cases or to given ranges of validity.

The aluminium industry showed a great interest about special joints due to the several advantages related to their use. But, at the same time, due to the lack of information about the design, the manufactures are forced to design the joints by means of expensive experimental tests.

The main objective of this work, supported by METRA S.p.A., is to overcome the lack of information about the mechanical behaviour of special joints. In particular, the aim is to define the main issues related to the joint geometry, the influence of load type and, mainly, the joint structural response by means of experimental tests. Then, on the basis of experimental results, the final aim is to develop numerical models able to predict the joint response, in order to provide a general design tool.

The work is focused on two different special joint systems: screw ports and bolt-channel joints. In particular, the first joint typology consists in a screw engaged in an open or closed slot of an extruded profile. The latter system consists in a track or channel section profile in which a bolt head, nuts or plates with threaded holes can be located.

This work is organized into four chapters.

In Chapter 1 a brief overview on the basis of aluminium alloy structures is reported. In particular, this chapter illustrates the main fields of application of aluminium structures, technological issues such as production processes and the fabrication stages, together with the basic information about the material mechanical behaviour.

After an overview on the joining techniques for aluminium structures, Chapter 2 describes the main properties of special joint systems, with particular regard to screw ports and bolt channel, and it illustrates their main applications. In addition, existing literature and standard specifications, together with the available formulations for strength prediction, are illustrated.

Chapter 3 deals with the whole experimental activity and it is divided into three parts. In the first one, tests results on used aluminium alloy, screw and materials are illustrated. The second part describes and analyses the pull-out tests on screwed joints in open and closed ports. In the third part the experimental tests on bolt-channel joints under three different load directions (slip, shear and pull-out) are illustrated and commented.

Chapter 4 describes the numerical phase. In this phase, on the basis of experimental data, numerical models in ABAQUS environment have been developed and calibrated by taking into account system non linearity.

At last, the main conclusions of this work, together with possible further research developments, are illustrated.

Chapter 1

GENERAL OVERVIEW ON STRUCTURAL USE OF ALUMINIUM AND ITS ALLOYS

1.1 EARLY HISTORY OF ALUMINIUM

Aluminium is the third most common element and the most abundant metal on the earth's crust in the measure of 8%. Nevertheless, aluminium can be considered a “young” material because its industrial use is relatively recent due to the complexities related to the separation of the element from its natural form.

The first to foresee the possibility to isolate the aluminium element was an English chemist and physicist, Sir Humphry Davy, in 1807. He was working on separation of salts by electrolysis and, in particular, on the alumina salts discovered at the end of eighteenth century by Guyton De Morveau during his studies on the ancient “allume”. The name with Latin derivation was used to identify a material of unknown composition employed in Egyptian civilization (Mazzolani, 1995). In 1821 in Les Baux-de-Provence, the French geologist Pierre Berthier discovered a hard, reddish and similar to clay material containing 25% of aluminium, which he named bauxite. Few years later (1825) a Danish chemist, Hans Christian Ørsted, succeeded to isolate tiny amounts of the metal by heating potassium amalgam with aluminium chloride, but he did not enhance his findings. Two years later (1827) the experiments of Ørsted were resumed by the German chemist Friedrich Wöhler, who obtained the first aluminium nugget that revealed some special properties of the material, as lightness and

brightness. In 1854, the first step to the industrial production was made by the French chemist Henri Etienne Sainte-Claire Deville, who developed a reduction process using sodium instead of potassium, which was more economic than the previous one. This allowed the commercial production and the increasing interest in this new metal. The first aluminium produced was employed to coin a medal in homage to Wöhler and to realize, on request of Napoleon III, eagles for the flag lances of the imperial regiment.

In 1886 an American engineer, Charles Martin Hall, and a French scientist, Paul Louis Touissant Héroult, independently invented the same electrolytic reduction process of alumina from which industrial production began. The process was later named Hall- Héroult process. In 1888 another important step for the aluminium growth, Karl Josef Bayer patented an economic process to extract alumina from bauxite. The combination of these two processes considerably reduced the price of aluminium and the first producing companies were born in France, Switzerland and USA. Nowadays, Bayer and Hall-Héroult processes are still used in current industrial production.

In the aftermath, aluminium was used in different applications with some success. Among the first applications, we can find the statue of Eros in Piccadilly Circus, London, cast in 1893, and the sheet metal roofing of the dome of the Church of San Gioacchino in Rome in 1897 (Figure 1.1). Both of these are still in pristine condition (Dwight, 1999).

The first aluminium alloy designation dates back to 1888 and since then a great number of aluminium alloys have been developed until the present day. The first alloy containing 4% copper was discovered at the beginning of twentieth century by a German metallurgist, Alfred Wilm (Müller, 2011).



Figure 1.1: First applications of aluminium: the statue of Eros in Piccadilly Circus; roofing of the dome of the San Gioacchino Church in Rome

1.2 STRUCTURAL APPLICATION OF ALUMINIUM

The success of aluminium and its alloys as structural material and the possibility to be competitive with common constructional materials as steel are based on some distinguishing prerequisites connected to physical and mechanical properties, fabrication process and technological features. In the following, the main properties of aluminium alloys are briefly summarized.

Aluminium alloys represent a wide family of structural materials, which covers the range of strength of common mild steels, debunking the false myth of a material not sufficiently strong to be used in structural application.

An important property of the aluminium and its alloys is the corrosion resistance. The exposed surface of aluminium reacts with oxygen in the air to form an inert aluminium oxide film only a few microns thick. The oxide film blocks further oxidation and it is self-repairing if damaged. For this reason, aluminium needs no protection against atmospheric or chemical corrosive agents.

Aluminium is a lightweight material, its density is about one-third that of steel. Therefore, this lightness gives great advantages in terms of weight reduction, but this feature is partially offset by the necessity

estimated that the 75% of ever produced aluminium is still in use. In addition, aluminium can be recycled over and over again without losing its main properties. The energy necessary to recycle aluminium, due to its low melting point, is just 5% of those originally used to extract it. Thus, it is possible to obtain the same material saving a very great amount of energy. For this reason, aluminium can be considered the perfect “eco-metal”.

Other attractive properties of aluminium are reflectivity, thermal conductivity, electric conductivity and non-toxicity.

Therefore, aluminium alloys can be considered economic, and then competitive, in all those applications in which their distinguishing prerequisites represent an important advantage. In particular, the three main properties to be exploited are (Mazzolani, 2003):

- Lightness;
- Corrosion resistance;
- Functionality of structural shapes.

The lightness property allows simplification and speeding of the erection phase, an ease to transport fully prefabricated components, a reduction of self-weight loads and also a reduction of energy cost due to movement both during erection and service phases. The applications which get more advantages from this prerequisite are all the structures in which live loads are small compared to dead loads such as long-span roof systems. They include reticular structures: planar, spatial (Figure 1.3) or curve, such as geodetic domes (Figure 1.4). Lightness represents an essential property for structures located in inaccessible places far from fabrication shop because of the transport economy and ease of erection. This is the case of prefabricated structures such as electrical transmission towers, staircases, provisional bridges, which can be carried completely assembled (Figure 1.5). Also structures having moving parts make the most of lightness because it means power savings under service. Examples of these structures are moving bridges (Figure 1.6) and the rotating crane bridges in the sewage plants (Figure 1.7).

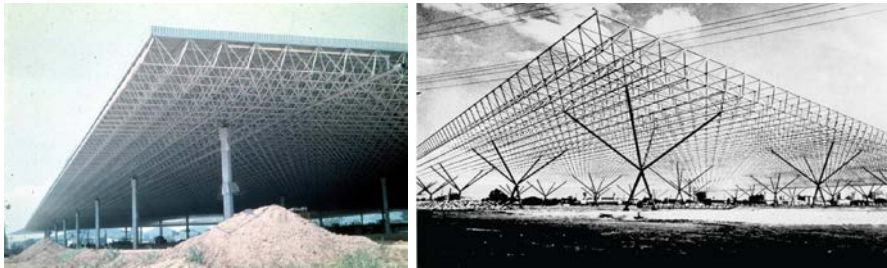


Figure 1.3: Reticular space structures: the International Congress Centre of Rio de Janeiro and the Interamerican Exhibition Center of Sao Paulo (Mazzolani, 2003)



Figure 1.4: One of two twin domes within of the thermal power plant of ENEL in North Torrevadliga near Civitavecchia (Mazzolani, 2010)



Figure 1.5: Erection of a fully prefabricated helideck (<http://aluminium.matter.org.uk>)



Figure 1.6: Riekerhaven bridge in Amsterdam
(<http://aluminium.matter.org.uk>)



Figure 1.7: The sewage plant pool of Po-Sangone in Turin (Mazzolani, 2006)

The main advantages of the good corrosion resistance of aluminium are the possibility to reduce the maintenance cost and to obtain a good performance in corrosive environments. Typical structures in humid and corrosive environments are swimming pool roofs, river bridges, hydraulic structures and offshore superstructures (Figure 1.8). The reduction or the absence of maintenance is necessary in all those special purpose structure for which maintenance works are

particularly difficult or must be limited, e.g. masts, lighting tower, sign motorway portals, etc. (Figure 1.9)



Figure 1.8: Offshore structures in the North Sea (Dwight, 1999)



Figure 1.9: A lighting tower and a motorway sign support (Mazzolani, 2012)

The functionality of structural shapes, due the extrusion process, makes it possible to improve the geometrical properties of cross-sections by designing a shape which optimizes the structural behaviour and, at same time, reduces weight saving material. Thanks to extrusion it is possible to obtain stiffer shapes without using built-up sections, so reducing machining as welding. Extruded shapes can be improved by introducing peculiar details aimed to develop easy, fascinating and advantageous systems for joining aluminium components to each other or to different material (Figure 1.10). In particular, this possibility represents the main topic on which the

present thesis is focused on. Finally, extrusion process allows to put material only where it is needed obtaining a more economic, efficient and rational shape of profiles.

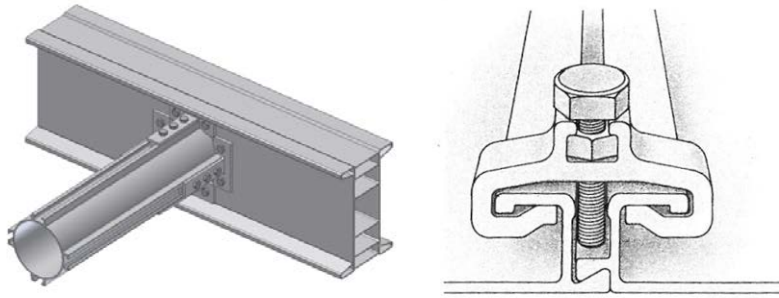


Figure 1.10: Examples of extruded shapes used for special joint systems

A list of general applications in structural engineering of aluminium alloys is given in Table 1.1 (Mazzolani, 2003). They are classified with regard to the prerequisite of lightness (L), corrosion resistance (C) and functionality of shapes (F), acting separately or together. This list includes not only typical civil engineering applications but all those ones in which aluminium alloy represent a convenient structural solution.

Table 1.1: The main structural applications of aluminium alloys (Mazzolani, 2003)

C	C+L	L
<ul style="list-style-type: none"> - Storage vessels - Lamp columns - Profiled roof and wall cladding - Support for railway overhead electrification - Enclosure structures for sewage works - Sound barriers Vehicle restraint systems - Sewage plant bridges - Silos* - Traffic signal gantries - Traffic signal poles 	<ul style="list-style-type: none"> - Lighting control loovers - Flag poles - Aircraft access bridges - Transmission towers - Bridge inspection gantries - Offshore structures (living quarters, bridges) - Tank flotation covers 	<ul style="list-style-type: none"> - Crane booms - Lorry mounted cranes - Pit props - Bridges* - Mobile bridge inspection gantries - Scaffolding systems - Ladders - Cherry pickers - Telescopic platforms - Masts for tents
C+F	C+F+L	F+L
<ul style="list-style-type: none"> - Domes over sewage tanks - Marina landing stages - Roof access staging - Dam logs - Curtain walling - Overcladding support systems - Pedestrian parapets - Chicken house structures - Wood drying kilns - Space structures (domes, etc.) - Exhibition stands* - Swimming pool roofs* - Canopies - Bus shelters - Green houses/Glass houses 	<ul style="list-style-type: none"> - Grating planks - Helidecks 	<ul style="list-style-type: none"> - Access ramps - Support for shuttering - Trackways (temporary) - Elevators for building materials - Scaffold planks - Trench supports - Grave digging supports - Loading ramps - Landing mats for aircraft - Access gangways - Shuttering support beams - Military bridges - Radio masts - Shuttering - Telescopic conveyor belt structures - Grandstand structures (temporary) - Building maintenance gantries - Fabric structure frames
	F	
	<ul style="list-style-type: none"> - Prefabricated balconies - Conveyor belt structures - Monorails - Robot support structures - Shuttering form work - Tunnel shuttering 	

1.3 FABRICATION PROCESSES

1.3.1 From ore to semi-fabricated products

The first step to obtain aluminium in metal form consists in the extraction of aluminium oxide (Al_2O_3), also known as “alumina”, from bauxite ore by means of the Bayer process. The extraction process is based on the fact that aluminium compounds dissolve in heated caustic soda but the most part of bauxite components do not and can be removed. In this way it is possible to separate pure aluminium oxide. A simplified scheme of the process is shown in Figure 1.11.

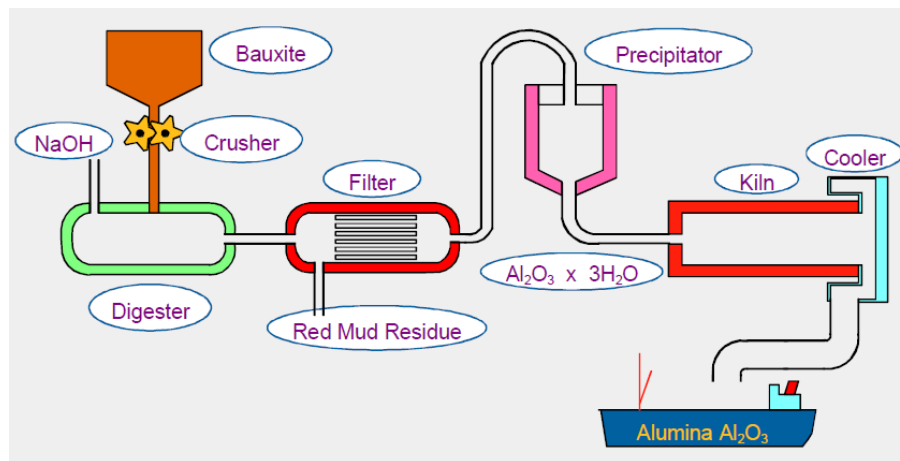


Figure 1.11: The Bayer Process (Budd, 1999)

The aluminium oxide is turned in metal form by electrolysis by means of the electrolytic process named “Hall-Hérout”. This takes place in a cell made of steel lined with carbon. The dimension of this cell is up to 10 m long, about 4 m wide and 1.5 m deep.

The electrolyte is the solution of aluminium oxide in a molten salt solution composed primarily of a mixture of sodium fluoride and aluminium fluoride. The electrical current flows from the carbon anodes through the electrolyte to the carbon liner and the cathode bus

bars. The carbon anodes are consumed during the electrolysis. The aluminium collects at the bottom of the cell and is removed. During the process the cell operates at a temperature of about 950°C and it is supplied by low voltage direct current (5V) with very high amperage (100-150 kA). The process is simply schematized in Figure 1.12.

The process requires large amounts of energy, modern smelters need about 13 kWh to produce 1 kg of aluminium. For this reason, smelters are usually located in those regions with plentiful cheap electricity or close to dedicate hydroelectric plants.

The result of this process is called primary aluminium. At the smelter the metal can be cast into ingots or larger blocks for subsequent remelting. The metal is usually alloyed at the smelter and then cast into cylindrical extrusion billets or rolling ingots in form of rectangular slabs. A semi-continuous process known as direct chill casting (DC) is employed (Budd, 1999).

There is also a secondary aluminium, which is obtained by recycling aluminium scrap. In recycling plants, aluminium scrap is checked, sorted according to composition and then melted in furnaces. Afterwards the molten material is cast or processed using the same methods as for primary processing.

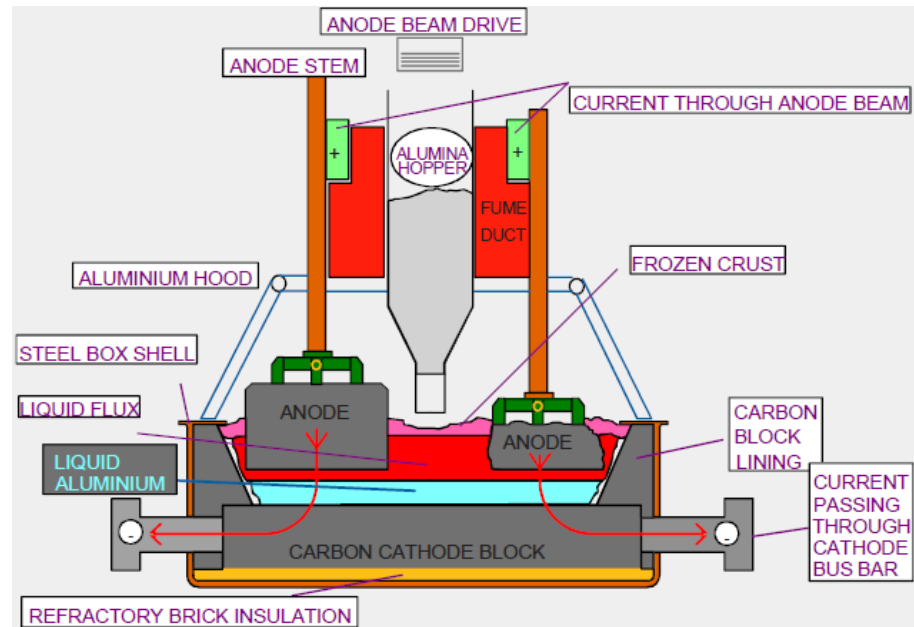


Figure 1.12: Hall-Héroult Process (Budd, 1999)

The material in form of billets or ingots is shipped to factories that make what are known as semi-fabricated products, which are the types of material required by end product manufacturers. In particular, semi-fabricated products are mainly obtained by means of one of the following processes:

- Casting;
- Forging;
- Rolling;
- Extrusion.

The casting process represents a very attractive way to obtain three-dimensional complex elements, even though it suffers some limitation in structural use. In effect, cast alloys have more variation on mechanical properties and less ductility than wrought ones (Kissel and Ferry, 2002). The molten metal is simply poured into a mould shaped essentially as the final part. Nowadays there are many casting process,

such as sand casting, shell casting, permanent mould and pressure die casting. The main differences lie on the type of used mould, on the pouring method and on the finishing of the final product.

In the forging process the metal is hammered or pressed into required shapes which have been cut into facing dies. The starting stock can be either cast blocks or extruded bars (Budd, 1999).

The rolling process is used to obtain aluminium flat products as sheets and plates. Rolling ingots in form of rectangular slabs are rolled to plates with thickness greater than 6 mm by hot-rolling process, similar to steel but involving lower temperature than steel. Further thickness reduction can be obtained by cold-rolling process. The rolling process induces work hardening proportional to the amount and the nature of alloying elements present in the product, and thus annealing processes are required to increase the ductility (Mazzolani, 1995).

1.3.2 Extrusion process

The extrusion process is the principal method of making aluminium structural shapes. The process consists in forcing heated metal through a shaped die. The extrusion process can be direct or indirect. In the first case the aluminium billet is pushed through the die while, in the latter one the press pushes the die into billet. In the following Section more information about direct extrusion process is given.

The majority of aluminium profiles is generally produced by means of direct extrusion process. This represents one of the biggest advantages of aluminium alloys. In effect, by means of this process it is possible to produce profiles of any shape that cannot be usually obtained by hot-rolling. This represents the main advantage of aluminium over steel (Mazzolani, 1995). The process consists in an extrusion billet pushed by a press through a die with a shaped opening that gives the desired profile configuration (Figure 1.13).

In the following the entire extrusion process is described.

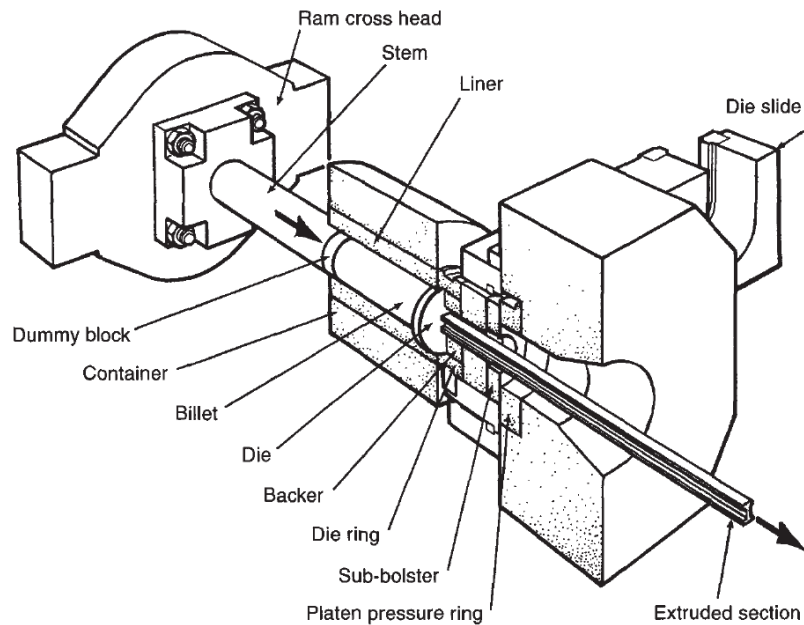


Figure 1.13: The extrusion process (Dwight, 1999)

The extrusion billet cut from DC cast log is preheated in an induced furnace (Figure 1.14a). Once the billet is brought at temperature of 460-480° C, it is inserted in the container of extrusion press. In order to avoid process problems due to thermal shock, also the die is preheated in a small furnace (Figure 1.14b). A pressure variable from 250 to 1000 N/mm² is applied by a hydraulic ram that pushes the billet through the die. The profile is then expelled from die and travels down the run-out table (Figure 1.14c). The maximum length of the extruded product depends on the billet volume and on the extrusion ratio, which is the ratio between the cross section of the billet and the cross section of the extruded profile. The optimal values of extrusion ratio are in the range between 10 and 50. Lower values can cause a worsening in properties, while greater values require an excessive pressure of ram with the possibility of die distortion and breakage. The length of the extruded profile can reach up to 40 m. In the case of heat-treatable alloys, the profile is quenched with water or air spray as it comes off

the press (Figure 1.14d). During the process the extrusions tend to distort and generally present an overall bow imperfection along the length. In order to correct it and to reduce residual stresses, the profile is subjected to the straightening process (Figure 1.14e). The profile is stretched up to the strain of $1\div 2\%$ by applying a high tension force on the straightening table. At this stage, the extrusion is cut in suitable lengths then, if it is required, in order to improve mechanical properties, the obtained elements can be further artificially aged in an air furnace (Figure 1.14f)

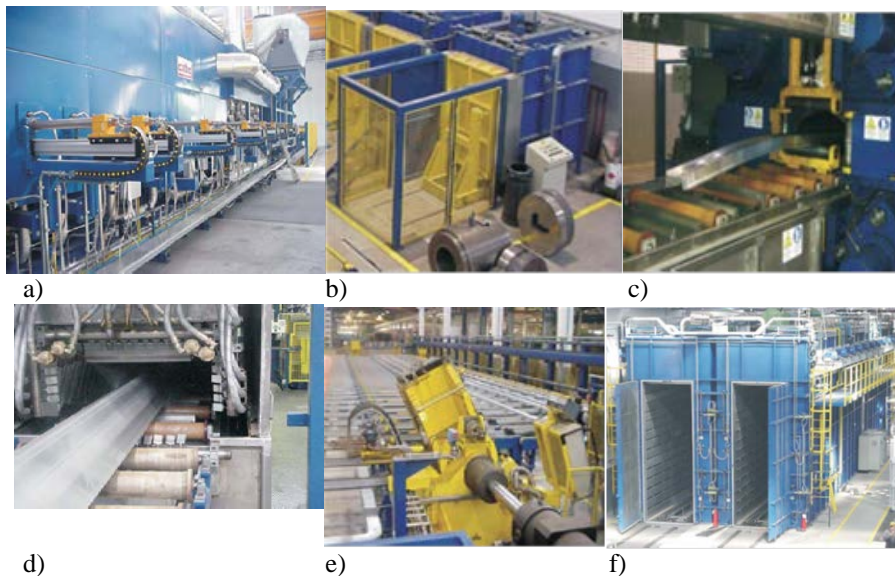


Figure 1.14: Extrusion phases - a) billet preheating, b) die preheating, c) extrusion, d) cooling, e) straightening, f) artificial aging (Carretta and Macillo, 2012)

The extruded products can be divided in two classes: solid and hollow profiles. This distinction is related to the big differences in the technology and manufacture of the dies. They are made of high temperature resistant tool steel and the aperture, corresponding to the profile cross-section, is cut by spark erosion. In case of solid profiles, the dies consist of a flat plate which forms the external shape of the extrusion (Figure 1.15b). More complex are the dies for hollow

extrusions. It is used a bridge die with a mandrel, which defines the section cavity, and the material flows around it during the extrusion (Figure 1.15b). In some cases, bridge dies are also used for so-called semi-hollow sections, which are open cross-sections having deep tongue and a narrow gap (Hydro, 2009). In order to increase the output, it is possible to extrude, in case of small sections, more than one profile per die by using multicavity dies, which allow to obtain up to ten profiles at the same time.

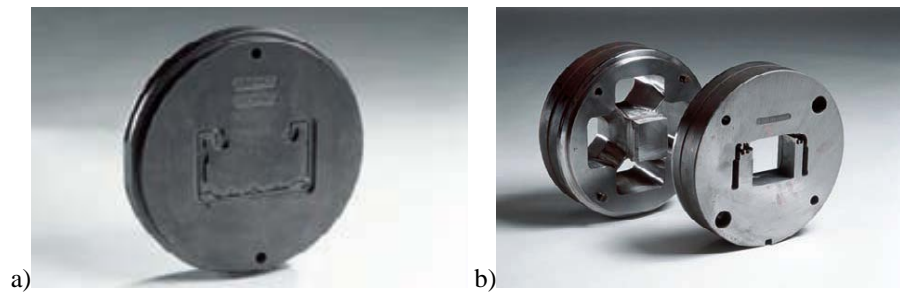


Figure 1.15: a) die for solid profiles; b) die for hollow profiles (Hydro, 2009)

The design of dies, and then of cross-section shapes, represents an important issue of extrusion. In order to improve the functionality and to reduce production costs, some design concepts have to be applied. In general, it is preferable to have sections with at least a symmetry axis to achieve a balanced flow of material during the process and to uniform the load on the die. Large thickness differences are to be avoided, because the material flows faster through the thicker parts than the thinner ones and the profile comes out as a curve. This problem is generally resolved by increasing the contact length in the die, and then the friction, for thicker parts. In addition, the thickness is a function of the extrusion width, indeed greater thicknesses are required for larger extrusions. In extrusion the sharp corners have to be avoided, because they increase the risk of die failure and reduce the permitted extrusion speed. They should be slightly rounded with a minimum radius of 0.03 mm (Dwight, 1999).

The maximum cross-section dimensions are limited by the press capacity that, for typical presses, ranges from 1000 and 12500 tonnes.

The size restrictions are generally expressed in terms of the Diameter of the Circumscribing Circle (DCC), which represents a conventional measure of maximum dimension in cross-section. Figure 1.16 shows the dimensional limits within which most extrusion plants can supply aluminium extrusions based on the DCC.

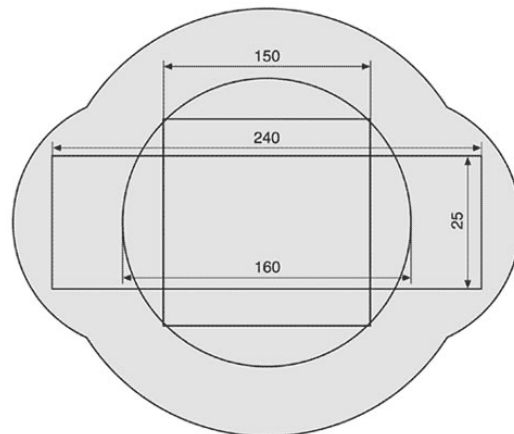


Figure 1.16: Typical limits of diameter of the circumscribing circle
(<http://www.aluminiumdesign.net>)

As far as the extrudability is concerned, all aluminium alloys can be extruded, but some type are less suitable than others. In general, strong alloys require high pressures, the extrusion speeds are too low and the products are not acceptable in terms of surface finishing and section complexity. The alloys of the 6000 series are the most suitable for the production of extruded profiles. In particular, alloys containing the lower limits of silicon and magnesium, e.g. 6060 and 6063, can be easily extruded with very high speeds, up to 100 m/min. The extrusions of such alloys have good surface finish, anodizing capability and maximum complexity of cross-section with the possibility to obtain minimum thickness values (Woodward, 1999). In addition, they are particularly suitable for hollow extrusions because they can flow readily through bridge dies and the material properties can be improved by quenching at the press.

1.4 CLASSIFICATION OF ALLOYS

1.4.1 Alloy designations

Despite its ductility and corrosion resistance, pure aluminium cannot be used in structural engineering applications because it is characterized by very low strength values. In order to increase its strength, different alloys have been developed. Several elements are used for aluminium alloys and their main properties are summarized below (Mazzolani, 1995):

- *Magnesium* reduces the melting point to 451°C (for this reason is also used as weld metal) and increases work-hardening ability and corrosion resistance to salted water;
- *Silicon* increases the strength and ductility and reduces the melting point. In combination with the magnesium it allows the precipitation hardening;
- *Zinc* strongly increases strength and allows hot or cold precipitation hardening;
- *Copper* gives an even greater strength increase and allows cold precipitation hardening, but reduces corrosion resistance, weldability and ductility.
- *Nickel* can increase the resistance under high-temperature conditions;
- *Titanium* reduces the grain size;
- *Zirconium* is a stabiliser element, which influences the temperability;
- *Chromium* increases the resistance to stress corrosion;
- *Iron* is usually an impurity which can increase the strength of pure aluminium if a low percentage is used.

The main alloying elements are magnesium, silicon, zinc and copper, the other ones are used only as additional elements.

The strength increasing provided by alloying like silicon, magnesium and copper is a consequence of the hardening produced by

the precipitation of their compounds (e.g. MgSi, CuAl₂), after the alloy has been put in solution.

Aluminium alloys are very numerous and represent a wide family of materials having different physical, mechanical, chemical and technological properties. In order to recognise them, it is necessary to make a differentiation and several classifications are commonly used. Aluminium alloys can be divided with respect to the fabrication process as follows:

- *Cast alloys*, which have to be remelted and then casted.
- *Wrought alloys*, which have to be hot worked or cold worked without being remelted like in hot- and cold-rolling process such as extrusion, forging and drawing.

The wrought aluminium alloys can be classified with respect to the treatment as follows:

- *non-heat-treatable alloys* also called work-hardenable alloys;
- *heat-treatable alloys*.

In the case of non-heat-treated alloys, the strength is generally increased by cold-working. Cold working can be obtained during the rolling process for plates or by means of straightening for profiles. Cold working causes a strength increasing with a reduction of ductility. If the material is heated to 350°C, the alloys return to the initial state. For this reason, the welding process implies a strength reduction in the so-called heat affected zone.

As far as heat-treatable alloys are concerned, the strength is improved by means of treating process such as quenching with water or air and natural or artificial aging. The effects of treating process disappear if the material is heated to between 200 and 350°C. Therefore, the heat input from welding process decreases the strength of the alloy to a value which is bounded by the properties of the material in the annealed stage and in the heat-treated stage (Mazzolani, 1995).

Another way to classify aluminium alloys is with respect to the chemical composition. This classification is particularly useful because the aluminium alloys are arranged in groups of alloys having similar mechanical and technological properties. There are two ways to classify aluminium alloys according to their chemical composition: numerical and alphanumeric designation.

The numerical designation is the most used and derives from the American nomenclature proposed by Aluminum Association. This alloys designation system considers two different nomenclatures for wrought and cast alloys. This designation for wrought alloys has been accepted by most international aluminium associations, which signed an accord to use it as given in the Teal sheets (Aluminum Association, 2009). The document provides the relevant designation and chemical composition of the alloys. This numerical designation for wrought alloys has been also introduced in European Standards by EN 573-1 (CEN, 2004b).

The designation system for wrought alloys consists of a four digits number, in which the first digit defines the main alloying element. In the case of pure aluminium (1xxx series), the last two digits represent the minimum aluminium percentage above 99.00%, while the second one is representative of the impurity level. In particular, second digit equal to 0 is for uncontrolled impurities while the values from 1 to 9 depend on the impurity level. In the other series, the second digit is equal to 0 for the main alloys and it varies between 1 to 9 for its modifications. The last two digits identify the individual alloys according to the registration order in the series. In Table 1.2 the numerical designation for wrought alloys is shown together with their main properties and applications.

The numerical designation for cast alloys is quite similar to those for wrought ones and, in Europe, it is defined by EN 1780-1 (CEN, 2002a).

In the alphanumeric designation each alloy is identified by a group of letters and figures divided into two parts. The first one represents the base material defined by “Al” symbol. In the latter one, the main alloying elements are indicated by means of their chemical

symbols sometimes followed by their percentage in the alloys, e.g. AlMgSi1. In Europe the alphanumerical designation is defined in EN 573-2 (CEN, 1994) and EN 1780-2 (CEN, 2002b) for wrought and cast alloys, respectively.

Table 1.2: Numerical designation for wrought alloys

Series	Alloying Elements		Properties	Application fields
1xxx	99% Aluminium	WH	Low strength, very high ductility, very high corrosion resistance	Tank, ceiling, panels
2xxx	Copper	HT	High strength, good ductility, low corrosion resistance, poor weldability	Aeronautic applications
3xxx	Manganese	WH	Middle-low strength, high ductility, high corrosion resistance, poor weldability	Panels, roof systems
4xxx	Silicon	HT	Similar to 3xxx series	Not often used, welding wires
5xxx	Magnesium	WH	High strength, good ductility, very high corrosion resistance, good weldability	Marine and aggressive environment application,
6xxx	Magnesium and silicon	HT	Good strength, good ductility, good corrosion resistance, good weldability	Extruded structures
7xxx	Zinc	HT	Very high strength	Military or specialised application
8xxx	Other	HT	Depends on alloying	-

WH: Work-hardenable alloys
HT: Heat-treatable alloys

1.4.2 Fabrication stage designation

The final mechanical properties of an aluminium product depend on the applied fabrication treatments. In case of heat-treatable alloys, their strength is generally improved by heating processes. On the contrary, the properties of non-heat-treatable alloys can only be

improved by cold-working after the last annealing operation and further heating is not possible as they remove the obtained increase of strength.

The fabrication stage of an aluminium alloy is identified by a symbol which follows the one of alloy designation. This symbol consists of a letter and, in some cases, one or more digits. The European Standard EN 515 (CEN, 1993) defines the properties and the specification of the different treatments and identifies them by the following symbols:

- *F rough stage fabrication*. This symbol is applied to work-hardened products, in which neither special control over thermal conditions nor strain-hardening is employed. Mechanical properties cannot be defined and therefore guaranteed in these work-hardenable products.
- *O annealed stage*. It is applied to wrought products which are annealed to obtain the lower strength temper and to cast products which are annealed to improve ductility. This is the most ductile stage. On the contrary, strength is very low.
- *H work-hardened stage*. This stage represents alloys whose strength is increased by cold working, with or without thermal treatments producing some reduction in strength. The symbol H is usually followed by two or three letters.
- *W Tempered non-stabilised stage*. An unstable temper applicable only to alloys which spontaneously age at room temperature after solution heat treatment. The symbol is followed by a number indicating the natural ageing period, e.g. W 1/2 h.
- *T Heat-treated stage*. It represents those products which are thermally treated, with or without supplementary strain-hardening. This T is always followed by one or more digits. The heat-treatment can be obtained by a combination of the following process: solution, tempering, natural ageing and quenching. Sometimes the heat treatment is followed by a cold-

working process in order to stabilise the alloy and to eliminate the stresses induced by the tempering process.

1.5 STRUCTURAL PROPERTIES OF ALUMINIUM

1.5.1 Physical and mechanical properties

The main physical properties of aluminium at room temperature, compared with those of steel, are given in Table 1.3. The values of these properties for aluminium alloys are generally very close to those of pure material.

As far as the most important parameters for structural point of view are concerned, the density of aluminium is about one third of that of steel with values ranging between 2600 and 2700 kg/m³, depending on alloy. On the contrary, the thermal expansion coefficient is twice that of steel and its values range for different alloys from $19 \cdot 10^{-6}$ to $25 \cdot 10^{-6} \text{ } ^\circ\text{C}^{-1}$.

Table 1.3: Physical properties of aluminium and steel

	Aluminium	Steel
Average density [kg/m ³]	2700	7850
Melting point [°C]	658	1450÷1530
Linear thermal expansion coefficient [°C ⁻¹]	$24 \cdot 10^{-6}$	$12 \cdot 10^{-6}$
Specific heat [cal/g]	0.225	0.12
Thermal conductivity [cal cm ⁻¹ s ⁻¹ °C ⁻¹]	0.52	0.062
Electrical resistivity [$\mu\Omega$ cm]	2.84	15.5
Young's modulus [N/mm ²]	68500	206000

The main mechanical properties of aluminium can be obtained by means of a tension test. The typical tensile stress vs. strain diagram is characterized by a continuous curve without yielding point (Figure 1.17). The diagram presents an initial linear elastic portion up to the proportional stress f_p , which generally corresponds to 0.01% residual

strain, followed by a non-linear portion up to the typical “knee” and a strain-hardening portion, whose slope depends on the type of alloy. Although the aluminium stress-strain curve presents a linear elastic portion, it is not possible to define clearly a yield strength as for steel. In the case of aluminium alloys, a conventional elastic limit stress corresponding to a 0.2% offset of strain from the initial straight-line portion of the curve is assumed. This stress, named 0.2% proof strength $f_{0.2}$, is internationally used in structural design with the same meaning of yield stress for steel. The ultimate stress f_t corresponds to a strain value which can be defined as the limit of “uniform elongation” corresponding to necking of the specimen. At the same time the testing machine records a load which decreases due to the failure of the test coupon, with a value of elongation equal to ε_t . This value is usually considered representative of the ductility of the material.

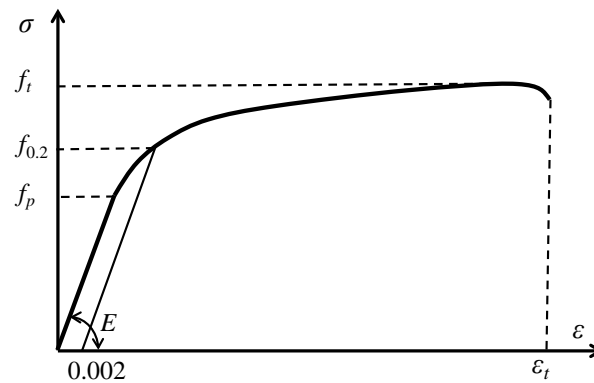


Figure 1.17: Typical stress-strain diagram of aluminium

The Young's modulus E of aluminium, corresponding to the slope of linear branch of stress-strain curve, is approximately 70000 N/mm^2 (it ranges from 68500 to 74500 depending on the alloy) and it is one third of those of steel. The Poisson's ratio ν is slightly higher than steel (0.30) and its value can be assumed equal to 0.33 as suggested by Baker and Roderick (1948), while the shear modulus G is equal to 27000 N/mm^2 .

As far as strength is concerned, aluminium alloys represent a large family of materials which covers a wide range of strength values. In effect, the elastic limit stress ranges from 10 N/mm² of pure aluminium to 500 N/mm² of 7xxx series alloys (Mazzolani, 1995).

The mechanical properties of aluminium, in particular the strength, strongly decrease with temperatures higher than 100°C. On the contrary, all aluminium properties increase with the decrease of temperature below room temperature, as shown in Figure 1.18 (Sharp, 1993). In addition, aluminium alloys do not present a transition temperature that is, in case of steel, the temperature below which brittle behaviour is most likely to occur. Therefore, aluminium is not prone to brittle fracture than steel and, for this reason, it is very suitable for low temperature applications (Mazzolani, 2003).

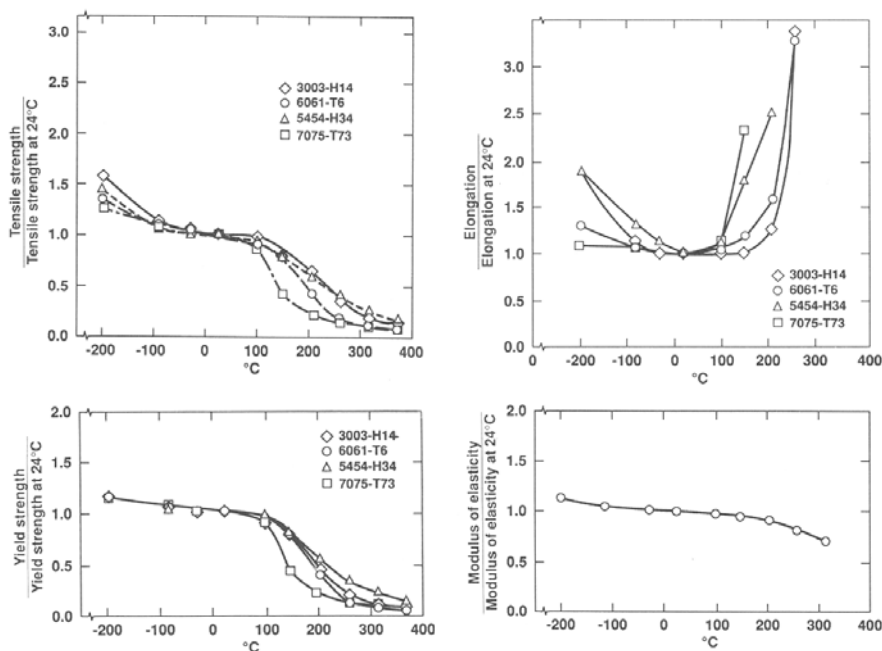


Figure 1.18: Effects of temperature on mechanical properties of aluminium alloys (Sharp, 1993)

1.5.2 Models for stress-strain law

The main difficulty in the development of theoretical analysis of static and stability problems of aluminium alloy structures is related to the model to be assumed for the material behaviour in terms of stress-strain law. As mentioned before, aluminium alloys are a wide family of materials having mechanical properties also considerably different from each other. In addition, the stress-strain curve has a continuous trend, which cannot be simplified in an elastic-perfectly plastic behaviour as for steel. Therefore, a generalized inelastic model has to be introduced. In this case, the elastic limit stress is not sufficient to model the stress-law, but it is necessary to take into account also other parameters, such as Young's modulus and strain-hardening ratio (Mazzolani, 1995).

The simplest way to describe the constitutive law of aluminium alloys is a piecewise linear model, which consist in two or more straight lines representing the elastic-hardening behaviour of the material. In the case of bi-linear model, the model consists of two lines (Figure 1.19a). The first one has a slope equal to the Young's modulus E , while the second one, which represents the strain-hardening portion, has a slope equal to the tangent modulus E_1 . The intersection of these two lines defines the conventional value of elastic limit stress f_p , which can be assumed equal to 0.2% proof strength. This model can be modified in a three-linear model by introducing an intermediate line corresponding to the knee of the actual curve (Figure 1.19b).

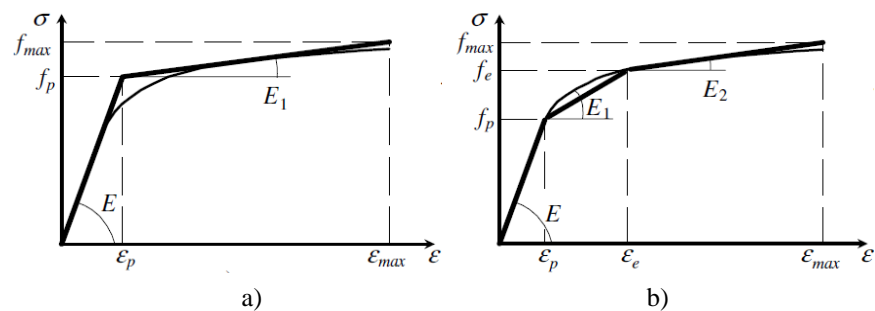


Figure 1.19: Piecewise linear models – a) bi-linear, b) three-linear

More complex models have to be used to describe accurately the actual stress-strain curve of aluminium alloys. In effect, the development of continuous models has been the subject of study of several authors, which formulated different proposals. Continuous models in the form $\sigma=\sigma(\varepsilon)$ were proposed by Baehre (1966) and Mazzolani (1972).

A widely used model is the generalized law in the form $\varepsilon=\varepsilon(\sigma)$, known as Ramberg-Osgood law (Ramberg and Osgood, 1943; Mazzolani, 1995). This law describes the aluminium stress-strain law through the definition of only three parameters. The expression of Ramberg-Osgood law is:

$$\varepsilon = \frac{\sigma}{E} + \left(\frac{\sigma}{B} \right)^n \quad (1.1)$$

where E is the Young's modulus, B and n are two parameters to be determined on the basis of experimental tests.

The meaning of these two parameters can be explained as follows. Defined $f_{\varepsilon 0}$ as the elastic limit stress which corresponds to a residual strain ε_0 , the Ramberg-Osgood law can be rewritten as follows:

$$\varepsilon = \frac{f_{\varepsilon 0}}{E} + \left(\frac{f_{\varepsilon 0}}{B} \right)^n \quad (1.2)$$

which gives

$$\frac{f_{\varepsilon 0}}{E} = \varepsilon - \varepsilon_0 \quad (1.3)$$

by substituting equation (1.3) in (1.2), it results:

$$\varepsilon_0 = \left(\frac{f_{\varepsilon 0}}{B} \right)^n \quad (1.4)$$

therefore

$$f_{\varepsilon 0} = B^n \sqrt[n]{\varepsilon_0} \quad (1.5)$$

by assuming $\varepsilon_0=0.002$ or, alternatively, $\varepsilon_0=0.001$, it results:

$$f_{0.2} = B^n \sqrt[n]{0.002} \quad ; \quad f_{0.1} = B^n \sqrt[n]{0.001} \quad (1.6)$$

whose ratio gives:

$$\frac{f_{0.2}}{f_{0.1}} = \sqrt[n]{2} \quad (1.7)$$

Therefore the exponent n of Ramberg-Osgood law is related to the strain-hardening ratio $f_{0.2}/f_{0.1}$, then to the heat-treatment of material. It gives the shape of inelastic portion of stress-strain curve and it can be expressed as:

$$n = \frac{\ln 2}{\ln \left(\frac{f_{0.2}}{f_{0.1}} \right)} \quad (1.8)$$

It can be noticed that when the ratio $f_{0.2}/f_{0.1}$ tends to 1, the exponent n tends to infinity and the law describes the behaviour of mild steels. On the contrary, for n equal to 1, corresponding to $f_{0.2}/f_{0.1}$ equal to 2, the law becomes linear (Figure 1.20). Intermediate values of n describe the behaviour of different aluminium alloys and decreasing values of the exponent correspond to alloys with higher strain-hardening. It is possible to classify aluminium alloys according to the Ramberg-Osgood exponent as follows (Mazzolani, 1995):

- $n < 10$ -20 non heat-treated alloys
- $n > 20$ -40 heat-treated alloys

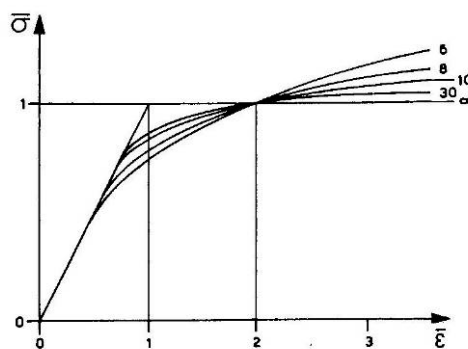


Figure 1.20: Influence of exponent n of Ramberg-Osgood law (Mazzolani, 1995)

For finite values of n , the parameter B defines the extent of curve portion in which the first term of the law is more significant than the second one.

By substituting B obtained from (1.5) into (1.1), the Ramberg-Osgood law assumes the generic form:

$$\varepsilon = \frac{\sigma}{E} + \varepsilon_0 \left(\frac{\sigma}{f_{\varepsilon_0}} \right)^n \quad (1.9)$$

in a completely general form, the evaluation of the exponent n requires the choice of two reference points: the conventional elastic limit and an arbitrarily selected one. In this case, the exponent n is given by:

$$n = \frac{\ln(\varepsilon_0/\varepsilon_x)}{\ln(f_{\varepsilon_0}/f_x)} \quad (1.10)$$

in which f_x is the reference stress and ε_x the corresponding residual strain.

The conventional elastic stress is usually assumed as the 0.2% proof strength and the Ramberg-Osgood law assume the classical form:

$$\varepsilon = \frac{\sigma}{E} + 0.002 \left(\frac{\sigma}{f_{0.2}} \right)^n \quad (1.11)$$

Basically, there are two alternatives for the choice of the second reference point: the stress corresponding to 0.1% residual strain ($f_{0.1}$) or the ultimate strength (f_{\max}), which is the top point of stress-strain curve (Figure 1.21). The choice of this point has a strong influence on the scatter between the experimental curve and the one predicted by the model. The best way to choose it must be based on the phenomenon to be analyzed. In effect, when it is necessary a good approximation in the range of moderately small deformation, it is preferable to use the 0.1% proof strength as second reference point. On the other hand, if the analysis is in the range of large plastic deformation, the ultimate stress shall be used (Mazzolani, 1995).

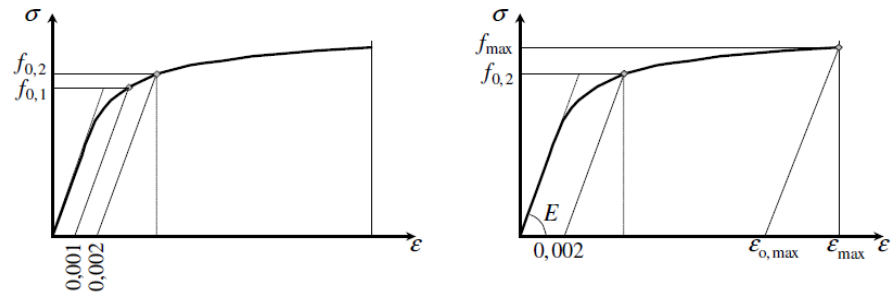


Figure 1.21: Choice of reference point for Ramberg-Osgood law

Chapter 2

DEFINITION AND PROPERTIES OF SPECIAL JOINTS

2.1 JOINING TECHNIQUES FOR ALUMINIUM STRUCTURES

2.1.1 General

Connections represent an important and very critical point in the design of any type of structures. A trustworthy performance of a structure passes through well designed joints because the structural analysis is based on assumptions about their behaviour. Then the results and the design are strongly influenced by the goodness of these assumptions.

Beside the structural design problems, joints influence also the costs of the structure. In effect, joints can represent an important part of construction costs and features like easiness, rapidity of assembly and reproducibility imply economical advantages and are important as well as quality and safety assurance. Other important features to be taken into account are detachability, durability, watertight and aesthetic qualities. All these features are fundamental in the choice of the most appropriate joining technique.

In the case of aluminium structures, a wide choice of joining techniques is available nowadays and they are able to fulfil the most different structural and non-structural requirements. In the following sections the properties of the main joining techniques for aluminium

structures are summarized. They are classified into two groups: “traditional” and “innovative” joints. The “traditional” group includes the most used joints that are also typical of steel structures, such as bolts, welds and rivets. The “innovative” joints are recent joining techniques and the mainly conceived for aluminium structures, such as adhesive, new welding technologies, clinching and special joints.

2.1.2 Traditional joints

In aluminium structures bolts are the most commonly used mechanical fasteners. A bolted joint consists of two or more plate elements connected by a screw with threaded shank and a nut. In order to uniform the pressure due to tightening, circular washers are fitted under the bolt head and the nut. Both aluminium and steel bolts are used. In order to avoid galvanic corrosion problems, steel bolts have to be superficially protected by galvanization or, alternatively, stainless steel bolts can be used (Figure 2.1). Aluminium bolts have a lower strength than steel ones but they have the advantage of avoiding the changes in tightness of joint due to thermal expansion. In case of steel bolts in aluminium female threads, insert threads are used to increase pull-out strength and to avoid that aluminium part become work due to frequent loosening and tightening of the bolt (Höglund, 1999). The main advantages lie in their capability of being detachable and easily assembled on site.

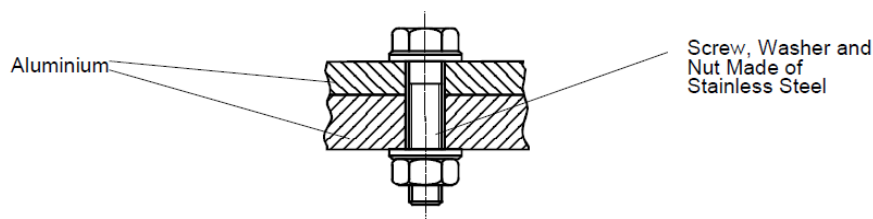


Figure 2.1: Bolted connection (Budde, 1999)

Welding of aluminium represents another widely used method of assembly. It is defined as the joining of materials by the use of heat or

sometimes force with or without a filler metal. Pure aluminium and many alloys (e.g. 6xxx, 7xxx series) are fully suitable to be welded. Different welding technologies are available for aluminium structures, among these, inert gas shielded processes (MIG and TIG) are the most used for structural applications and they can be obtained in ordinary workshops (Figure 2.2). In both Metal Inert Gas (MIG) and Tungsten Inert Gas (TIG) procedures, the fusion of material is protected by an inert gas (argon or helium) and it is caused by high temperatures in the electric arc between the electrode and the parent material. In MIG procedure the arc is drawn by a metal wire electrode, which is also the filler material, and by the work piece. In TIG procedure the electrode is made of tungsten and the filler material is usually introduced manually. MIG welding is more used than TIG due to its better penetration and its higher operational speed. The advantages of welded connections are saving of work and material, absence of drilling and overlap, tight joints, and no crevice corrosion in case of butt welds (Soetens and van Hove, 2003). The main disadvantage consists of the strength reduction in the case of heat treated and cold worked alloys due to the heat input in the so-called Heat Affected Zone (HAZ).

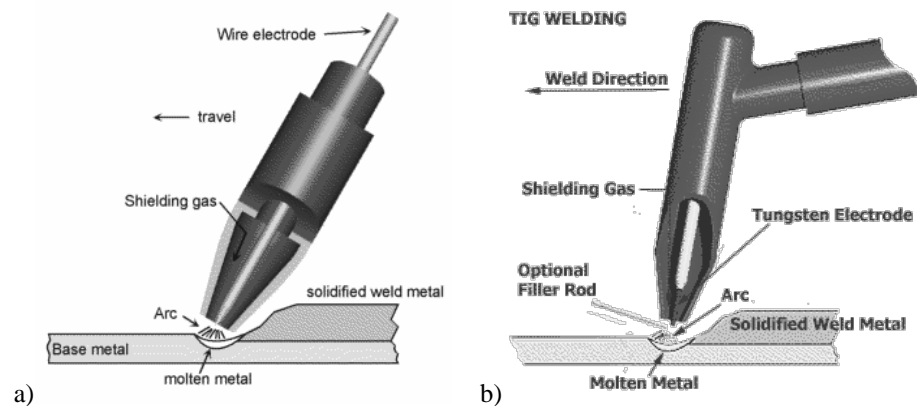


Figure 2.2: a) MIG, b) TIG welding procedure

Aluminium solid rivets are a traditional joining system that has been considered outdated and uneconomical, for a long time. Recently, riveting was rediscovered and it is mainly used for special-purpose applications in the aerospace industry (Budde, 1999). Aluminium solid rivets are driven while cold. The shaft is inserted into the holes of the elements to be connected and with a pneumatic hammer a rounded head is formed on the rear face (Figure 2.3a). Contrarily to hot-driven rivets, cold-driven rivets do not shrink and therefore do not press the sheets together (Soetens and van Hove, 2003). Hence, cold-driven rivets are loaded in a similar way to bolts and it is advisable to avoid in joint under tension.

Other mechanical fasteners typically used in aluminium structures that belong to the rivet family are huckbolts and blind rivets.

Huckbolts have an intermediate behaviour between that of rivets and bolt one (Figure 2.3b). They are made of high strength material as steel. Once the bolt is inserted, a socket is threaded over the projecting grooved portion of the shaft. A special tool grips the end of the shaft and compresses the socket until the external part of the shaft breaks off at the preformed notch (Rørvik, 1998). This system can be rapidly assembled and provides a secure connection that can be used for high stress joints.

Blind or pop rivets were developed in aircraft industry (Figure 2.3c). They are made of stainless steel aluminium and they are generally used in joints for thin-walled structures. One of the advantages of this joint typology is the possibility to be applied in that case where there is access only from one side, e.g. a sheet attached to a hollow profile (Rørvik, 1998).

Blind rivets consist of a hollow shaft and a pull-stem which serves as a tool that forms the closing head. The rivet is mounted by pulling the stem out with a special tool, whereby the stem head is drawn into the protruding rivet material to form the closing head. When the pulling force exceeds a certain level, the stem breaks at a predetermined position (notched or break-stem). The breaking point can be chosen to lie either in the shaft or at the rivet head (Budde, 1999).

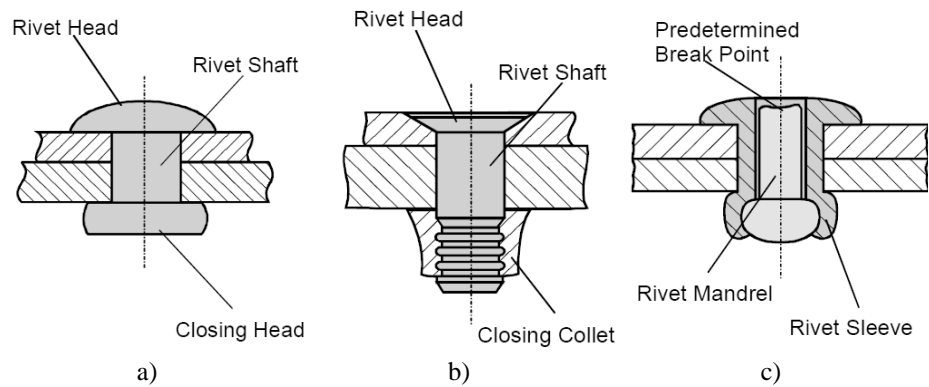


Figure 2.3: a) solid rivet, b) huckbolt, c) blind rivet (Budde, 1999)

In thin-walled structures, screws represent the most used joining system (Figure 2.4). Self-tapping screws (thread forming) are usually installed in predrilled or punched holes, while self-drilling screws have a drilling cutter or a sharp point able to realize their own hole. The great advantage of self-drilling screw is the rapidity of execution because they can drill the hole and fasten the sheets to be connected in only one operation.

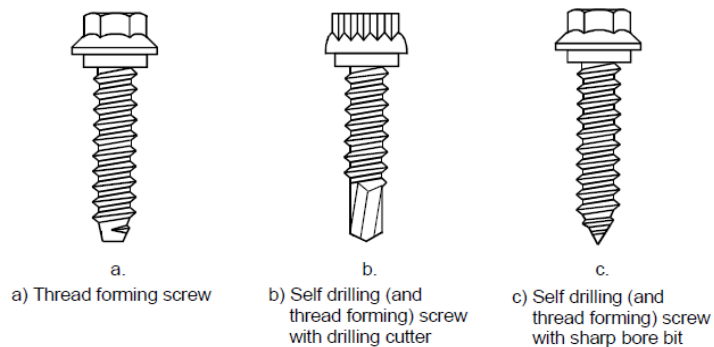


Figure 2.4: Self-tapping and self-drilling screws (Höglund, 1999)

2.1.3 Innovative joints

A typical joining system used in aluminium applications is adhesive bonding. Such system is becoming very important because it can exploit the geometrical possibilities enabled by extrusion (Figure 2.5). Adhesive bonding is not widely used in structural application but it is a very familiar system in the field of the aerospace industry. Adhesive bonding is defined as the process of joining parts using a non-metallic substance (adhesive) which undergoes a physical or chemical hardening reaction causing the parts to join together through surface adherence (adhesion) and internal strength of the adhesive (cohesion). The adhesive types generally used in structural application are phenolic adhesive systems, epoxides, and acrylics. In case of semi structural applications, polyurethanes, hot melt systems, and silicones are used, while typical adhesive for non-structural applications are: cyanoacrylates and contact adhesives. This system has many advantages respect to traditional systems as mechanical fastener and welding but also some disadvantages (Soetens and van Hove, 2003). The main advantages are the possibility to have continuous joints with no holes as for fasteners and no heat input, as for welding, which implies a strength reduction of the parent metal, a more uniform stress and strain distributions, low level of stress concentrations in particular for cyclic loaded structures, possibility to join aluminium with other materials and more flexibility in designing. On the other hand, main adhesives disadvantages are: specific joint design, very low strength to tension force, need of large surface areas, particular attention to surface treatment and curing time, restricted structural behaviour at high temperature.

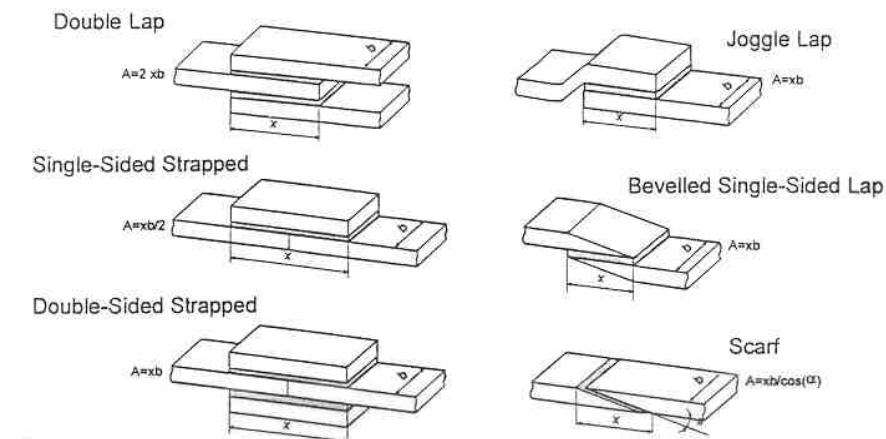


Figure 2.5: Adhesive bonded joints (Soetens and van Hove, 2003)

Friction Stir Welding (FSW) represents a quite recent development in welding processes and it gives several advantages in aluminium applications. The friction stir welding process consists in a specially shaped rotation pin which moves between the abutting faces of the joint generating frictional heat that creates a plasticised region around the tool (Figure 2.6). The contact of the shouldered region of the tool with the workpieces also generates significant frictional heat as well as preventing plasticised material from being expelled. The tool is moved along the joint line, forcing the plasticised material to coalesce behind the tool in order to form a solid-phase joint (Soetens and van Hove, 2003). Therefore, this system allows to weld without any filler or additional material. The main advantages provided by friction stir welding are: a more increased strength than traditional fusion welding, leakproofness, low thermal stress and reduced thermal deformation, repeatability. Other innovative welding procedures that can be used are: laser, explosion, ultrasonic, diffusion, cold and hot pressure welding.



Figure 2.6: Friction stir welding (<http://www.aluminiumdesign.net>)

Another “innovative” joining process is clinching systems which are widely accepted and used for fastening aluminium shaped sheet components and profile components in undetachable joints. Clinching covers processes for direct joining in which the material undergoes a local plastic deformation with or without local incision (Budde, 1999). Different clinching processes are available for various joining purposes depending on sheet materials and thicknesses (Figure 2.7).

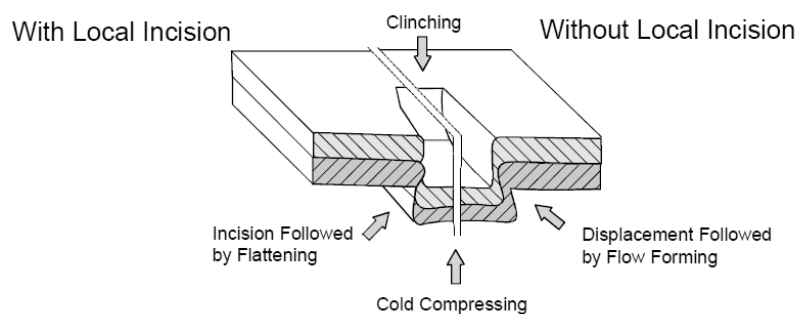


Figure 2.7: Clinching (Budde, 1999)

A typical and handcrafted technique for joining aluminium is the folding process for straight-edged sheets which present a great number of variations (Figure 2.8). Such joints are created through the following steps: folding manually or automatically, interlocking, pressing together and locking by displacing the sheet edges. Great importance lies in the overlap area which should be neither too narrow nor too large in order to avoid low strength joints or waste of material (Budde, 1999).

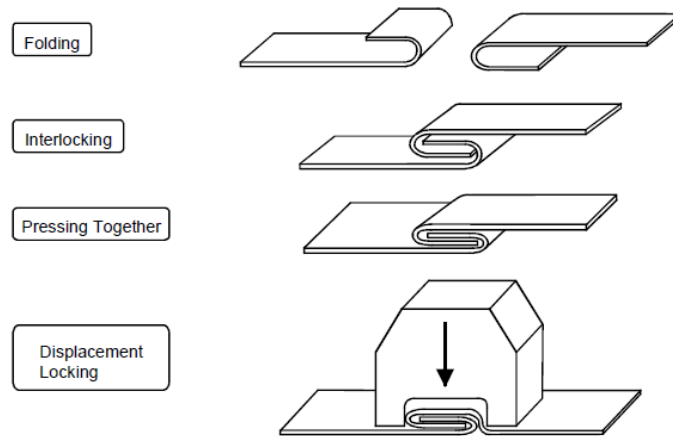


Figure 2.8: Folding process (Budde, 1999)

In some applications different joining techniques are combined in so called hybrid joints. These systems are generally a combination of mechanical fasteners and welds or adhesive bonding. The combination of joining techniques allows to exploit the advantages and to reduce the negative factors related to the single used system as much as possible.

Joining techniques often used in aluminium structures are the so-called “Special” or “non-conventional” joints, which exploit the wide variety of shape possibilities provided by the extrusion process. The mechanical behaviour of these systems represents the topic of the present work. In the following Section the peculiarities and the principles at the base of the studied joint systems together with the main applications are deeply illustrated.

2.2 SPECIAL JOINTS

2.2.1 General information

In aluminium structures the elements and profiles are usually obtained by means of extrusion process that, as known, allows many possibilities of cross-sectional shapes. In particular, extruded shapes can be customized according to the different possible uses by incorporating essential design features, such as stiffener, rib, bulbs, slots and tracks (Figure 2.9). These features can be exploited to conceive, in a more rational way, systems that join together aluminium profiles. The achievable joining methods are various and they can or cannot involve the combination with other types or fasteners.

A typical system that does not need the presence of additional mechanical fasteners is the Snap-fit joint. Such system is mainly used in windows frames and for joining panels side by side on trucks (Höglund, 1999). Snap-fit joint is self-locking system and consists in exerting an action that flexes the mating parts until one of them slips over a raised lip on the other part. Once over this lip, the flexed parts snap back to their normal shape and the lip prevents them from separating (Figure 2.10).

Other special joint systems consist in tracks and slots obtained in the extruded shapes in which mechanical fasteners, such as bolts and screws, can be located. This system typology includes the so-called screw port and bolt-channel joints, which represent the object of investigation of the present work and are fully described in the following.

Finally, thanks to extrusion possibility it is possible to realise a creative joining system which provides many advantages such as the easiness and rapidity of assembly, machining reduction, optimization and saving of the parent material with a consequent cost reduction.

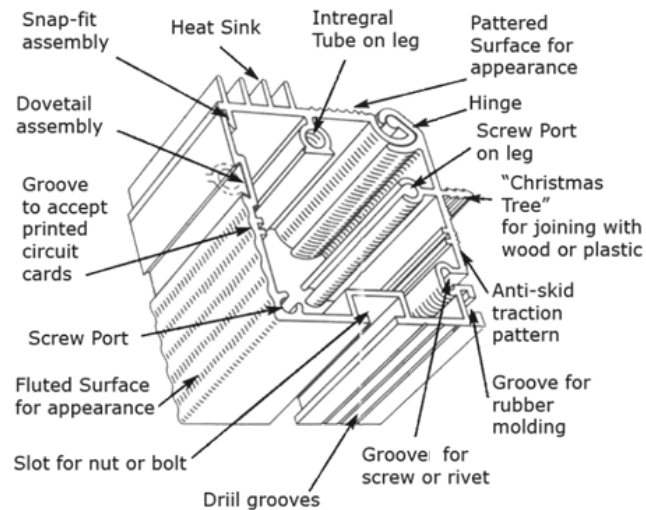


Figure 2.9: Possible feature for joining aluminium profiles (AEC, 2013)

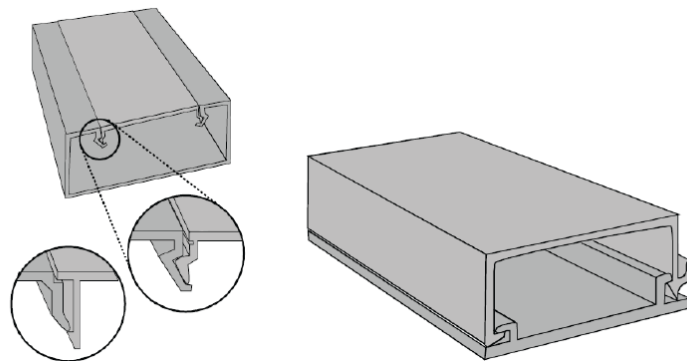


Figure 2.10: Snap-fit joint (Höglund, 1999)

2.2.2 Screw port joints

Screw port joints are commonly used to join aluminium profiles for different structural and non structural applications. This system usually consists in an open or closed slot, obtained by extrusion, in which a screw is installed. The screw port or slot can be threaded by machining in case of metric screws, even if in the most common

solution self-tapping screws are used. The screw port may have different configurations, the main ones are illustrated in Figure 2.11.

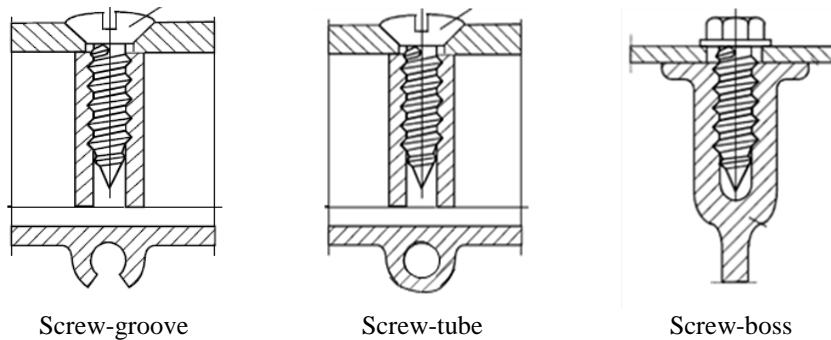


Figure 2.11: Screw port configuration

The screw-groove configuration consists in an open slot obtained by extrusion in which the screw is engaged in the longitudinal direction of profile. The slot opening is usually 60° and it can be located in correspondence of corners or along flat elements of the section. An irrelevant additional amount of material is needed in order to obtain screw grooves, so the fabrication costs are significantly lower compared to conventional methods of drilling and threading screw holes (Hydro, 2009).

In the present work, closed port configuration is named Screw-tube and it develops longitudinally to the profile. In the experimental phase of this work, this system has been schematized by means of an isolated aluminium tube in which self-tapping or metric screw can be located. The latter is only a simplified scheme, because close ports are generally present in extruded profiles and, more frequently, in solid aluminium blocks. Closed ports are often used in case where large screw diameters are required (Sapa, 2009).

Screw-boss, or also screw chase, is a system consisting in a channel of the extruded profile in which a screw can be located at the right angle with the profile axis. This system allows a “stepless fastening”, so the screw joint can be made at any point along the profile, as it shown in Figure 2.12 (<http://www.aluminiumdesign.net>).

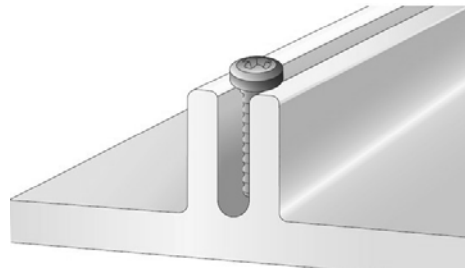


Figure 2.12: Screw-boss system (Sapa, 2009)

Some possible applications of screw port joint, with particular reference to the screw-groove system, so as provided in Sapa Design Manual (Sapa, 2009), are shown Figure 2.13.

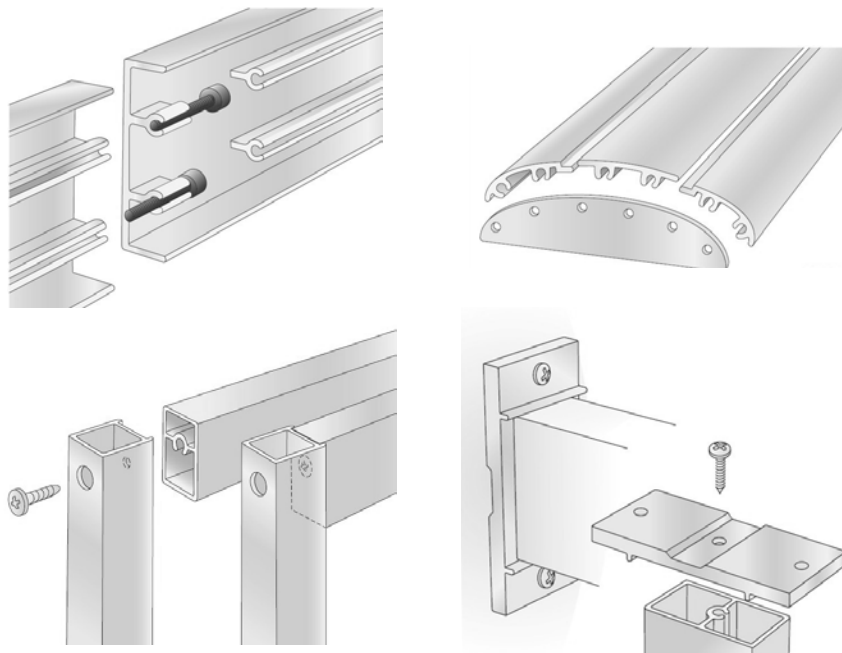


Figure 2.13: Screw port joint application (Sapa, 2009)

2.2.3 Bolt-channel joints

The bolt-channel joint system consists in an extruded section with a track in which the head or nut of bolts that connect the profile with the other joint components can be located (Figure 2.14a). This joining technique allows to set the bolts anywhere along the profile length without any machining. In addition, the joint position can be easily relocated by moving the bolt head along the track (Sapa, 2009).

In the case of joints with more bolts disposed at a given distance, a plate with threaded holes can be introduced in the track defining the bolt position, as shown in Figure 2.14b. In general, plates with threaded hole can be located into the channel and be used as nuts. This solution has been adopted in the experimental investigation presented in this work.

As an alternative to the above solution, special bolt or nuts can be used for bolt-channel joints. T-bolts are very common and advantageous because it is possible to install directly the bolt in the desired position in the channel without the need to slide it from the end of the profile. Also rhombus nuts are commonly used because, after turning, they results self-locked inside the channel.

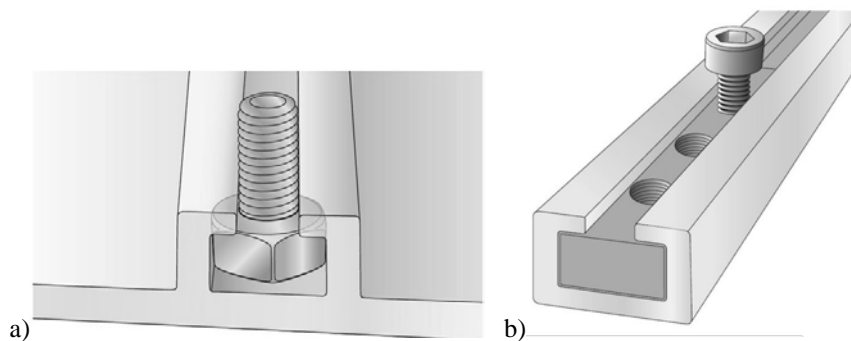


Figure 2.14: Bolt-channel joint (Sapa, 2009)

Possible applications of bolt-channel system are indicated in Sapa Design Manual (Sapa, 2009), such as the end-to-end joint that uses a plate with threaded holes and the T-joint with angles and bolts, shown in Figure 2.15.

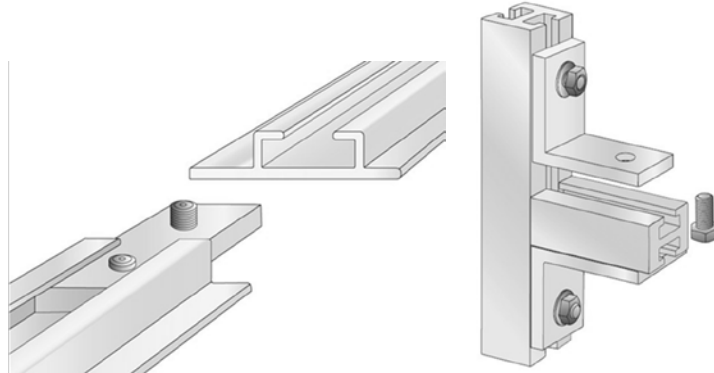


Figure 2.15: Application of bolt-channel joints (Sapa, 2009)

2.2.4 Main applications

Special joints are frequently used for joining aluminium structures in numerous applications, structural or not. The fields of application are wide including not only buildings and civil engineering but also automotive and railway industries. Most common building applications of such joints are façade, doors and windows fixture, but many interesting and creative solutions are worldwide spread. In this Section just some possible applications are presented.

A classic use of bolt-channel joints is T-slotted profile system. A T-slotted profile consists in a semi hollow extruded profile with a square cross-section having, at each side, one or more slots with the aim to receive special bolt heads or nuts. These profiles can be joined together all along their length by introducing simple elements, such as angle and gusset plates. The result is a versatile modular system which allows to obtain any type of frame structure. An example of this type of application is Modulsystem40 produced by METRA (2012), which is specially used to obtain industrial furniture such as support frames for machines, shelves and machine guarding (Figure 2.16). This system is also used to support systems for solar panel plants. A similar system is provided by Roxroth (2011) which allows to assemble framing structures in a faster and cheaper way. With The Roxroth system is possible to obtain a wide range of framing structures as workstations, medical applications, machine frames and base,

enclosures, aerospace applications and creative architectural applications (Figure 2.17)

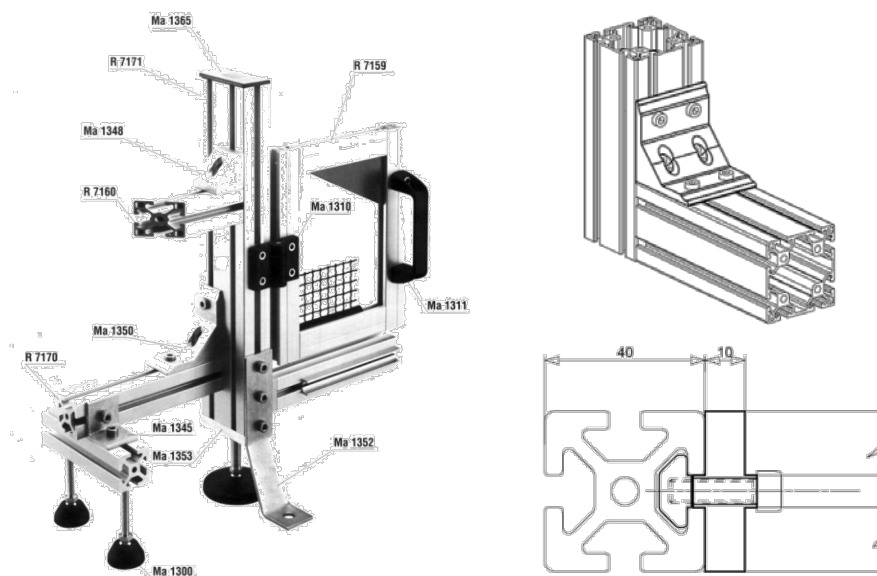


Figure 2.16: Modulsystem by METRA (2012)



Figure 2.17: Roxroth Aluminum structural framing (<http://www.boschrexroth.com>)

Special joints are often used in curtain walls applications. An example is Poliedra-sky system by METRA (2011a). In this case, screw-boss joints are used to fix the glasses to the aluminium structures of the curtain wall (Figure 2.18). Another application of screw-boss joints by METRA (2011b) is in Energymodul system, where the screw-boss elements are used to fix solar panels to the support structure, as shown in Figure 2.19.

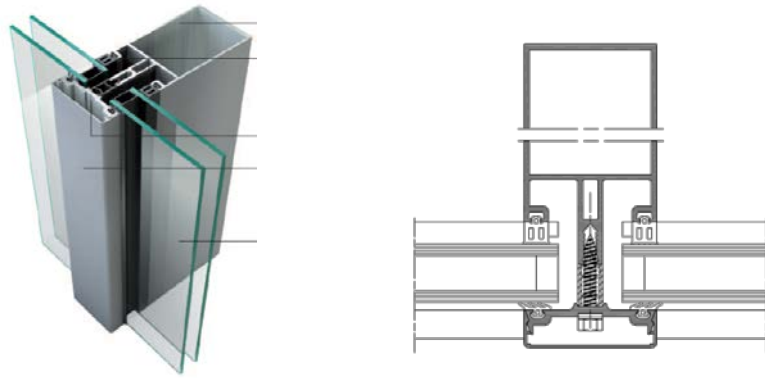


Figure 2.18: Screw-boss joint in curtain walls (METRA, 2011a)

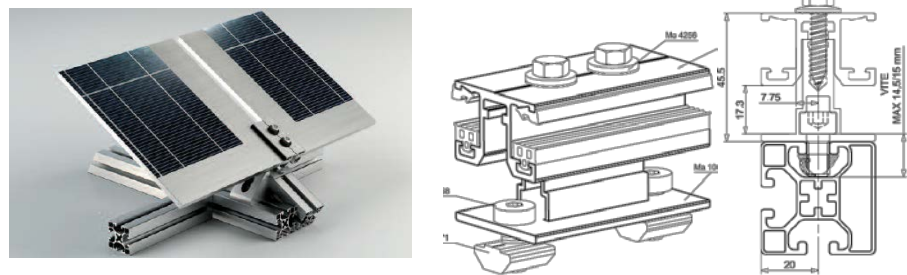


Figure 2.19: Screw-boss joint in solar panel structures (METRA, 2011b)

Another interesting use of special joints is provided by Aluscalae (<http://www.aluscalae.it>), who proposes a modular system with aluminium alloy extruded for staircases where the steps are joined to supporting beams by means of a screwed connection in a closed port

(Figure 2.20). A similar system used for industrial staircases and flooring is provided also by Sapa (2012). The extruded profiles used for steps or floor are connected to the main structures by means of screw-groove and bolt-channel systems (Figure 2.21)

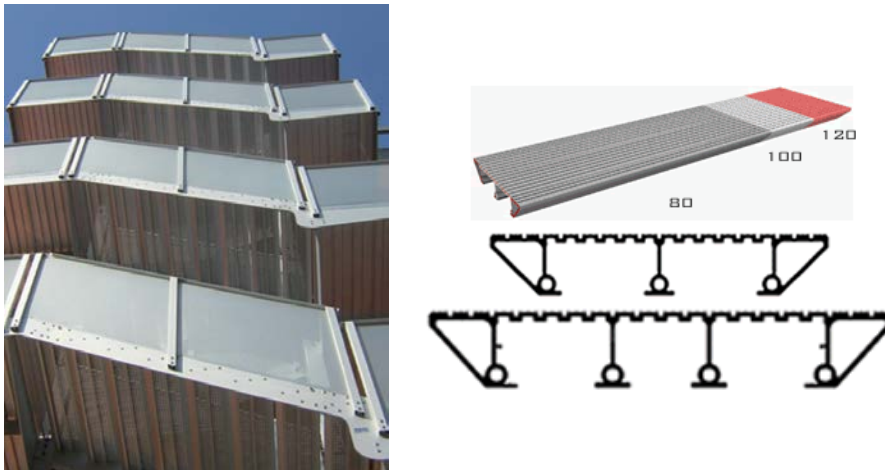


Figure 2.20: Aluscalae staircase system (<http://www.aluscalae.it>)

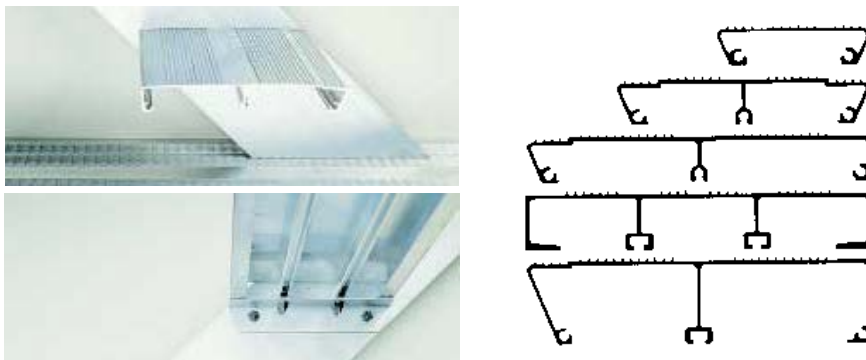


Figure 2.21: Sapa industrial stairway systems (Sapa, 2012)

Special joint is also used in MakeABridge® system by MAADI Group (MAADI, 2011). It is a weld-free aluminium modular system for pedestrian bridges up to 24 m. The main applications of the system are walkways, overpasses, footbridges, trail bridges and gangways. The modular system consists in tubular element with a closed port in

the centre. The elements are connected together through a cast aluminium node where the joint is made by a metric bolt in the closed port of the element (Figure 2.22).



Figure 2.22: MakeABridge® system (MAADI, 2011)

2.3 REVIEW OF THE EXISTING LITERATURE ON SPECIAL JOINTS

2.3.1 State of the art

Although special joint systems are currently and widely used in aluminium applications, also with structural aims, very little information about their mechanical behaviour is available.

In literature, only two experimental studies cover this research topic and they represent the basis of the main formulation for predicting the joint strength. These studies are briefly summarised in the following Sections.

2.3.2 Hellgren (1996)

Hellgren (1996) conducted a wide experimental program on both bolt-channel and screw-groove joining systems. In particular, 247 tests on bolt channel and 160 tests on screw-groove joint have been performed.

The main objective of this research was to investigate the behaviour and to determine the strength and stiffness of commonly used types of bolt-channel and screw-groove joints.

As far as bolt-channel tests are concerned, an AW 6063-T6 aluminium profile with a channel suitable for 8 mm diameter bolts was selected to extract of the used test specimens. The tested bolt-channel configuration was the one where bolt head is fitted into the channel. The joints were tested by considering three test series corresponding to different load directions: a force parallel along the channel, a shear transversal force and a pull-out action. For each series, the influence of bolt head shape was investigated. Stainless steel metric threaded bolts with hexagonal head and special designed T-bolt were used. In the case of pull-out tests, the influence of web channel thickness (1.0, 2.0 and 3.0 mm) was investigated.

The tests on screw-groove joints were carried out under tension load on two different screw-groove extruded shapes. The investigation parameters were: aluminium alloy temper, type of screw and the effective embedment length. For each selected shape the assumed aluminium alloy tempers were AW 6063-T4 and AW-6063-T6. Two different types of screw were selected: a 6.3 mm diameter self-tapping screw and a DG-type screw with 6.0 mm diameter. For each combination of the above assumed parameters, the effective embedment length varied between 5, 10, 15 and 20 mm.

In conclusion, some empirical design methods for the joint ultimate strength calculation were proposed on the basis of experimental findings.

2.3.3 Menzemer et al. (2008)

The experimental program presented in Menzemer et al. (2008) dealt with the pull-out behaviour of self-tapping fasteners in aluminium slot extrusion. The main objective of the study was to investigate the influence of the different parameters that affect the joint strength.

In this study, 79 pull-out tests on 19 different screw-groove joint configurations were carried out. Such tests results are also provided in Deliwala (2007). 6 different extrusion profiles provided by 4 manufacturers were selected. The aluminium alloys used for profiles were 6063-T5 and 6061-T6. Each manufacturer supplied coated steel or stainless steel self-tapping screw for the provided screw slot. The screw diameter was one of the investigation parameter, 4.8, 5.5 and 6.3 mm diameter were assumed. The influence of screw embedment length was taken into account by varying it from 6.35 to 38.1 mm. The failure exhibited by tests was always due to slot opening and pull-out of the fastener, without any fastener rupture.

On the basis of experimental data, the Authors proposed a simply design formulation to evaluate the pull-out strength, which was also adopted in the latest edition of Aluminum Design Manual (Aluminum Association, 2010).

2.4 CODE SPECIFICATIONS AND DESIGN MANUALS

Main codes and specifications for aluminium structures do not provide clear indications about the design of special joints. Only little information and design formulations are given in some specification documents or design manuals. An overview of the main aluminium structure codes and design documents is illustrated hereafter.

Eurocode 9 (EC9) is a very comprehensive document which covers all the main features of aluminium structures design and it represents the main European standard in this field. The document is subdivided into five parts:

- EN 1999-1-1 General structural rules (CEN, 2007a);
- EN 1999-1-2 Structural fire design (CEN, 2007b);
- EN 1999-1-3 Structures susceptible to fatigue (CEN, 2007c);
- EN 1999-1-4 Cold-formed structural sheeting (CEN, 2007d);
- EN 1999-1-5 Shell structures (CEN, 2007e).

In the general part, EN 1999-1-1, the design rules for “traditional” connections, such as bolts, rivets, pins and welding, are provided. The same part provides also information about adhesive bonding joints. In addition, this part proposes also a new method for T-stub joint calculation together with a joint classification based on strength, stiffness and ductility. The rules for design of typical joining system used in thin-walled structures, such as self-tapping/drilling screws and blind rivets, are provided in part 1.4 (EN 1999-1-4). As far as special joints are concerned, the part 1.1 mentions screw-groove, among other joining methods not covered by the standard, specifying that the use of these joints is possible only if appropriate experimental tests are carried out. Therefore, special joints may be used only through design assisted by tests.

Another important international document concerning aluminium structural design is the Aluminum Design Manual (ADM) provided by the Aluminum Association (2010). This document is a guideline which includes an aluminium structural design specification (Part I) accompanying commentary (Part II), a supplemental design guide (Part III), material properties (Part IV), properties of common shapes (Part V), design aid tables (Part VI) and illustrative design examples (Part VII). In Part I, beside the design specification for bolted, riveted and welded joints, pull-out strength formulation for screws in holes (screw-tube) and screws in screw slots (screw-groove) are provided. In particular, for pull-out of screw-groove joints the formulation proposed in Menzemer et al. (2008) has been adopted. Background information about introduced special joints are given in Part II. Basic notions about adhesive bonding, nesting, interlocking and snap-fit joints are illustrated in Part III.

Special joints design is widely treated by Italian Recommendations for aluminium structures CNR-DT 208/2011 (CNR, 2011). The contents of these recommendations are substantially based on Eurocode 9, but it introduces some innovative features, such as special joints and the component method for connections design. The design specifications for special joints are substantially based on literature formulations with little modifications. In particular, CNR-DT 208/2011 provides design rules for screw-groove and bolt-channel joints and general information on snap joints.

Design information about special joints are not only provided by standards and specifications, but also by manufacturer as in the case of the Design Manual published by Sapa (2009). This document is a comprehensive guide on aluminium alloy concerning main material properties, possibilities of application, alloys selection, joining techniques, tolerance, corrosion, economic and structural calculations. In the chapter dedicated to joining techniques, the Design Manual presents a bank of different joining possibilities for extruded profiles with particular reference to screw port, bolt-channel and snap-fit joints, where suggested dimensions for such special joints are also provided. Some design formulations for special joints, screw-groove and bolt-channel, are proposed in the structural calculation chapter.

Information about the sliding lateral strength of screw chase (screw-boss) is provided in the guideline for fastener design in curtain walls AAMA TIR A9-91 (AAMA, 1991). An addendum of this document (AAMA, 2000) introduces, on the basis of about 400 experimental results, the design formulation for screw-tube pull-out which is also adopted by Aluminum Design Manual.

2.5 FORMULATION FOR STRENGTH PREDICTION

As it is shown in the previous section, the main codes in the field of aluminium structures do not provide clear information about the design of special joints. The available formulations for the strength prediction of such joints are generally derived from experimental

results. These formulations provided by standards, specifications and design manuals together with their range of validity are illustrated and described hereafter.

As far as screw-groove joints are concerned, the Design Manual by Sapa (2009) provides indications about slot thickness and diameter dimensions, which are adopted also by CNR-DT 208/2011 (CNR, 2011). Similar indications for slot diameter are given by ADM (Aluminum Association, 2010), while the slot thickness has to be greater than 1.27 mm or $t/2$ (Figure 2.23). These indications, representing the range of validity of proposed design formulations, are given in Table 2.1.

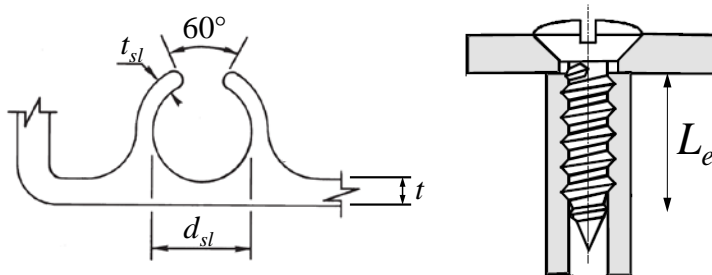


Figure 2.23: Assumed symbols for screw-groove joints

Table 2.1: Range of validity of screw-groove joint

Screw diameter d [mm]	Sapa / CNR DT-208		ADM
	Slot diameter d_{sl} [mm]	Slot thickness t_{sl} [mm]	Slot diameter d_{sl} [mm]
3.5	3.1 ± 0.15	1.5	-
4.2	3.8 ± 0.15	1.5	3.7
4.8	4.2 ± 0.20	1.5	4.3
5.5	4.9 ± 0.20	2.0	4.8
6.3	5.6 ± 0.20	2.0	5.8

Different formulations for pull-out ($F_{o,Rd}$) strength prediction of screw-groove are available. Such formulations are given in the following. The Equation (2.1) is the formulation proposed by Hellgren (1996) on the basis of experimental results, while the one suggested by Sapa is given by Equation (2.2). The formulation expressed in (2.3)

is the one proposed on experimental basis by Menzemer et al. (2008), which is adopted by Aluminium Association in the ADM and, with some modification, also by CNR-DT 208 (2.4).

$$F_{o,Rd} = 0.45 \frac{f_u}{1.2\gamma_{M2}} \left(L_e + \frac{d}{2} \right) 2t_{sl} \quad (2.1)$$

$$F_{o,Rd} = 1.6 \frac{L_e f_u}{\gamma_{M2}} \quad (2.2)$$

$$F_{o,Rd} = \phi 0.29 d L_e f_u \quad (2.3)$$

$$F_{o,Rd} = \frac{0.2 d L_e f_u}{\gamma_{M3}} \quad (2.4)$$

where L_e is the effective embedment length, d is the screw diameter, t_{sl} is the slot thickness (Figure 2.23), f_u is the ultimate strength of the aluminium slot.

Each formulation provides an own safety factor, Hellgren and Sapa suggest to assume, according EC9 (CEN 2007b), γ_{M2} equal to 1.25, while ADM and CNR-DT 208 are more conservative and assume the values of 0.50 and 1.50 for ϕ and γ_{M3} , respectively. For each formulation, the strength linearly increases with the embedment length (L_e) and screw diameter (d), with the exception of Sapa formulation which provides constant strength on varying of diameter.

Information about the prediction of shear strength of screw-groove joints is provided by Sapa and, in case of shear force applied towards the slot opening, it can be evaluated as follows:

$$F_{v,Rd} = (2t_{sl} + 0.16L_e) \frac{f_u}{\gamma_{M2}} \quad (2.5)$$

This formulation is also adopted by CNR DT-208 assuming a safety factor γ_{M3} equal to 1.50. Sapa suggests that in case of force perpendicular to the slot opening, the joint strength can be conservatively calculated through (2.5). On the other hand, if the force is applied towards the close part of the slot, the screw represents the weak component of the joint.

Formulations for the prediction of pull-out strength of screw in closed ports (screw-tube) are given in ADM which adopted the formulations provided by AAMA (2000). Two sets of formulations corresponding to UNC thread and spaced thread are given. For each type of thread three equations, corresponding to different failures that develop on varying of embedment length, are provided. In case of UNC (coarse) thread, the pull-out strength is given by the following equations:

for $1.5 \leq L_e \leq 3$ mm

$$F_{o,Rd} = \phi K_s d L_e f_0 \quad (2.6)$$

for $3 < L_e < 6.3$ mm

$$F_{o,Rd} = \phi [1.2 d f_0 (0.25 - L_e) + 1.16 A_{sn} f_u (L_e - 0.125)] \quad (2.7)$$

for $6.3 \leq L_e \leq 10$ mm

$$F_{o,Rd} = \phi 0.58 L_e A_{sn} f_u \quad (2.8)$$

where K_s is equal to 1.01 for $1.5 \leq L_e \leq 2$ mm and 1.20 for $2 \leq L_e \leq 3$ mm, f_0 is the conventional elastic limit strength of the aluminium slot, f_u the ultimate strength of the aluminium slot, A_{sn} is the internal thread stripping area and ϕ is the safety factor to be assumed equal to 0.50.

On the other hand, the pull-out strength for spaced thread can be evaluated by following equations:

for $1 \text{ mm} \leq L_e \leq 2/n$

$$F_{o,Rd} = \phi K_s d L_e f_0 \quad (2.9)$$

for $2/n \leq L_e \leq 4/n$

$$F_{o,Rd} = \phi 1.2 d f_0 (4/n - L_e) + 3.26 d f_u (L_e - 2/n) \quad (2.10)$$

for $2/n \leq L_e \leq 10$ mm

$$F_{o,Rd} = \phi 1.63 d L_e f_u \quad (2.11)$$

where K_s is equal to 1.01 for $1 \leq L_e \leq 2$ mm and 1.20 for $2 \text{ mm} \leq L_e \leq 2/n$ mm and n is the number thread for unit length of screw.

As far as bolt-channel joints are concerned, the Design Manual by Sapa provides the bolt track dimensions (Figure 2.24) representing the

range of validity of the proposed design formulations. This range of validity, given in Table 2.2, is assumed also by CNR-DT208.

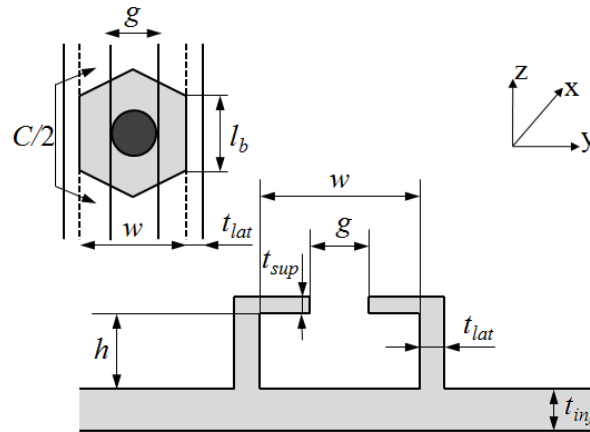


Figure 2.24: Assumed symbols for bolt-channel joints

Table 2.2: Range of validity of bolt-channel joint

Bolt diameter	Internal width w [mm]	Internal height h [mm]	Channel opening g [mm]
M4	7.3±0.15	4.0	4.4
M5	8.3±0.15	5.5	5.4
M6	10.3±0.20	6.0	6.4
M8	13.4±0.20	8.0	8.5
M10	16.5±0.20	9.5	10.7
M12	18.5±0.20	12.5	12.7
M14	21.7±0.20	14.0	15.0
M16	24.7±0.20	16.0	17.0

The joint strength for force acting in parallel direction to the channel, which produces the slipping of bolts or plate inside the channel, can be calculated, according to Sapa and Hellgren, through the following equation:

$$F_{x,Rd} = 200 \frac{M_v}{\gamma_{M2}} \quad (2.12)$$

where M_v is the bolt torque in Nm and γ_{M2} is the partial safety factor assumed equal to 1.25.

On the other hand, CNR-DT 208 recommends to evaluate this strength as well as bolted slip resistant joints by applying a partial safety factor γ_{M3} equal to 1.50, as follows:

$$F_{x,Rd} = \frac{n\mu}{\gamma_{M2}} F_{p,Cd} \quad (2.13)$$

where n is the number of friction interfaces, μ is the friction coefficient and $F_{p,Cd}$ is the bolt preloading force.

The strength of bolt-channel joint subjected to transversal shear force can be calculated by the Equations (2.14) and (2.15), as provided by Hellgren and CNR DT-208, respectively.

$$F_{y,Rd} = \frac{\sqrt{2}f_u t_{inf} l_b}{1.2\gamma_{M2}} \quad (2.14)$$

$$F_{y,Rd} = \frac{1.2l_b t_{lat} f_u}{\gamma_{M3}} \quad (2.15)$$

where f_u is the ultimate strength of the aluminium channel, t_{inf} is the thickness of lower flange of the channel, t_{lat} is the webs thickness of the channel, l_b is the contact length between the web of the channel and the bolt head (Figure 2.24), γ_{M2} and γ_{M3} are the partial safety factor assumed equal to 1.25 and 1.50, respectively.

It has to be noticed that the two formulations have a very similar structure, both depend on the contact length of bolt inside the channel, but Hellgren formulation considers that failure occurs on lower flange (t_{inf}), while according to CNR DT-208 it does in the web. For this loading direction, Sapa evaluated the strength as 70% of the values determined for a traditional bolted joint subjected to shear.

Formulations for the pull-out strength of bolt-channel joint are provided by Hellgren and Sapa as follows:

$$F_{z,Rd} = \frac{f_u t_{sup} C}{\sqrt{3}\gamma_{M2}} \quad (2.16)$$

$$F_{z,Rd} = 1.2 \frac{g t_{sup} f_u}{\gamma_{M2}} \quad (2.17)$$

where t_{sup} is the thickness of upper flanges of the channel, C is the bolt head perimeter in contact with upper flanges of the channel, g is the width of channel opening (Figure 2.9).

Both formulations consider as possible failure mode the shearing of channel web by the bolt head. CNR-DT 208 adopted both formulations assuming the partial safety factor γ_{M3} and suggesting the use of (2.17) because it provides more conservative strength values.

Chapter 3

EXPERIMENTAL CHARACTERIZATION OF THE STRUCTURAL BEHAVIOUR OF SPECIAL JOINTS

3.1 DEFINITION OF EXPERIMENTAL CAMPAIGN

Although some experimental campaigns have been carried out, the information about the structural behaviour of special joint systems for aluminium structures are few and incomplete. The available predictive formulations for such joints are based on a small number of tests and can be considered reliable only for the tested geometrical configurations. In addition, many achievable and commonly used configurations are not covered by the existing test results.

In order to overcome this lack of information and to investigate other possible joint configurations, a wide experimental program on special joints for aluminium structures has been defined and carried out. The experimental campaign has been financially supported by METRA S.p.A., which also provided all the tested specimens. The experimental tests have been performed at the testing laboratory of the Department of Structures for engineering and architecture (DIST) of the University of Naples “Federico II”.

The experimental program has foreseen a total number of 71 tests, of which 45 on screwed joints and 26 on bolt-channel systems.

The tests under tension loads on screw joints have been carried out on three different typologies of screw slot. In particular, the joint configurations defined in Chapter 2 as screw-groove, screw-tube and

screw-boss have been tested. For screw-groove and screw-tube systems the influence of different parameters has been investigated, such as the aluminium alloy and the screw in terms of thread type, diameter and embedment length. The aluminium ports for screw-groove joints have been extracted from two different extruded profiles made of AW 6060-T5 aluminium alloy while, in the case of screw-tube joints, they have been obtained by turning process from an extruded bar of AW 6082-T6 alloy. The only configuration tested for screw-boss consists in two coupled extruded profile made of AW 6060-T5 alloy. The cross-sections of profiles employed to obtain the aluminium slot for screwed joint specimens are shown in Figure 3.1.

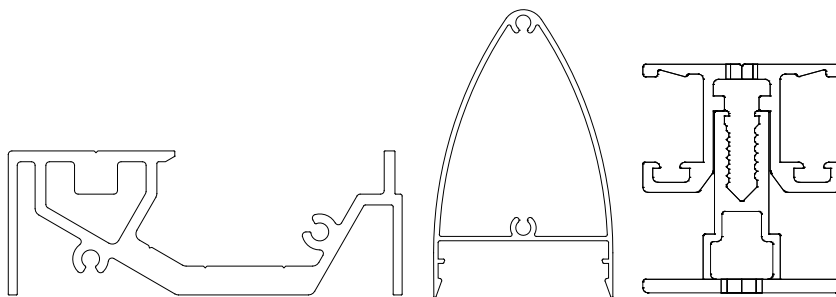


Figure 3.1: Extruded profiles used in screw joint tests

The 26 tests carried out on bolt-channel joints investigated the influence of the load direction and the bolt diameter. The considered loading directions are three: an axial force that induces slipping of bolt along the channel, a transversal shear and a pull-out force. Two different aluminium channels, made of AW 6005A-T6 alloys, corresponding to two different bolt diameters alloys, are used. These channels are extracted from the extruded profiles shown in Figure 3.2.

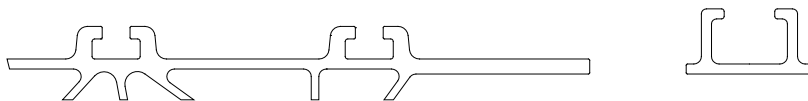


Figure 3.2: Extruded profiles used in bolt-channel tests

In order to define the mechanical properties of used material, the experimental program has foreseen 8 tensile tests on aluminium coupons and 3 tensile tests on steel representative of self-tapping screw material.

In the present Chapter the results of this experimental campaign are presented. Section 3.2 illustrates the results of tests on materials. The detailed test programs, the descriptions of specimens, the information about set-up and instrumentation together with the experimental results are presented in Sections 3.3 and 3.4 for screwed joint and bolt-channel, respectively.

3.2 TESTS ON MATERIALS

3.2.1 Tests on aluminium alloys

Tensile tests on all the aluminium alloy materials used for test specimens have been carried out. The tested materials are: 1.2 mm thick AW 6060-T5, 2.5 mm thick AW 6060-T5, 2.5 mm thick AW 6082-T6 and 4.0 mm thick AW 6005A-T6. These aluminium alloys are representative of 5.5 mm diameter screw-groove, 4.8 mm diameter screw-groove, screw-tube and bolt-channel specimens, respectively. For each type of alloys 2 tensile tests have been performed.

Test coupons sizes are defined according to EN 10002-1 (CEN, 2001), in particular, proportional test pieces are used for materials with thickness lower than 3 mm (AW 6060-T5 and AW 6082-T6), while non-proportional test pieces are used for AW 6005A-T6 alloys. Figure 3.3 shows the sizes of test coupons corresponding to the different investigated alloys and the extraction position from the extruded profile, with exception of AW 6005A-T6 coupons that are obtained by cutting.

The tests have been performed by a universal testing machine MTS 810, while an extensometer with gauge length of 50 mm is used for

strain measurements. The loading rate is 0.05 mm/s and data has been recorded with a frequency of 5 Hz.

Test results are summarised in Table 3.1, where for each tested alloy the average values of Young's modulus (E), 0.1% proof strength ($f_{0.1}$), 0.2% proof strength ($f_{0.2}$), ultimate strength (f_u), ultimate strain (ϵ_u) and the exponent of the Ramberg-Osgood law (n_p) together with the corresponding nominal values provided by Eurocode 9 (CEN, 2007a) are given.

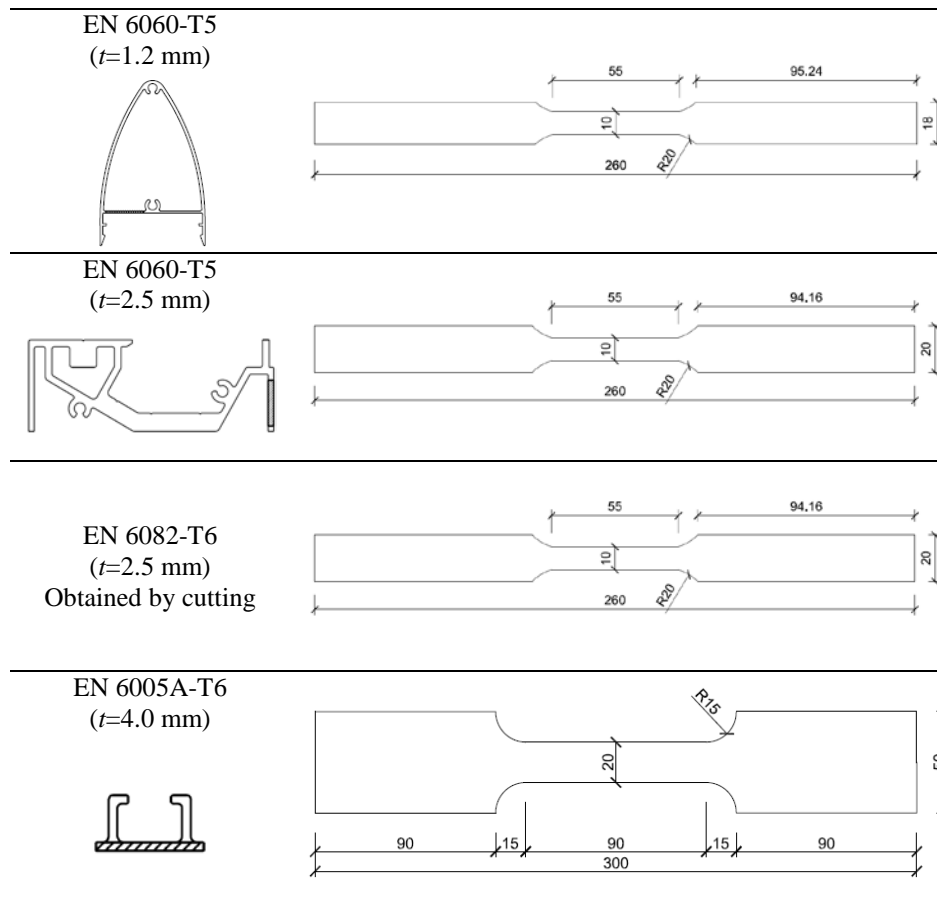


Figure 3.3: Test coupons for different tested aluminium alloys

Table 3.1: Results of test on aluminium alloys

Material		E [MPa]	$f_{0.1}$ [MPa]	$f_{0.2}$ [MPa]	f_u [MPa]	ϵ_u [%]	n_p
AW 6060-T5 ($t=1.2$ mm)	Exp. (Av.)	64470	212	216	247	7	27
	Nominal	70000		120	160		
AW 6060-T5 ($t=2.5$ mm)	Exp. (Av.)	65008	200	206	241	7	22
	Nominal	70000		120	160		
AW 6082-T6 ($t=2.5$ mm)	Exp. (Av.)	66364	272	276	309	7	32
	Nominal	70000		250	295		
AW 6005A-T6 ($t=4.0$ mm)	Exp. (Av.)	63963	231	235	279	10	23
	Nominal	70000		215	255		

The experimental results are substantially in good agreement with nominal values with exception of AW 6060-T5 alloys which show a large increase of 0.2% proof and ultimate strength up to 80% and 50%, respectively. Lower increases with respect of nominal values are exhibited by AW 6082-T6 and AW 6005A-T6 alloys with maximum variation of 10% and 9% for 0.2% proof and ultimate strength, respectively. Finally, the experimental values of Young modulus are slightly lower than nominal ones with a maximum variation of 9%.

Figure 3.4 provides the experimental stress-strain curves for one of the tested aluminium alloys while, in Figure 3.5, all the tested coupons are shown. Detailed information about test results carried out on aluminium alloys is given in Appendix A.

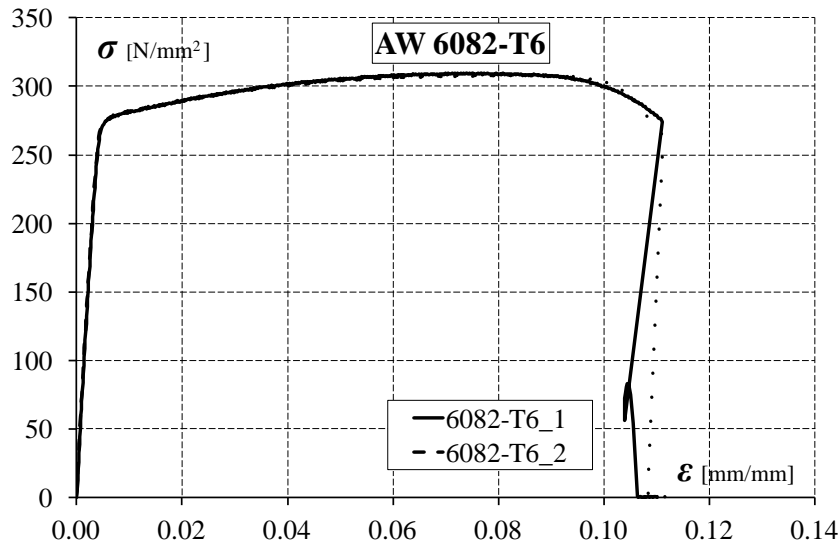


Figure 3.4: Experimental stress-strain curves for AW 6082-T6

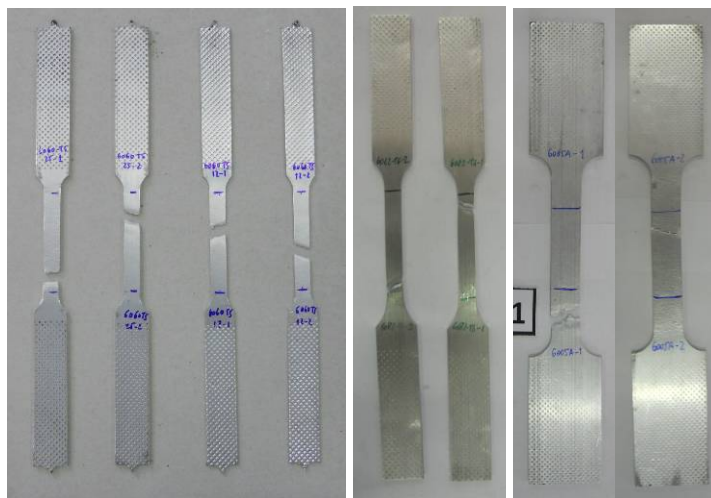


Figure 3.5: Tested aluminium coupons

3.2.1 Tests on screw material

In order to define the mechanical properties of screw material used in the experimental campaign, 3 tensile tests have been carried out. The specimen consists of a 6.3 mm diameter self-drilling screw

produced by the same manufacturer and made of the same steel grade of the screw used for joint tests. The selected screw for material tests has a length of 240 mm with a non threaded portion of 170 mm.

The tests have been performed by a universal testing machine MTS 810, in which the screw head is grabbed with the holder used for screwed joint tests, described in Section 3.3.2. On the other hand, the screw point is directly clamped to the wedge grip of testing machine for a length of 90 mm, so that the threaded portion of screw is completely inside the wedge grip (Figure 3.6). Strain has been recorded by an extensometer with gauge length of 50 mm. The loading rate is 0.05 mm/s and data has been recorded with a frequency of 5 Hz.



Figure 3.6: Tensile test on screw material

The test results in terms of stress-strain curves are given in Figure 3.7, which shows that material does not present a clearly defined yielding strength. Therefore, the 0.2% proof strength has been considered as the conventional elastic limit strength. Table 3.2 shows the results in terms of Young's modulus (E), 0.2% proof strength ($f_{0.2}$), ultimate strength (f_u) and ultimate strain (ϵ_u) values. It can be noticed that strength values are little scattered with a coefficient of variation

lower than 5%. More detailed information about the results of each test is provided in Appendix A.

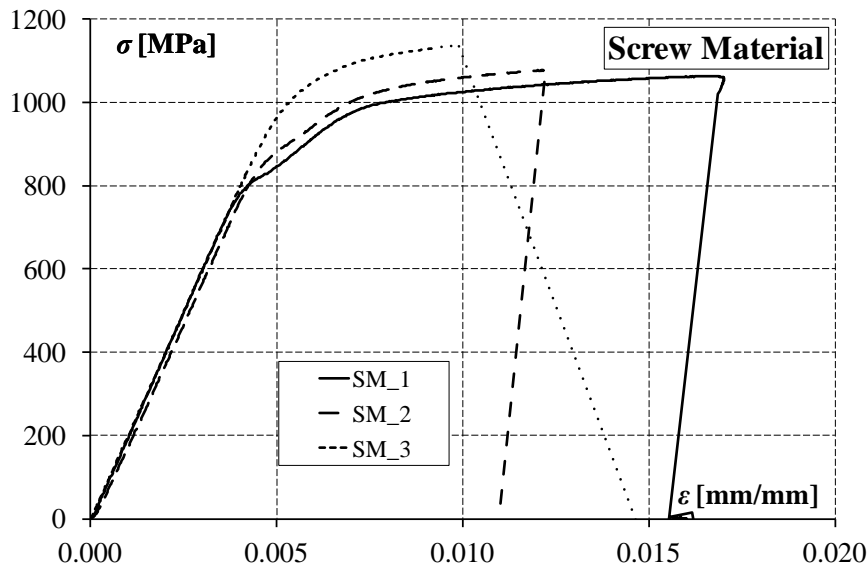


Figure 3.7: Experimental stress-strain curve for screw material

Table 3.2: Results of test on screw material

	E [MPa]	$f_{0.2}$ [MPa]	f_u [MPa]	ϵ_u [%]
Average	199852	1026	1093	1.3
Standard deviation	-	31.1	52.9	-
C.O.V.	-	0.03	0.05	-

3.3 TESTS ON SCREWED JOINTS

3.3.1 Test specimen and program

The existing experimental program about “special” screwed joints (Hellgren, 1996, Menzemer et al. 2007) investigated only the response of screw-groove joints under tension load and no literature is available

about the behaviour of other possible joint configurations, such as screw-tube and screw-boss. For these reasons, the present experimental program has foreseen 45 tests, of which 13 on screw-groove, 28 on screw-tube and 4 on screw boss. The specimens have been tested under tension load, investigating the influence of such parameters: screw thread type (self-tapping or metric), screw diameter and embedment length. About the embedment length, in order to understand some results given in the following section, an important explanation has to be made. The embedment length considered as investigation parameter is the nominal embedment length that is the total length of screw inside the aluminium slot, but the length parameter influencing the joint response is the effective embedment length. The latter is the screw length that fully threads the aluminium slot and it can be assumed as the difference between the nominal embedment length and screw point length, as shown in Figure 3.8.

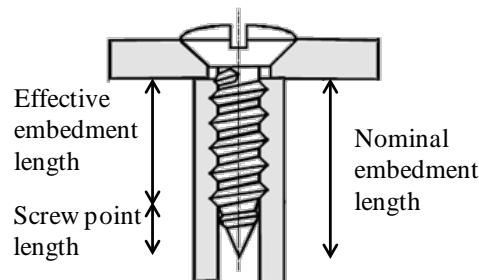


Figure 3.8: Nominal vs. Effective embedment length

Two different aluminium slots for screw-groove specimens, corresponding to 4.8 and 5.5 mm diameter self-tapping screws, have been considered. The specimens have been extracted from extruded profiles made of AW 6060-T5 aluminium alloy. The slot dimensions of both specimens (Figure 3.9) are in the ranges suggested in Design Manual by Sapa (2009) and in Aluminum Design Manual (Aluminum Association, 2010), given in Section 2.5. For both screw diameters nominal embedment length of 15 mm has been considered and, only

for 5.5 mm screw diameter, also specimens with nominal embedment length of 30 mm have been tested.

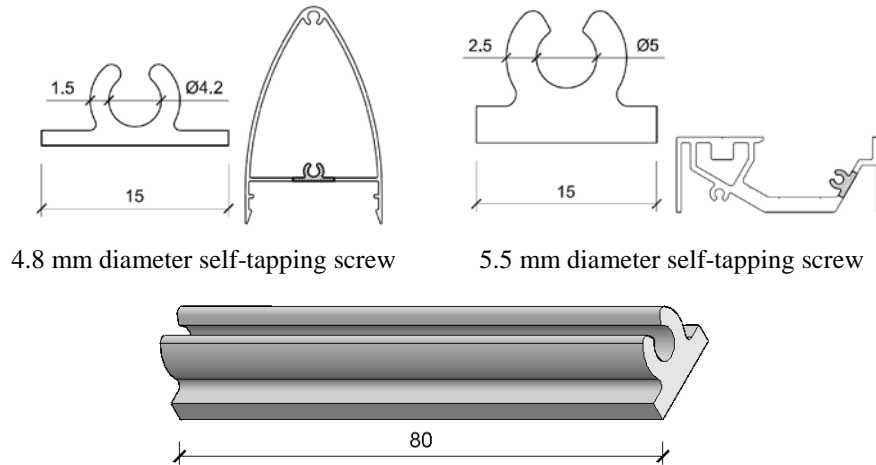


Figure 3.9: Screw-groove specimens

In the case of screw-tube specimens, three different aluminium closed ports have been employed. These elements consist in aluminium tube obtained by turning of an extruded bar of AW 6082-T6 alloy. The internal diameter and the thickness of specimens have been defined in such a way to have similar dimensions to those of the corresponding screw-groove in terms of screw diameter according to the Sapa Design Manual. Two self-tapping screw diameters have been investigated: 5.5 and 6.3 mm. In addition, a closed port with a threaded hole for M6 bolt has been selected. In this case, two bolt grades have been considered: 8.8 and 12.9 grade. The cross-section of specimens is illustrated in Figure 3.10. Specimen with nominal embedment lengths of 10 and 15 mm have been tested for all the investigated diameter while, for 5.5 mm diameter specimen, the additional length of 7.5 mm has been tested.

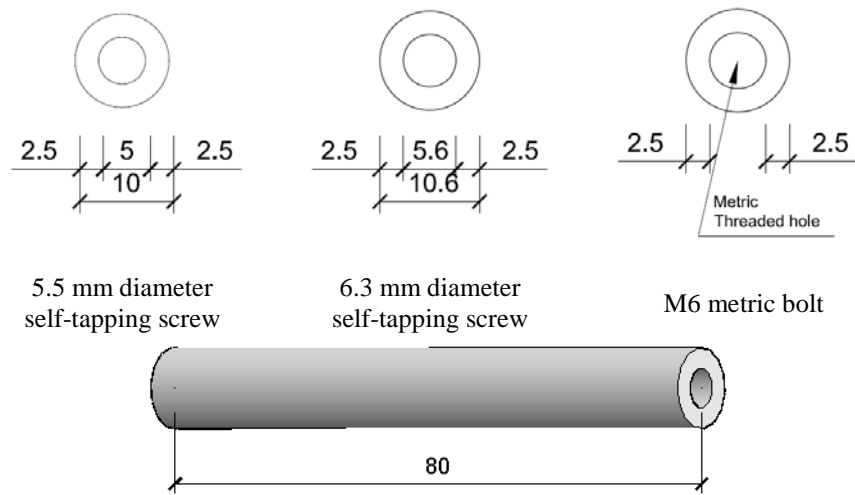


Figure 3.10: Screw-tube specimens

Only one geometry of specimen for screw-boss has been considered. It consists in two extruded elements coupled by means of two 6.3 mm diameter self-tapping screws with a nominal embedment length of 15 mm (Figure 3.11). The width of the channel for screws is 5.2 mm, which is higher than the value of 4.7 ± 0.2 mm suggested by Sapa. The internal surface of the screw channel is knurled in order to facilitate the tapping operation.

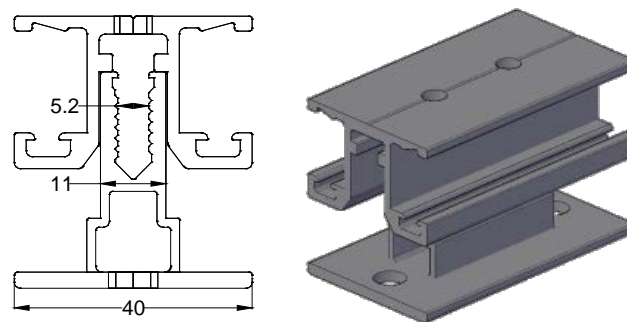


Figure 3.11: Screw-boss specimen

The test program is summarised in Table 3.3, where the parameters under investigation are reported for each specimen series. The series label defines the specimen typology. Namely, the first group of characters indicates the joint typology (SG: screw-groove; ST: screw-tube; SB: screw-boss), the second group represents the fastener diameter (4.8, 5.5 or 6.3 mm for self-tapping screw; M6 and M6H for metric bolt of 8.8 and 12.9 grade, respectively), the third group of digits identifies the nominal embedment length (7.5, 10, 15 or 30 mm). For instance, the label SG-5.5-15 refers to a screw-groove specimen with 5.5 mm screw diameter and nominal embedment length of 15 mm.

Table 3.3: Test program for screwed joints

Series Label	Screw diameter [mm]	Nominal Embedment Length [mm]	Alloy	n. test
SG-4.8-15	4.8	15	6060-T5	5
SG-5.5-15	5.5	15	6060-T5	5
SG-5.5-30	5.5	30	6060-T5	3
ST-5.5-7.5	5.5	7.5	6082-T6	5
ST-5.5-10	5.5	10	6082-T6	5
ST-5.5-15	5.5	15	6082-T6	3
ST-6.3-10	6.3	10	6082-T6	2
ST-6.3-15	6.6	15	6082-T6	2
ST-M6-10	M6 (8.8 grade)	10	6082-T6	3
ST-M6-15	M6 (8.8 grade)	15	6082-T6	5
ST-M6H-15	M6 (12.9 grade)	15	6082-T6	3
SB-6.3-15	6.3	10	6060-T5	4
Total n. of tests:				45

3.3.2 Test set-up and instrumentation

The structural response of screwed joints has been evaluated by testing specimens which reproduce the typical joints configurations. In the case of screw-groove and screw-tube systems, the specimen consists of an aluminium screw port, as described in Section 3.3.1, having 80 mm length, in which at both edges a screw is engaged for a

given nominal embedment length. All the used screws are 70 mm long with cylindrical head with the exception of the 8.8 grade M6 metric bolts that are 80 mm long with hexagonal head. The tension load has been applied to the specimen by means of two steel holders, clamped in machine wedge grip, in which a $38 \times 80 \times 5$ mm steel plate with a hole in the centre is placed. In the plate hole the tested screw are installed in such a way to be pulled by the plate through the holder. Both holder and plate are made of S355 steel grade. The geometrical dimensions of the holder are illustrated in Figure 3.12, while a typical tested specimen placed in the test machine is shown in Figure 3.13.

The screw-boss specimen presents some differences with respect to the other ones. There are two 6.3 mm diameter self-tapping screws, which unlike the previous specimens, are loaded in parallel. In this case, the load is directly applied to the profiles wings by the steel holder, as shown in Figure 3.14.

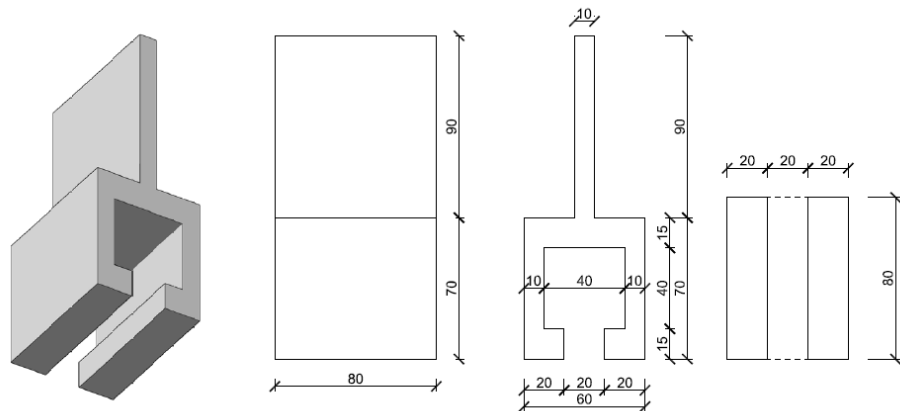


Figure 3.12: Set-up for screwed joint tests



Figure 3.13: Screw-tube specimen

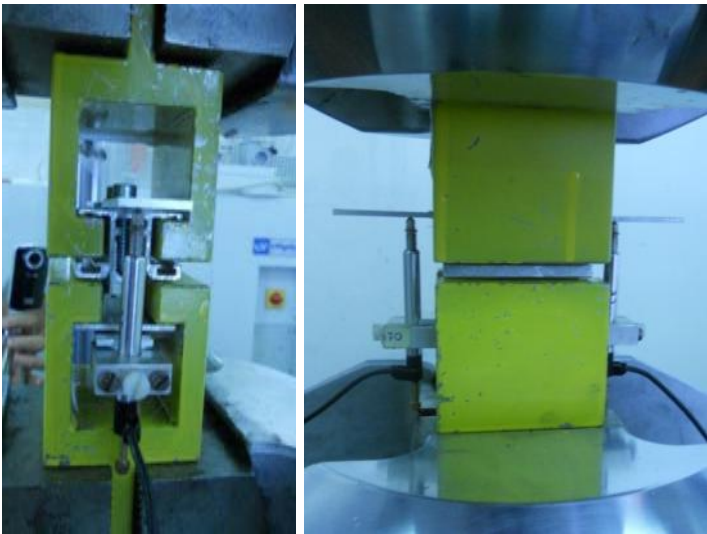


Figure 3.14: Screw-boss specimen

The tests have been performed by means of a universal test machine MTS 810, which has load capacity of ± 500 kN. For screw-groove and screw tube specimens, two linear variable differential transducers (LVDTs) with stroke length of 10 mm have been used to measure displacements of two at the slot edge, while a LVTD with

stroke length 20 mm measured the global response of the specimen. Only two LVDTs are used for screw-boss specimens. All the tests are performed in displacement control with a loading rate of 0.02 mm/s and data has been recorded with a frequency of 10 Hz.

3.3.3 Test Results

Screwed joint test results are summarised in Table 3.4. In this table, for each specimen series the parameters that define the structural behaviour together with the observed failure mechanism are provided. In particular, the considered parameters that define the structural behaviour are the average, the standard deviation and the coefficient of variation values of strength (F_{max}), evaluated as the maximum recorded load, and the average values of stiffness (k), evaluated as the slope of the first significant linear portion on the experimental curve. In the case of screw-boss joints, due to the configuration that produces a different load distribution, the strength and stiffness values provided in Table 3.4 are the values per single screw, evaluated as the total strength divided by 2 that is the number of screws of the specimen.

Table 3.4: Experimental results of screwed joints tests

Series Label	F_{max}			k [kN/mm]	Failure mode
	Average [kN]	Standard dev.[kN]	C.o.V.		
SG-4.8-15	3.62	0.21	0.06	5.06	P
SG-5.5-15	6.10	0.93	0.15	6.66	P
SG-5.5-30	12.60	0.51	0.04	8.48	P
ST-5.5-7.5	7.32	1.26	0.17	8.12	P
ST-5.5-10	12.76	0.71	0.06	9.06	P*
ST-5.5-15	14.24	0.27	0.02	9.29	S
ST-6.3-10	9.62	-	-	10.32	P
ST-6.3-15	18.9	-	-	11.45	A
ST-M6-10	14.61	1.41	0.10	8.59	P
ST-M6-15	17.40	0.32	0.32	10.0	S
ST-M6H-15	19.39	0.08	0.003	12.72	A
SB-6.3-15	2.35	0.07	0.03	3.87	P

P: screw pull-out; S: screw failure; A: aluminium failure
* screw failure occurred for one specimen

As far as screw-groove tests are concerned, the observed failure mechanism is always the pull-out of screw from its slot (Figure 3.15). In case of SG-4.8-15 and SG-5.5-30 series this failure mode is combined by a pronounced bending deformation of aluminium slot, as shown in Figure 3.16. The experimental results in terms of load vs. displacement ($F-d$) curves are shown in Figure 3.17. By comparing the results of SG-4.8-15 and SG-5.5-15 specimens, it can be noticed that the influence of the diameter from 4.8 to 5.5 mm revealed an increase of strength equal to 69%. In case of 5.5 mm screw diameter, the doubling of the nominal embedment length from 15 to 30 mm implied an increase of more than two times of strength (106%). The scatter of strength values are in the range from 4% to 15% with lower values with increasing embedment length (5.5 mm screw diameter series). In terms of stiffness, a slight increase can be observed passing from 4.8 to 5.5 mm screw diameter and for increasing embedment length.

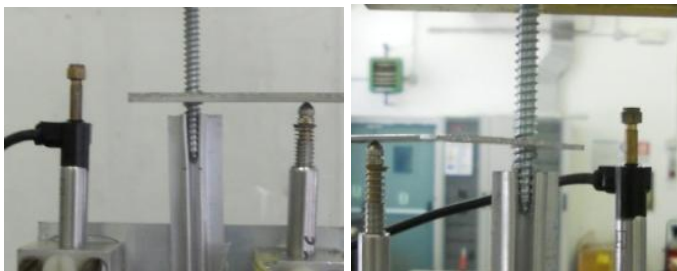


Figure 3.15: Pull-out failure of screw-groove joints



Figure 3.16: Bending deformation of screw slot

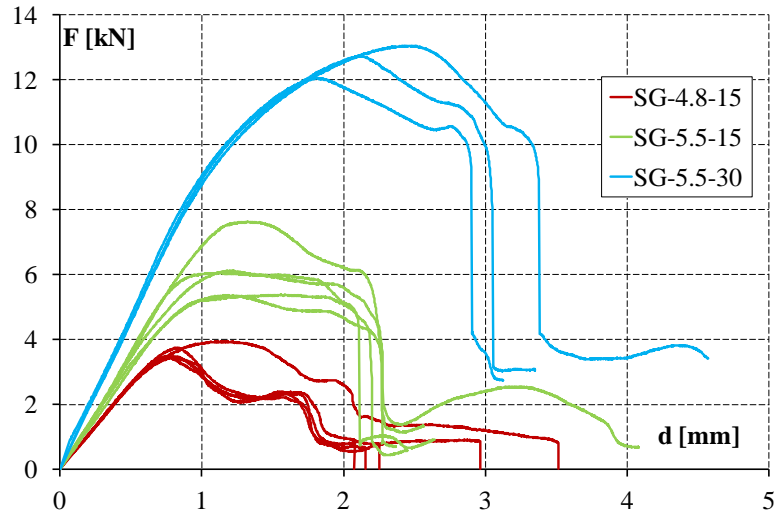


Figure 3.17: Experimental curves of screw-groove joints

Only one screw-boss configuration (SB-6.3-15) has been tested, so it represents an isolated case. The screw pull-out failure (Figure 3.18) occurred and, in terms of strength, the values are very low scattered with a coefficient of variation of 3% (Figure 3.19). By comparing the SB-6.3-15 results with those of other open slot configurations with equal nominal embedment length, it can be noticed that, although a greater screw diameter is used, the strength per one screw is 35% and 61% lower than those exhibited by SG-4.8-15 and SG-5.5-30. This difference can be explained by the lower interaction surface between the screw and the aluminium slot respect to the screw-groove systems.

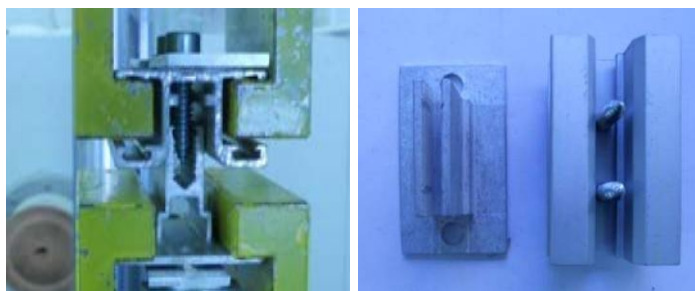


Figure 3.18: Failure mechanism of SB-6.3-15

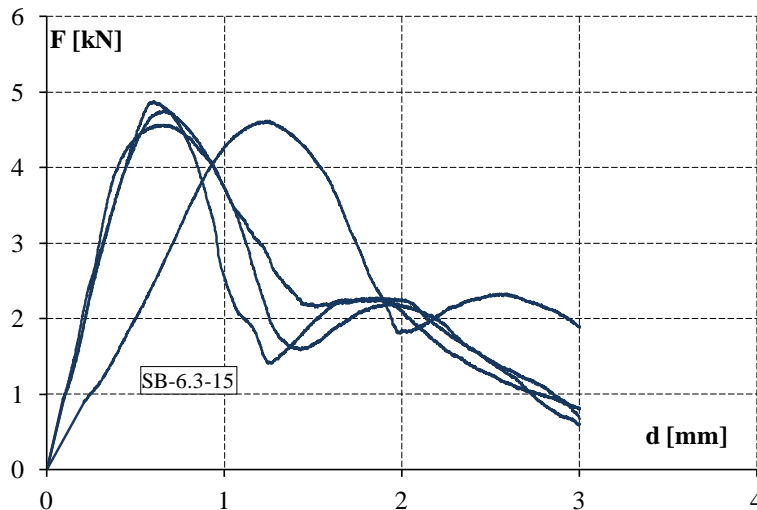


Figure 3.19: Experimental curves of screw-boss joints

As far as screw-tube tests are concerned, the observed failure mechanisms are three (Figure 3.20): screw pull-out from its slot, tension failure of the screw and tension failure of the aluminium tube. For all the series having nominal embedment length of 7.5 and 10 mm, the failure is due to the screw pull-out, with exception of only one test of ST-5.5-10 series where screw failure occurred. Tension failure of screw occurred for ST-5.5-15 and ST-M6-15 series while, in the case of ST-6.3-15 and ST-M6H-15 series, the failure of aluminium tube occurred. It can be notice that in case of M6 metric bolt series the change of bolt grade from 8.8 to 12.9 implies the moving of failure from screw to aluminium.



Figure 3.20: Failure mechanism in screw-tube joints: a) screw pull-out; b) screw failure; c) aluminium failure

The experimental results in terms of load vs. displacement ($F-d$) for ST-5.5 series are shown in Figure 3.21. In this case, the experimental evidence shows a high strength increase (78%) for a little difference of nominal embedment length (33%). This can be explained by considering the effective embedment length as the parameter that really influences the joint response. Given for the examined diameter the point length of 5 mm, according ISO 1478 (ISO, 1999), the effective embedment length are 2.5 and 5 mm for nominal values of 7.5 and 10 mm, respectively. Therefore, there is a difference of effective length of 100% which can justify the observed strength increase. On the other hand, the variation of nominal embedment length from 10 to 15 implies an increase of strength of 11% with the change of failure mode. The scatter of strength is in the range from 2% and 17% with higher values for lower nominal embedment length.

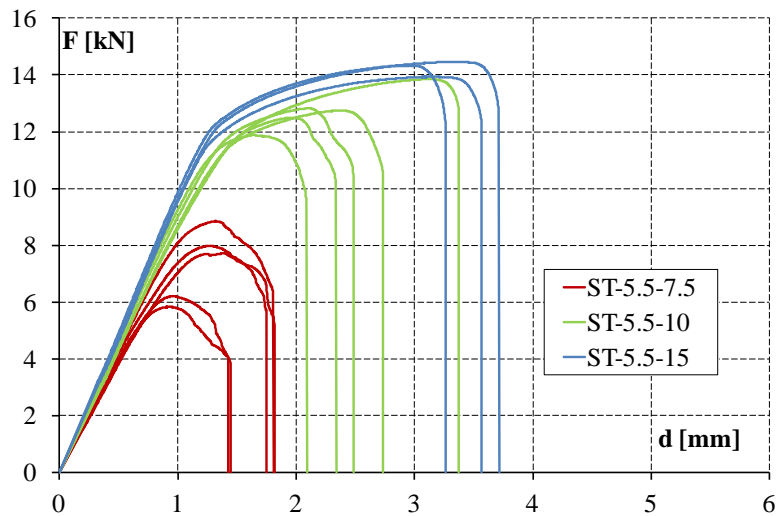


Figure 3.21: Experimental curves of screw-tube joints (SG-5.5)

The experimental results in terms of load vs. displacement ($F-d$) for ST-6.3 series are shown in Figure 3.22. By comparing the results it can be observed a 96% increase of strength from 10 to 15 mm nominal embedment length with a change of failure mode from pull-out to aluminium failure. It can be noticed that the average strength of

ST-6.3-10 is 25% lower than the one of smaller diameter ST-5.5-10. Also this finding is due to the difference of effective embedment length. In effect, for a 6.3 mm diameter screw the point length is 6 mm (ISO, 1999) and it is greater than the 5 mm points of 5.5 mm diameter, then the corresponding effective resisting length are 4 mm and 5 mm for ST-6.3-10 and ST-5.5-10, respectively. Also in this case, the stiffness values are slightly increasing with the nominal embedment length.

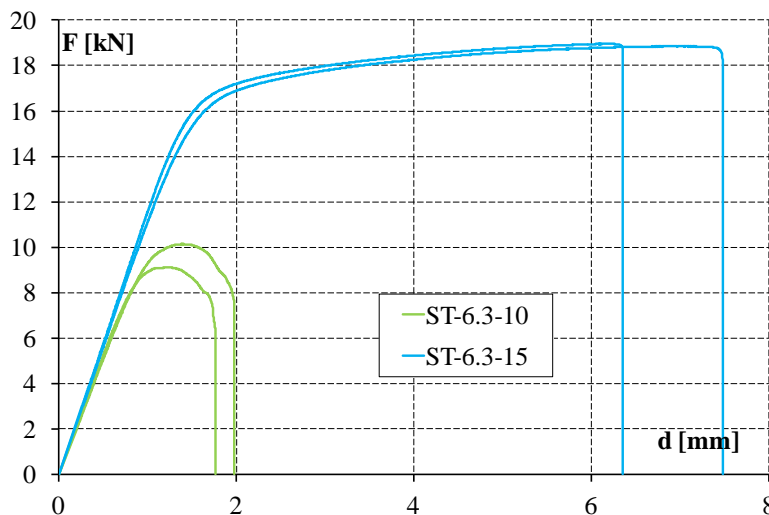


Figure 3.22: Experimental curves of screw-tube joints (SG-6.3)

The experimental results in terms of load vs. displacement ($F-d$) for ST-M6 series are shown in Figure 3.23. The results in terms of strength present an increase of 19% from 10 to 15 mm nominal embedment length with a change in failure mode from pull-out to screw failure while, by changing the bolt grade from 8.8 to 12.9, the strength increase of 11% and failure is from aluminium side. In addition, by comparing the strength results of ST-M6-10 to the other ST series having same nominal embedment length, it can be noticed that the metric threaded screws are 14% and 52% more strength than ST-5.5-10 and ST-6.3-10. This can be explained by the difference of thread pitch (1 mm of M6 vs. 1.8 mm of 5.5 and 6.3 mm diameter

screws) and by the difference in terms of effective embedment length that is close to the nominal one for metric screws while, in case of self-tapping screws, it is halved. The strength results are low scattered with a maximum coefficient of variation of 10%. Also this case confirms a decreasing trend of scatter with increase of nominal embedment length and that the stiffness values are slightly increasing with the nominal embedment length.

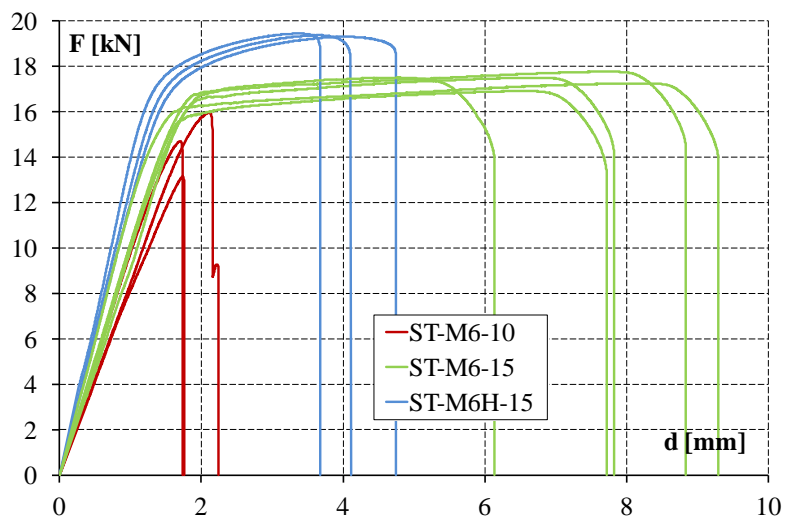


Figure 3.23: Experimental curves of screw-tube joints (SG-M6)

As a general remark, it can be noticed that the most scattered results are always for lower values nominal embedment length (7.5 to 10 mm). These cases correspond to the failure mode of screw pull-out. Such mechanism is strictly related to the embedment length and then it is more sensitive than other failure mode to little variation of this length. As a consequence, the assembly imperfection, in terms of little difference between actual and nominal embedment, can strongly influence the structural response. In addition, this phenomenon is more pronounced in the case of small values of nominal embedment length where a little assembly imperfection can imply a great difference in terms of strength.

More detailed information about the results of single test on screwed joints is provided in Appendix B.

3.3.4 Failure mechanism considerations

The chart of Figure 3.24 shows the trend of failure mechanism in screwed joints as function of different parameters.

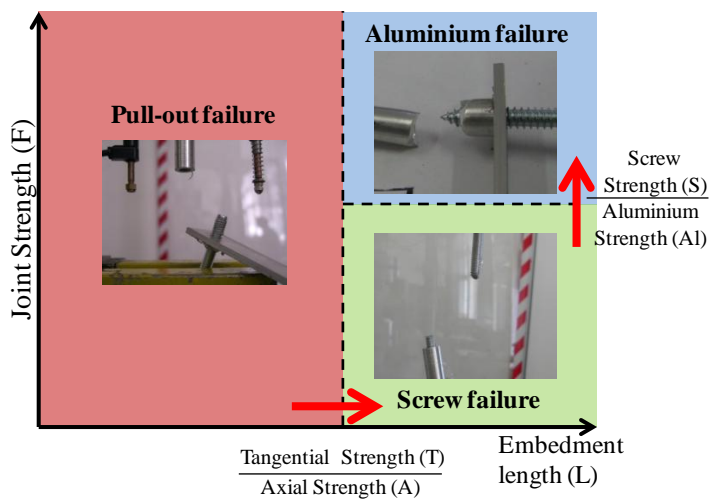


Figure 3.24: Failure mechanism chart for screw joints

In particular, it can be noticed that the joint tangential strength defined as the one of the interaction between the screw and aluminium slot, which corresponds to the pull-out failure mechanism, increases with the embedment length. On the other hand, the axial strength related to the tension failure of screw or aluminium slot is constant and independent from the embedment length. Therefore, it can be defined a transition length, corresponding to the ratio between the tangential and axial strength (T/A) equal to 1, which defines the variation of failure mechanism from pull-out ($T/A < 1$) to an axial failure ($T/A > 1$). In the right part of the chart, corresponding to axial failures, a dividing line, which separates the field of screw and aluminium failure, can be defined. In this case, the transition line

corresponds to the ratio between the screw and aluminium slot strength (S/Al) equal to 1, and its position moves up with the increase of aluminium alloy strength.

Figure 3.25 shows the chart drawn on the basis of experimental results of screw-tube joints. In this case, the transition embedment length is 10 and 15 mm, while the transition line for axial failure corresponds to about 18 kN.

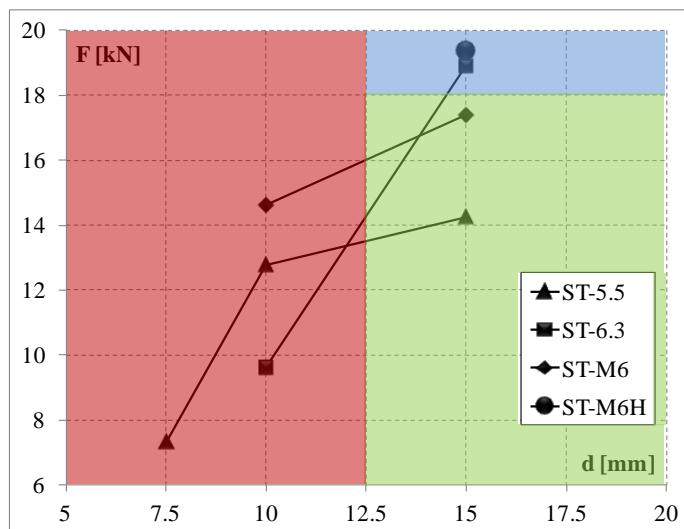


Figure 3.25: Experimental based failure chart

3.3.5 Experimental vs. predicted strength

In this Section, values of strength of screwed joint obtained by experimental tests are compared to those estimated through the available prediction formulations, illustrated in Section 2.5. In particular, the formulations are applied for all the screw-groove and screw-tube series that exhibited the pull-out failure, since they are calibrated on this failure mode. All the considered formulations are applied by considering the experimental values of aluminium alloys given in Section 3.2 and by assuming the safety factors equal to 1. The

effective embedment length has been evaluated as the difference of nominal embedment length and the nominal length of screw point.

The predicted values of strength for screw-groove joints estimated through the formulation proposed by Hellgren (2.1), Sapa Manual (2.2), Menzemer et al. and ADM (2.3), CNR-DT 208 (2.4), together with the ratio between the predicted and the experimental values are given in Table 3.5.

Table 3.5: Comparison between predicted and experimental strength for screw-groove joints

Series	Exp.[kN]	Hellgren (2.1)		Sapa (2.2)	
		Pred. [kN]	Pred./Exp.	Pred. [kN]	Pred./Exp.
SG-4.8-15	3.62	3.56	0.98	4.23	1.17
SG-5.5-15	6.10	5.65	0.93	3.86	0.63
SG-5.5-30	12.6	12.4	0.99	12.43	0.77
Pred./Exp. Aver.			0.96	0.86	
Pred./Exp. St. dev.			0.03	0.28	
Pred./Exp. C.o.V.			0.04	0.33	
Series	Exp.[kN]	Menzemer et. al /ADM (2.3)		CNR DT-208 (2.4)	
		Pred. [kN]	Pred./Exp.	Pred. [kN]	Pred./Exp.
SG-4.8-15	3.62	3.68	1.02	2.54	0.70
SG-5.5-15	6.10	3.84	0.63	2.65	0.43
SG-5.5-30	12.60	9.61	0.77	6.63	0.53
Pred./Exp. Aver.			0.80	0.55	
Pred./Exp. St. dev.			0.20	0.14	
Pred./Exp. C.o.V.			0.24	0.24	

From the comparison of results, it has to be noticed that CNR-DT 208, for the examined cases, strongly underestimates of 50% the experimental values on average. Sapa and ADM formulations overestimate the strength of SG-4.8-15 with an error of 17% and 2%, respectively, and underestimate the strength of both SG-5.5-15 and SG-5.5-30 with errors up to 37%. These formulations, for the examined cases, present errors on average of 14% and 24%, respectively. Hellgren slightly underestimate the strength with an

average error equal to 4%. In this case, the differences between predicted and experimental values have very low scatter (4%), and then this formulation would seem to be the one that provides the best prediction.

In Table 3.6 the comparison of values estimated by ADM formulations for closed ports (screw-tube) and experimental ones is given. For each series, the reference of used formulation according the range of validity is specified. In the case of ST-M6-10 series, the formulations provided for UNC screw have been used, while the ones for spaced screws have been used for ST-5.5-75 and ST-5.5-10 series.

Table 3.6: Comparison between predicted and experimental strength for screw-tube joints

Series	Exp.[kN]	ADM		
		Equation	Pred. [kN]	Pred./Exp.
ST-5.5-7.5	7.32	(2.9)	4.55	0.62
ST-5.5-10	12.8	(2.10)	11.8	0.92
ST-6.3-10	9.62	(2.10)	9.22	0.96
ST-M6-10	14.6	(2.8)	20.9	1.43

From the comparison of results, the ADM formulation (2.8) used for ST-M6-10 overestimate the experimental values of 43% while, for ST-5.5-7.5 the formulation (2.9) provides strength values of 38% lower than the experimental ones. A good estimation of strength is given by the formulation (2.10) used for ST-5.5-10 and ST-6.3-10, with errors equal to 8% and 6%, respectively.

3.4 TESTS ON BOLT-CHANNEL JOINTS

3.4.1 Test specimen and program

The experimental program is aimed to investigate the structural response of so-called Bolt-channel joint systems. The main objective is to define the influence of extruded channel geometry, the bolt

diameter and the direction of loads. Just a little literature about these joints is available and only one experimental study was carried out before (Hellgren, 1996), in which bolt-channel joints were obtained by locating bolt head in the extruded channel and the influence of head type was investigated.

In the present experimental program a variation of bolt-channel system has been tested. Instead of the bolt-head, a steel plate with a threaded hole is located in the channel and the joint is made by tightening a bolt to this plate. Practically, the holed steel plate behaves as a bolt nut, which hereafter is simply named plate nut. No information, tests results or design rules, are available for this joint configuration.

Two aluminium channels, suitable for M10 and M18 bolt diameter, have been selected to be used as bolt-channel specimens. The M10 channel has been extracted from an extruded profile while, for M18 specimens, a specific extruded channel has been employed (Figure 3.26). Both profiles were made of AW 6005A-T6 aluminium alloy, all used bolts are of 8.8 grade and the steel plates used as bolt nuts are made of S355 steel grade (Figure 3.27).

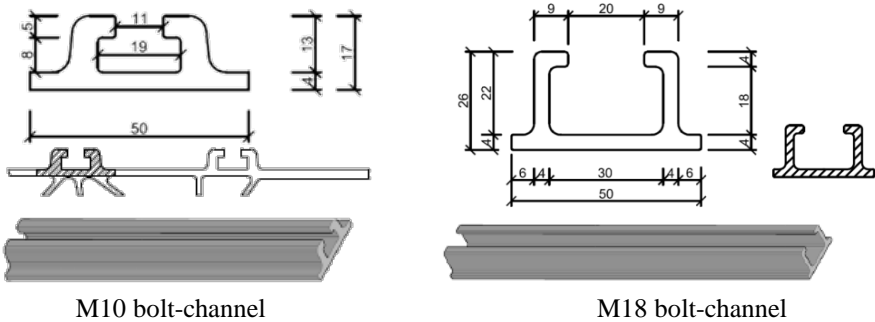


Figure 3.26: Bolt-channel specimens

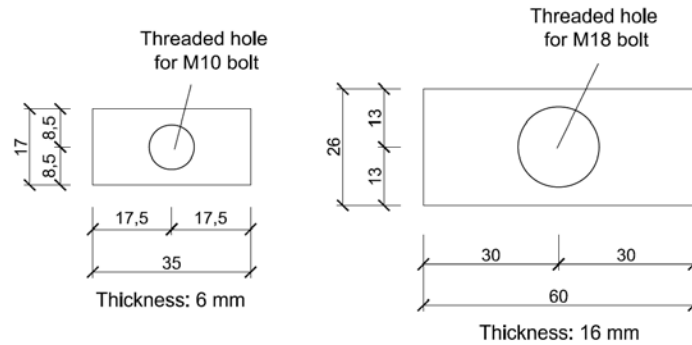


Figure 3.27: Steel plate nuts

In order to take into account the possible load condition that can occur in the different applications of bolt-channel joints, tests have been carried out under three different directions.

The first load direction consists of a force parallel with the track that induces a slipping of bolt and plate nut along the aluminium channel. This case, in the following, is simply named slip tests. Three series of slip tests have been carried out, one for M10 specimens and, in order to evaluate the effects on structural response of bolt preload, two for M18 specimens, corresponding to two different values tightening torques. The second load direction is a transversal force that produces shear actions in the aluminium channel. For this case, named shear, two series (M10 and M18) have been tested. The last considered load direction is a tension force which tends to pull-out the plate from the aluminium channel. Also in this case, in the following named pull-out, two series (M10 and M18) have been tested.

The whole test program for bolt-channel joints is summarised in Table 3.7, where the different parameters under investigation are given for each specimen series. The series label defines the specimen typology. Namely, the first group of characters (BC) means bolt-channel, the second group represents the loading direction (SL: slip, PO: pull-out and SH: shear), the third group of digits identifies the bolt diameter (10, and 18) and the final character identifies the different tightening torque.

Table 3.7: Test program for screwed joints

Series Label	Load direction	Bolt diam. [mm]	Tight. torque [Nm]	Alloy	n. test
BC-SL-10	Slip	M10	40	6005A-T6	6
BC-SL-18A	Slip	M18	93	6005A-T6	4
BC-SL-18B	Slip	M18	60	6005A-T6	4
BC-SH-10	Shear	M10	40	6005A-T6	3
BC-SH-18	Shear	M18	100	6005A-T6	3
BC-PO-10	Pull-out	M10	-	6005A-T6	3
BC-PO-18	Pull-out	M18	-	6005A-T6	3
Total n. of tests:					26

3.4.2 Slip tests

3.4.2.1 Test set-up and instrumentation

The test specimens and set-up for slip tests of bolt-channel have been designed with the aim to have a simple joint in which only the desired action and mechanism can be developed. The specimens consist in aluminium channels with cross-section described in Figure 3.26 with length of 75 mm and 100 mm for M10 and M18 configurations, respectively (Figure 3.28). Inside the channel the plate nut is located at a depth of 5 mm with respect to the top edge.

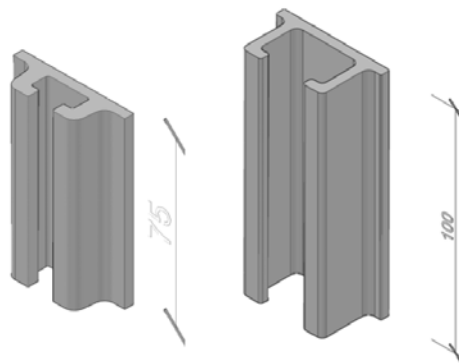


Figure 3.28: Aluminium channels for slip tests

The M10 specimens have been tightened with a torque of 40 Nm, which corresponds to 60% of maximum preloading force, calculated according EN 1999-1-1 (CEN, 2007a). In the case of M18 specimens, the influence of the tightening torque has been investigated by considering two different torque values, 60 and 93 Nm, that correspond to 25% and 15% of preloading force, respectively. These low values of tightening torque are assumed to limit the excessive deformation induced by tightening operation in the small thickness element of aluminium channel.

During the test, the specimen is laid by contact to a T-shaped steel element clamped in bottom wedge grip. The test consists in applying a compression load to the plate nut, by means of a steel flat plate clamped in the top wedge grip of testing machine. The tests set-up is illustrated in Figures 3.29.

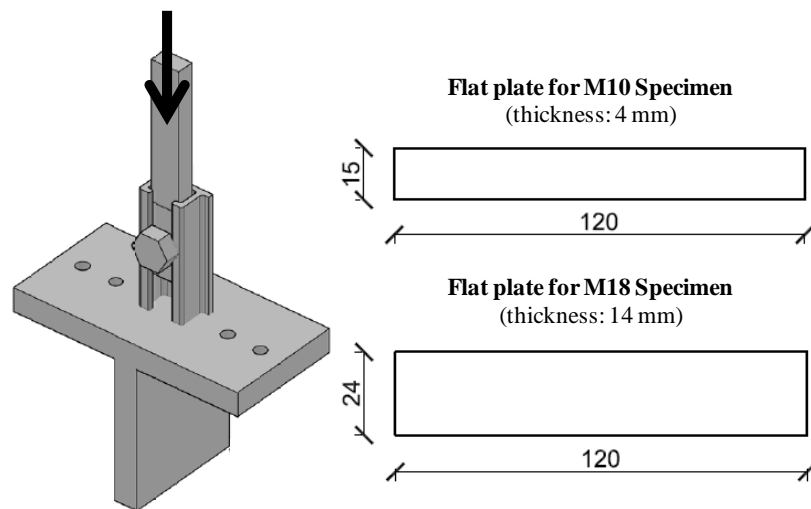


Figure 3.29: Dimension of slip tests set-up

The tests have been performed by means of a universal tests machine MTS 810, which has load capacity of ± 500 kN. The slip displacements have been measured by means of a LVDT with stroke length of 10 mm placed on bolt head (Figure 3.30). The tests are

performed in displacement control with a loading rate of 0.02 mm/s and data has been recorded with a frequency of 10 Hz.



Figure 3.30: Set-up and instrumentation for slip tests

3.4.2.2 Test results

The results of slip joint tests are summarised in Table 3.8. In this table, for each specimen series the parameters that define the structural behaviour, strength and stiffness, are provided. In particular, for strength (F_{max}) the values of the average, the standard deviation and the coefficient of variation are given. The strength has been assumed as the first peak or the plateau of the experimental curve depending on its shape. The joint stiffness (k) has been assumed as the slope of the first significant linear portion on the experimental curve.

Table 3.8: Experimental results of slip test on bolt-channel joints

Series Label	F_{max}			k [kN/mm]
	Average [kN]	Standard dev.[kN]	C.o.V.	
BC-SL-10	4.77	0.94	0.20	31.9
BC-SL-18A	7.02	0.97	0.14	37.3
BC-SL-18B	6.88	1.67	0.24	34.5

In Figure 3.31, the deformed configuration of the M10 and M18 specimens is illustrated. For all tested series, the failure mechanism consists in the slipping of bolt and plate nut inside the aluminium channel up to maximum possible displacement.

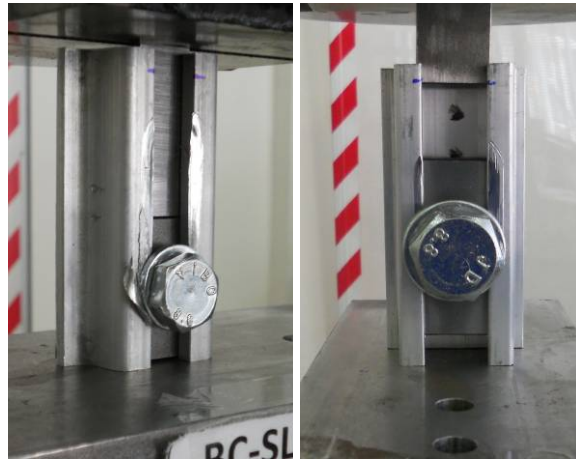


Figure 3.31: Deformed configuration of slip test specimens

Figure 3.32 shows the experimental results in terms of load vs. displacement ($F-d$) curves. These curves are limited at 10 mm displacement that corresponds to maximum capacity of the used LVDT. By comparing the results of BC-SL-10 specimens with BC-SL-18B ones, which are characterized by similar values of preloading force of about 20 kN, it can be observed an increase of strength of about 44% with the variation of bolt diameter from 10 to 18 mm, while the stiffness increase is of 8%. In the examined cases, the influence of the tightening torques, and then of preloading force, is limited. In effects, the variation of 55% of tightening torque implies a very small increase (2%) in terms of average strength, while the stiffness increase is 8%. It has to be noticed that all the results are quite scatter with coefficient of variation ranging from 14% to 24%. This finding can be explained by the joint sensitivity to the assembly imperfections. These imperfections consist of a non perfectly axis alignment between the channel and the plate nuts because of the

tightening, which tends to rotate the plate nuts with a consequently unforeseen contact inside the channel that can influence the response. In addition, the effect of tightening implies a squashing and local thickness reduction of channel parts in contact with the plate nut which implies, in some cases, a marked material removal with a possible influence on strength values Figure 3.33. More detailed information about the single results of slip tests on bolt-channel is provided in Appendix C.

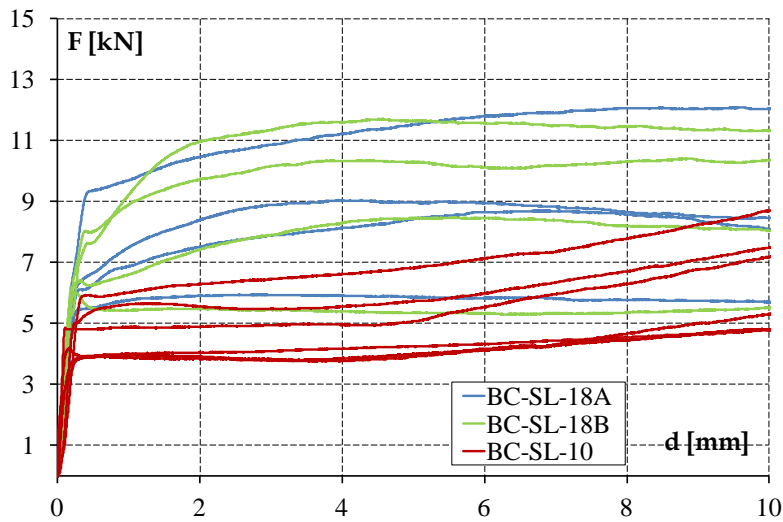


Figure 3.32: Experimental curves of slip tests on bolt-channel joints

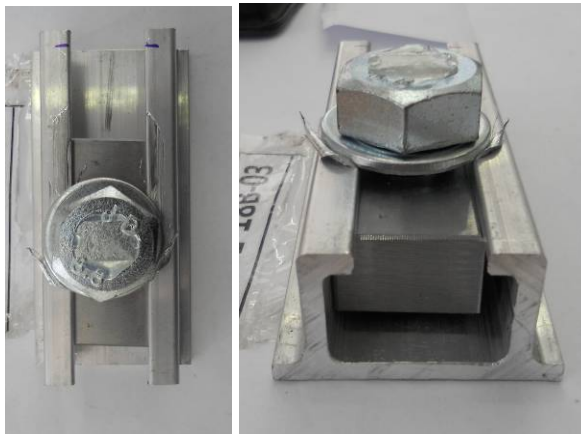


Figure 3.33: Material removal in slip test specimen

3.4.1 Shear tests

3.4.1.1 Test set-up and instrumentation

The test specimens and set-up for shear tests of bolt-channel have been designed with the aim to reproduce the transversal load transfer in such type of joint, to promote the aluminium failure and to avoid unwanted and non significant mechanisms, such as the fastener failure or the bearing of connected steel plate. The specimens consist in aluminium channels with cross-section described in Figure 3.26 with length of 250 mm and 400 mm for M10 and M18 configurations, respectively (Figure 3.34). The plate nut of investigated connection is located in the middle of aluminium channel.

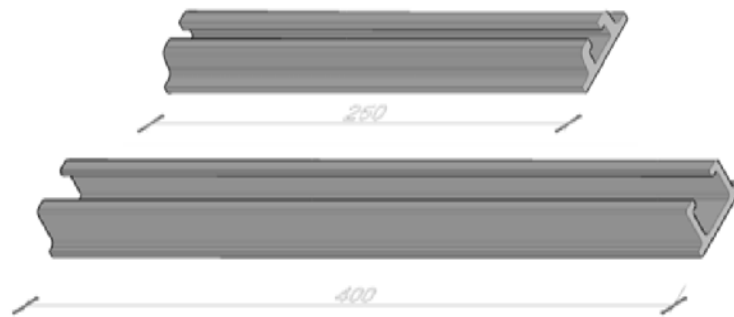


Figure 3.34: Aluminium channels for shear tests

The test set-up consists of U-shaped plate, clamped to the bottom wedge grip of testing machine. The ends of such plate are connected to the channel by means of a plate nut for two bolts with a system similar to the tested one. The edge connection has been designed to be oversized with respect to the tested one. A plate with a hole, clamped the top wedge grip, is used to apply the shear load to the bolt shank of the tested joint. All the set-up plates (Figure 3.35) are made of S355 steel and their thickness has been defined in order to avoid the bearing failure. The bolts of tested and oversized connection are tightened with a torque of 40 and 100 Nm for M10 and M18 specimens, respectively.

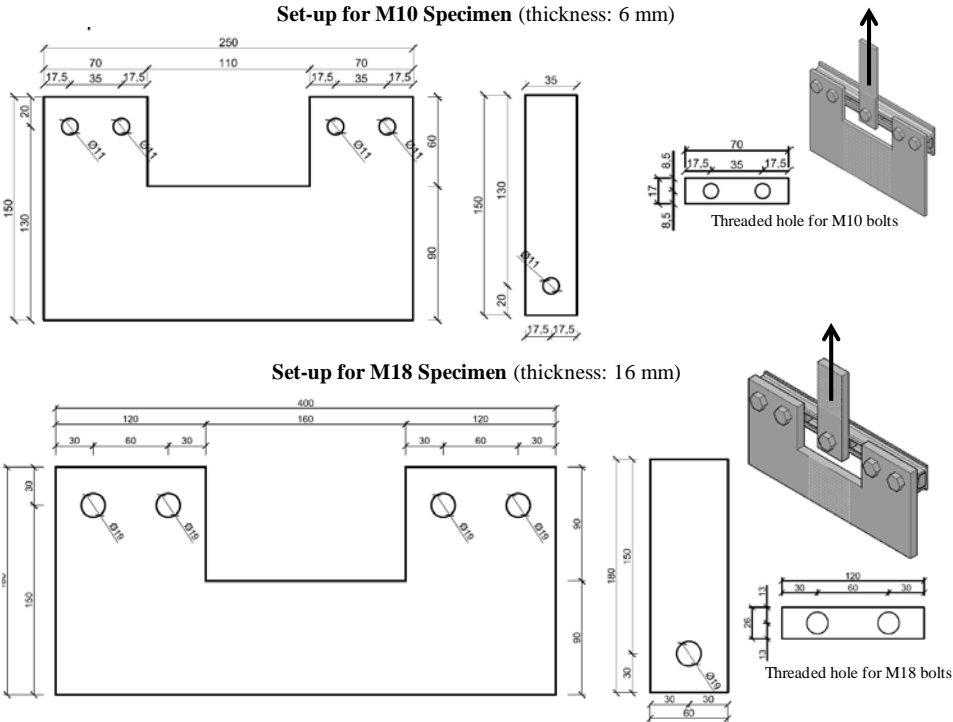


Figure 3.35: Shear tests set-up

The tests have been performed by applying a tension load by means of a universal tests machine MTS 810. The displacements of tested connection have been measured by means of a LVDT with stroke length of 10 mm placed on bolt head (Figure 3.36). Two additional LVDTs are disposed at the channel edges to measure the displacement of oversized connections (Figure 3.37). The tests are performed in displacement control with a loading rate of 0.02 mm/s and data has been recorded with a frequency of 10 Hz.



Figure 3.36: Set-up and instrumentation for shear tests



Figure 3.37: LDVTs for oversized connections measurement

3.4.1.2 Test results

Table 3.9 summarises the results of shear tests on bolt-channel joints. In this table, for each specimen series the parameters that define the structural behaviour together with the observed failure mechanism are provided. In particular, (F_{max}) the values of the average, the standard deviation and the coefficient of variation of strength and the average value of stiffness (k) are given. The strength has been assumed as peak load of the experiment curve, while the

stiffness has been evaluated as the slope of the first significant linear portion on the experimental curve.

Table 3.9: Experimental results of shear test on bolt-channel joints

Series Label	F_{max}			k [kN/mm]	Failure mode
	Average [kN]	Standard dev.[kN]	C.o.V.		
BC-SH-10	20.8	0.60	0.03	20.4	BF
BC-SH-18	49.3	1.83	0.04	8.32	W

BF: Failure occurred in channel bottom flange
W: Failure occurred in channel web

The final deformed configuration and the failure mechanism of BC-SH-10 series is shown in Figure 3.38. A crack development in the bottom flange close to the corner with web of aluminium channel was observed. The specimens present also an evident deformation of top flange and web on the loaded side, while the bolts and the plate nut do not appear deformed.

In the case of BC-SH-18 series a crack developed from the top flange on the loaded side to all the web depth and along the intersection between this one and the bottom flange, as shown in Figure 3.39. Also in this case no deformation in bolt and plate nut occurred.

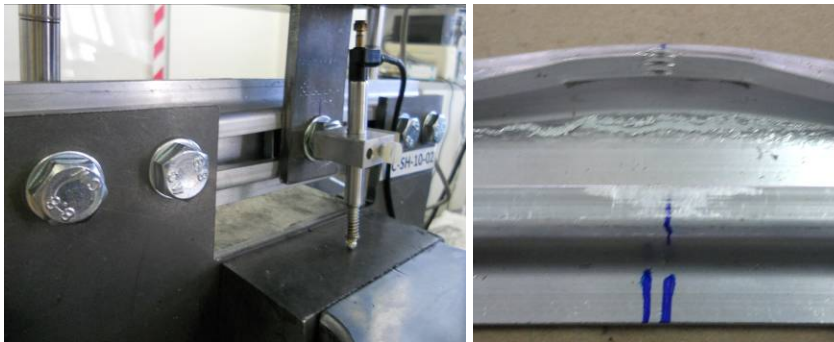


Figure 3.38: Failure mechanism in BC-SH-10 series



Figure 3.39: Failure mechanism in BC-SH-18 series

Figure 3.40 shows the experimental results in terms of load vs. displacement ($F-d$) curves. It can be observed that the two investigated configurations showed a great variation in terms of deformation capacity. In particular, in the case of BC-SH-10 the failure occurs for displacement of about 5 mm while for BC-SH-18 displacement greater than 20 mm has been reached. In terms of strength, an increase of 137% from BC-SH-10 to BC-SH-18 has been observed. On the contrary, BC-SH-10 specimens resulted 2.5 times stiffer than BC-SH-18 ones. In addition, the strength values for both series are very low scattered with coefficient of variation lower than 4%.

The low scattered values demonstrate that, for the investigated cases, the shear strength of bolt-channel joint is not influenced by assembly issues and imperfections. The low sensitivity to imperfections is also confirmed by the symmetrical global response up to the failure for both investigated systems (Figure 3.41).

More detailed information about the single results of bolt-channel joints shear tests is provided in Appendix C.

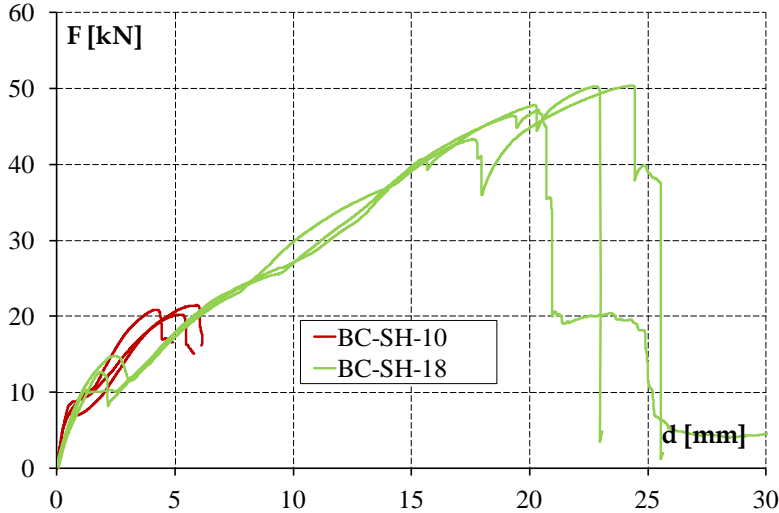


Figure 3.40: Experimental curves of shear tests on bolt-channel joints



Figure 3.41: Deformed configuration of BC-SH-10



Figure 3.42: Deformed configuration of BC-SH-18

3.4.2 Pull-out tests

3.4.2.1 Test set-up and instrumentation

The test specimens and set-up for pull-out tests of bolt-channel have been designed with the aim to reproduce the behaviour of such type of joint under tension load perpendicular to the aluminium channel. The specimens consist in aluminium channels with cross-section described in Figure 3.26 with length of 200 mm for both M10 and M18 configuration (Figure 3.43).

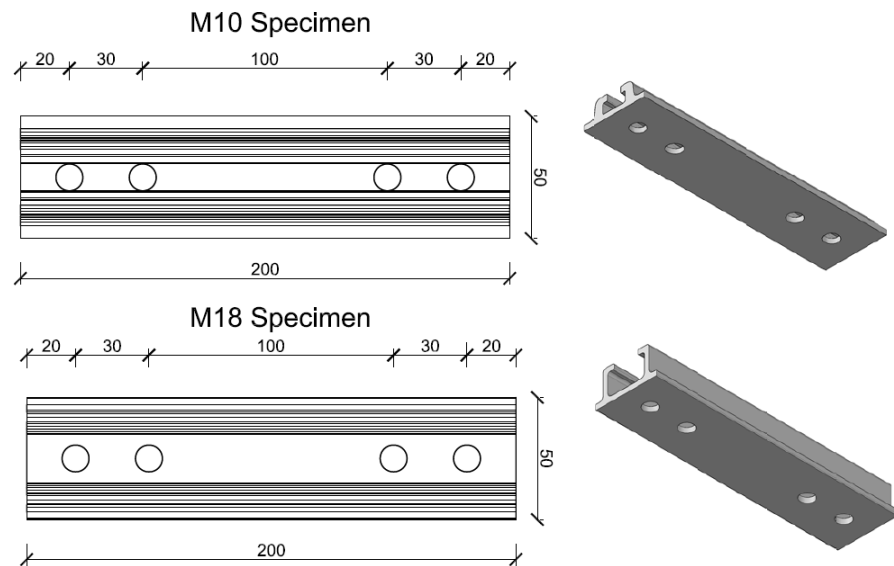


Figure 3.43: Aluminium channels for pull-out tests

The test set-up consists of T-shaped element, made of S355 steel, which is clamped to the bottom wedge grip of testing machine (Figure 3.44). The specimen is fixed to this steel element by means of 4 M10 bolts of 12.9 grade, placed inside the channel as shown in Figure 3.45. The tested connection is located in middle of aluminium channel and it consists in a plate nut tightened with a 180 mm long threaded bar. The bar is pulled by means of a holder element clamped in top wedge grip of testing machine. The holder element is the same used

for screwed joints, described in Section 3.3.2, but, in this case, the threaded bar is installed in a 20 mm thick internal plate.

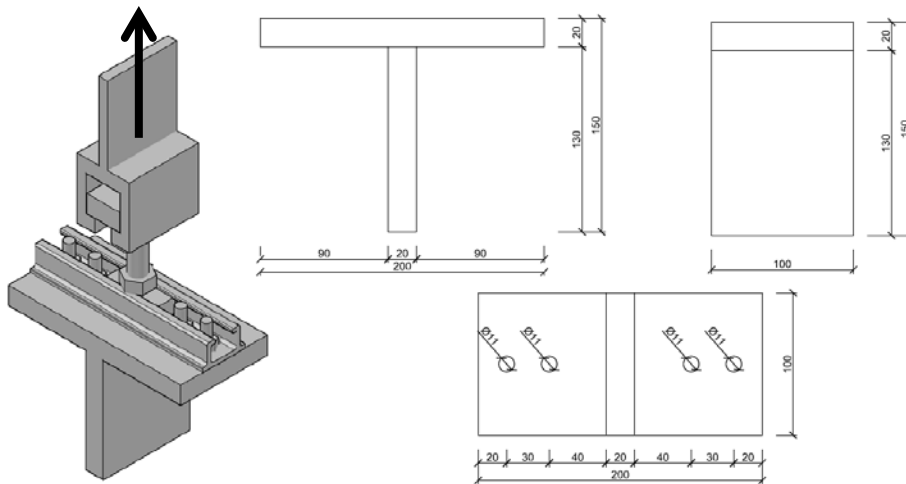


Figure 3.44: Pull-out tests set-up



Figure 3.45: Specimen to set-up connection

The tests have been performed by applying a tension load by means of a universal tests machine MTS 810. The displacements have been measured through a LVDT with stroke length of 20 mm placed between the holder and the T-shaped element (Figure 3.46). The tests are performed in displacement control with a loading rate of 0.02 mm/s and data has been recorded with a frequency of 10 Hz.



Figure 3.46: Set-up and instrumentation for pull-out tests

3.4.2.2 Test results

Table 3.10 summarises the results of pull-out tests on bolt-channel joints. In this table, for each specimen series the parameters that define the structural behaviour together with the observed failure mechanism are provided. In particular, (F_{max}) the values of the average, the standard deviation and the coefficient of variation of strength and the average value of stiffness (k) are given. The strength has been assumed as peak load of the experiment curve while the stiffness has been evaluated as the slope of the first significant linear portion on the experimental curve.

Table 3.10: Experimental results of pull-out tests on bolt-channel joints

Series Label	F_{max}			k [kN/mm]	Failure mode
	Average [kN]	Standard dev.[kN]	C.o.V.		
BC-PO-10	33.3	0.33	0.01	21.1	PO
BC-PO-18	42.8	2.93	0.07	25.5	TF

PO: Pull-out of threaded bar

TF: Failure occurred in channel top flange

The final deformed configuration and the failure mechanism of BC-PO-10 series are shown in Figure 3.47. For all the specimens the observed failure corresponded to the pull-out of threaded bar from the plate nut with shearing of both plate nut and bar threads. In correspondence to the failure, the plate nuts resulted strongly deformed and a crack developed along one of the top flanges.



Figure 3.47: Failure mechanism in BC-PO-10 series

The observed failure mechanism of BC-PO-18 series is due to aluminium channel, as shown in Figure 3.48. A crack occurred at the one of top flanges which tended to propagate along the web. In this case threaded bar and plate did not present any type of deformation.

It has to be noticed that the response of both specimen series was strongly non symmetrical and probably influenced by assembly issues. In effects, during the tightening the plate nut tends to rotate in the channel or, due to the clearance, it can be not perfectly centred in the channel. This could explain the development of cracks on only one side of the channel.

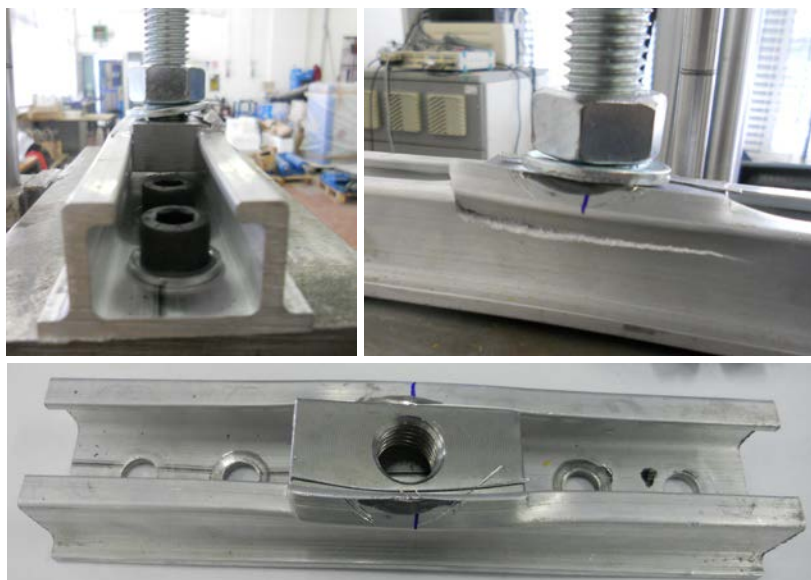


Figure 3.48: Failure mechanism in BC-PO-18 series

Figure 3.49 shows the experimental results in terms of load vs. displacement ($F-d$) curves. It can be observed that BC-PO-18 series showed a slightly higher deformation capacity with respect to BC-PO-18. The response BC-PO-18 was, in average, 29% and 21% greater than BC-PO-10 in terms of strength and stiffness, respectively. Despite the fact that the joint response is, for both series, markedly non symmetrical, the strength values for both series are quite low scattered with coefficient of variation lower than 7%. As a consequence, it would seem that the influence of assembly imperfections is evident in failure and deformed shape of the joint but does not affect the strength scattering.

More detailed information about the single results of bolt-channel joints pull-out tests is provided in Appendix C.

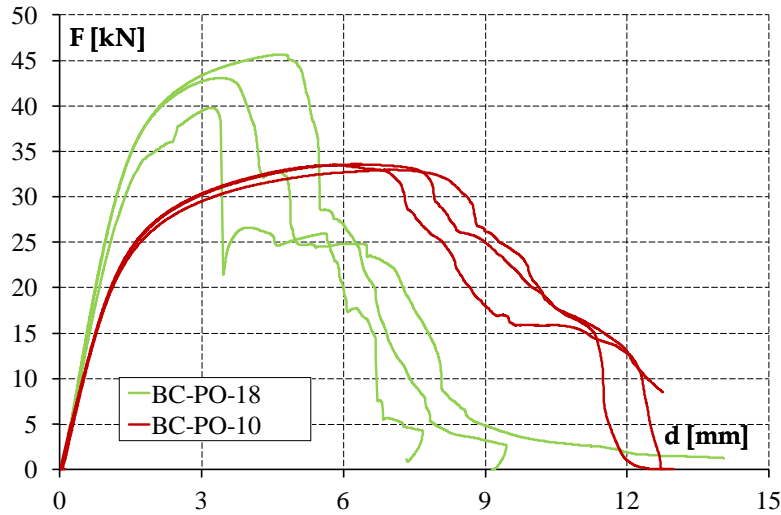


Figure 3.49: Experimental curves of pull-out tests on bolt-channel joints

3.4.3 Experimental vs. predicted strength

In this Section, values of strength of bolt-channel obtained by experimental tests are compared to those estimated through the available prediction formulations, illustrated in Section 2.5. The formulations are applied by considering the experimental values of aluminium alloys given in Section 3.2 and by assuming the safety factors equal to 1.

In case of the evaluation under slipping load, the formulation provided by CNR-DT 208 has been applied by calculating the bolt preloading force as follows:

$$F_{p,Cd} = 0.2M_v d \quad (3.1)$$

where M_v is the applied tightening torque and d is the bolt diameter.

The values obtained by the formulation proposed by Hellgren and Sapa (2.12) and the one of CNR-DT 208 (2.13) are compared with experimental results in Table 3.11.

Table 3.11: Comparison between predicted and experimental slip strength for bolt-channel joints

Series	Exp.[kN]	Hellgren/Sapa (2.12)		CNR-DT 208 (2.13)	
		Pred. [kN]	Pred./Exp.	Pred. [kN]	Pred./Exp.
BC-SL-10	4.77	8.00	1.68	6.00	1.26
BC-SL-18A	7.02	12.0	1.74	5.00	0.73
BC-SL-18A	6.88	18.6	2.65	7.75	1.10

It has to be noticed that the formulation (2.12), in the examined cases, strongly overestimates the strength with errors ranging from 68% to 165%. On the other hand, CNR-DT 208 provides a better estimation of strength with error ranging from 10% to 27%.

As far as shear strength is concerned, the results obtained by applying the formulation provided by Hellgren (2.14), CNR-DT 208 (2.15) and the indication of Sapa are summarized in Table 3.12.

Table 3.12: Comparison between predicted and experimental shear strength for bolt-channel joints

Series	Exp. [kN]	Hellgren (2.14)		CNR-DT 208 (2.15)		Sapa	
		Pred. [kN]	Pred./ Exp.	Pred. [kN]	Pred./ Exp.	Pred. [kN]	Pred./ Exp.
BC-SH-10	20.8	46.0	2.21	69.0	3.32	19.5	0.94
BC-SH-18	49.3	78.9	1.60	78.9	1.60	35.2	0.71

The results show that both Hellgren and CNR-DT 208 formulations give higher values than experimental ones with errors in the range from 60% to 232%. Sapa suggestion to evaluate the strength as 70% of the one evaluated for a common bolted joint is, for the examined case, quite conservative with errors ranging from 6% to 29%.

Table 3.13 shows the prediction of bolt-channel pull-out strength according to the formulation suggested by Hellgren (2.16) and Sapa (2.17).

Table 3.13: Comparison between predicted and experimental pull-out strength for bolt-channel joints

Series	Exp.[kN]	Hellgren (2.16)		Sapa (2.17)	
		Pred. [kN]	Pred./Exp.	Pred. [kN]	Pred./Exp.
BC-PO-10	33.3	66.0	1.98	18.4	0.55
BC-PO-18	42.8	85.1	1.99	26.8	0.63

The comparison of predicted values with experimental ones shows that the strength obtained with Hellgren formulation is about 2 times the experimental values. On the other hand, Sapa formulation strongly underestimates the strength with errors of up to 45%.

As general remark, the available formulations are calibrated on the basis of experimental tests carried out on specimens where the bolt head is located into the channel. This configuration is different from the one investigated in this work and this could explain the great difference between predicted and experimental values. In addition, the formulations that well approximate the experimental results are the one for slip strength given in CNR-DT 208 and the indication about shear strength suggested by Sapa. Both formulations are not calibrated on tests results but they are derived from design rules of traditional bolted joints.

Chapter 4

NUMERICAL MODEL CALIBRATION OF SPECIAL JOINTS

4.1 GENERALITIES ON FINITE ELEMENT ANALYSIS

The complexity of the behaviour of physical phenomena in the creation cannot be simply and directly grasped or understood by human mind. Hence the idea of subdividing a complex whole system into its individual components or elements, which can be readily understood and rebuilt in the original system to individuate the overall behaviour. This is the typical way undertaken by engineers and scientists to study very complex phenomena (Zienkiewicz and Taylor, 2000).

In many cases, an adequate model can be obtained by subdividing the problem in a finite number of elements. These problems, named discrete, are suitable to be readily solved by computers also in case of very large number of elements. On the other hand, there are some cases in which the mentioned subdivision is continued indefinitely and the problem can be defined in terms of infinitesimal concepts and can be solved by differential equation. In this case, named continuous problem, since the finite capacities of computers, the solution can be obtained only by mathematical manipulation, which represents a feasible way only for oversimplified problems. In order to overcome these difficulties, several methods of discretization have been proposed. All methods involve an approximation of the real

continuum problem which tends to be better as the number of considered elements increases (Zienkiewicz and Taylor, 2000).

The possibilities to approach the problem are different and they depend basically on the object selected for discretization. From mathematical point of view, it is possible to operate directly on differential equation governing the problem, such as in case of finite difference methods, weighted residual procedure or other approximate techniques. On the other hand, the engineering approach is more intuitive and consists in subdividing in finite portions the physical domain. Finally, it is possible to define the Finite Element Methods as “a method of approximation to continuous problems such that the continuum is divided into a finite number of parts (elements), the behaviour of which is specified by a finite number of parameters, and the solution of the complete system and an assembly of its elements follows precisely the same rules as those applicable to standard discrete problems” (Zienkiewicz and Taylor, 2000). The standard discrete problems can be defined as a problem in which it is possible to define a set of parameters which describe the behaviour of each element of system and through them it is possible to define equations able to compute the unknown system parameters and to define the whole system behaviour.

Numerical analysis performed with finite Element Methods can be able to characterize the mechanical behaviour of complex systems and can be useful where the classical linear theory of the elasticity is not able to give an accurate interpretation of the problem. This is the case of structures having complex and wide geometry or whose mechanical behaviour is influenced by several sources of non-linearity, such as material plasticity, large displacements, contact interactions and imperfections. The results of numerical analysis allow to investigate some parameters or issues that cannot be measured or caught by means of experimental procedure. So additional or complementary information can be obtained by numerical analysis of experimental studied systems. Numerical models are very useful to investigate the mechanical behaviour of structures whose condition is not reproducible by experimental tests or because it would be too

expensive, such as extreme loading or very large structures. In addition, reliable models calibrated on the basis of experimental results can be employed to perform parametrical analysis, in which some parameters can be varied by defining the mechanical behaviour without the with no need for further expensive experimental tests.

On the basis of the latter consideration and, in order to provide a tool of general validity, numerical models of special joint systems have been calibrated on the results of experimental tests provided in Chapter 3. The models presented in this study are entirely developed by means of ABAQUS 6.10 (Simulia, 2010), that is a general-purpose finite element computer program. This program has been selected on the basis of its versatility and capability of facing up complex problems with different source of non-linearity. In particular, the models have been developed in ABAQUS/CAE an interactive environment used to create finite element models, submit and monitor analyses and evaluate results.

As far as numerical modelling of special joints is concerned, no literature is available with exception of a preliminary modelling carried out for this study and described in Macillo et al. (2011), in which a numerical model reproducing the experimental tests performed on bolt-channel joint by Hellgren (1996) has been calibrated.

In the present Chapter, the calibration of numerical models of screw-tube and bolt-channel joints is illustrated. In particular, screw-tube joints have been axisymmetrically modelled, in addition, the description of the models, the mesh sensitivity analysis and the comparison of numerical results with experimental ones are presented in Section 4.2. Similar information for bolt-channel joints under shear and pull-out loadings is provided in Section 4.3.

4.2 SCREWED JOINT MODELS

4.2.1 Axisymmetric model

In the present study a model for screw-tube joints have been calibrated on the basis of experimental results. This model aims to reproduce the joint behaviour experimentally obtained, so providing a useful and general tool able to investigate the structural response of geometries different from tested ones.

The screw-tube joints are rather complex to be modelled due to their geometry, particularly to the helical continuous configuration of screw thread and just that part is the most involved in loading transfer and interaction contact phenomena. As it was shown in Chapter 3, the overall behaviour and the failure mode are strongly dependent on the interface between screw threads and aluminium slot. This feature implies, in modelling phase, a specific care in the definition of interaction properties, type of elements, integration methods and, particularly, the mesh size. In effect, the mesh size covers a fundamental role in the good calibration and performance of model and, as in this case, where the interaction is focused on the contact in correspondence to the screw threads, a very refined mesh is needed. As a consequence, a three-dimensional model would be defined by a very large number of nodes and elements requiring a huge computational effort and with great difficulties in managing.

Therefore, a three dimensional modelling would seem complicated to be performed and some compromises have to be taken into account to overcome and reduce these difficulties. For this reason, screw-tube joints have been modelled by considering the axisymmetry of the problem. The advantages of this assumption consist in dealing with a three-dimensional system as a plane problem. Thanks to symmetry, only two components of displacements in any plane section of the system along its symmetry axis define entirely the state of strain and stress. This implies an important reduction of nodes and elements in the model, as well as saving computation effort.

The tested screw-groove specimen is actually axisymmetric in terms of loads, boundary condition and overall geometry. In particular, the only source of non symmetry lies in the helical configuration of screw thread and in the corresponding internal aluminium thread, metric or formed by screw. Therefore, the assumption of axisymmetry represents a simplification of model geometry, in particular, the effects of lead angle and the helix of thread profile were neglected but, at same time, this simplification allows to obtain a very refined mesh on thread contacts without huge increasing of computation efforts. This approach is usually used to study the behaviour of threaded connection under tension loads.

Several studies have been conducted in order to define the influence of helical thread configuration on the behaviour of threaded connection with reference to the approximation of axisymmetric assumptions. Chen and Shih (1999) investigated the helical effects in threaded connections on the load distribution of each thread by comparing results of three-dimensional, axisymmetric numerical model and analytical methods on UNC and UNF threaded bolts axially loaded. The numerical results provided that the load ratio obtained by three-dimensional and axisymmetric model is quite similar, then the helical effect does not influence and the model simplification can give a good estimation of load distribution. A comparison of three-dimensional model with two-dimensional axisymmetric one of a bolt subjected to axial load has been conducted by Johnson et al. (2000). In this case, both models approaches exhibited quite similar results in terms of equivalent stress and contact pressure distribution. Hobbs et al. (2003) carried out a study on the nut thread run-out effect on the stress distribution in bolt by using finite element methods. The study focused on a metric bolt under uniform axial load modelled by means of three-dimensional and axisymmetric models and by considering the bolt material as linear. The obtained results of axisymmetric model were in good agreement with those of an earlier photoelastic study with a slightly higher stress prediction. In order to obtain a more accurate prediction of stress distribution, the Authors suggest to create a number of models representing different

positions around the helix. In the two Fukuoka's studies, one about an accurate geometry model proposal for helical thread (Fukuoka and Nomura, 2008) and another on finite element analysis on fatigue behaviour of helical thread (Fukuoka, 2011), different finite element model, both three dimensional and axisymmetric, have been performed. The comparison of the analyses results confirmed that using axisymmetric models, stress concentrations at the thread root can be analyzed within acceptable accuracy. In addition, axisymmetric model has been used in Williams et al. (2008) to study the behaviour of a simple single-bolted-joint under tensile separating loads, which provided a reasonable agreement between finite element results and experimental analysis. Another application of axisymmetric model is given in Chen et al. (2010) which used a finite element model to validate a new analytical method for evaluating the load distribution on cylindrical pipe thread connection.

Based on the above consideration, an axisymmetric model for the screw-tube joints has been developed, its description and results are hereafter discussed.

4.2.2 Model description

As discussed in the previous Section, the model for screw-tube joints has been developed by taking into account the axisymmetric condition. The FEM model consists in two parts: the screw and the aluminium slot. The two parts have been introduced in the ABAQUS software as plane sketches corresponding to the sections of the parts along their axisymmetric axis. In addition, only one half of the aluminium slot has been considered, in agreement with the symmetry of specimen respect the x-axis, as shown in Figure 4.1. In order to take into account the actual geometry of aluminium slots, the average measured values of internal and external diameter of each slot series are considered, because of the little differences between the nominal and actual values (see Appendix B). In particular, the assumed values for each series are illustrated in Table 4.1. As far as the screw geometry is concerned, the assumed threaded profiles are the nominal

ones provided by ISO 1478 (ISO, 1999) and UNI 5542 (UNI, 1965) for self-tapping screws (ST-5.5 and ST-6.3 series) and metric bolts (ST-M6 series), respectively. Also in case of aluminium slot for ST-M6 series the internal threaded geometry is assumed according to ISO 1478. A detail of threaded profile for self-tapping screws and metric bolts is shown in Figure 4.2.

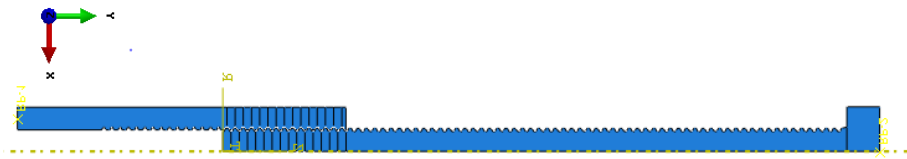


Figure 4.1: Geometry of FEM model

Table 4.1: Assumed dimension for aluminium slots

Series	d_{int} [mm]	d_{ext} [mm]
ST-5.5	10.0	4.80
ST-6.3	10.7	5.55
ST-M6	10.9	5.30

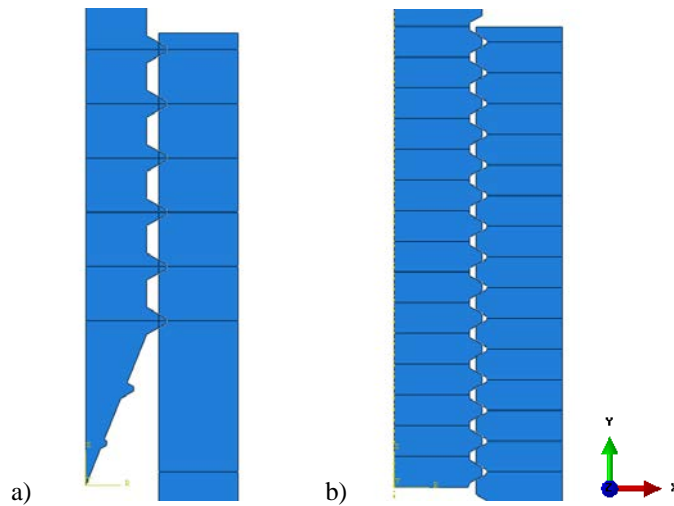


Figure 4.2: Threaded profile for self-tapping screw (a) and metric bolt (b)

In order to interpret the correct behaviour of the model also for large deformations, ABAQUS requires that the material is defined in terms of “true stress” (σ_{true}) and “true strain” (ε_{true}). These values can be obtained from the engineering ones (σ_{eng} , ε_{eng}) through the following transformation formulae:

$$\sigma_{true} = \sigma_{eng} (1 + \varepsilon_{eng}) \quad \varepsilon_{true} = \ln(1 + \varepsilon_{eng}) \quad (4.1)$$

In addition, ABAQUS requires the material plasticity defined in terms of true plastic strain (ε_{pl}), which can be obtained by subtracting from the total true strain the elastic part as follows:

$$\varepsilon_{pl} = \varepsilon_{true} - \sigma_{true} / E \quad (4.2)$$

In particular, the aluminium material (AW 6082-T6) has been modelled by Ramberg-Osgood law drawn on the basis of experimental results provided in Section 3.2.1. In order to correctly catch the behaviour material for large deformation, the 0.2% proof strength ($f_0=276$ MPa) and ultimate strength ($f_u=309$ MPa) have been considered as reference points. The other material constants are: $E=66300$ MPa (Young’s modulus) and $\nu=0.30$ (Poisson’s ratio). Finally, the obtained Ramberg-Osgood curve is transformed in terms of “true stress” and “true strain” values through Equation (4.1). The experimental (eng.), the obtained Ramberg-Osgood (eng.) and the implemented “true stress-strain” curve are superimposed in Figure 4.3.

Three different types of material laws have been considered for self-tapping screw material, 8.8 and 12.9 bolt grades, respectively. The material properties of self-tapping screws have been defined through the experimental tests depicted in Section 3.2.2 while, for 8.8 and 12.9 bolt grades, nominal values provided by ISO 898-1 (ISO, 2009) have been considered. For each material a bilinear law is assumed, where the material elastic constants are: $E=200000$ MPa and $\nu=0.30$. The material plasticity for the different assumed materials is defined by the true stress and true strain values. Such values for each material type together with the models series in which they are employed are summarized in Table 4.2.

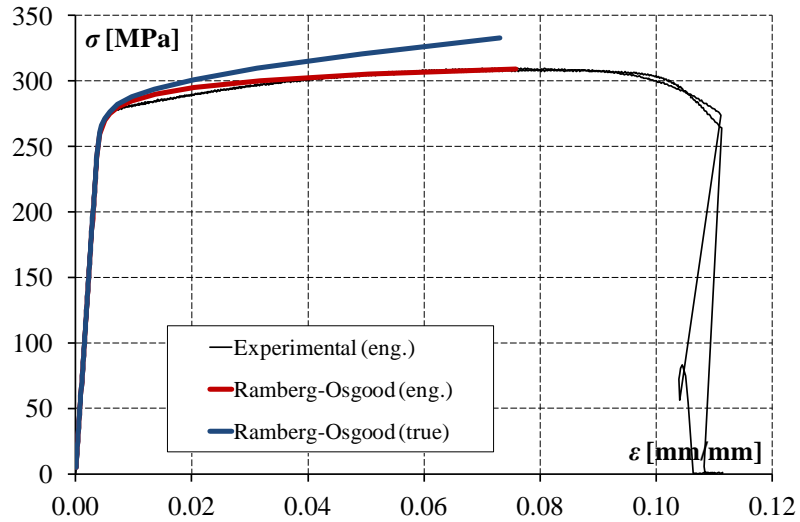


Figure 4.3: Engineering vs. true stress-strain curve for AW 6082-T6

Table 4.2: Assumed screws material properties

Screw Material	true yield stress [MPa]	true ultimate stress [MPa]	true ultimate plastic strain	Model series
Self-tapping	1031	1107	0.007	ST-5.5-XX, ST-6.3-XX
8.8 Grade	642	896	0.11	ST-M6-XX
12.9 Grade	1106	1318	0.07	ST-M6H-XX

Contact interaction has been defined between the external thread of screw and internal thread of aluminium slot, corresponding to the highlighted lines in Figure 4.4. The interaction has been defined as a tangential “penalty” contact characterized by a friction coefficient of 0.3.

The assumed boundary conditions are symmetry about y-axis ($U_x=U_{Rz}=0$), corresponding to the axisymmetric condition, and symmetry about x-axis ($U_y=U_{Rz}=0$), in correspondence of aluminium slot middle section. The pulling load consists in a uniform displacement along y-axis applied up to collapse to a reference point rigidly coupled to the top of the screw head. Figure 4.5 shows the assumed loads and boundary conditions.

The analyses consist in only one general static step carried out by means of ABAQUS standard implicit solver, which uses the Newton-Raphson method, an incremental iterative technique to solve non-linear problems (Simulia, 2010).

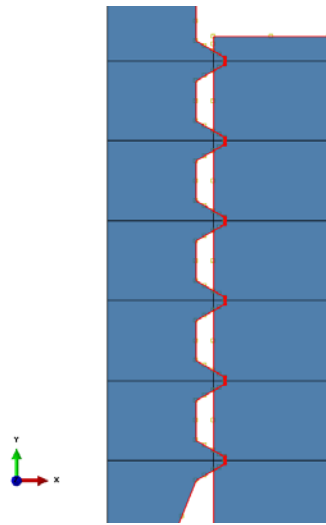


Figure 4.4: Interaction contact definition

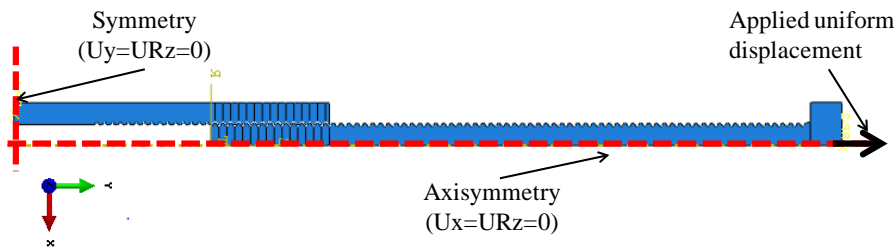


Figure 4.5: Model load and boundary conditions

4.2.3 Mesh sensitivity analysis

In order to investigate the influence of mesh size, a sensitivity analysis has been carried out on the model reproducing the ST-M6H-15 specimen. The model has been meshed with a 6-node modified quadratic axisymmetric triangle (CAX6M). A second-order

(quadratic) element has been chosen because it allows to achieve more accurate results in case of complex contact problems.

The parts have been meshed in order to have a more refined mesh and a perfect node alignment in correspondence of interaction surface between the external screw threads and the internal aluminium threads. The mesh size has been increased along the screw and slot diameter with the aim to limit the number of element in the zone that is not affected by contact interaction and strong stress concentrations. Therefore, the mesh size can be defined by two values, the minimum one in the contact zone and the maximum one in the peripheral model zones.

The sensitivity analysis has been conducted considering three different mesh configurations: coarse, intermediate and fine (Figure 4.6). Table 4.3 summarises the assumed mesh size, the obtained number of node and elements together with the CPU time consuming, normalised to intermediate configuration, for each considered mesh configuration.

By comparing the analysis results in terms of force vs. displacement curve (Figure 4.7), it can be observed that the investigated mesh sizes do not influence significantly the global model response. Therefore, the adopted mesh for all implemented screw-tube models is the intermediate one, which allows to contain computational analysis time obtaining the same results accuracy of the fine model.

Table 4.3: Mesh parameters

Mesh config.	Minimum mesh size [mm]	Maximum mesh size [mm]	No. of Elements	No. of Nodes	Normalized CPU Time
Coarse	0.08	0.80	11605	35232	0.42 (12 min)
Intermediate	0.04	0.40	24726	74734	1.00 (28 min)
Fine	0.02	0.02	95904	288794	12.65 (349 min)

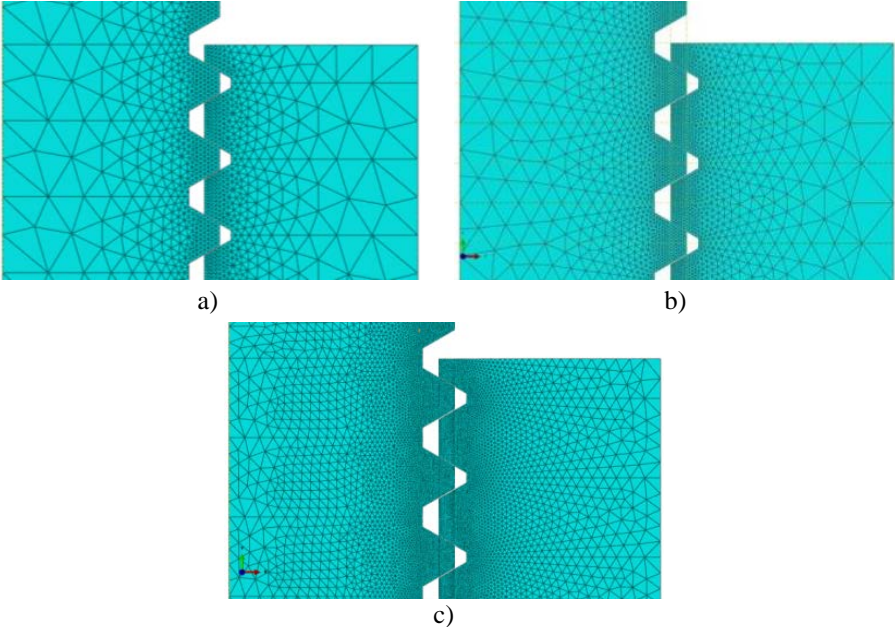


Figure 4.6: Assumed mesh size (a) coarse , (b) intermediate, (c) fine

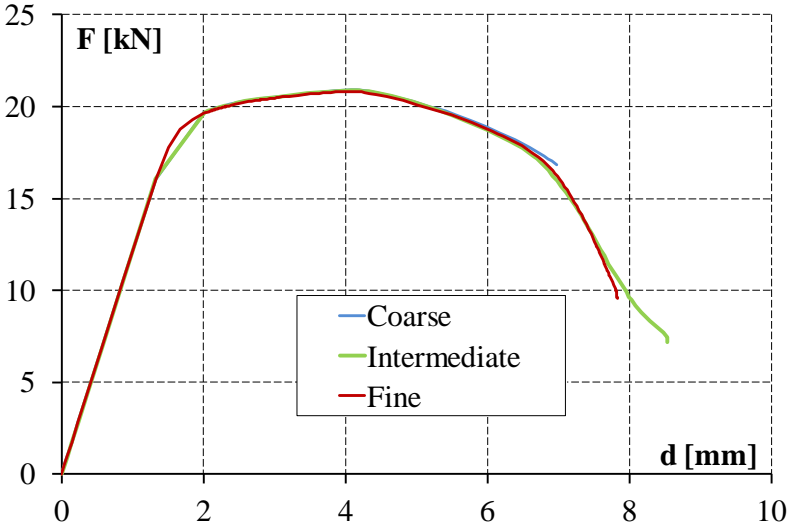


Figure 4.7: Mesh sensitivity analysis results

4.2.4 Numerical vs. experimental results

The comparison between numerical and experimental results of screw-tube joints is described hereafter. Seven screw-tube configurations have been implemented through the model above proposed. The modelled configuration corresponds to the tested ST-5.5-10, ST-5.5-15, ST-6.3-10, ST-6.3-15, ST-M6-10, ST-M6-15 and ST-M6H-15 series, described in Section 3.3.

For each modelled series, the results in terms of load vs. displacement ($F-d$) curves and the comparison between experimental and numerical failure mechanism are illustrated in Figures 4.8 to 4.21. Table 4.4 summarises the comparison between numerical and experimental results in terms of joint strength (F_{max}) and stiffness (k).

The numerical results are substantially in good agreement with the experimental ones. The different failure mechanisms experimentally observed are readily caught by the model. The only exception is represented by ST-M6-10 model, in which the numerical model shows the screw failure instead of the pull-out one exhibited in the experimental tests.

With exception of this case, the proposed model always shows results in good agreement with experimental ones in terms of strength with an error ranging from 1% to 8%. In particular it can be observed that, in case of pull-out failure, the model tends to underestimate the strength. On the other hand, the numerical strength corresponding to axial failure (self-tapping screw or aluminium) results slightly higher than the experimental one.

Also in terms of stiffness, the model shows results in good agreement with the experimental ones. In this case, the error ranges from 1% to 10%. It has to be noticed that the maximum error for stiffness occurs in ST-M6-15, which has the same bolt properties (material and geometry) as ST-M6-10. So this problem in catching response of ST-M6 joint could be ascribed to discrepancy between assumed (nominal) and actual values of material properties and thread geometry.

Finally, it can be observed that, despite the axisymmetric simplification, in most cases, the proposed model is able to predict with acceptable approximation the structural response of the joint.

Table 4.4: Comparison between numerical and experimental results

Series		F_{max} [kN]	k [kN/mm]	Failure mechanism
ST-5.5-10	Numerical	12.74	8.96	P
	Experimental	12.76	9.06	P
	Error	-1%	-1%	
ST-5.5-15	Numerical	15.03	9.42	S
	Experimental	14.24	9.29	S
	Error	+6%	+1%	
ST-6.3-10	Numerical	8.99	10.22	P
	Experimental	9.62	10.32	P
	Error	-7%	-1%	
ST-6.3-15	Numerical	20.12	10.89	A
	Experimental	18.90	11.46	A
	Error	+6%	-5%	
ST-M6-10*	Numerical	16.60	10.62	S
	Experimental	14.61	8.59	P
	Error	+14%	+24%	
ST-M6-15	Numerical	16.61	10.98	S
	Experimental	17.40	10.0	S
	Error	-5%	+10%	
ST-M6H-15	Numerical	20.90	12.15	A
	Experimental	18.38	12.71	A
	Error	+8%	+4%	

P: screw pull-out; S: screw failure; A: aluminium failure

* failure mechanism not caught

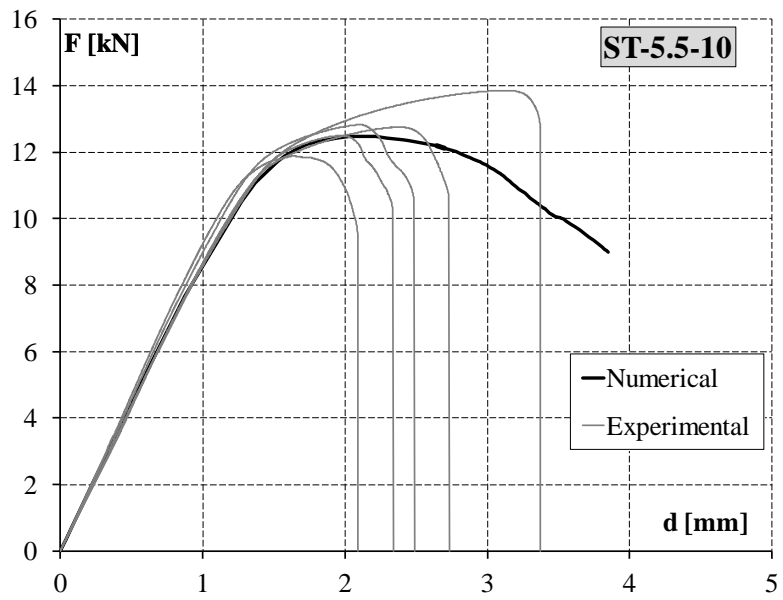


Figure 4.8: Numerical vs. Experimental results for ST-55-10

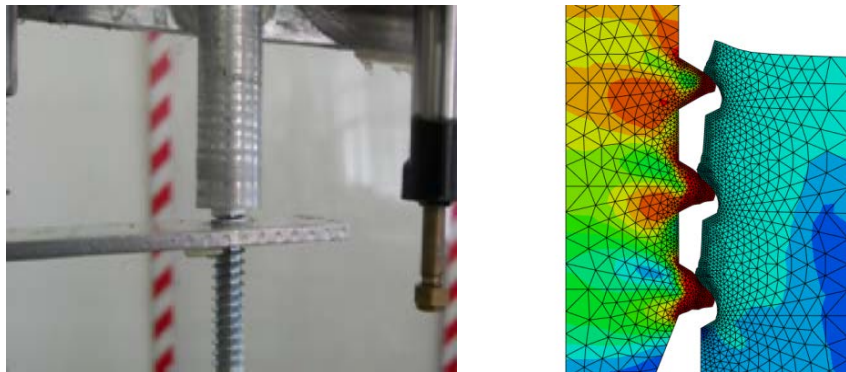


Figure 4.9: Failure mechanism for ST-55-10

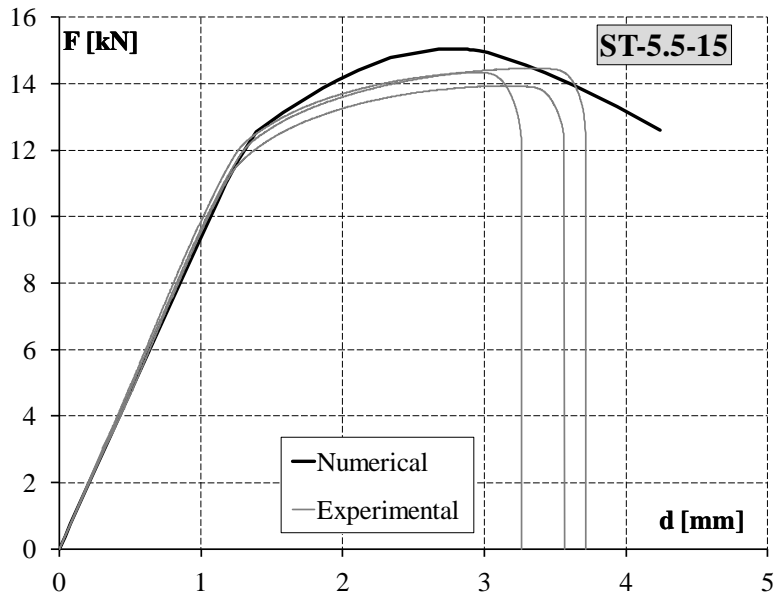


Figure 4.10: Numerical vs. Experimental results for ST-5.5-15

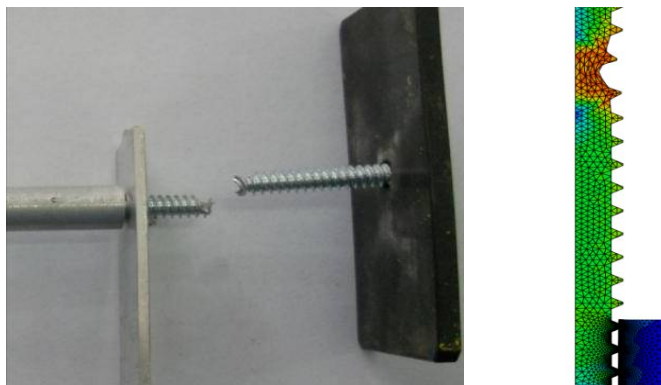


Figure 4.11: Failure mechanism for ST-5.5-15

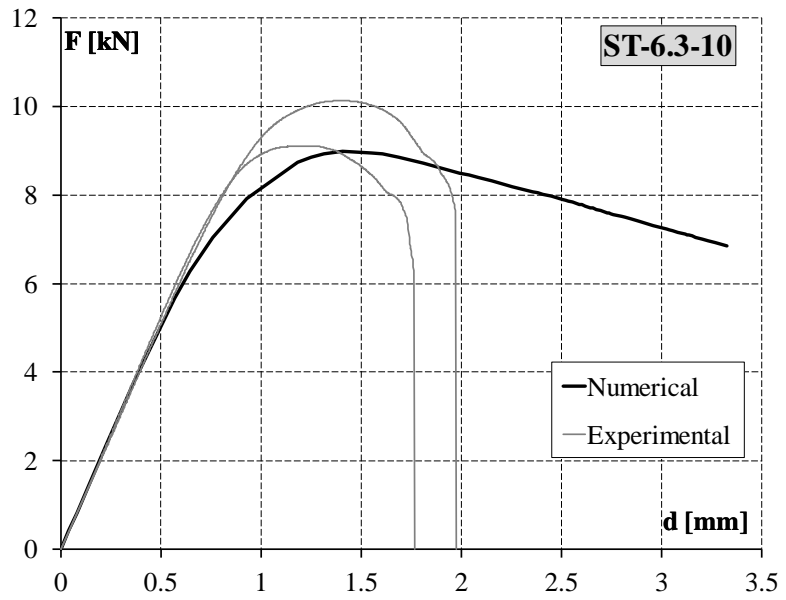


Figure 4.12: Numerical vs. Experimental results for ST-63-10

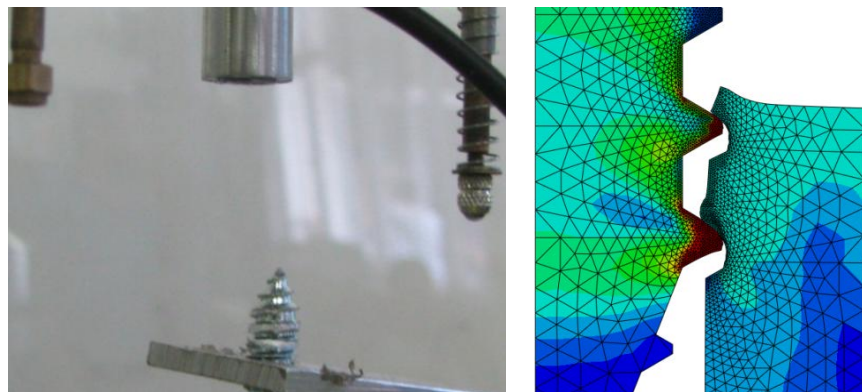


Figure 4.13: Failure mechanism for ST-63-10

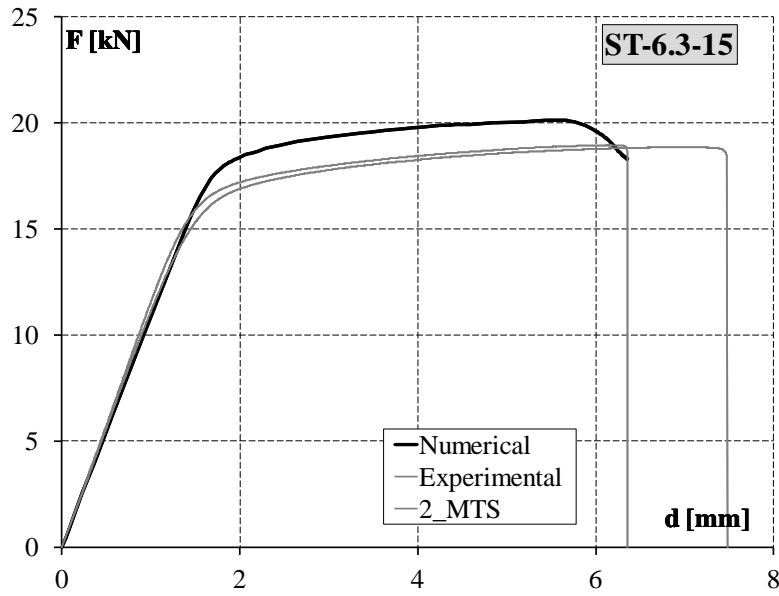


Figure 4.14: Numerical vs. Experimental results for ST-63-15

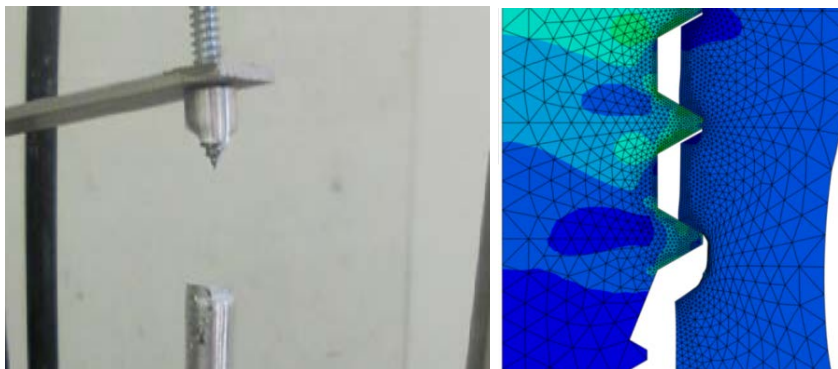


Figure 4.15: Failure mechanism for ST-63-15

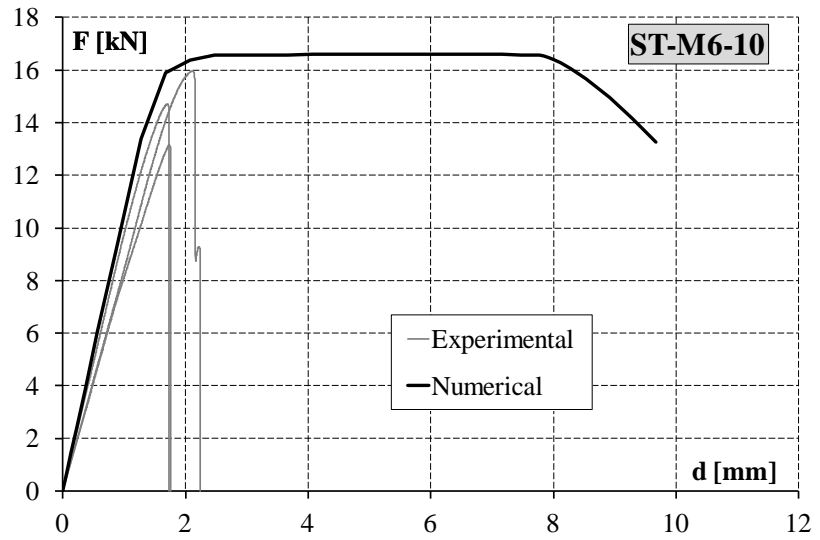


Figure 4.16: Numerical vs. Experimental results for ST-M6-10

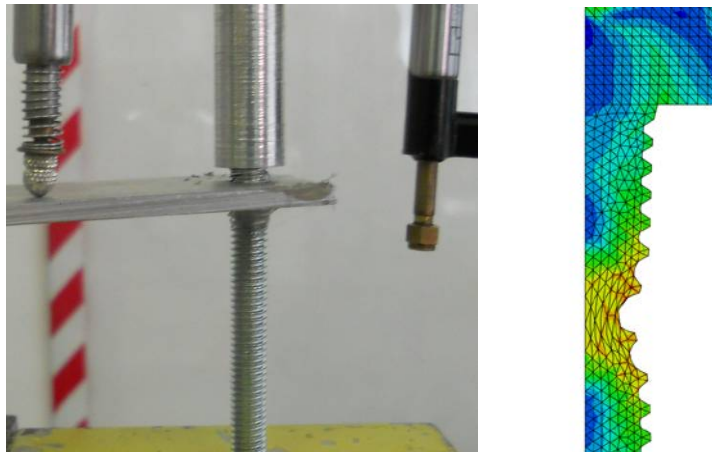


Figure 4.17: Failure mechanism for ST-M6-10

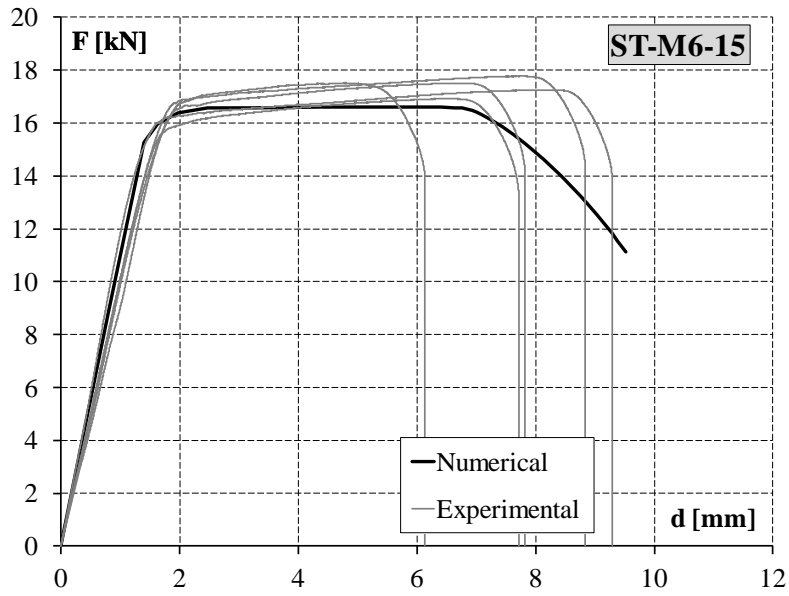


Figure 4.18: Numerical vs. Experimental results for ST-M6-15



Figure 4.19: Failure mechanism for ST-M6-15

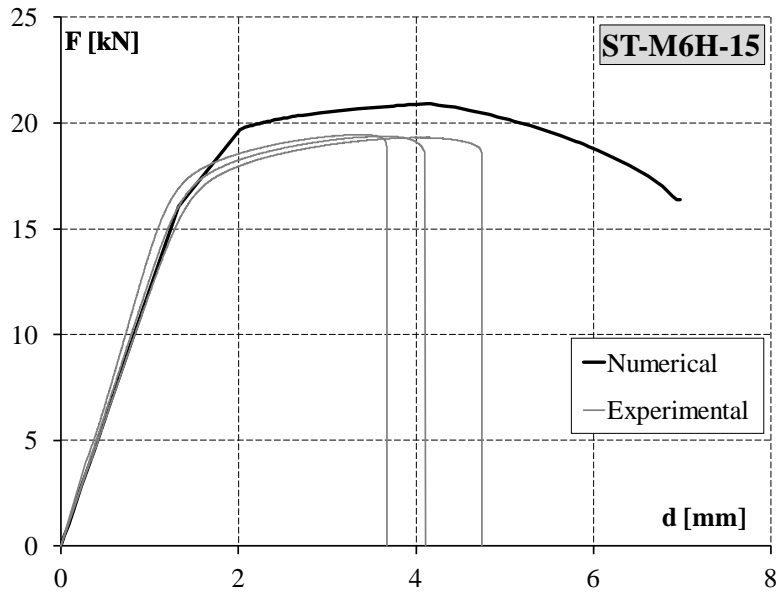


Figure 4.20: Numerical vs. Experimental results for ST-M6H-15



Figure 4.21: Numerical vs. Experimental results for ST-M6H-15

4.3 BOLT-CHANNEL MODELS

4.3.1 General assumption

In the present Section the calibration and results of bolt-channel joints modelling is described and discussed. In particular, two models representative of bolt-channel joint under transversal shear and pull-out force have been developed. The models have been calibrated on the basis of experimental results of BC-SH-18 and BC-PO-18 specimens. The common assumption of two models, such as material and geometries, are shown below.

The aluminium alloy used for both specimens is the AW 6005A-T6 alloys. The mechanical properties have been defined on the basis of experimental results provided in Section 3.2.1. The stress vs. strain relationship has been modelled by Ramberg-Osgood law defined by considering the 0.2% proof strength ($f_0=235$ MPa) and ultimate strength ($f_u=279$ MPa) as reference points. This assumption is generally assumed for analysing problems in the range of large deformation (Mazzolani, 1995). The material constants that define the linear behaviour of material are: $E=63900$ MPa (Young's modulus) and $\nu=0.30$ (Poisson's ratio). In order to implement the material properties as requested by ABAQUS, the obtained Ramberg-Osgood curve is transformed in terms of "true stress" and "true strain" values through Equation (4.1). The experimental (eng.), the obtained Ramberg-Osgood (eng.) and the implemented "true stress-strain" curves are superimposed in Figure 4.22.

As far as the bolt and plate nut are concerned, a geometrical simplification has been assumed. These two specimen components have been modelled as only one part. This assumption has been made on the basis of the observed experimental failures that, in the considered cases, did not exhibit any mutual deformation of the two components. Also the bolt washers have been considered as only one part with the bolt. In addition, another simplification concerns the bolt head geometry that is considered as cylindrical instead of hexagonal in order to avoid complex and heavy mesh configuration. The part

representing bolt and plate nuts has been mechanically characterized by two different materials, corresponding to the two modelled components. In particular, the bolt is characterized by an 8.8 grade material, whose nominal properties have been considered according to ISO 898-1 (ISO, 2009). The material of plate nuts is a S355 steel grade and the assumed nominal properties are provided by EN 10025-2 (CEN, 2004a). The latter material has been assumed also for the modelling experimental set-up parts. For each material a bilinear law is assumed, where the material elastic constants are: $E=200000$ MPa and $\nu=0.30$. The material plasticity for assumed materials is defined by the true stress and true strain values, summarized in Table 4.5.

In addition, for all parts implemented in the model nominal geometric dimensions have been assumed.

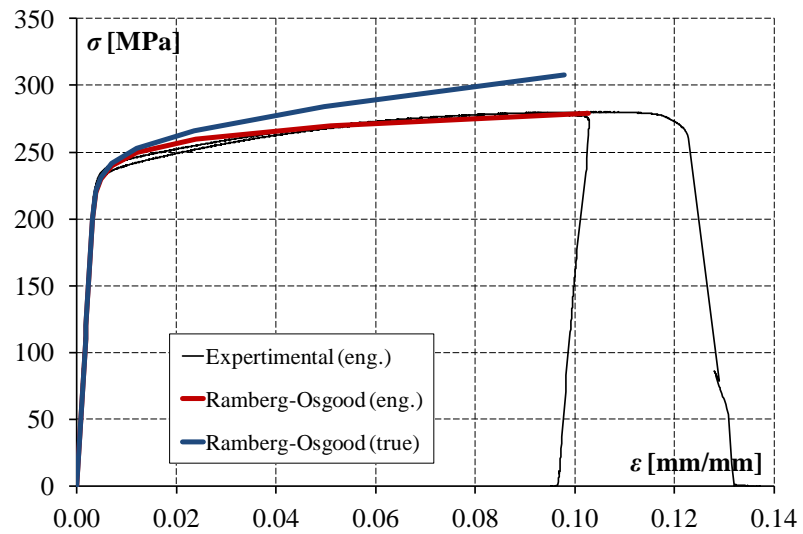


Figure 4.22: Engineering vs. true stress-strain curve for AW 6005A-T6

Table 4.5: Assumed material properties

Screw Material	true yield stress [MPa]	true ultimate stress [MPa]	true ultimate plastic strain	Model series
8.8 Grade	642	896	0.11	Bolts
S355	356	622	0.22	Plate nut, set-up part

4.3.2 Shear model

4.3.2.1 Model description

The model reproducing the experimental tests of bolt-channel under shear loads (BC-SH-18) has been implemented by means of three geometrical parts: the aluminium channel, the bolt with plate nuts and the set-up plate used to apply the loads (Figure 4.23). The parts have been introduced in the ABAQUS software as three dimensional solid deformable parts. In addition, only one half of the actual geometry has been considered with the aim to exploit the model symmetry with respect to middle plane of the whole specimen. The material properties of different parts have been assigned according to the assumption of Section 4.3.1.

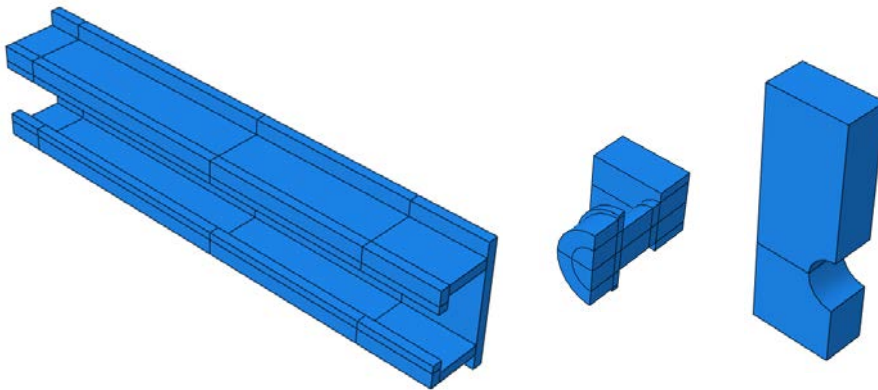


Figure 4.23: Implemented model parts

Surface-to-surface contacts have been used to model all the interactions. In particular, the assumed interactions are: plate nut-aluminium channel, bolt shank-aluminium channel, bolt shank-plate hole, plate-aluminium channel, and bolt washer-plate. In this interaction, the steel surfaces have always been assumed as master. The interactions have been modelled with tangential “penalty” contact and a normal “hard-contact” behaviour. The friction coefficient has been assumed equal to 0.3.

In Figure 4.24, the model assembly with the assumed boundary conditions is depicted. In particular, the symmetry with respect of middle plane has been assumed by restraining this plane against the translation along x-axis ($U_x=0$) and the rotation about y- and z-axis ($U_{Ry}=U_{Rz}=0$). The support condition at the channel ends has been schematized by restraining the internal surface of the aluminium channel top flanges in the effective contact zone with the internal plate of set-up system (Figure 4.25). In particular, the upper one has been restrained against translation along x- and z- axis ($U_x=U_z=0$) while, in the lower one, all translations ($U_x=U_y=U_z=0$) have been impeded.

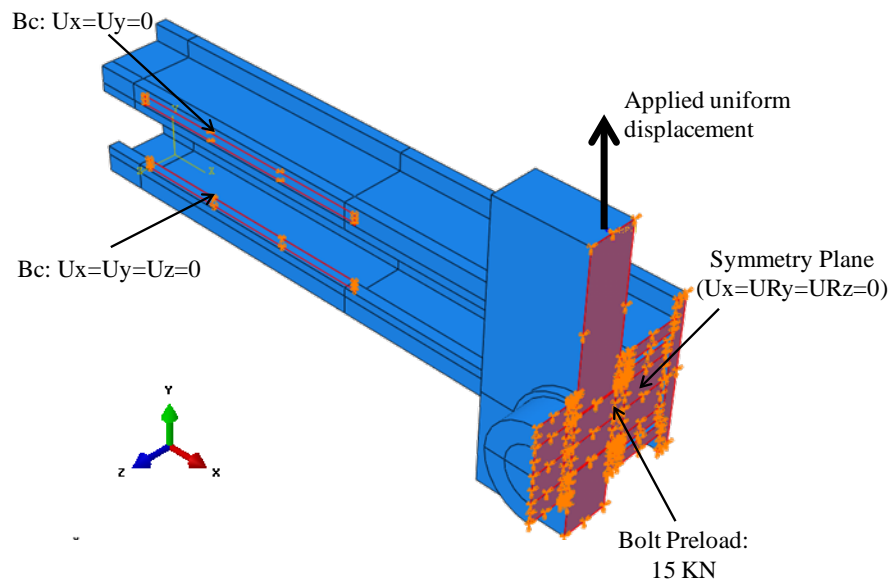


Figure 4.24: Model load and boundary conditions

The bolt tightening has been simulated by means of the “bolt load” ABAQUS option, which is usually used to model tightening forces or length adjustments in bolts or fasteners. The assumed bolt load is of 15 kN for the considered half model geometry, which corresponds to the tightening torque of 100 Nm applied to the specimen in the experimental phase. In order to reproduce the load condition, at a

reference point coupled to the top surface of set-up plate a uniform displacement along y-axis has been applied.

The analysis consists in two general static steps carried out by means of the Newton-Raphson incremental method. In the first step the bolt-load is applied while, in the second one, the pulling load is gradually applied up to a displacement of 30 mm.

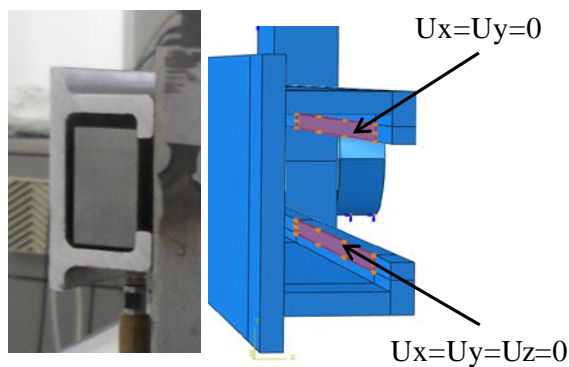


Figure 4.25: Boundary condition at channel ends

4.3.2.2 Mesh sensitivity analysis

In order to investigate the influence of mesh size, a sensitivity analysis has been carried out on the proposed model. The model has been meshed by means of an 8-node linear brick with reduced integration and hourglass control (C3D8R). This hexahedral element is generally used in ABAQUS environment in case of three-dimensional problems related to material plasticity and contact interactions because it usually provides good results with reduced computational time.

The parts have been meshed in order to have a more refined mesh in model zone involved in contact interactions. In particular, the plate nut and the adjacent zone of aluminium channel have been more finely meshed than the peripheral zone. Therefore, the finite element mesh has been generated by considering two reference sizes, a finer one for the zone involved in contact interactions and a greater one for the other zone.

The sensitivity analysis has been conducted considering three different mesh configurations: coarse, intermediate and fine (Figure 4.26). The considered mesh sizes, the obtained number of node and elements together with the CPU time consuming, normalised to intermediate configuration, for each considered mesh configuration are summarised in Table 4.6.

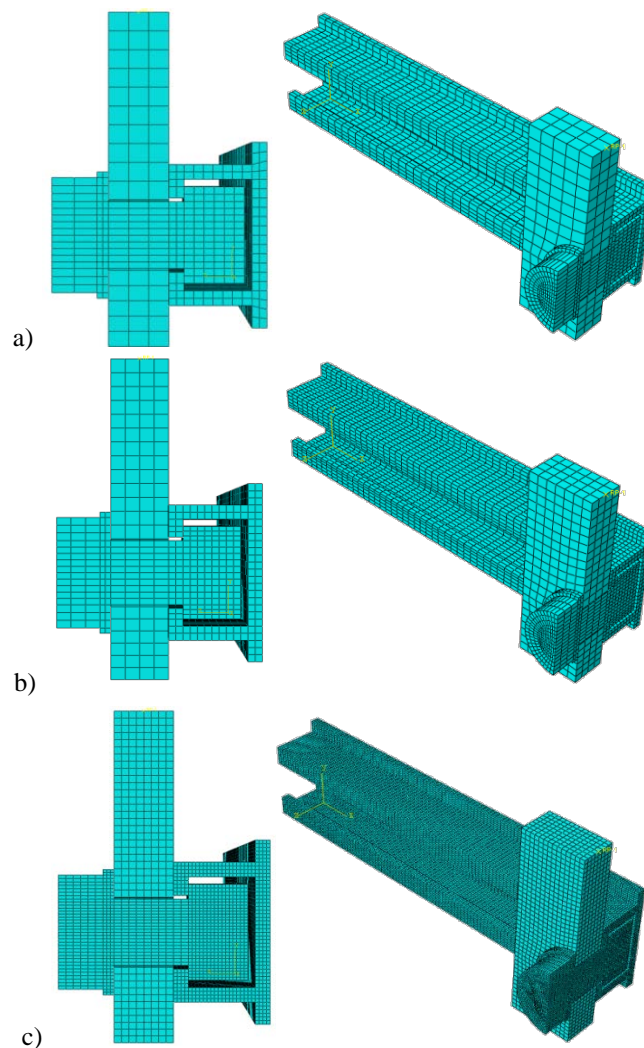
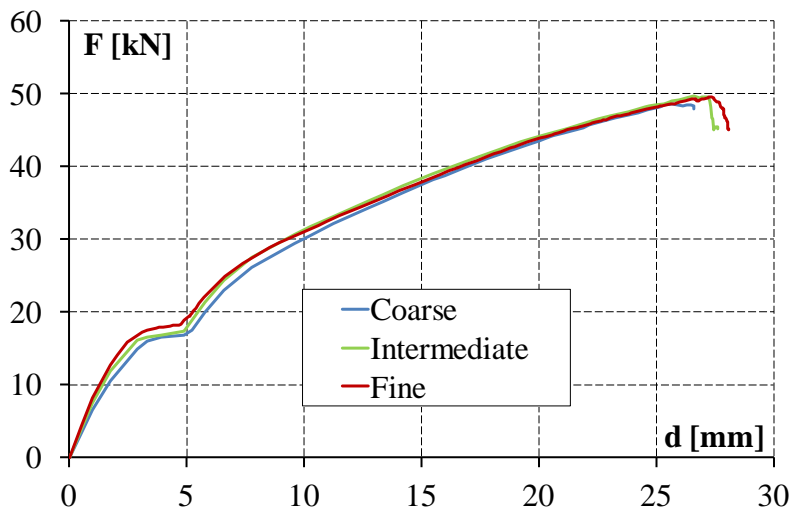


Figure 4.26: Assumed mesh size (a) coarse , (b) intermediate, (c) fine

Table 4.6: Mesh parameters

Mesh config.	Minimum mesh size [mm]	Maximum mesh size [mm]	No. of Elements	No. of Nodes	Normalized CPU Time
Coarse	2.5	5.0	11004	18748	0.64 (20 min)
Intermediate	2.0	4.0	17616	29517	1.00 (44 min)
Fine	1.0	2.0	105902	150813	32.7 (1454 min)

By comparing the analysis results in terms of force vs. displacement curve (Figure 4.27), it can be observed that the investigated mesh sizes do not significantly influence the global model response. Little difference can be noticed in the first part of curves up to 10, where the coarse model curve is slightly lower than the others. In addition, coarse model analysis stopped before it catches the post-peak behaviour. On the basis of this consideration, the adopted mesh is the intermediate one, which allows to contain computational analysis time with very similar results with respect to the fine model.

**Figure 4.27: Mesh sensitivity analysis results**

4.3.2.3 Numerical vs. experimental results

The reliability of the proposed model for bolt-channel joint subjected to shear transversal load can be proved by comparing the numerical with experimental results. Figure 4.28 shows the superimposition of numerical and experimental results in terms of load vs. displacement ($F-d$) curves. The numerical curve describes with acceptable approximation the experimental ones, but there are some differences especially for displacement beyond 5 mm. The slipping plateau of curve due to clearance is slightly higher than those experimentally obtained. The main difference on response curve consists in the marked irregularity in experimental curve, probably depending on local phenomena related to the assembly imperfection.

The comparison between numerical and experimental results in terms of joint strength (F_{max}) and stiffness (k) is provided in Table 4.7. The model catches in very good agreement with experimental results the joint strength with an error of 1%. On the other hand, the model underestimates the initial stiffness of about 10%.

It has to be noticed that the numerical results match in good approximation the experimental ones also in terms of deformed configuration at failure. Figure 4.29 shows a frontal view of the experimental and numerical deformed configurations, which appear substantially similar. Also the comparison between final deformed configuration at the middle section and the end of the aluminium channel, given in Figures 4.30 and 4.31, shows a good agreement of numerical deformed shape with the experimental one.

Although some little imperfections are present, especially in terms of shape of load vs. displacement curve, the proposed model is sufficiently accurate and it can be considered a useful tool to understanding the joint structural behaviour.

Table 4.7: Comparison between numerical and experimental results

	F_{max} [kN]	k [kN/mm]
Numerical	49.7	7.51
Experimental	49.3	8.32
Error	+1%	-10%

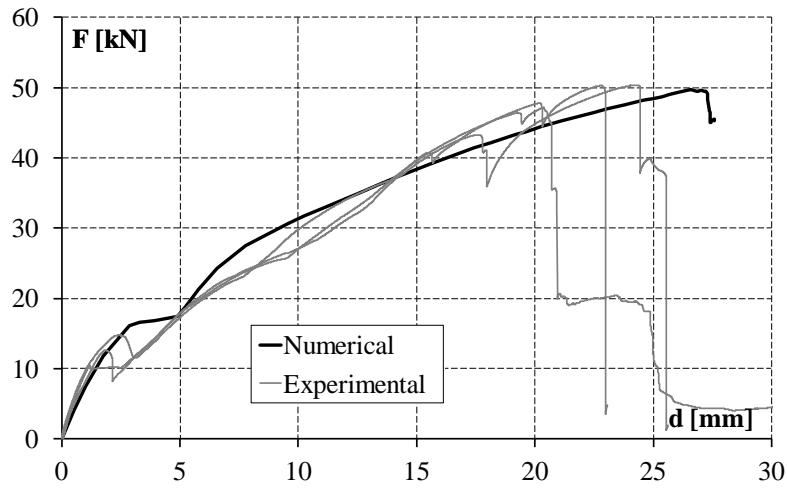


Figure 4.28: Comparison between numerical and experimental response curves

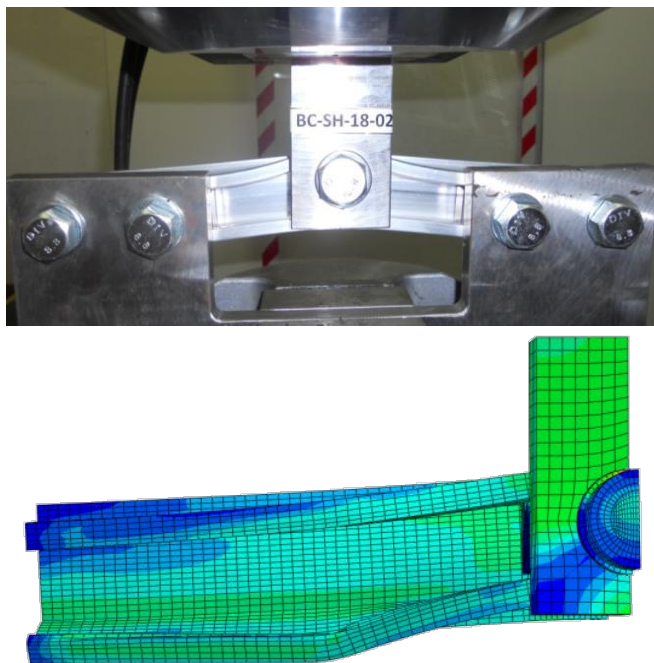


Figure 4.29: Deformed configuration at failure – frontal view

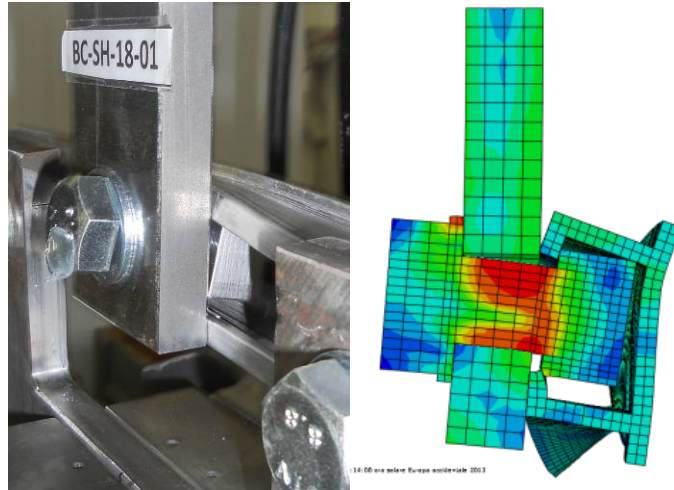


Figure 4.30: Deformed configuration at middle section

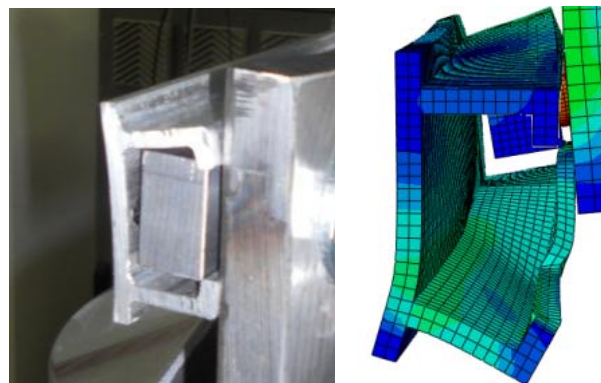


Figure 4.31: Deformed configuration of aluminium channel end (experimental vs. numerical)

4.3.3 Pull-out model

4.3.3.1 Model description

The experimental tests of bolt-channel under pull-out loads (BC-PO-18) have been modelled by implementing in ABAQUS three geometrical parts: the aluminium channel, the bolt with plate nuts and a set-up part. The latter schematize the surface of the set-up T-shaped steel element where the aluminium channel is laid on and connected

by bolts. This part has been implemented as a rigid discrete planar shell. The remaining two parts have been introduced as three dimensional solid deformable parts. Also for this reason, only one half of the actual geometry has been considered by exploiting the model symmetry with respect to middle plane of the whole specimen (Figure 4.32). The material properties of the aluminium channel and the bolt with plate nut have been assigned according to the assumption of Section 4.3.1, while the set-up part, assumed as rigid, does not need any material assignment.

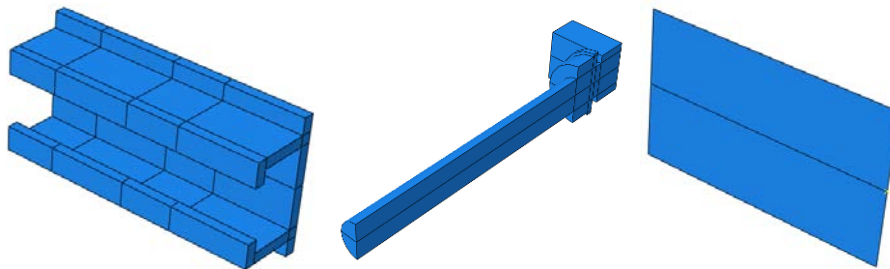


Figure 4.32: Implemented model parts

Surface-to-surface contacts have been used to model the interactions between plate nut and aluminium channel and between bolt washer and aluminium, where the steel surfaces have been assumed as master. These interactions consist in a tangential “penalty” contact, with a friction coefficient of 0.3 and a normal “hard-contact” behaviour.

The model assembly and the assumed boundary conditions are shown in Figure 4.33. The symmetry condition at middle plane has been assumed by restraining this plane against the translation along x-axis ($U_x=0$) and the rotation about y- and z-axis ($U_{Ry}=U_{Rz}=0$).

The support condition between the aluminium channel and the rigid shell that schematize the set-up element has been modelled by a surface-to-surface interaction defined only by the “hard-contact” behaviour. In addition, the set-up bolted connection has been considered by assigning specific boundary conditions to the two

reference points coupled with the areas corresponding to the bolts positions. In particular, each reference point has been restrained against x and y translations and, in order to take into account the bolt deformability, in z direction a spring with stiffness of 900 kN/mm has been introduced (Figure 4.34).

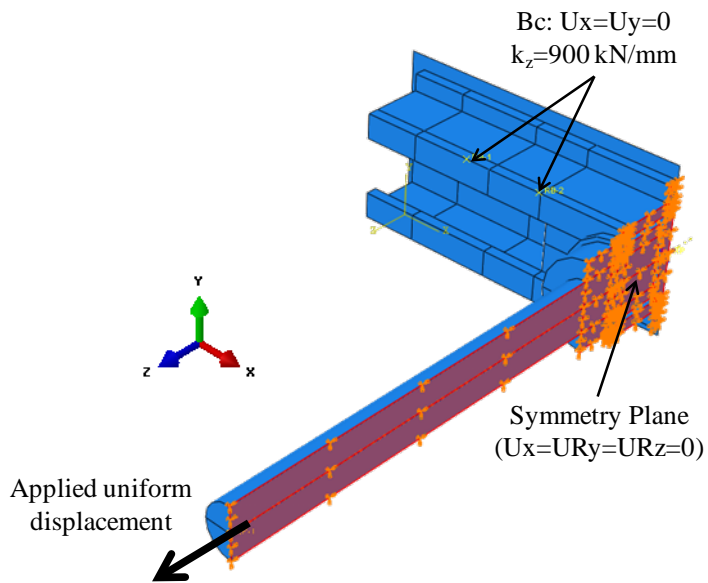


Figure 4.33: Model load and boundary conditions

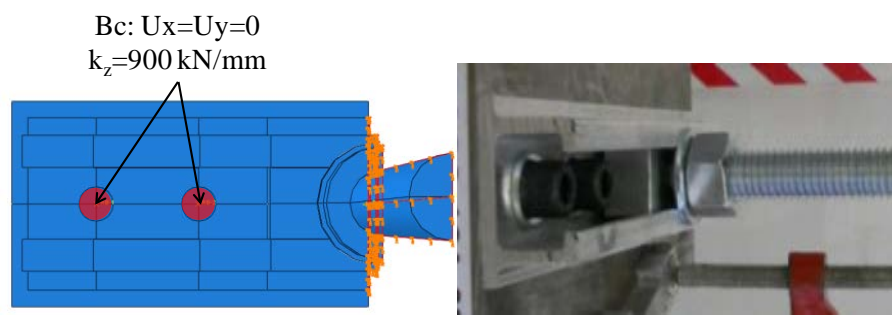


Figure 4.34: Boundary condition at the connection with set-up

The loading condition consists in applying a uniform displacement up to 6 mm along z-axis to a reference point rigidly coupled to the end of bolt shank. Also in this case Newton-Raphson method has been used in the analysis, which consists in only one general static step.

As it is observed in Section 3.4.4, although the specimens were nominally symmetric, their exhibited experimental response was strongly non-symmetric in terms of deformed configuration. In order to catch this issue by numerical model, the presence of imperfections has been taken into account and calibrated. The imperfections have been introduced by locating the plate nuts in not centred position with respect of aluminium channel, as shown in Figure 4.35. Therefore, in addition to the perfectly symmetric model, simply named “perfect”, three models corresponding to imperfection amplitude of 0.25, 0.50 and 1.00 mm have been analysed.

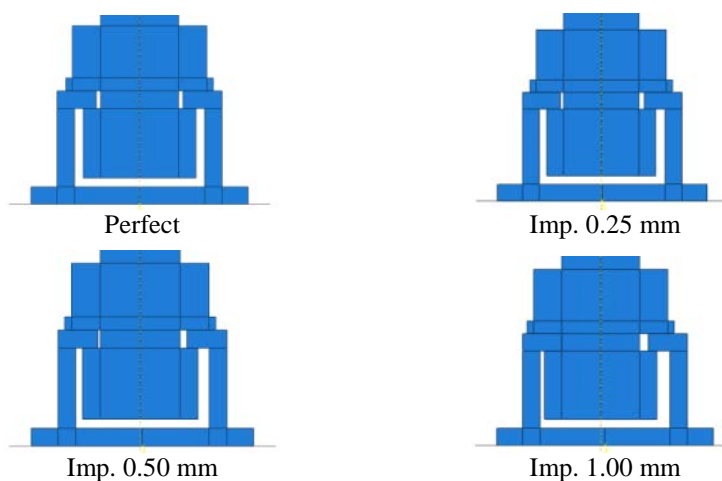


Figure 4.35: Model imperfection calibration

4.3.3.2 Mesh sensitivity analysis

Also for this model, the influence of mesh size has been investigated by means of a sensitivity analysis. This investigation has been performed by considering the “perfect” model. As for the BC-SH-18 model, the selected mesh elements are the 8-node linear brick

with reduced integration and hourglass control (C3D8R). Also in this case a more refined mesh in model zone involved in contact interactions has been assumed. In particular, the plate nut and the adjacent zone of aluminium channel have been more finely meshed than the peripheral zone.

The sensitivity analysis has been conducted considering three different mesh configurations: coarse, intermediate and fine (Figure 4.36). Table 4.8 provides the values for each considered mesh configuration of sizes, number of node and elements together with the CPU time consuming, normalized to intermediate configuration.

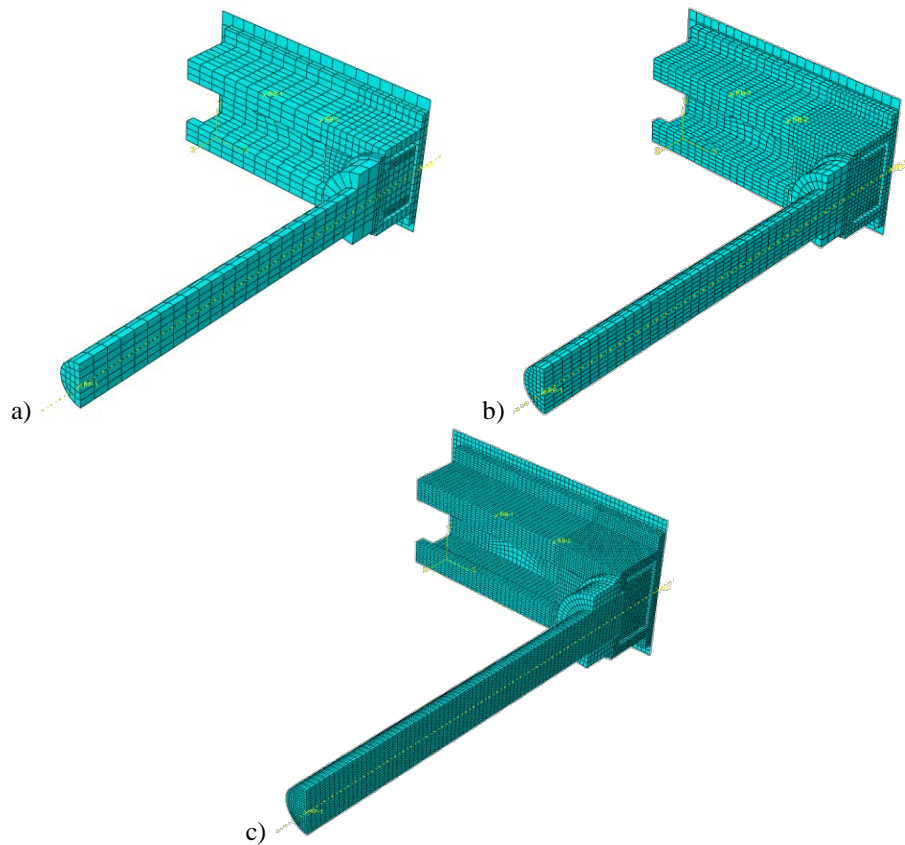
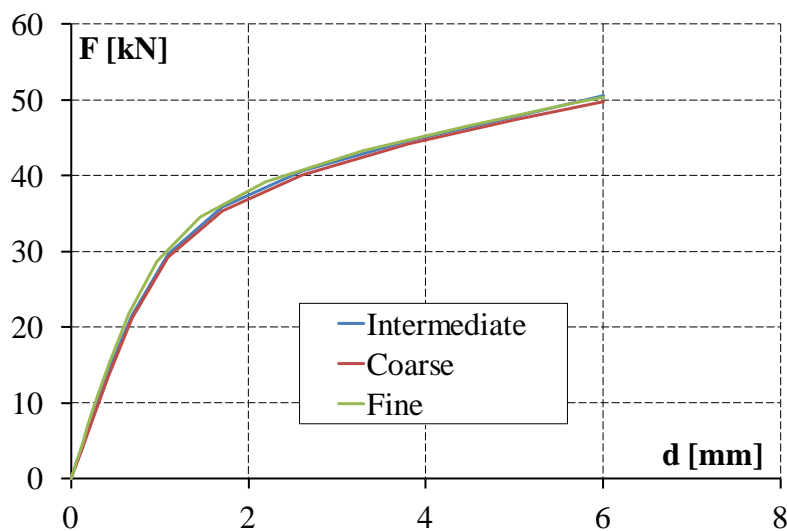


Figure 4.36: Assumed mesh size (a) coarse , (b) intermediate, (c) fine

Table 4.8: Mesh parameters

Mesh config.	Minimum mesh size [mm]	Maximum mesh size [mm]	No. of Elements	No. of Nodes	Normalized CPU Time
Coarse	3.0	6.0	8335	14053	0.61 (11 min)
Intermediate	2.0	4.0	14027	23138	1.00 (18 min)
Fine	1.0	2.0	73905	106168	15.2 (265 min)

By comparing the analysis results in terms of force vs. displacement curve (Figure 4.37), it can be observed that the investigated mesh sizes do not significantly influence the global model response. Therefore, the intermediate mesh configuration has been selected to perform the analyses of the models corresponding to the different assumed configuration. The selected configuration allows to contain computational analysis time guaranteeing a good results accuracy.

**Figure 4.37: Mesh sensitivity analysis results**

4.3.3.3 Numerical vs. experimental results

The comparison between the results of the numerical models corresponding to different imperfection amplitudes and experimental ones, in terms of load vs. displacement ($F-d$) curves, is shown in Figure 4.38. The numerical curves for the analysed model describe with good approximation the full experimental range. The curves related to perfect and 0.25 mm imperfect models are practically identical as for the deformed configuration and the stress distribution, which are shown in Figure 4.39. In effect, the deformed configuration of 0.25 mm imperfect model is substantially symmetric. As a consequence, this imperfection amplitude does not seem to influence significantly the model response. On the other hand, the curves of 0.50 mm and 1.00 mm imperfect model do not fully develop the applied displacement. In addition, and the corresponding deformed configurations, given in Figure 4.39, are clearly non symmetric.

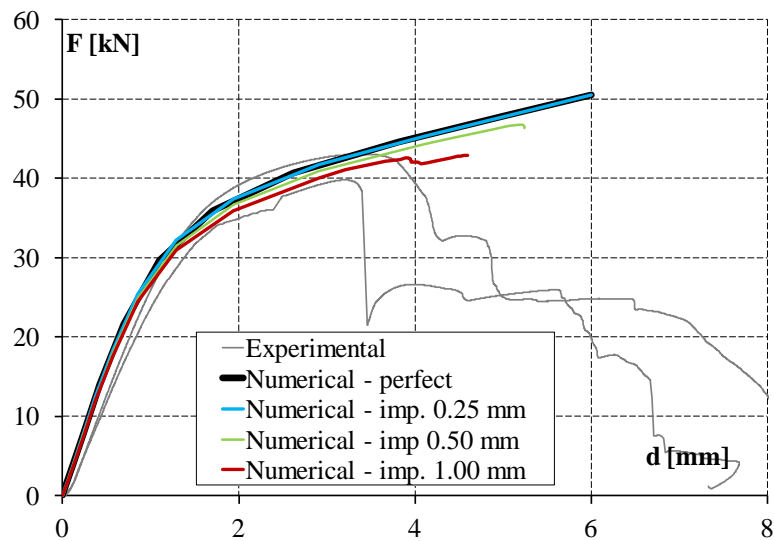


Figure 4.38: Comparison between numerical and experimental response curves

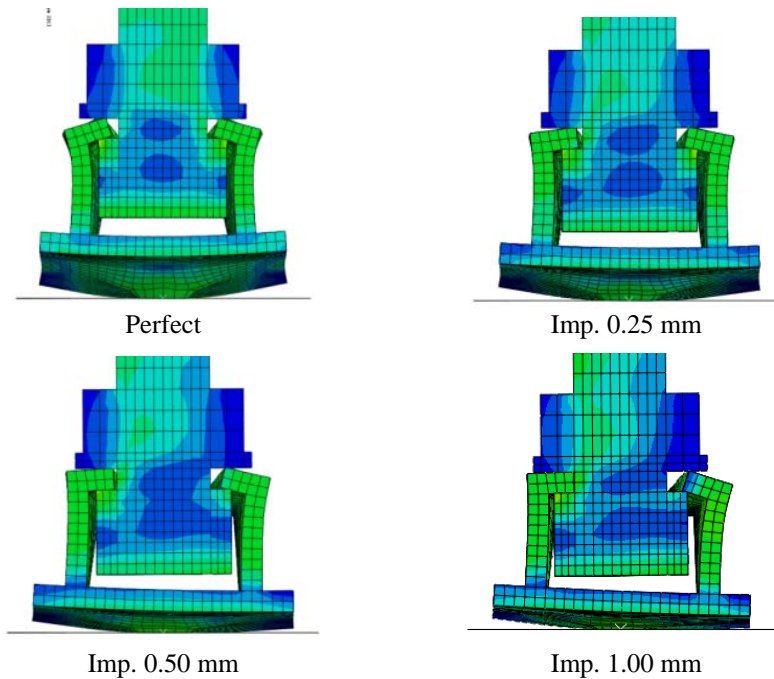


Figure 4.39: Deformed configurations for the assumed imperfections

Table 4.9 shows the comparison between numerical and experimental results in terms of joint strength (F_{max}) and stiffness (k). Also in this case, it is possible to notice the small influence of 0.25 mm imperfection because the strength and the stiffness are equal to those of the perfect model. By comparing the numerical results with experimental ones, the perfect model overestimates both strength and stiffness with errors of 18% and 15%, respectively. The strength error decreases with higher imperfection amplitude and results equal to 8% and 0.2% for 0.50 and 1.00 mm imperfect models, respectively. A lower error reduction can be observed in terms of stiffness. In particular, 0.50 mm and 1.00 mm imperfect models make an error in stiffness evaluation of 12% and 10%, respectively. On the basis of the above considerations, the 1.00 mm imperfect model would seem to match in best approximation the experimental results. In addition, this is also confirmed by the comparison between the deformed configuration of such model and the experimental one. In effect,

numerical deformed configuration matches in very good way the experimental one, as it is shown in Figures 4.40 to 4.42.

Finally, it can be noticed that by considering the influence of imperfections, the proposed model is able to catch in good approximation the experimental results and it can be used for the prediction of joint response.

Table 4.9: Comparison between numerical and experimental results

	F_{max} [kN]	F_{max} Error	k [kN/mm]	k Error
Experimental	42.8		28.6	
Perfect	50.5	+18%	33.2	+15%
Imp. 0.25 mm	50.5	+18%	32.8	+15%
Imp. 0.50 mm	46.3	+8%	32.1	+12%
Imp. 1.00 mm	42.9	+0.2%	31.5	+10%

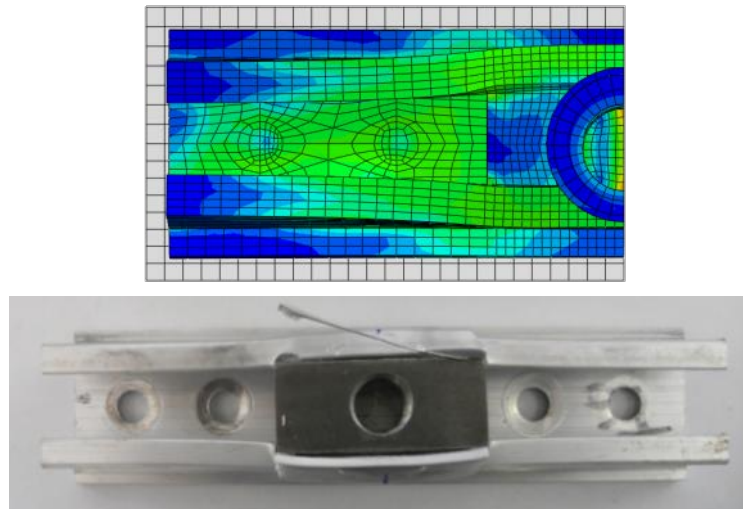


Figure 4.40: Deformed configuration – frontal view

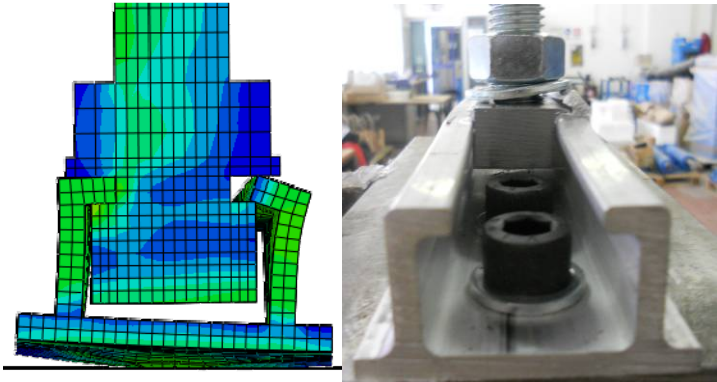


Figure 4.41: Deformed configuration at middle section

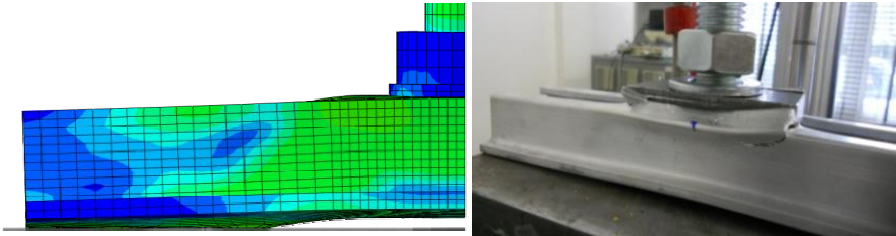


Figure 4.42: Deformed configuration – lateral view

CONCLUSIONS

The evaluation of mechanical behaviour of special joints by means of experimental tests and numerical analyses has been the main objective of this work.

The work has been focused on two typologies of special joints: screwed joints in open and closed port under pull-out loads and bolt-channel joints under three different loading directions (i.e., slip, shear and pull-out).

The main conclusions based on the results of the experimental and numerical phases are summarised hereafter.

In screw joint tests three different failure mechanisms, namely the pull-out of the screw, the tension failure of the screw or of the aluminium slot, have been observed. In the case of open screw ports (screw-groove and screw-boss specimen), the observed joint failure was always due to pull-out. On the contrary, in the case of closed port joints (screw-tube), the screw pull-out occurred in specimens with low values of nominal embedment length (7.5 and 10 mm), while for higher values (15 mm) the axial failure mode consisted of the rupture of the screw or the aluminium under tension.

It has been observed, in case of pull-out failure, that the main parameter influencing the strength of the screwed joints the effective embedment length, which represents the length of the effective threaded portion of the screw in the slot. In addition, for such mechanism, it has also been observed that strength results more scattered, with coefficient of variation ranging from 10% to 17%, than the other cases where the scatter is always lower than 2%. These

findings could be ascribed to the higher sensitivity of the pull-out mechanism to assembly and imperfection issues.

As far as Bolt-channel joint tests results are concerned, slip tests showed high scattered results (14-24%). Also in this case, the strength values would seem strongly influenced by the assembly and the imperfections. In effect, it has been observed that due to the tightening the plate nut rotates inside the aluminium channel causing unforeseen contacts, which could influence the response. In addition, for the examined case, it has been observed that a variation of 55% of tightening torque does not substantially influence the joint response with a corresponding strength increase of 2%.

Assembly and imperfections would seem not to influence the shear test response of the bolt-channel, which is globally symmetric and presents very low scattered values in terms of strength (3-4%). In addition, it has been observed a great difference in terms of deformation capacity and strength of the two investigated configurations, corresponding to M10 and M18 bolts, with a strength increase of 137% for M18 bolt configuration.

Although the low scattered results, ranging from 1% to 7%, the deformed configuration exhibited in pull-out tests was always strongly non symmetric and probably influenced by assembly imperfections. In terms of strength, the M18 configuration showed strength values 29% greater than those obtained in M10 configuration tests.

A numerical model that simulates the tests on closed port screwed joints has been developed by means of ABAQUS computer code. Due to the need of a very refined mesh in contact zones, a simplification on geometry has been made by introducing the axisymmetric condition. This allowed to strongly reduce the computational time which, in case of three-dimensional analyses, would be prohibitive. The numerical model results able to catch the failure mode observed in the experimental phase. The numerical results are in very good agreement with experimental ones with errors ranging from 1% to 7% for strength, and from 1 to 15% for stiffness.

Finite element models for bolt-channel joint under shear and pull-out loadings have been calibrated. In the case of shear the numerical

results are in good agreement with respect to experimental ones. In particular, the model reliably catches the strength with an error of 1%, while it underestimates the stiffness with an error of 10%. In order to match the non symmetric experimental response, the model reproducing the pull-out tests on bolt-channel has been calibrated taking into account the influence of imperfections. The configuration corresponding to an imperfection amplitude of 1 mm matches in best approximation with the experimental results with errors of +0.2% and +10% for strength and stiffness, respectively.

In order to extend the experimental data to geometrical configurations, not considered in this work, a parametric analysis, based on the proposed models, can be performed with the aim to deeply investigate the influence of different parameters on the structural response of special joints. The results of such analysis could be the basis for the optimization of the joint geometry and for the development of design formulations proposals.

REFERENCES

AAMA (1991), *Metal Curtain Wall Fasteners*, AAMA TIR A9-91, American Architectural Manufacturers Association (AAMA), Schaumburg IL.

AAMA (2000), *Metal Curtain Wall Fasteners Addendum*, AAMA TIR A9-91 (2000 Addendum), American Architectural Manufacturers Association (AAMA), Schaumburg IL.

AEC (2013), *Aluminum extrusion manual*, Aluminum Extruder Council (AEC), Wauconda IL.

aluMATTER, <http://aluminium.matter.org.uk>

Aluminium Design, <http://www.aluminiumdesign.net>

Aluminum Association (2009), *International Alloy Designations and Chemical Composition Limits for Wrought Aluminum and Wrought Aluminum Alloys*, The Aluminum Association inc., Arlington VA.

Aluminum Association (2010), *Aluminum Design Manual*, The Aluminum Association inc., Arlington VA.

Aluscalae s.r.l, <http://www.aluscalae.it>

Baehre, R. (1966), *Trycktastravorav elasloplastikc material-nagrafragestillningat*, Tekn. Dr Arne Johnson Ingenjorsbyra, Report No. 16.

Baker, J.F., Roderick, J.W. (1948), *The strength of light alloy struts*, Research Report No. 3, The Aluminium Development Association, London.

Bosch Rexroth, <http://www.boschrexroth.com>

- Bosh Rexroth (2011), *Aluminum Structural Framing System - Version 7.0*, Bosch Rexroth Corporation, Charlotte, NC.
- Budd, G. (1999), "Resources and Production of Aluminium", in *Training In Aluminium Application Technologies*, TALAT Lecture 1101, CD-Rom.
- Budde, L. (1999), "Definition and Classification of Mechanical Fastening Methods", in *Training In Aluminium Application Technologies*, TALAT Lecture 4101, CD-Rom.
- Carretta, E., Macillo, V. (2012), "Selezione delle leghe", in *La progettazione strutturale delle leghe di alluminio*, Mazzolani, F.M. (ed.). Officine Grafiche Francesco Giannini & figli, Italy, pp. 49-91.
- CEN (1993), *EN 515 Aluminium and aluminium alloys - Wrought products - Temper designations*, European Committee for Standardization (CEN), Bruxelles.
- CEN (1994), *EN 573-2 Aluminium and aluminium alloys - Chemical composition and form of wrought products - Part 2: Chemical symbol based designation system*, European Committee for Standardization (CEN), Bruxelles.
- CEN (2001), *EN 10002-1 Metallic materials – Part 1: Method of test at ambient temperature*, European Committee for Standardization (CEN), Bruxelles.
- CEN (2002a), *EN 1780-1 Aluminium and aluminium alloys - Designation of alloyed aluminium ingots for remelting, master alloys and castings - Part 1: Numerical designation system*, European Committee for Standardization (CEN), Bruxelles.
- CEN (2002b), *EN 1780-2 Aluminium and aluminium alloys - Designation of alloyed aluminium ingots for remelting, master alloys and castings - Part 2: Chemical symbol based designation system*, European Committee for Standardization (CEN), Bruxelles.
- CEN (2004a), *EN 10025-2 - Hot rolled products of structural steels - Part 2: Technical delivery conditions for non-alloy structural steels*, European Committee for Standardization (CEN), Bruxelles.
- CEN (2004b), *EN 573-1 Aluminium and aluminium alloys - Chemical composition and form of wrought products - Part 1: Numerical designation system*, European Committee for Standardization (CEN), Bruxelles.

- CEN (2007a), *EN 1999-1-1 - Eurocode 9 - Design of aluminium structures - Part 1-1: General structural rules*, European Committee for Standardization (CEN), Bruxelles.
- CEN (2007b), *EN 1999-1-2 - Eurocode 9 - Design of aluminium structures - Part 1-2: Structural fire design*, European Committee for Standardization (CEN), Bruxelles.
- CEN (2007c), *EN 1999-1-3 - Eurocode 9 - Design of aluminium structures - Part 1-3: Structures susceptible to fatigue*, European Committee for Standardization (CEN), Bruxelles.
- CEN (2007d), *EN 1999-1-4 - Eurocode 9 - Design of aluminium structures - Part 1-4: Cold-formed structural sheeting*, European Committee for Standardization (CEN), Bruxelles.
- CEN (2007e), *EN 1999-1-5 - Eurocode 9 - Design of aluminium structures - Part 1-5: Shell structures*, European Committee for Standardization (CEN), Bruxelles.
- Chen, J.J., Shin Y.S. (1999), "A study of the helical effect on the thread connection by three dimensional finite element analysis", *Nuclear Engineering and Design*, Elsevier, 191(1999), pp 109-116.
- Chen, S.J., An, Q., Zhang, Y., Gao, L.X., Li, Q. (2010), "Loading Analysis on the Thread Teeth in Cylindrical Pipe Thread Connection", *Journal of Pressure Vessel Technology*, ASME, Vol. 132. pp. 031202 1-8.
- CNR (2011), *CNR-DT 208/2011 Istruzioni per la progettazione, l'esecuzione ed il controllo di strutture di alluminio*, Consiglio Nazionale delle Ricerche, Roma.
- Deliwala, J. (2007), *An investigation of the extrinsic factors affecting the pull-out strength of aluminum alloy extrusions*, MSc Thesis, University of Akron.
- Dwight, J. (1999), *Aluminium Design and Construction*, Taylor & Francis Group, London.
- Fukuoka T., Nomura, M. (2008), "Proposition of Helical Thread Modeling With Accurate Geometry and Finite Element Analysis", *Journal of Pressure Vessel Technology*, ASME, Vol. 130. pp. 011204 1-6.
- Fukuoka T., Nomura, M., Fuchikami, T.(2011) "Finite Element Analysis of the Cyclic Stress Amplitude of Threaded Fasteners Using Helical Thread Models" *Journal of Pressure Vessel Technology*, ASME, Vol. 133. pp. 061201 1-7.

- Hellgren, M. (1996), *Strength of Bolt-Channel and Screw-Groove Joints in Aluminium Extrusions*, KTH Royal Institute of Technology, Licentiate Thesis, Stockholm.
- Hobbs, J.W., Burguete, R.L., Patterson, E.A. (2003), "Investigation into the Effect of the Nut Thread Run-Out on the Stress Distribution in a Bolt Using the Finite Element Method", *Journal of Mechanical Design*, ASME, Vol. 125. pp. 627-632.
- Höglund, T. (1999), "Design of joints", in *Training In Aluminium Application Technologies*, TALAT Lecture 2302, CD-Rom.
- Hydro (2009), *Extrusion Design Manual - A world of opportunities*, Hydro Aluminum North America, Linthicum MD.
- ISO (1999), *ISO 1478 - Tapping screw thread*, International Organization for Standardization (ISO) Genève.
- ISO (2009), *ISO 898-1 - Mechanical properties of fasteners made of carbon steel and alloy steel - Part 1: Bolts, screws and studs with specified property classes - Coarse thread and fine pitch thread*, International Organization for Standardization (ISO), Genève.
- Johnson, D.H., Englund, R.B., McAnlis, B.C., Sari, K.C., Colombet, D., *Three-dimensional modeling of a bolted connection*, Penn State-Erie, Erie, PA, Tech. Rep., 2000.
- Kissel, J.R., Ferry, R.L. (2002), *Aluminum Structures - A Guide to Their Specifications and Design (Second edition)*, John Wiley & Sons, Inc., New York.
- MAADI (2011), *MakeABridge® weld-free aluminium modular bridge system*, MAADI Group Inc., Montreal.
- Macillo, V., Fiorino, L., Mazzolani F.M. (2011), "Sistemi di giunzione speciale per elementi estrusi di alluminio", In Proceedings of *XXIII Giornate Italiane della Costruzione in Acciaio, Congresso C.T.A.* Lacco Ameno (NA) Italy, 9-12 October 2011. Doppiovoce, Naples, pp. 61-68.
- Mazzolani, F.M. (1972), "La caratterizzazione della legge σ - ϵ e l'instabilità delle colonne di alluminio", *Costruzioni Metalliche*, No. 3.
- Mazzolani, F.M. (1995), *Aluminium Alloy Structures (Second edition)*, E & FN SPON, London.
- Mazzolani, F.M. (2003), "Design Criteria for Aluminium Structures: Technology, Codification and Applications", in *Aluminium Structural*

- Design* (CISM course n. 443), ed. F.M. Mazzolani, Springer-Verlag, Wien, New York.
- Mazzolani, F.M. (2006), “Structural Applications of Aluminium in Civil Engineering”, *Structural Engineering International*, International Association for Bridge and Structural Engineering, Vol. 4, pp. 1-4.
- Mazzolani, F.M. (2010), “Two Twin Aluminium Domes of the Enel Plant in Civitavecchia (Italy)”, in proceedings of *11th International Aluminium Conference - INALCO 2010*, pp. 57-66.
- Mazzolani, F.M. (2012), “L’impiego delle strutture di alluminio nell’Ingegneria Civile”, in *La progettazione strutturale delle leghe di alluminio*, Mazzolani, F.M. (ed.). Officine Grafiche Francesco Giannini & figli, Italy, pp. 5-48.
- Menzemer, C.C., Deliwala, J., Kissell, J.R. (2008), “Pull-Out Strength of Self Tapping Fasteners in Aluminum Screw Slot Connections”, *Light metal age*, October 2008, pp. 22-26.
- METRA (2011a), *Modulenergy - Catalogo generale*, METRA S.p.A., Rodengo Saiano.
- METRA (2011b), *Facciate continue*, METRA S.p.A., Rodengo Saiano.
- METRA (2012), *Modulsystem40*, METRA S.p.A., Rodengo Saiano.
- Müller, U. (2011), *Introduction to Structural Aluminium Design*, Whittles Publishing, Dunbeath, UK.
- Ramberg, W. and Osgood, W.R. (1943), *Description of stress-strain curves by three parameters*, NACA Technical Note No. 902.
- Rørvik, T. (1998), *Aluminium Structures: introduction to Material Technology and Structural Design according to Eurocode 9*, TAS Courses.
- Sapa (2009), *Design Manual*, Sapa Profiler AB, Stockholm.
- Sapa (2012), *Industrial stairways & handrailings in Aluminium*, Sapa Building System AB, Vetlanda.
- Sharp, M.L. (1993), *Behavior and Design of Aluminum Structures*, McGraw-Hill, Inc., New York.
- Simulia (2010), *Abaqus Analysis User’s manual, version 6.10*, Dassault Systemes Simulia Corporation.

- Soetens, F., van Hove, B.W.E.M. (2003), "Design of Connections", in *Aluminium Structural Design* (CISM course n. 443), ed. F.M. Mazzolani, Springer-Verlag, Wien, New York.
- UNI (1965), *UNI 5542 - Filettature metriche ISO a profilo triangolare. Dimensioni limite per filettature con diametri da 1,6 fino a 39 mm*, Ente Nazionale Italiano di Unificazione (UNI), Roma.
- Williams, J.G., Anley, R.E., Nash, D.H., Gray, T.G.F. (2009), "Analysis of externally loaded bolted joints: analytical, computational and experimental study". *International Journal of Pressure Vessels and Piping*, Elsevier, 86 (7). pp. 420-427.
- Woodward, R. (1999), "Aluminium Extrusion: Alloys, Shapes and Properties", in *Training In Aluminium Application Technologies*, TALAT Lecture 1302, CD-Rom.
- Zienkiewicz, O.C., Taylor, R.L. (2000), *The Finite Element Method Volume 1: The Basis (fifth edition)*, Butterworth-Heinemann, Oxford.

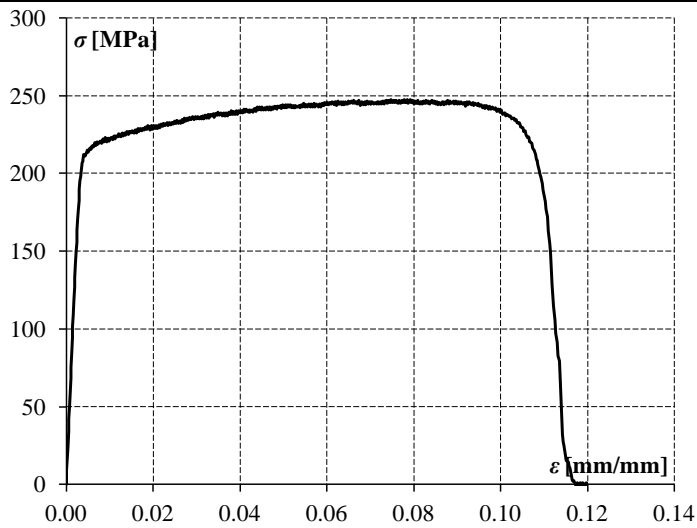
Appendix A

TESTS ON MATERIALS

6060 T5-1.2_1



Specimen Dimension	
Width [mm]	9.13
Thickness [mm]	1.19
Section Area [mm ²]	10.86
Test Results	
E [MPa]	65130
$f_{0.1}$ [MPa]	212
$f_{0.2}$ [MPa]	216
f_u [MPa]	247
ϵ_u	0.079
n_p	26.5

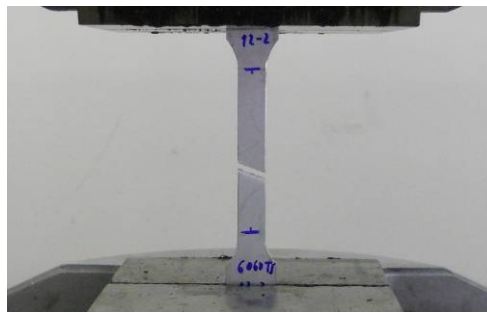


Annotations:

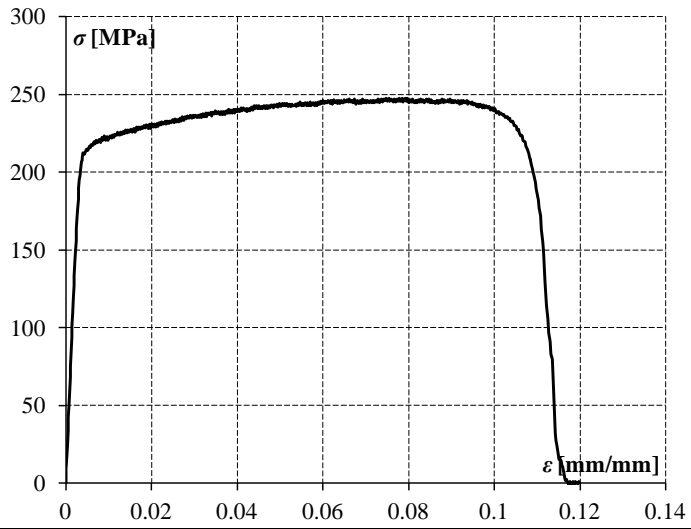
6060 T5-1.2_2



Specimen Dimension	
Width [mm]	9.14
Thickness [mm]	1.19
Section Area [mm ²]	10.88

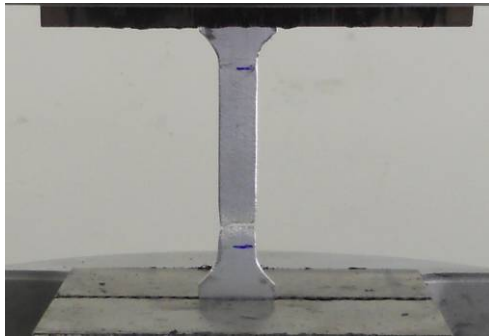


Test Results	
E [MPa]	63810
$f_{0.1}$ [MPa]	211
$f_{0.2}$ [MPa]	217
f_u [MPa]	247
ϵ_u	0.075
n_p	27.1

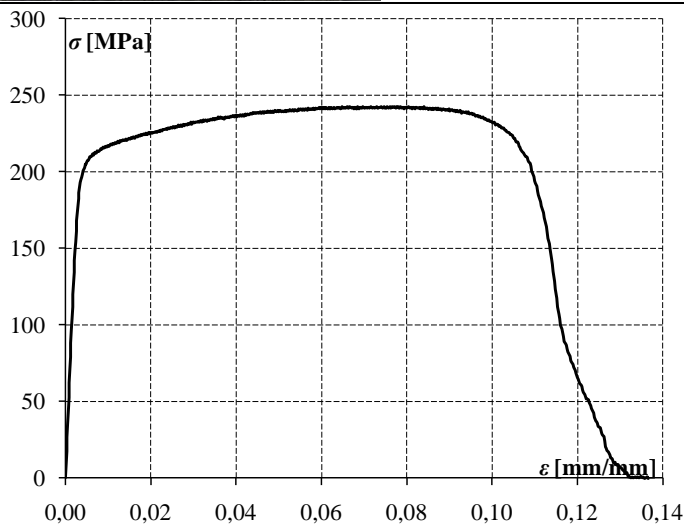


Annotations:

6060 T5-2.5_1



Specimen Dimension	
Width [mm]	9.30
Thickness [mm]	2.43
Section Area [mm ²]	22.6
Test Results	
E [MPa]	64087
$f_{0.1}$ [MPa]	203
$f_{0.2}$ [MPa]	208
f_u [MPa]	243
ϵ_u	0.066
n_p	22.2



Annotations:

6060 T5-2.5_2

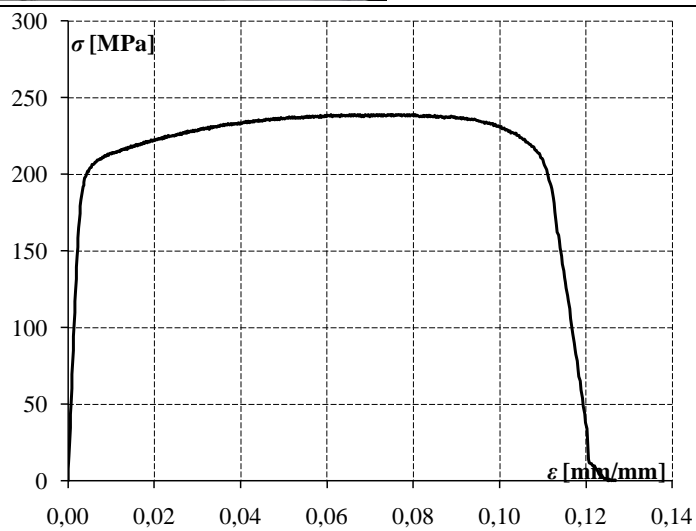


Specimen Dimension

Width [mm]	9.30
Thickness [mm]	2.46
Section Area [mm ²]	22.9

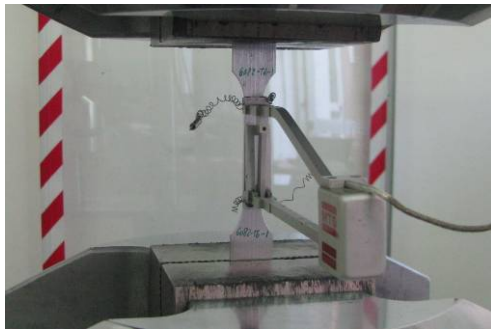
Test Results

E [MPa]	65292
$f_{0.1}$ [MPa]	198
$f_{0.2}$ [MPa]	204
f_u [MPa]	239
ϵ_u	0.075
n_p	22.8

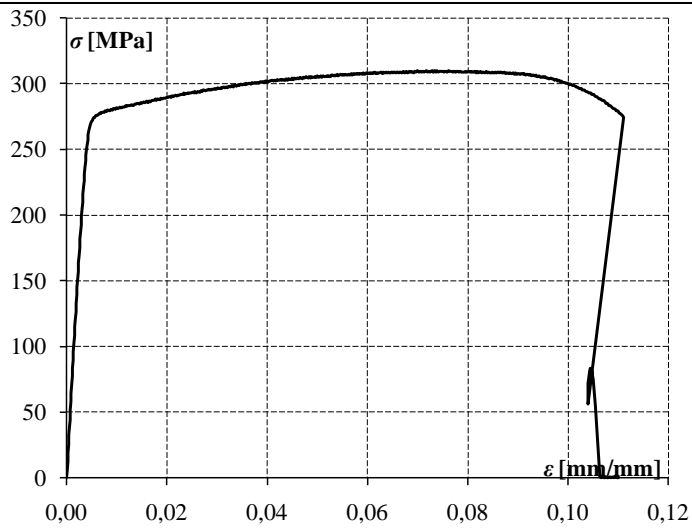
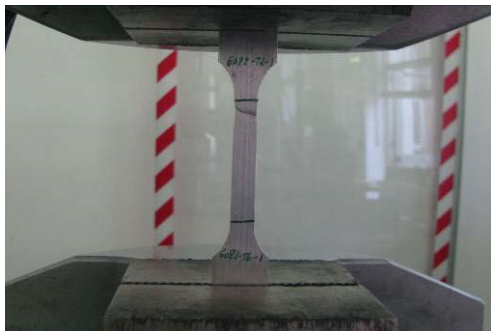


Annotations:

6082 T6_1



Specimen Dimension	
Width [mm]	10.33
Thickness [mm]	2.87
Section Area [mm ²]	29.6
Test Results	
E [MPa]	65693
$f_{0.1}$ [MPa]	272
$f_{0.2}$ [MPa]	276
f_u [MPa]	310
ϵ_u	0.073
n_p	30,7



Annotations:

6082 T6_2

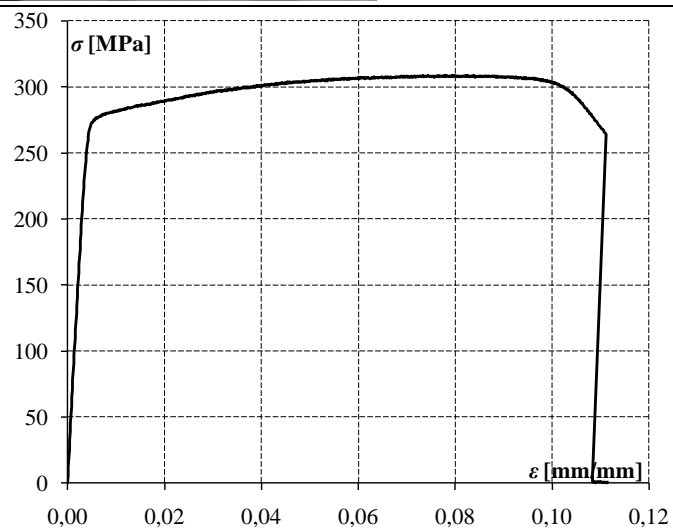


Specimen Dimension

Width [mm]	10.2
Thickness [mm]	2.74
Section Area [mm ²]	27.9

Test Results

E [MPa]	67035
$f_{0.1}$ [MPa]	273
$f_{0.2}$ [MPa]	276
f_u [MPa]	309
ϵ_u	0.078
n_p	32.5



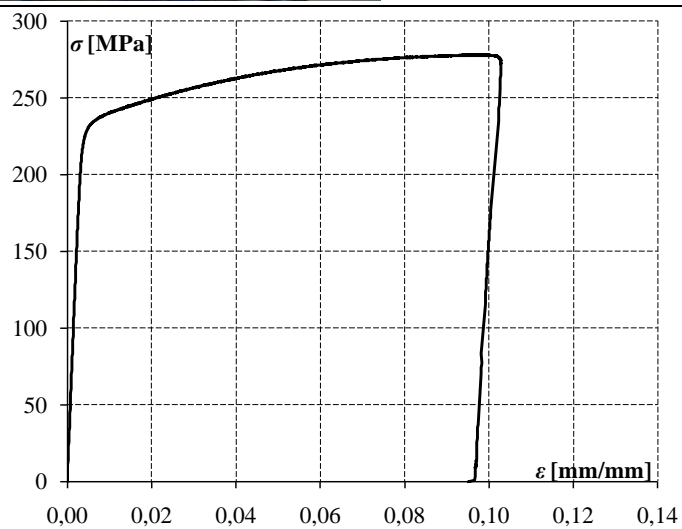
Annotations:

6005A T6_1**Specimen Dimension**

Width [mm]	20.5
Thickness [mm]	4.20
Section Area [mm ²]	86.1

Test Results

E [MPa]	63460
$f_{0.1}$ [MPa]	228
$f_{0.2}$ [MPa]	233
f_u [MPa]	278
ε_u	0.096
n_p	21.6

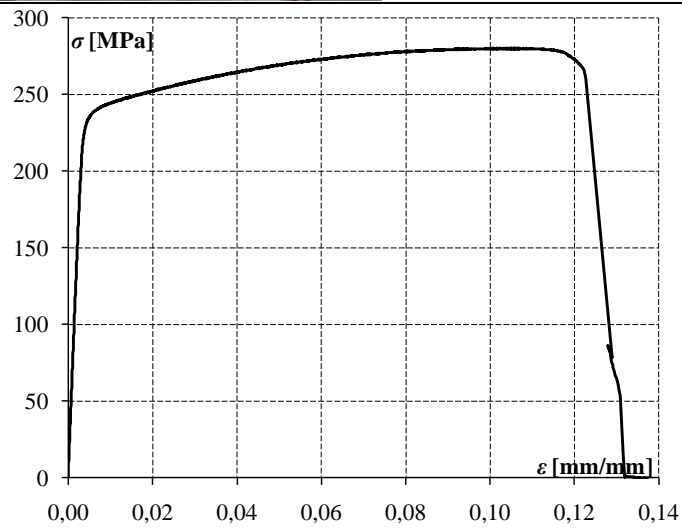


Annotations: Fracture out of the gauge length

6005A T6_2**Specimen Dimension**

Width [mm] 20.1

Thickness [mm] 4.20

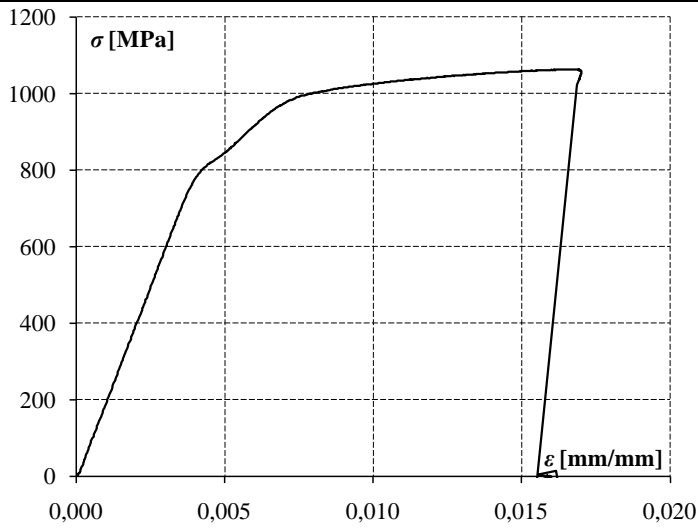
Section Area [mm²] 83.9**Test Results** E [MPa] 64412 $f_{0.1}$ [MPa] 233 $f_{0.2}$ [MPa] 278 f_u [MPa] 280 ϵ_u 0.104 n_p 23.8

Annotations:

SM_1



Specimen Dimension	
Diameter [mm]	5.40
Section Area [mm ²]	23.2
Test Results	
E [MPa]	200611
$f_{0.1}$ [MPa]	868
$f_{0.2}$ [MPa]	967
f_u [MPa]	1064
ϵ_u	0.017



Annotations: Fracture out of the gauge length

SM_2

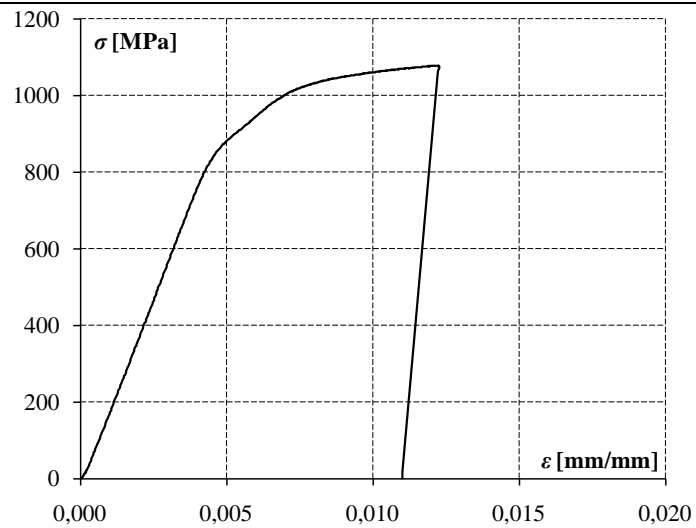


Specimen Dimension

Diameter [mm] 5.50

Section Area [mm²] 23.6

Test Results

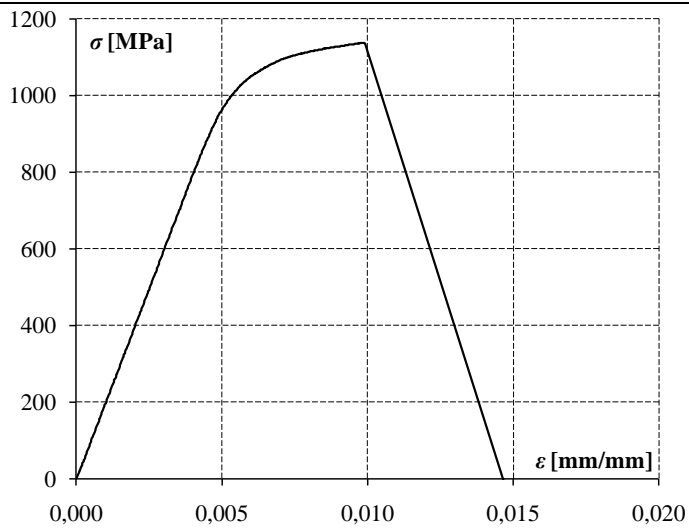
 E [MPa] 197840 $f_{0.1}$ [MPa] 923 $f_{0.2}$ [MPa] 1006 f_u [MPa] 1078 ϵ_u 0.012

Annotations: Fracture out of the gauge length

SM_3



Specimen Dimension	
Diameter [mm]	5.50
Section Area [mm ²]	23.6
Test Results	
E [MPa]	201104
$f_{0.1}$ [MPa]	1065
$f_{0.2}$ [MPa]	1106
f_u [MPa]	1137
ϵ_u	0.010



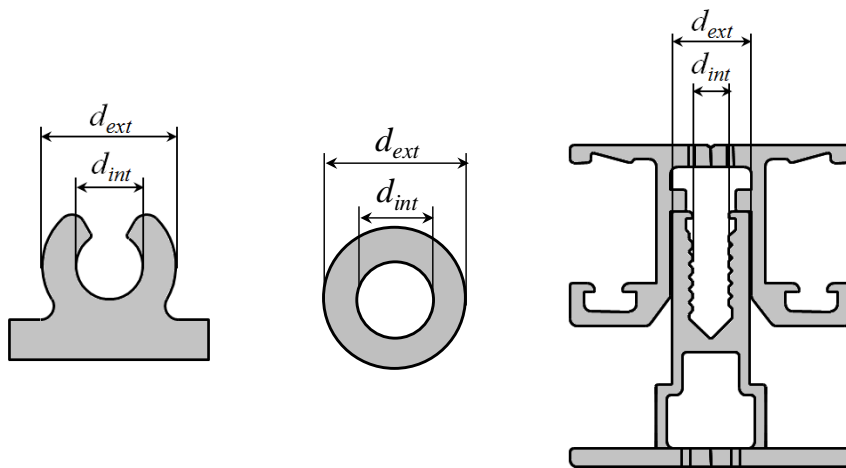
Annotations: Fracture occurred at screw head (out of the gauge length)

Appendix B

TESTS ON SCREWED JOINTS

Measured dimensions of Screwed joint Specimens

The dimensions of each specimen have been measured with a slide gauge. Hereafter the main geometrical parameter are summarised.



Measured dimensions for SG-4.8 specimens

Label	d_{ext}	d_{int}
SG-4.8-15_1	7.11	4.20
SG-4.8-15_2	7.04	4.14
SG-4.8-15_3	7.11	4.19
SG-4.8-15_4	7.10	4.23
SG-4.8-15_5	7.12	4.19
Average	7.10	4.19
Standard dev.	0.032	0.032
C.o.V.	0.004	0.01

Measured dimensions for SG-5.5 specimens

Label	d_{ext}	d_{int}
SG-5.5-15_1	9.97	5.09
SG-5.5-15_2	9.96	5.02
SG-5.5-15_3	9.99	5.02
SG-5.5-15_4	9.98	5.04
SG-5.5-15_5	10.0	5.01
SG-5.5-30_1	9.98	5.03
SG-5.5-30_2	9.98	5.01
SG-5.5-30_3	9.99	5.02
Average	9.98	5.03
Standard dev.	0.012	0.0261
C.o.V.	0.001	0.01

Measured dimensions for ST-5.5 specimens

Label	d_{ext}	d_{int}
ST-5.5-7.5_1	10.10	4.79
ST-5.5-7.5_2	9.98	4.76
ST-5.5-7.5_3	9.97	4.78
ST-5.5-7.5_4	10.05	4.77
ST-5.5-7.5_5	9.97	4.72
ST-5.5-10_1	9.98	4.79
ST-5.5-10_2	10.09	4.78
ST-5.5-10_3	9.97	4.86
ST-5.5-10_4	10.00	4.77
ST-5.5-10_5	10.09	4.75
ST-5.5-15_1	9.98	4.77
ST-5.5-15_2	9.95	4.77
ST-5.5-15_3	9.98	4.78
Average	10.01	4.78
Standard dev.	0.052	0.030
C.o.V.	0.005	0.006

Measured dimensions for ST-6.3 specimens

Label	d_{ext}	d_{int}
ST-6.3-10_1	10.68	5.56
ST-6.3-10_2	10.70	5.55
ST-6.3-15_3	10.65	5.53
ST-6.3-15_4	10.74	5.57
Average	10.69	5.55
Standard dev.	0.038	0.017
C.o.V.	0.004	0.003

Measured dimensions for ST-M6 specimens

Label	d_{ext}	d_{int}
ST-M6-10_1	10.95	5.31
ST-M6-10_2	10.87	5.25
ST-M6-10_3	10.95	5.30
ST-M6-15_1	10.85	5.25
ST-M6-15_2	10.90	5.31
ST-M6-15_3	10.90	5.30
ST-M6-15_4	10.88	5.30
ST-M6-15_5	10.91	5.29
ST-M6H-15_1	10.93	5.30
ST-M6H-15_2	10.87	5.32
ST-M6H-15_3	10.94	5.30
Average	10.90	5.29
Standard dev.	0.035	0.023
C.o.V.	0.003	0.004

Measured dimensions for SB-6.3 specimens

Label	d_{int}	d_{ext}
SB-6.3-15_1	10.67	5.10
SB-6.3-15_2	10.61	5.11
SB-6.3-15_3	10.63	5.20
SB-6.3-15_4	10.60	5.20
Average	10.63	5.15
Standard dev.	0.031	0.055
C.o.V.	0.003	0.01

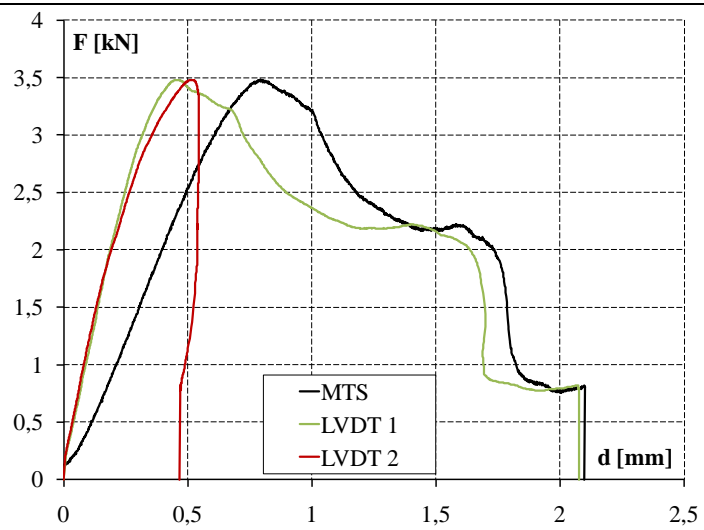
Instrumentation legend

LVDT 1: transducer placed at slot end

LVDT 2: transducer placed at slot end

LVDT A: transducer placed between the set-up holders

SG-4.8-15_1

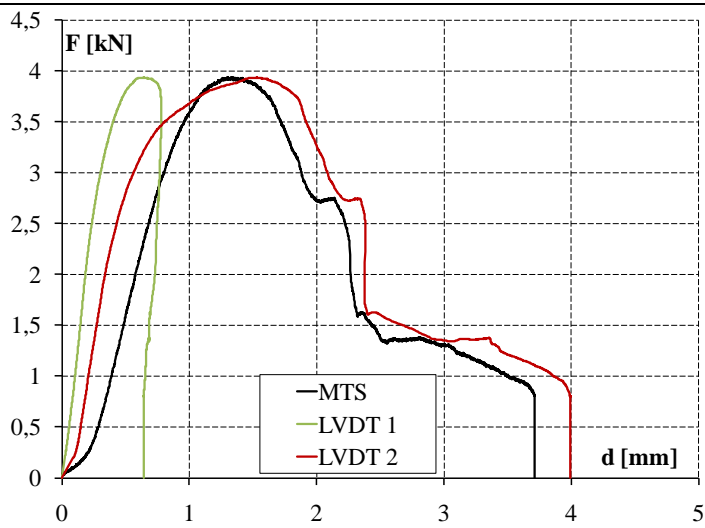


Test Results

Strength F_{max} [kN/mm]	3.48
Stiffness k [kN/mm]	5.15
Failure Mechanism:	Pull-out

Annotations:

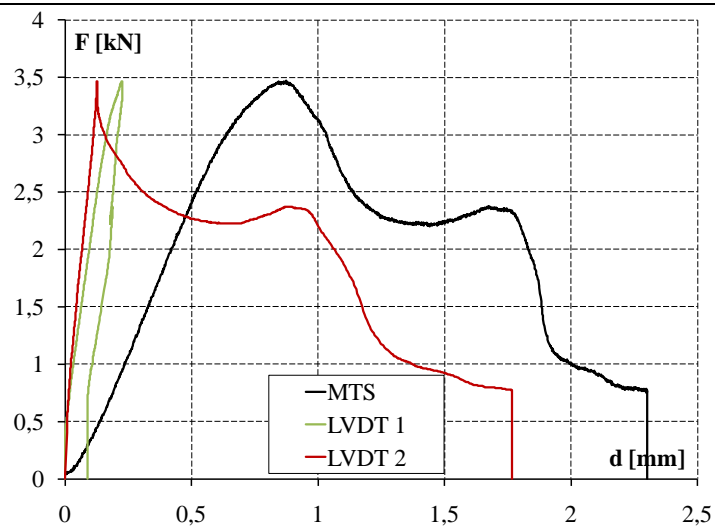
SG-4.8-15_2



Test Results

Strength F_{max} [kN/mm]	3.93
Stiffness k [kN/mm]	4.96
Failure Mechanism:	Pull-out
Annotations:	

SG-4.8-15_3

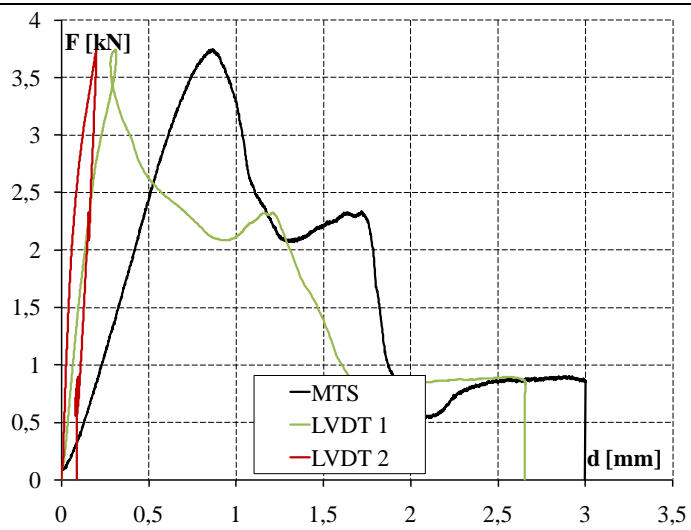


Test Results

Strength F_{max} [kN/mm]	3.46
Stiffness k [kN/mm]	5.14
Failure Mechanism:	Pull-out

Annotations:

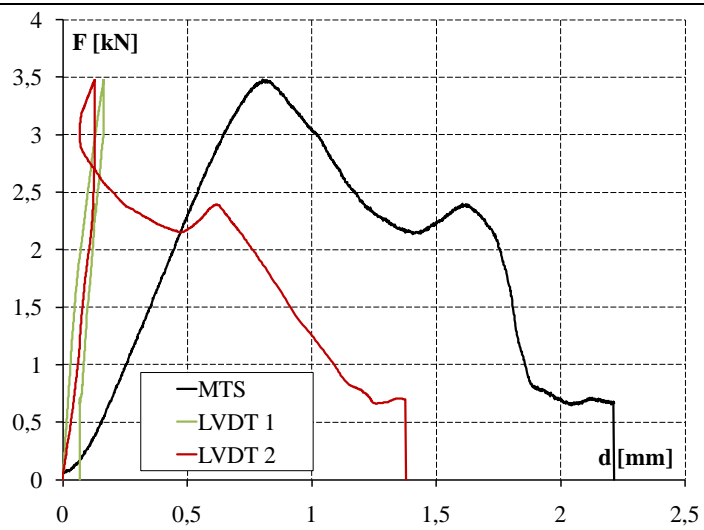
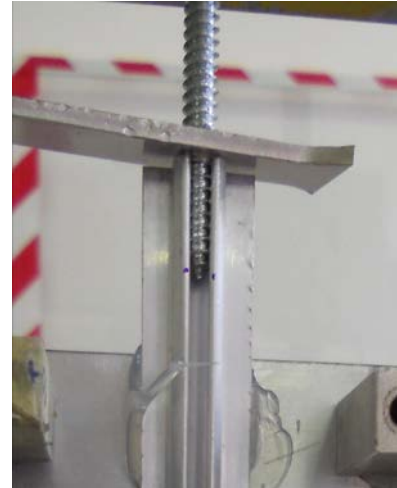
SG-4.8-15_4



Test Results

Strength F_{max} [kN/mm]	3.74
Stiffness k [kN/mm]	5.05
Failure Mechanism:	Pull-out
Annotations:	

SG-4.8-15_5

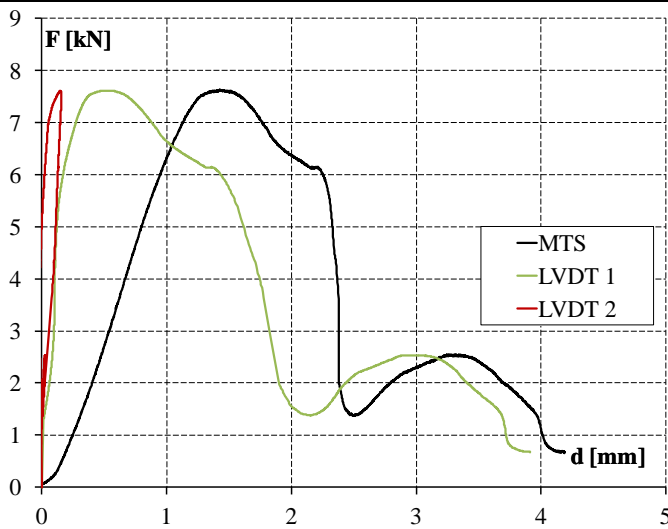


Test Results

Strength F_{max} [kN/mm]	3.47
Stiffness k [kN/mm]	5.02
Failure Mechanism:	Pull-out

Annotations:

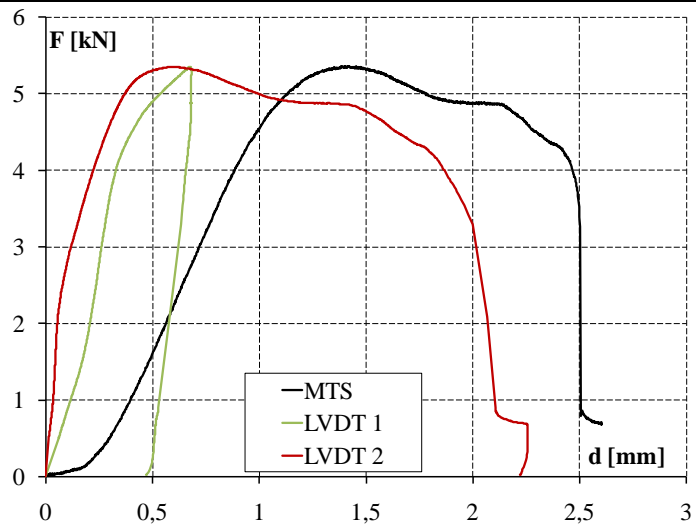
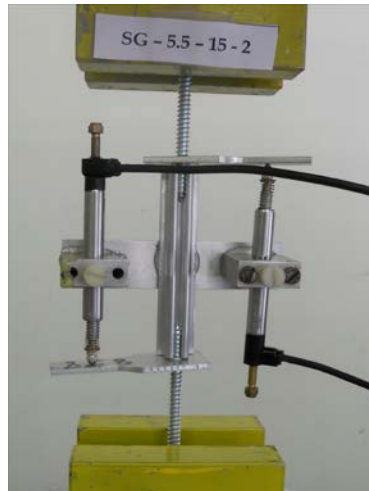
SG-5.5-15_1



Test Results

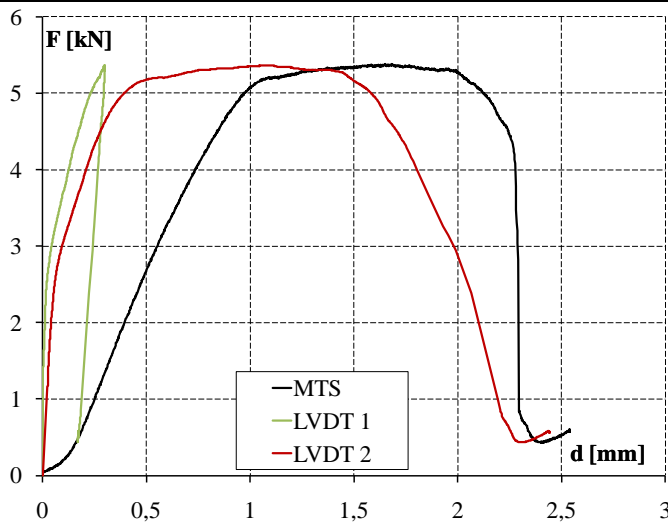
Strength F_{max} [kN/mm]	7.62
Stiffness k [kN/mm]	6.81
Failure Mechanism:	Pull-out
Annotations:	

SG-5.5-15_2



Test Results	
Strength F_{max} [kN/mm]	5.35
Stiffness k [kN/mm]	6.05
Failure Mechanism:	Pull-out
Annotations:	

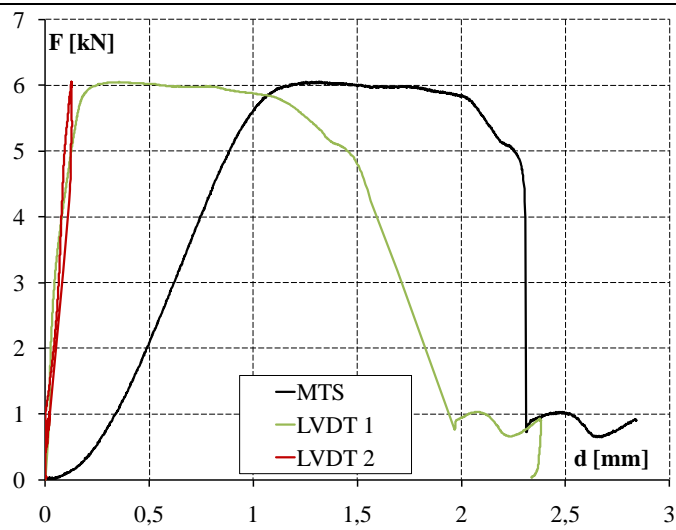
SG-5.5-15_3



Test Results

Strength F_{max} [kN/mm]	5.36
Stiffness k [kN/mm]	6.82
Failure Mechanism:	Pull-out
Annotations:	

SG-5.5-15_4

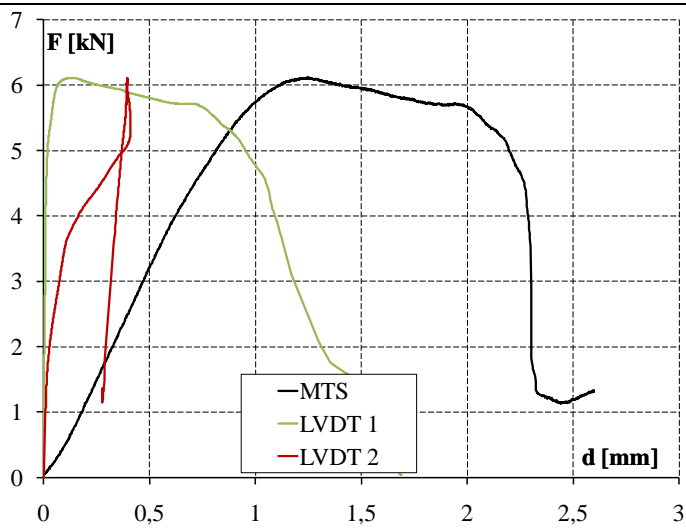
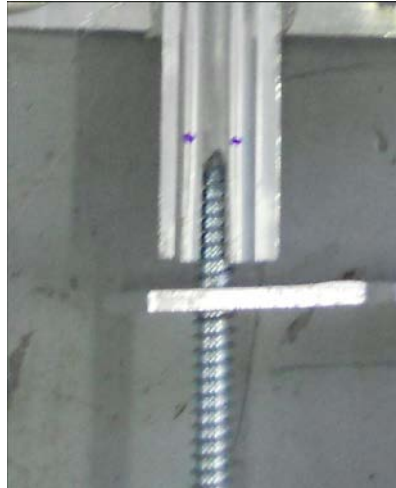


Test Results

Strength F_{max} [kN/mm]	6.05
Stiffness k [kN/mm]	6.87
Failure Mechanism:	Pull-out

Annotations:

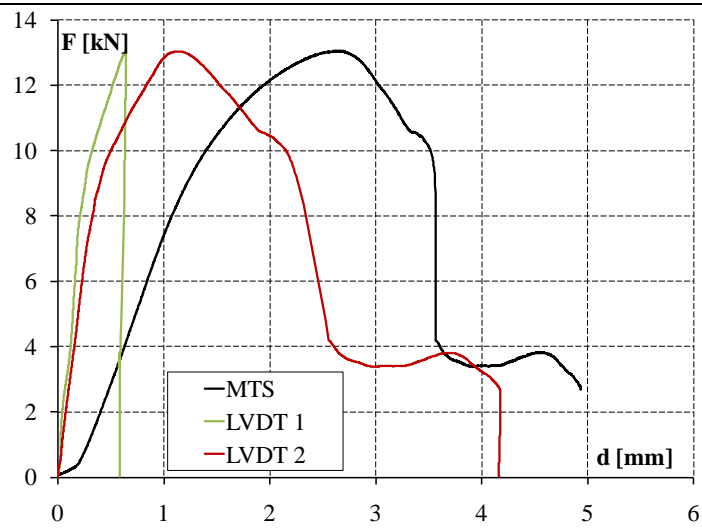
SG-5.5-15_5



Test Results

Strength F_{max} [kN/mm]	6.11
Stiffness k [kN/mm]	6.77
Failure Mechanism:	Pull-out
Annotations:	

SG-5.5-30_1



Test Results

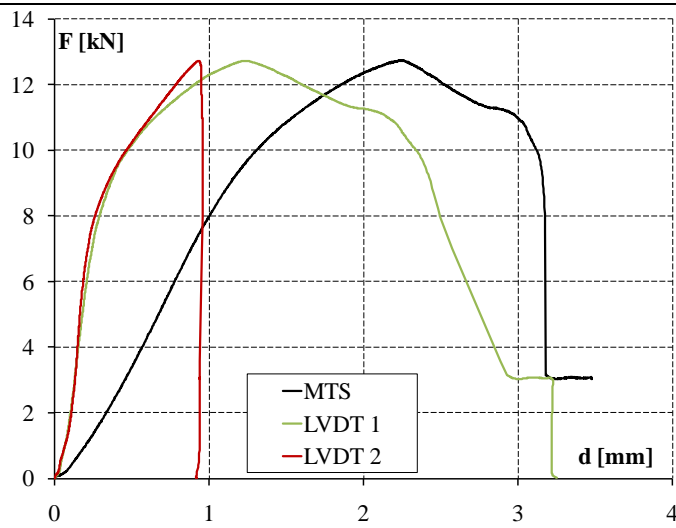
Strength F_{max} [kN/mm]	13.04
----------------------------	-------

Stiffness k [kN/mm]	8.59
-----------------------	------

Failure Mechanism:	Pull-out
--------------------	----------

Annotations:	
--------------	--

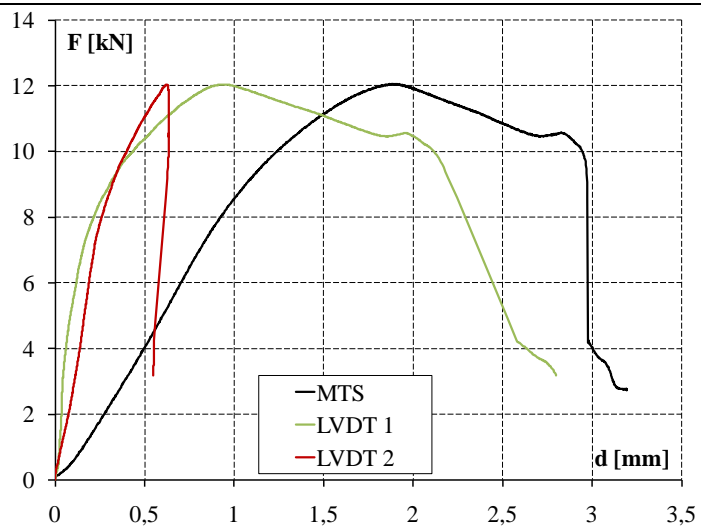
SG-5.5-30_2



Test Results

Strength F_{max} [kN/mm]	12.73
Stiffness k [kN/mm]	8.09
Failure Mechanism:	Pull-out
Annotations:	

SG-5.5-30_3



Test Results

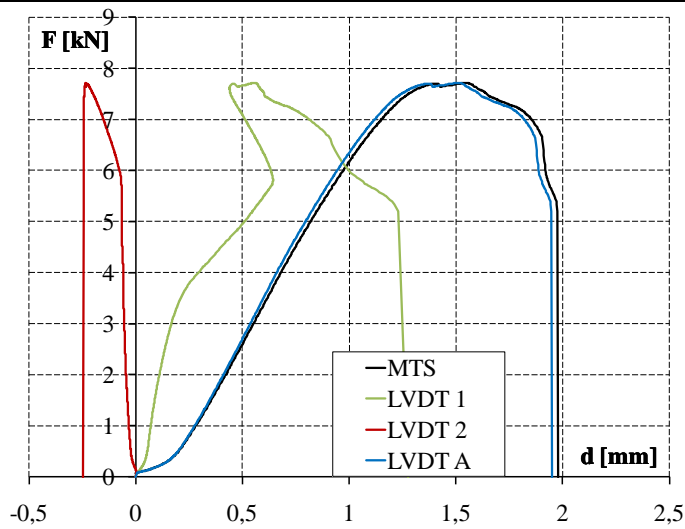
Strength F_{max} [kN/mm]	12.04
----------------------------	-------

Stiffness k [kN/mm]	8.75
-----------------------	------

Failure Mechanism:	Pull-out
--------------------	----------

Annotations:	
--------------	--

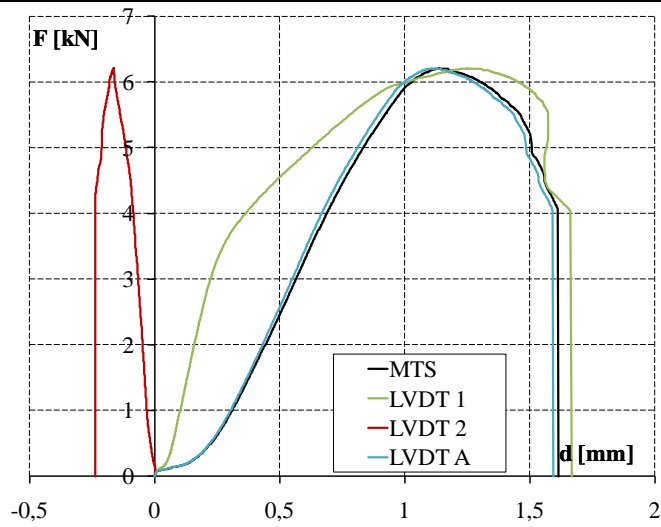
ST-5.5-7.5_1



Test Results

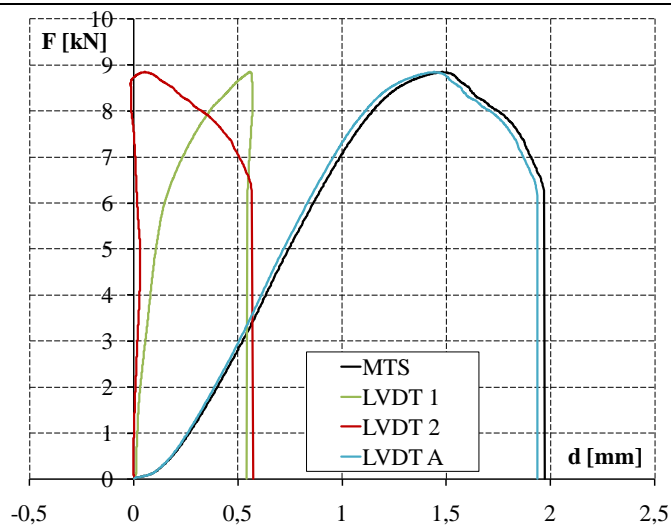
Strength F_{max} [kN/mm]	7.71
Stiffness k [kN/mm]	7.66
Failure Mechanism:	Pull-out
Annotations:	

ST-5.5-7.5_2



Test Results	
Strength F_{max} [kN/mm]	6.21
Stiffness k [kN/mm]	8.08
Failure Mechanism:	Pull-out
Annotations:	

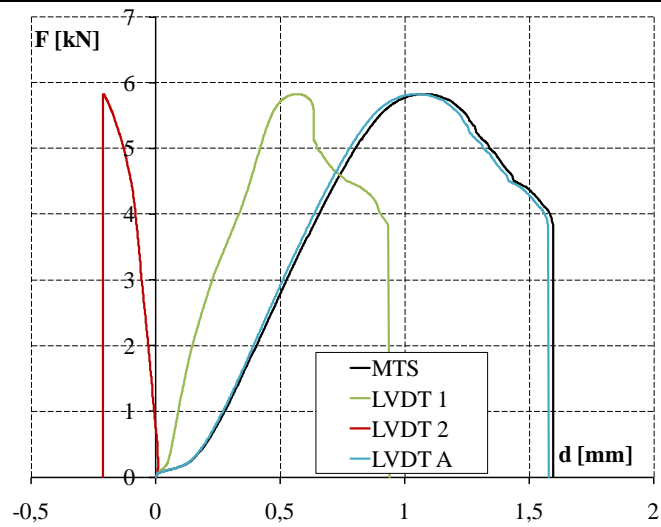
ST-5.5-7.5_3



Test Results

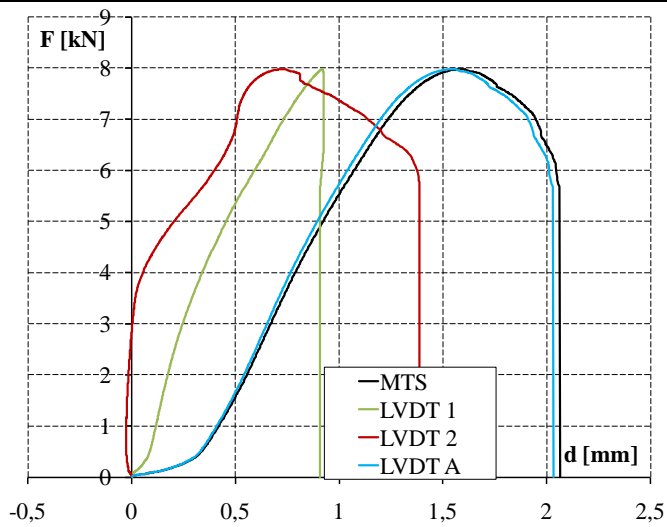
Strength F_{max} [kN/mm]	8.85
Stiffness k [kN/mm]	8.75
Failure Mechanism:	Pull-out
Annotations:	

ST-5.5-7.5_4



Test Results	
Strength F_{max} [kN/mm]	5.85
Stiffness k [kN/mm]	7.97
Failure Mechanism:	Pull-out
Annotations:	

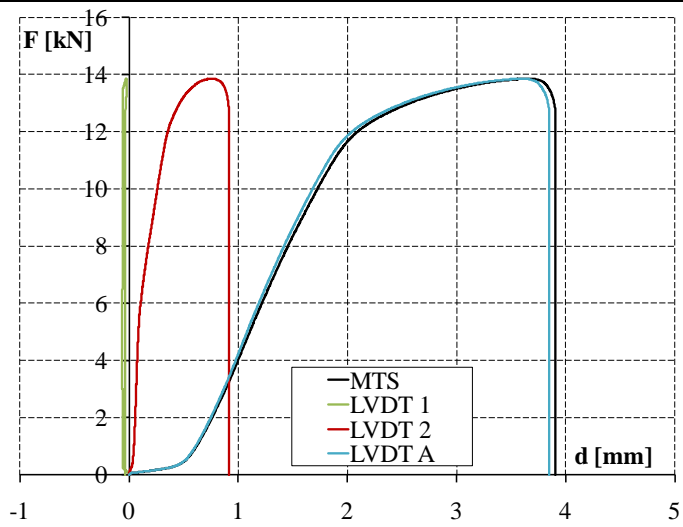
ST-5.5-7.5_5



Test Results

Strength F_{max} [kN/mm]	7.98
Stiffness k [kN/mm]	8.42
Failure Mechanism:	Pull-out
Annotations:	

ST-5.5-10_1



Test Results

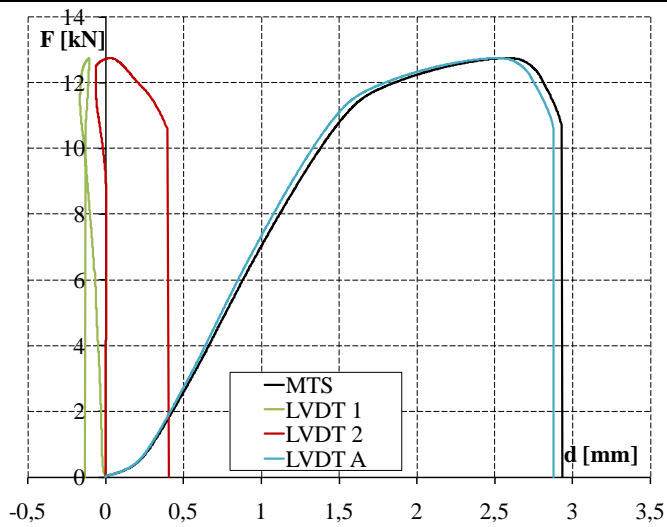
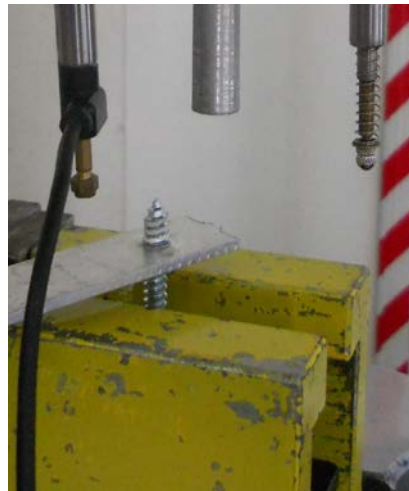
Strength F_{max} [kN/mm]	13.85
----------------------------	-------

Stiffness k [kN/mm]	8.77
-----------------------	------

Failure Mechanism:	Screw failure
--------------------	---------------

Annotations:	
--------------	--

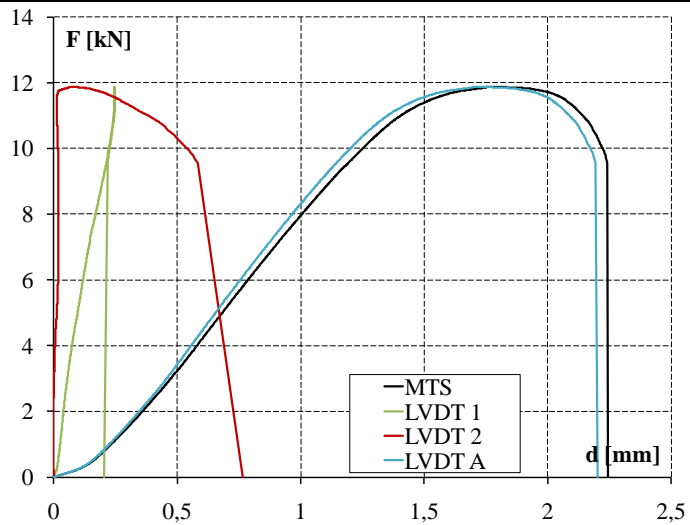
ST-5.5-10_2



Test Results

Strength F_{max} [kN/mm]	12.75
Stiffness k [kN/mm]	8.83
Failure Mechanism:	Pull-out
Annotations:	

ST-5.5-10_3

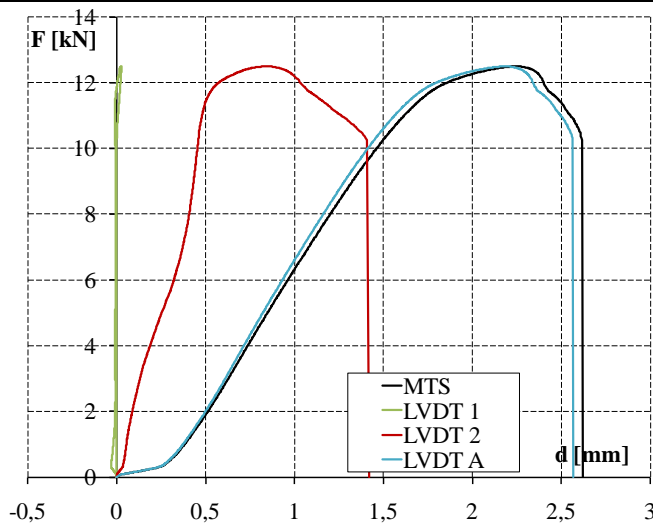


Test Results

Strength F_{max} [kN/mm]	11.88
Stiffness k [kN/mm]	9.39
Failure Mechanism:	Pull-out

Annotations:

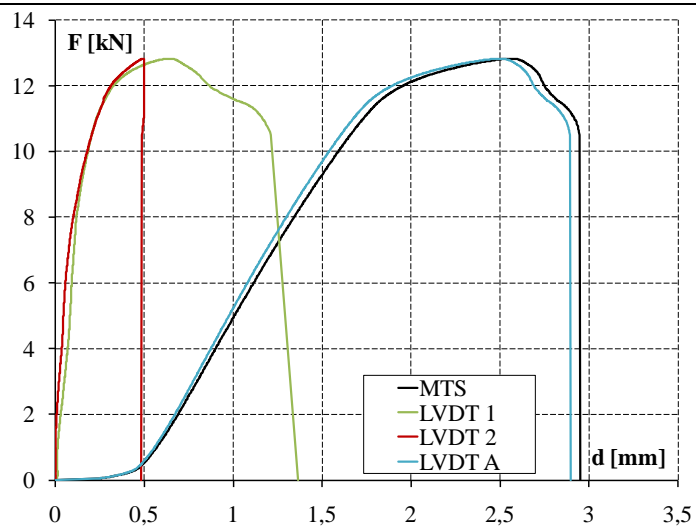
ST-5.5-10_4



Test Results

Strength F_{max} [kN/mm]	12.49
Stiffness k [kN/mm]	8.89
Failure Mechanism:	Pull-out
Annotations:	

ST-5.5-10_5



Test Results

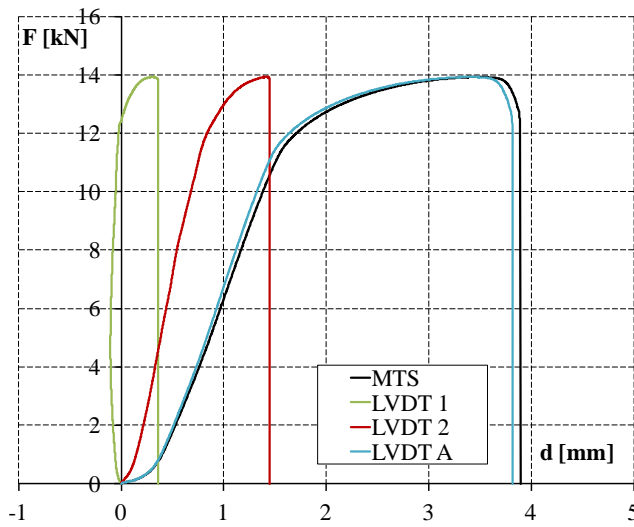
Strength F_{max} [kN/mm]	12.82
----------------------------	-------

Stiffness k [kN/mm]	9.42
-----------------------	------

Failure Mechanism:	Pull-out
--------------------	----------

Annotations:	
--------------	--

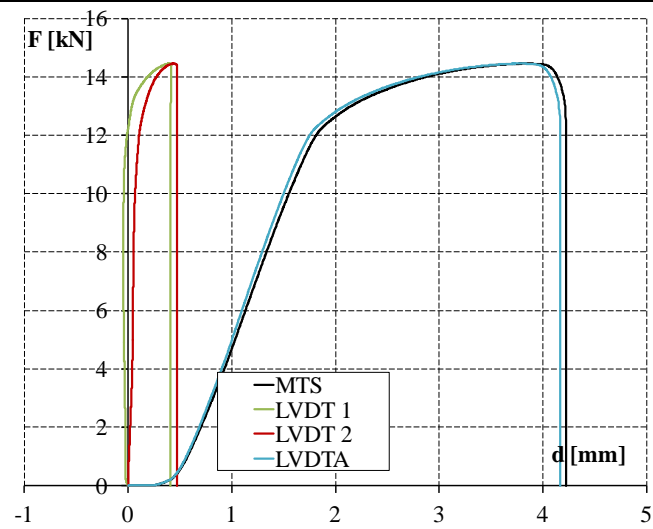
ST-5.5-15_1



Test Results

Strength F_{max} [kN/mm]	13.93
Stiffness k [kN/mm]	9.09
Failure Mechanism:	Screw failure
Annotations:	

ST-5.5-15_2



Test Results

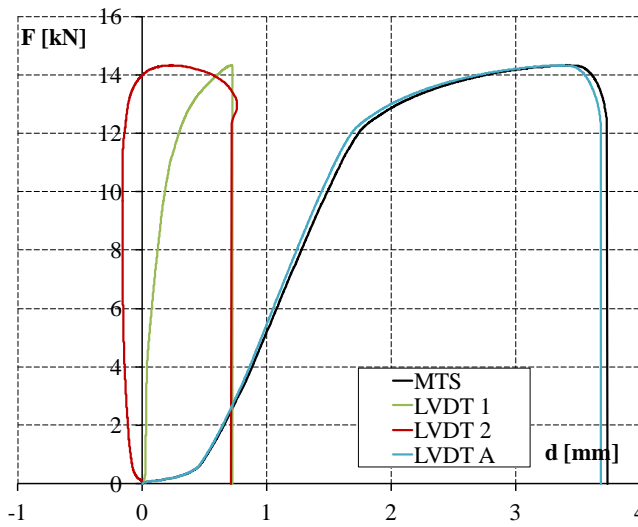
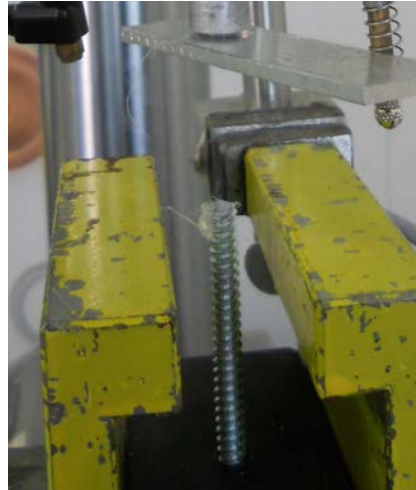
Strength F_{max} [kN/mm]	14.46
----------------------------	-------

Stiffness k [kN/mm]	9.33
-----------------------	------

Failure Mechanism:	Screw failure
--------------------	---------------

Annotations:	
--------------	--

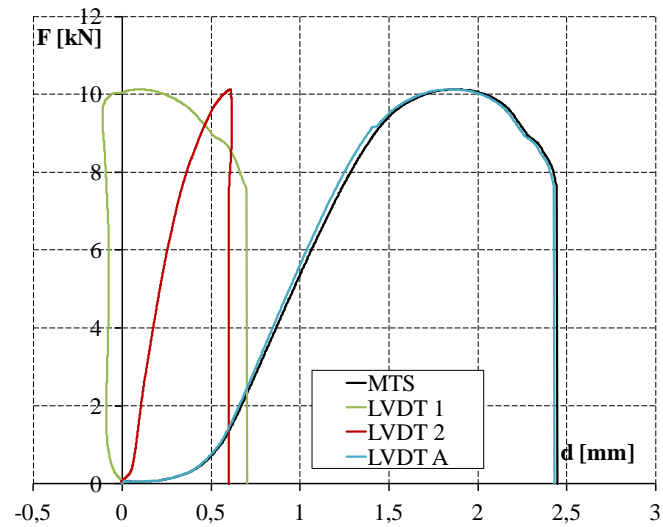
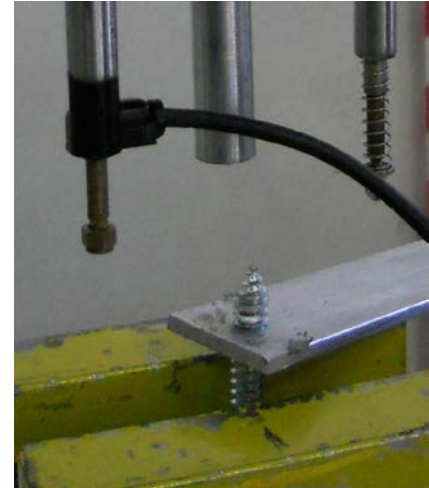
ST-5.5-15_3



Test Results

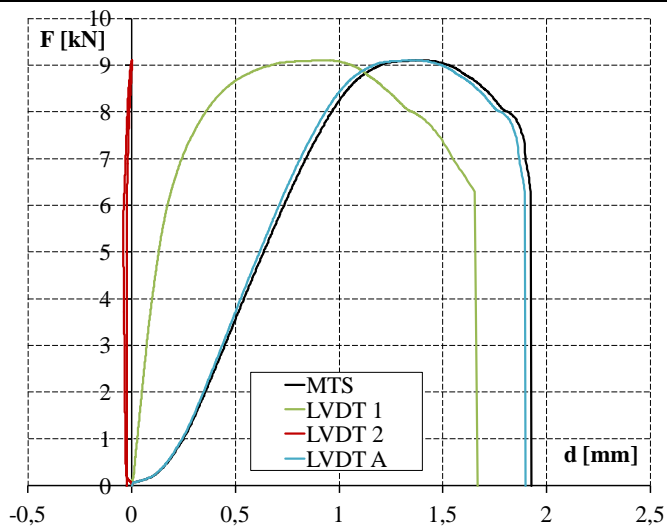
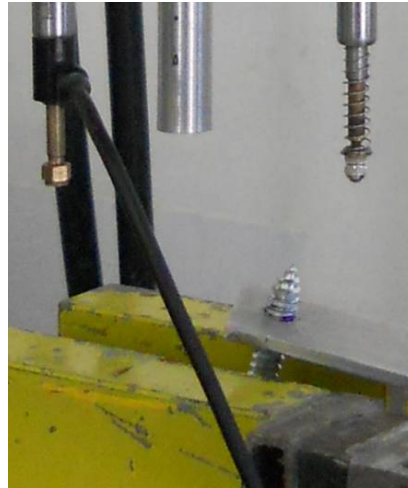
Strength F_{max} [kN/mm]	14.33
Stiffness k [kN/mm]	9.44
Failure Mechanism:	Screw failure
Annotations:	

ST-6.3-10_1



Test Results	
Strength F_{max} [kN/mm]	10.13
Stiffness k [kN/mm]	10.49
Failure Mechanism:	Pull-out
Annotations:	

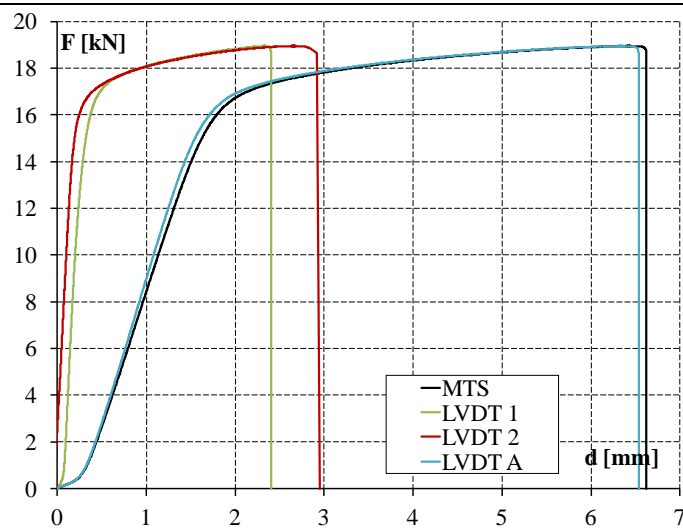
ST-6.3-10_2



Test Results

Strength F_{max} [kN/mm]	9.10
Stiffness k [kN/mm]	10.14
Failure Mechanism:	Pull-out
Annotations:	

ST-6.3-15_1



Test Results

Strength F_{max} [kN/mm]

18.95

Stiffness k [kN/mm]

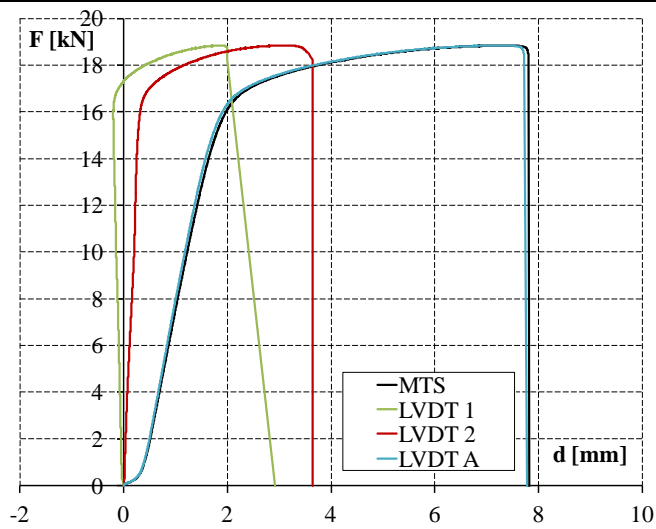
11.70

Failure Mechanism:

Aluminium failure

Annotations:

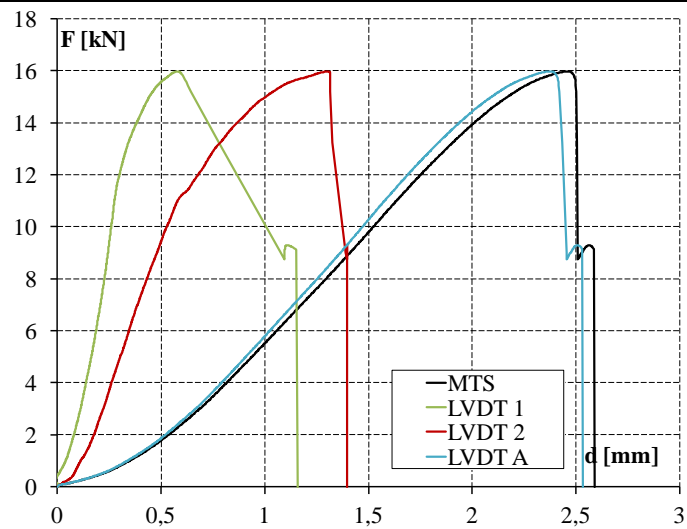
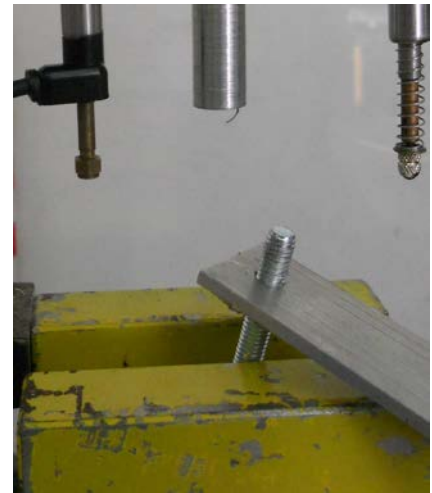
ST-6.3-15_2



Test Results

Strength F_{max} [kN/mm]	18.85
Stiffness k [kN/mm]	11.21
Failure Mechanism:	Aluminium failure
Annotations:	

ST-M6-10_1



Test Results

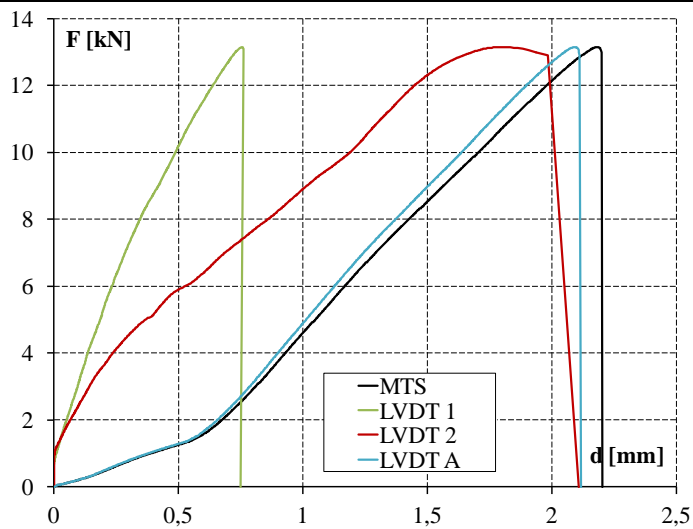
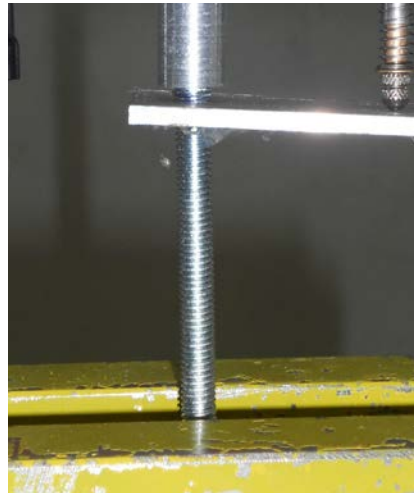
Strength F_{max} [kN/mm]	15.96
----------------------------	-------

Stiffness k [kN/mm]	7.92
-----------------------	------

Failure Mechanism:	Pull-out
--------------------	----------

Annotations:

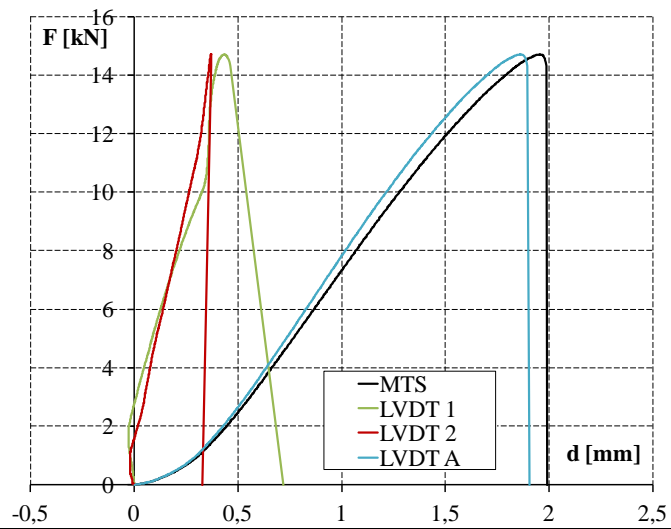
ST-M6-10_2



Test Results

Strength F_{max} [kN/mm]	13.15
Stiffness k [kN/mm]	8.09
Failure Mechanism:	Pull-out
Annotations:	

ST-M6-10_3

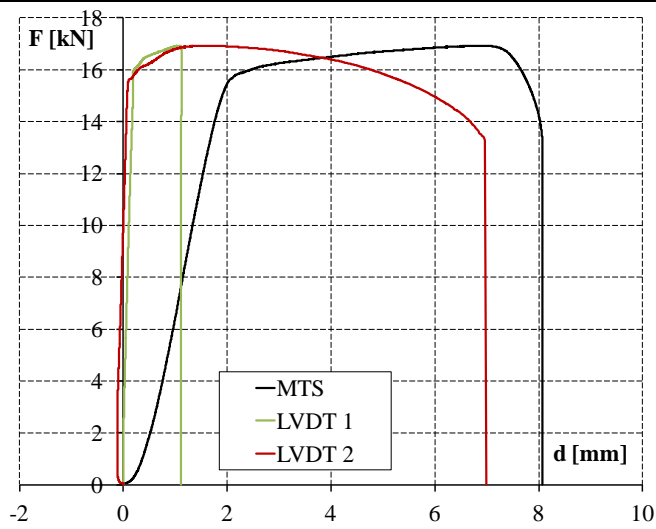
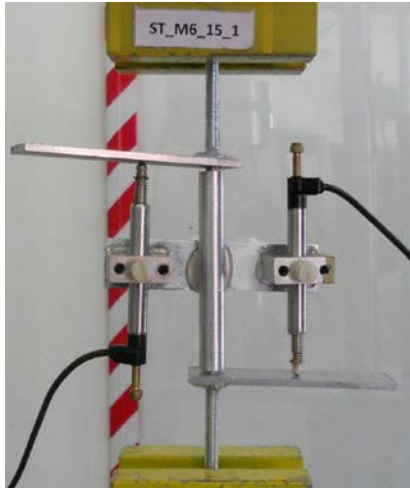


Test Results

Strength F_{max} [kN/mm]	14.71
Stiffness k [kN/mm]	9.75
Failure Mechanism:	Pull-out

Annotations:

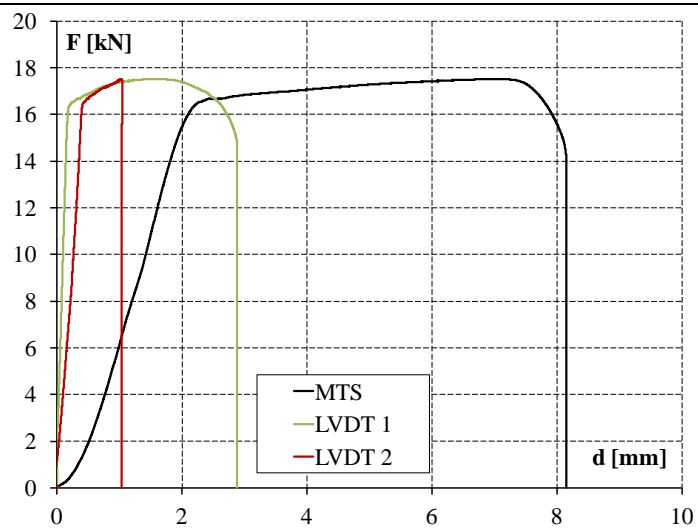
ST-M6-15_1



Test Results

Strength F_{max} [kN/mm]	16.92
Stiffness k [kN/mm]	9.85
Failure Mechanism:	Screw failure
Annotations:	

ST-M6-15_2



Test Results

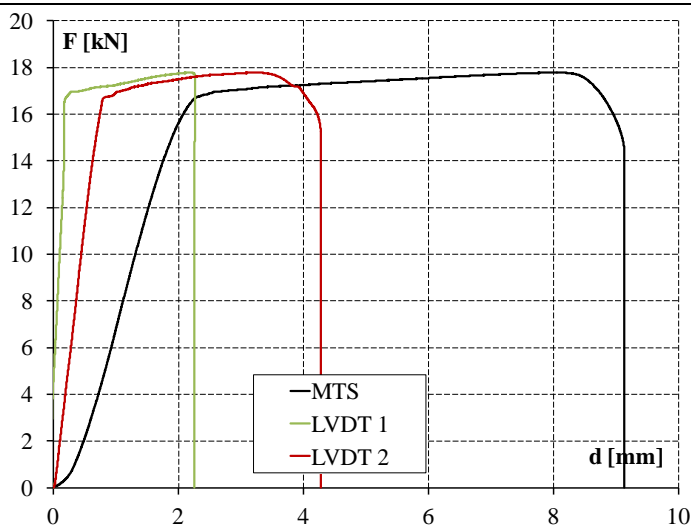
Strength F_{max} [kN/mm]	17.51
----------------------------	-------

Stiffness k [kN/mm]	8.94
-----------------------	------

Failure Mechanism:	Screw failure
--------------------	---------------

Annotations:

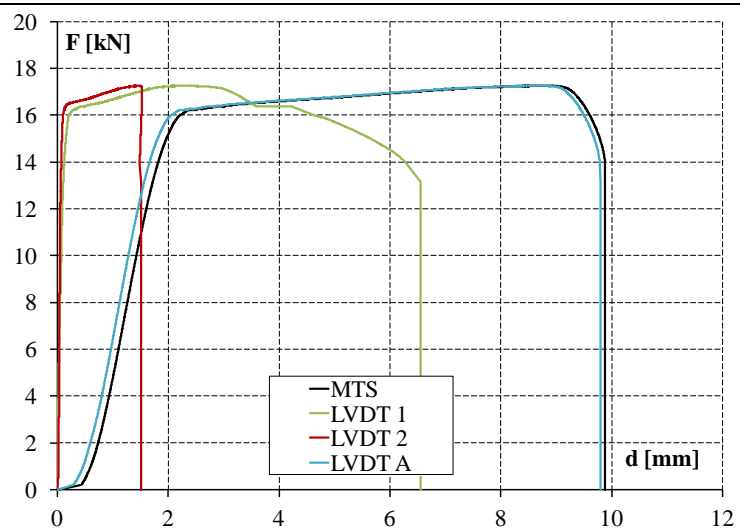
ST-M6-15_3



Test Results

Strength F_{max} [kN/mm]	17.78
Stiffness k [kN/mm]	9.52
Failure mechanism:	Screw failure
Annotations:	

ST-M6-15_4



Test Results

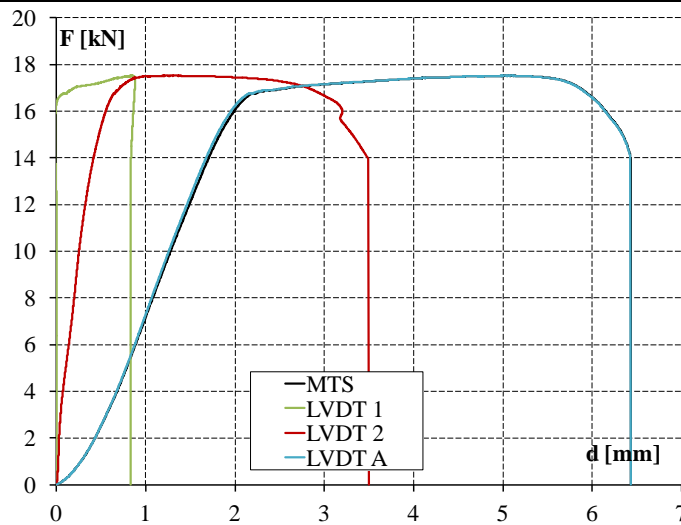
Strength F_{max} [kN/mm]	17.26
----------------------------	-------

Stiffness k [kN/mm]	12.01
-----------------------	-------

Failure Mechanism:	Screw failure
--------------------	---------------

Annotations:

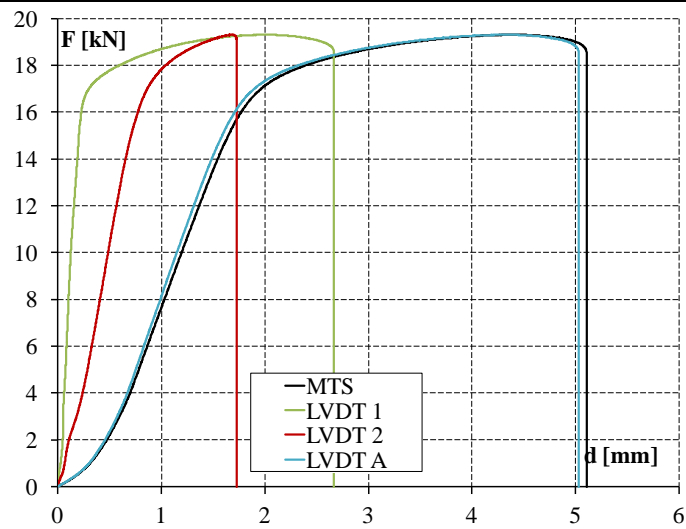
ST-M6-15_5



Test Results

Strength F_{max} [kN/mm]	17.52
Stiffness k [kN/mm]	9.85
Failure Mechanism:	Screw failure
Annotations:	

ST-M6H-15_1



Test Results

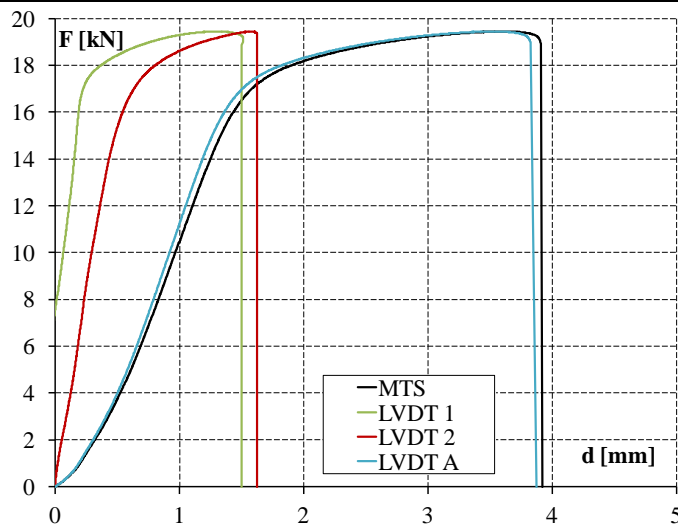
Strength F_{max} [kN/mm]	19.31
----------------------------	-------

Stiffness k [kN/mm]	12.02
-----------------------	-------

Failure Mechanism:	Aluminium failure
--------------------	-------------------

Annotations:

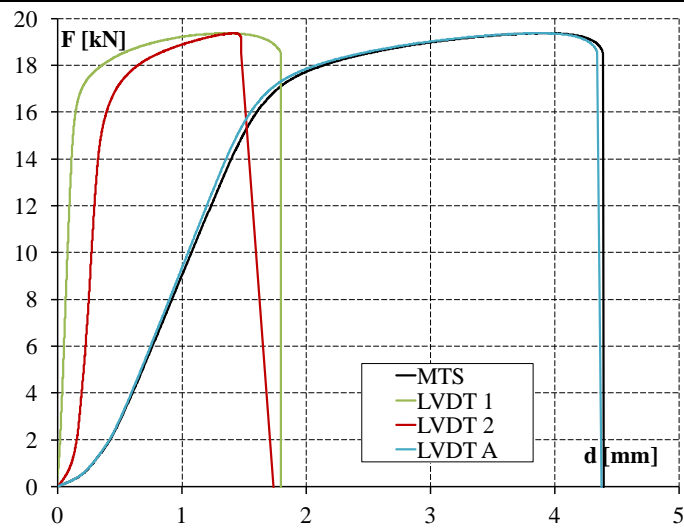
ST-M6H-15_2



Test Results

Strength F_{max} [kN/mm]	19.53
Stiffness k [kN/mm]	13.53
Failure Mechanism:	Aluminium failure
Annotations:	

ST-M6H-15_3



Test Results

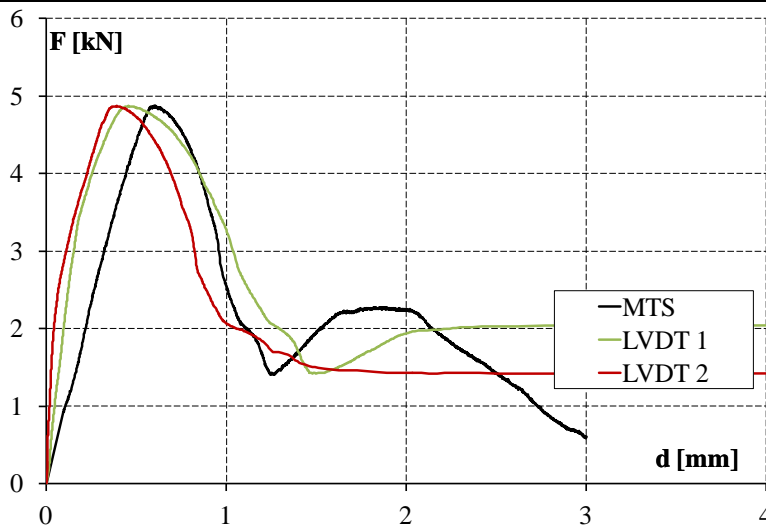
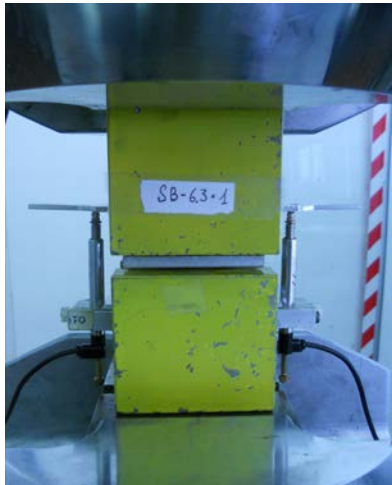
Strength F_{max} [kN/mm]	19.38
----------------------------	-------

Stiffness k [kN/mm]	12.60
-----------------------	-------

Failure Mechanism:	Aluminium failure
--------------------	-------------------

Annotations:

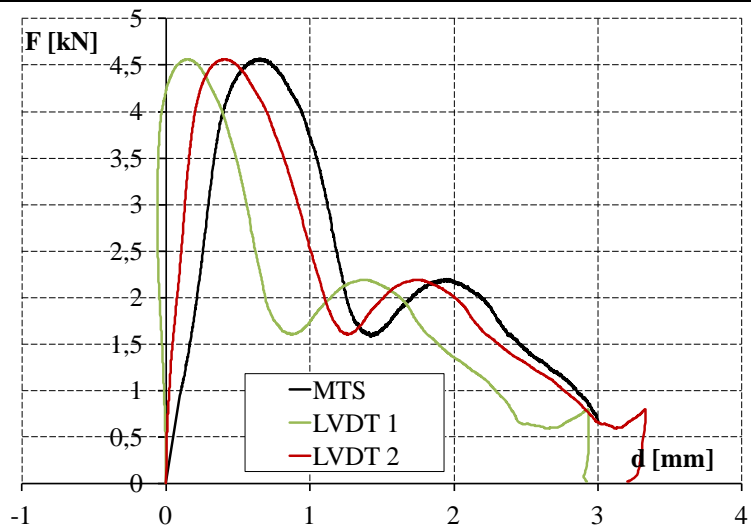
SB-6.3-15_1



Test Results

Strength F_{max} [kN/mm]	4.87
Stiffness k [kN/mm]	8.72
Failure Mechanism:	Pull-out
Annotations:	

SB-6.3-15_2

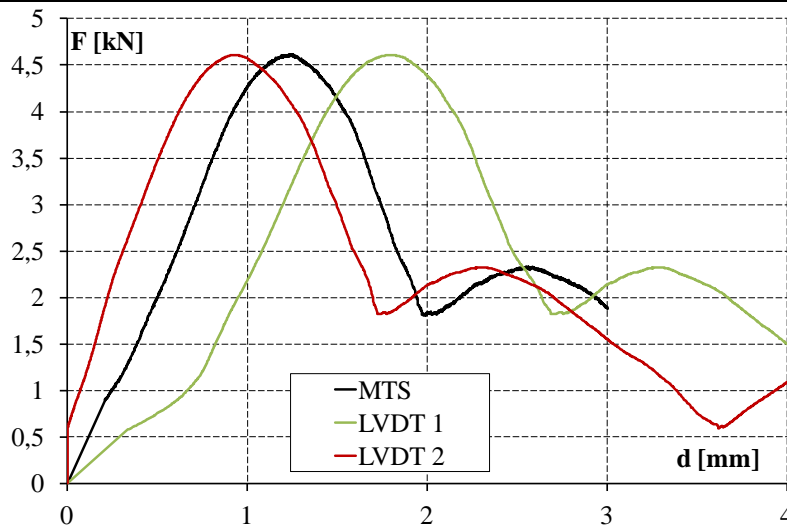


Test Results

Strength F_{max} [kN/mm]	4.56
Stiffness k [kN/mm]	8.59
Failure Mechanism:	Pull-out

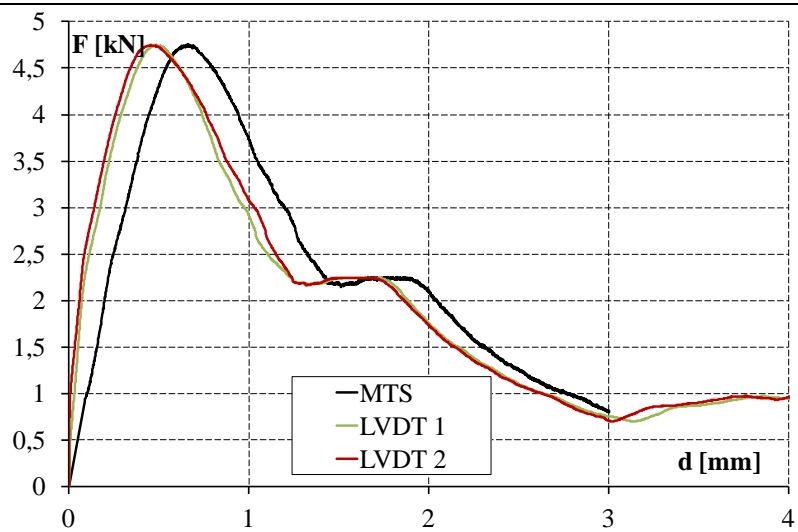
Annotations:

SB-6.3-15_3



Test Results	
Strength F_{max} [kN/mm]	4.61
Stiffness k [kN/mm]	3.78
Failure Mechanism:	Pull-out
Annotations:	

SB-6.3-15_4



Test Results

Strength F_{max} [kN/mm]	4.75
----------------------------	------

Stiffness k [kN/mm]	3.86
-----------------------	------

Failure Mechanism:	Pull-out
--------------------	----------

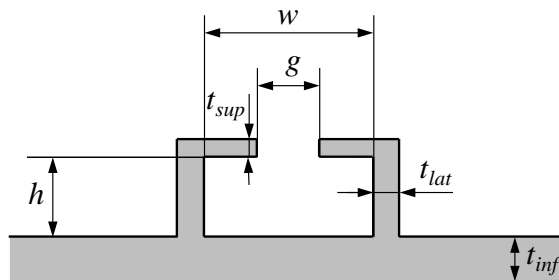
Annotations:

Appendix C

TESTS ON BOLT-CHANNEL JOINTS

Measured dimensions of Bolt-Channel Specimens

The dimensions of each specimen have been measured with a slide gauge. Hereafter the main geometrical parameter are summarised.



Measured dimensions for M10 specimens

Label	g	w	h	t_{int}	t_{lat}	t_{sup}
BC-SL-10_01	11.65	19.16	8.20	3.43	6.51	4.88
BC-SL-10_02	11.62	19.10	8.15	3.55	6.00	5.10
BC-SL-10_03	11.64	19.09	8.08	3.63	6.50	4.98
BC-SL-10_04	11.62	19.14	8.15	3.51	6.44	4.97
BC-SL-10_05	11.61	19.08	8.13	3.42	6.39	4.99
BC-SL-10_06	11.66	19.22	8.14	3.52	6.36	4.90
BC-SH-10_01	11.65	19.13	8.12	3.09	6.36	5.11
BC-SH-10_02	11.20	18.98	8.14	3.02	6.31	5.01
BC-SH-10_03	11.59	19.14	8.07	3.46	6.29	5.13
BC-PO-10_01	11.61	19.16	8.18	3.39	6.26	5.05
BC-PO-10_02	11.64	19.13	8.08	3.57	6.31	4.91
BC-PO-10_03	11.62	19.14	8.16	3.57	6.35	4.96
Average	11.59	19.12	8.13	3.43	6.34	5.00
Standard dev.	0.13	0.06	0.04	0.19	0.13	0.08
C.o.V.	0.01	0.003	0.005	0.06	0.02	0.02

Measured dimensions for M18 specimens

Label	g	w	h	t_{int}	t_{lat}	t_{sup}
BC-SL-18A_01	20.28	30.13	18.13	3.98	3.94	3.93
BC-SL-18A_02	20.05	30.08	18.00	3.96	3.90	4.33
BC-SL-18A_03	20.35	30.10	18.09	3.95	3.94	4.12
BC-SL-18A_04	20.20	29.79	18.00	3.97	3.96	4.17
BC-SL-18B_01	20.24	30.13	18.15	3.97	3.98	4.03
BC-SL-18B_02	20.20	30.18	18.05	3.97	3.99	4.15
BC-SL-18B_03	20.21	30.19	18.03	3.95	3.96	4.22
BC-SL-18B_04	20.05	30.00	18.14	3.97	3.93	4.08
BC-SH-18_01	20.50	30.25	18.13	3.97	3.92	4.03
BC-SH-18_02	20.54	30.27	17.93	3.99	3.95	4.09
BC-SH-18_03	20.48	30.23	18.14	3.95	3.92	3.96
BC-PO-18_01	20.31	30.08	18.12	4.09	3.96	3.97
BC-PO-18_02	20.29	30.13	18.06	4.04	3.97	4.01
BC-PO-18_03	20.35	29.93	18.11	4.07	4.00	4.12
Average	20.29	30.11	18.08	3.99	3.95	4.09
Standard dev.	0.15	0.13	0.07	0.05	0.03	0.11
C.o.V.	0.01	0.004	0.004	0.01	0.01	0.03

Instrumentation legend***Slip tests***

LVDT: transducer placed on bolt head

Shear tests

LVDT-B: transducer placed on bolt head

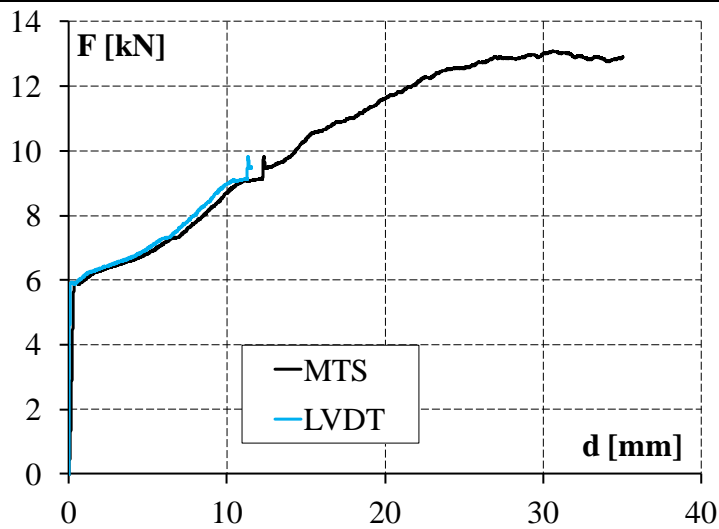
LVDT-S1: transducer placed at right support

LVDT-S2: transducer placed at left support

Pull-out tests

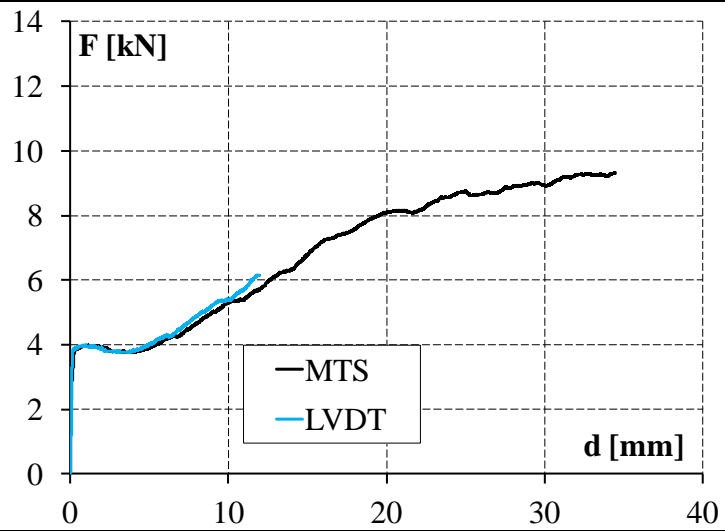
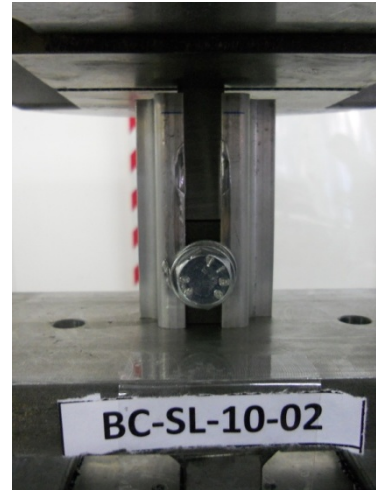
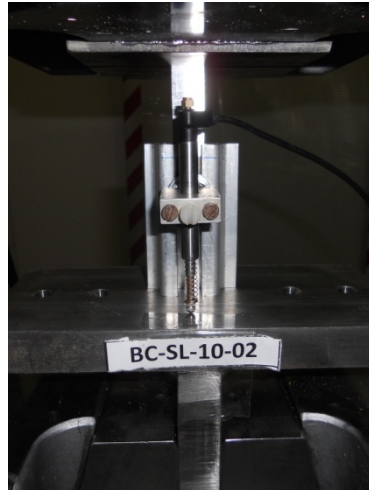
LVDT: transducer placed between the holder and the T-shaped element

BC-SL-10_1



Test Results	
Strength F_{max} [kN/mm]	5.94
Stiffness k [kN/mm]	25.23
Failure Mechanism:	Slipping up to max possible displacement
Annotations:	

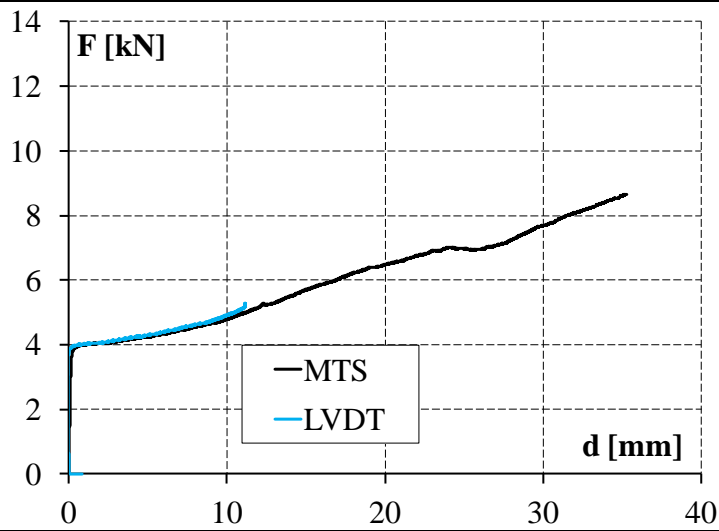
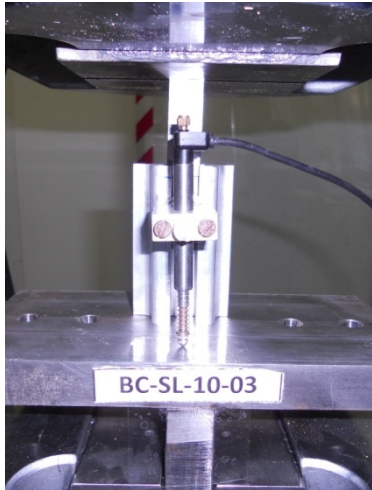
BC-SL-10_2



Test Results

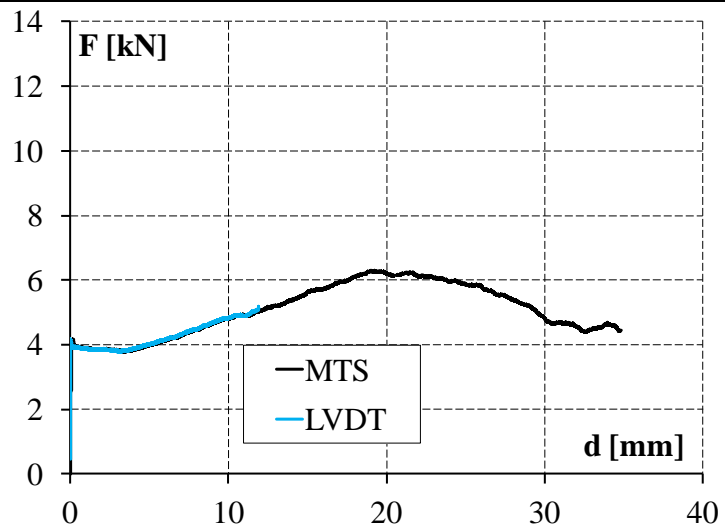
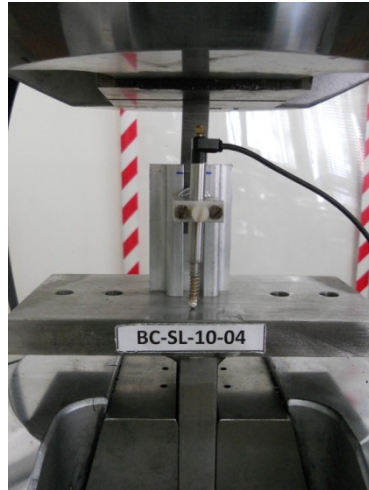
Strength F_{max} [kN/mm]	3.96
Stiffness k [kN/mm]	16.20
Failure Mechanism:	Slipping up to max possible displacement
Annotations:	

BC-SL-10_3



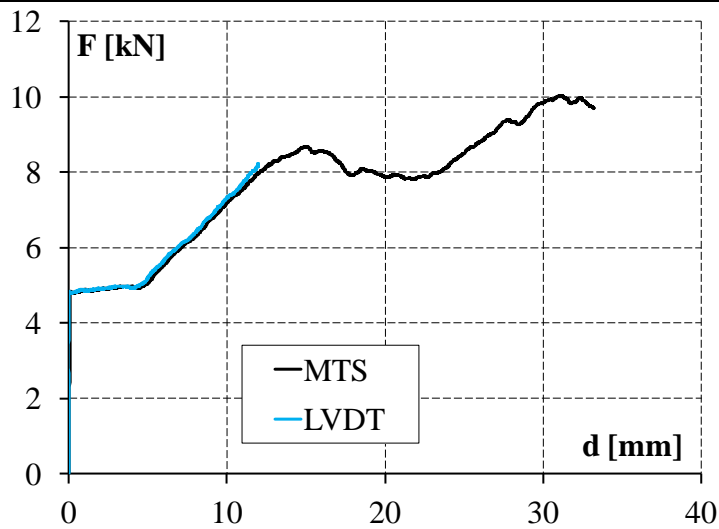
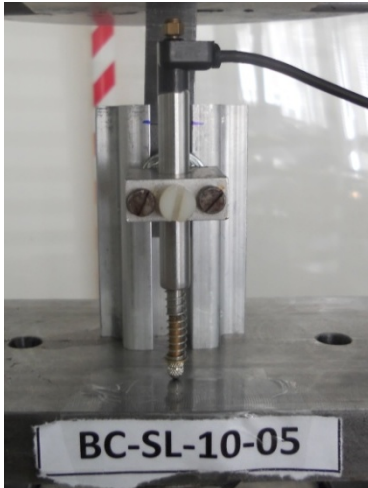
Test Results	
Strength F_{max} [kN/mm]	4.04
Stiffness k [kN/mm]	26.36
Failure Mechanism:	Slipping up to max possible displacement
Annotations:	

BC-SL-10_4



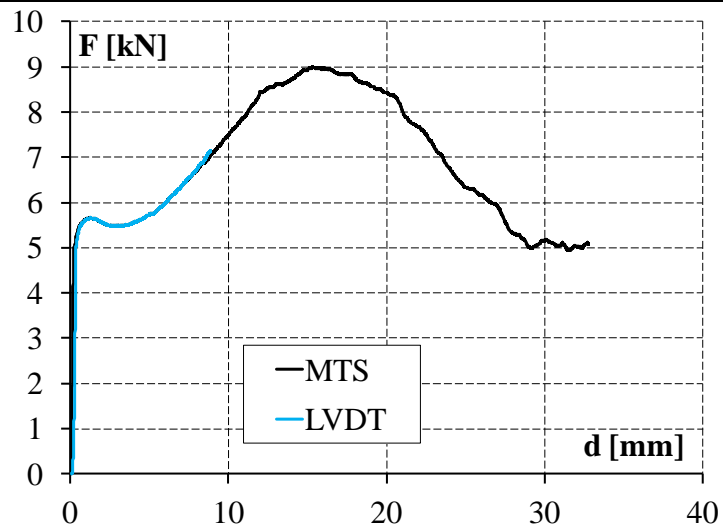
Test Results	
Strength F_{max} [kN/mm]	4.18
Stiffness k [kN/mm]	30.49
Failure Mechanism:	Slipping up to max possible displacement
Annotations:	

BC-SL-10_5



Test Results	
Strength F_{max} [kN/mm]	4.86
Stiffness k [kN/mm]	59.89
Failure Mechanism:	Slipping up to max possible displacement
Annotations:	

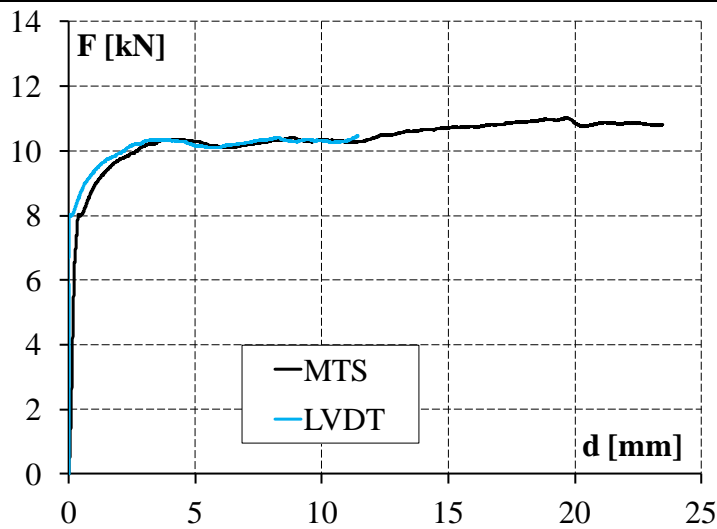
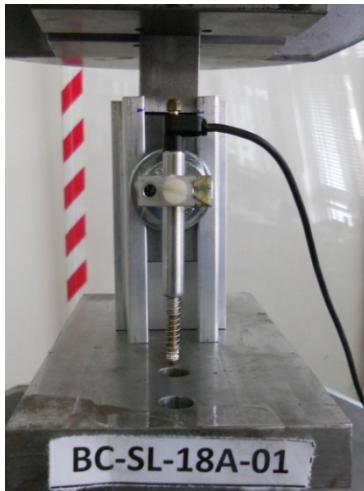
BC-SL-10_6



Test Results

Strength F_{max} [kN/mm]	5.66
Stiffness k [kN/mm]	32.91
Failure Mechanism:	Slipping up to max possible displacement
Annotations:	

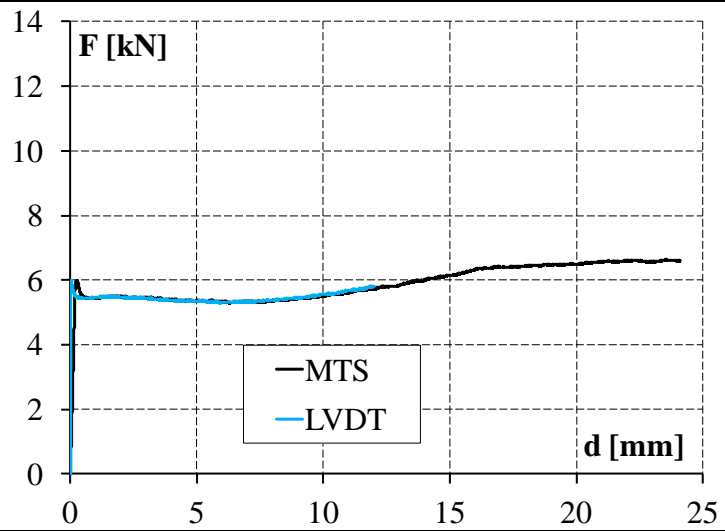
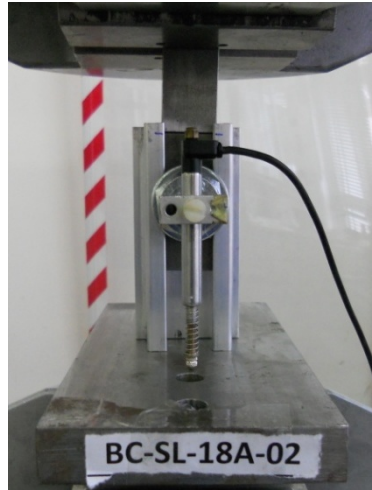
BC-SL-18A_1



Test Results

Strength F_{max} [kN/mm]	8.04
Stiffness k [kN/mm]	37.90
Failure Mechanism:	Slipping up to max possible displacement
Annotations:	

BC-SL-18A_2



Test Results

Strength F_{max} [kN/mm]

6.00

Stiffness k [kN/mm]

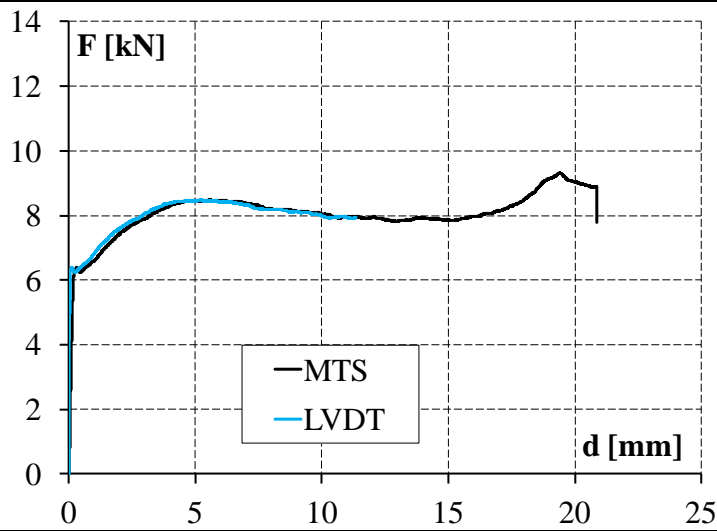
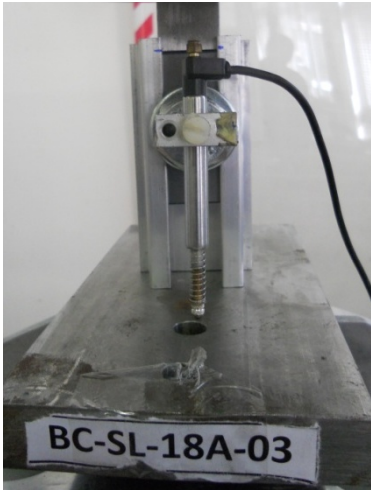
33.10

Failure Mechanism:

Slipping up to max possible displacement

Annotations:

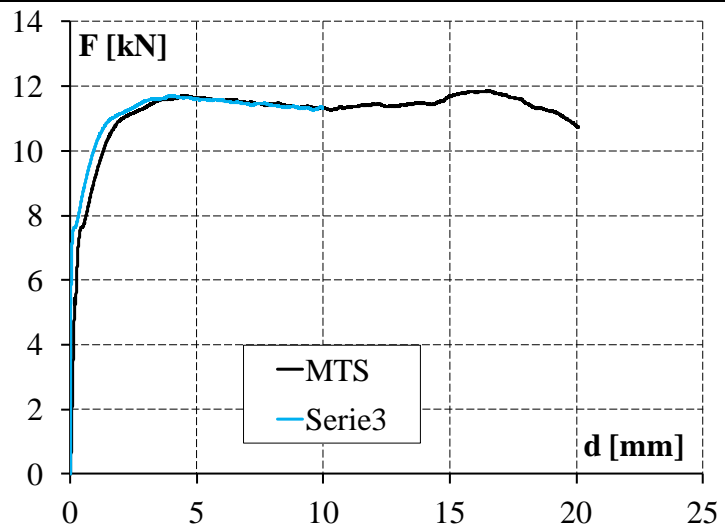
BC-SL-18A_3



Test Results

Strength F_{max} [kN/mm]	6.40
Stiffness k [kN/mm]	41.80
Failure Mechanism:	Slipping up to max possible displacement
Annotations:	

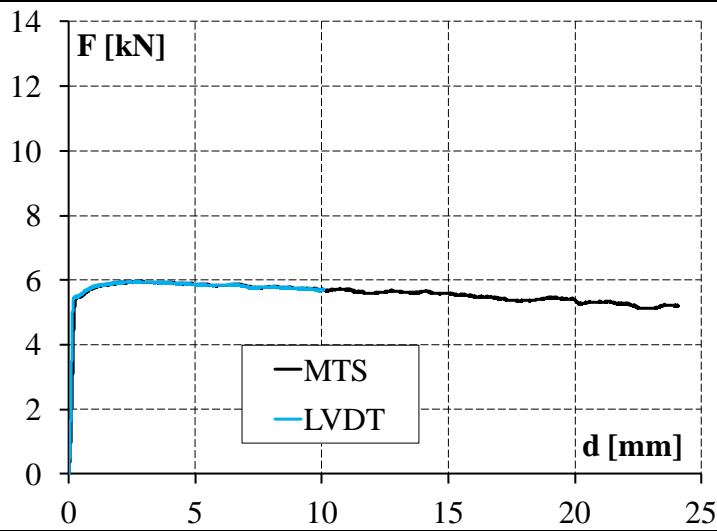
BC-SL-18A_4



Test Results

Strength F_{max} [kN/mm]	7.63
Stiffness k [kN/mm]	36.40
Failure Mechanism:	Slipping up to max possible displacement
Annotations:	

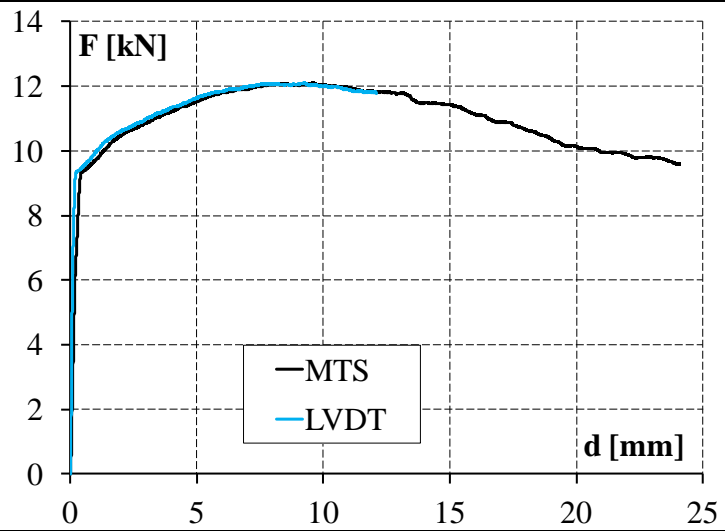
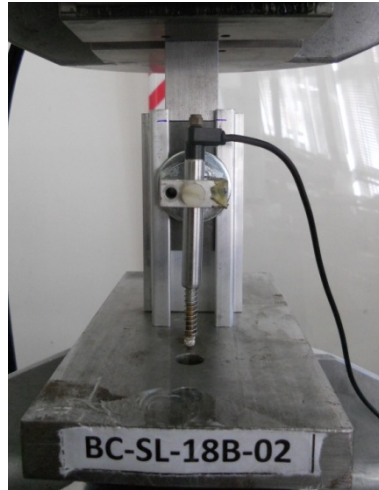
BC-SL-18B_1



Test Results

Strength F_{max} [kN/mm]	5.50
Stiffness k [kN/mm]	31.30
Failure Mechanism:	Slipping up to max possible displacement
Annotations:	

BC-SL-18B_2



Test Results

Strength F_{max} [kN/mm]

9.30

Stiffness k [kN/mm]

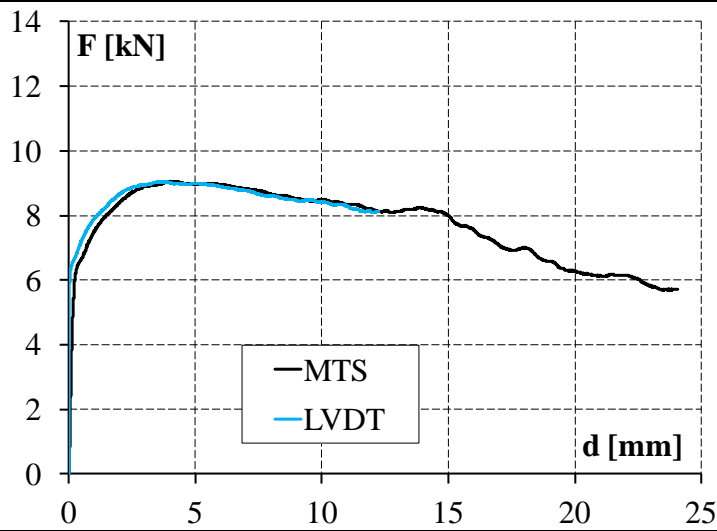
34.50

Failure Mechanism:

Slipping up to max possible displacement

Annotations:

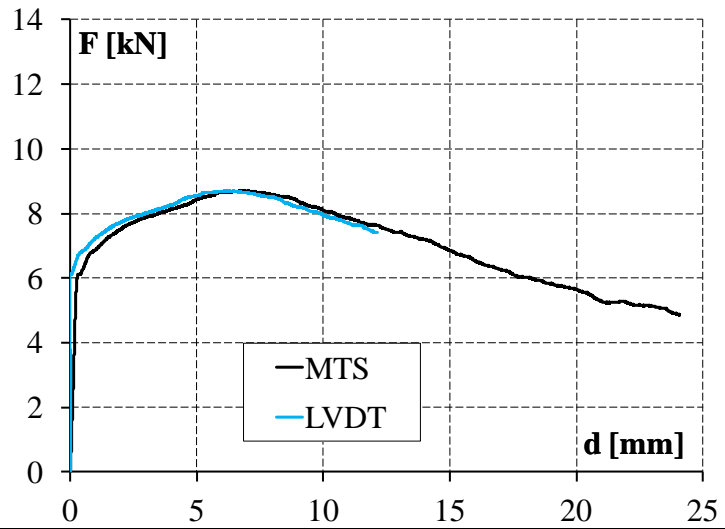
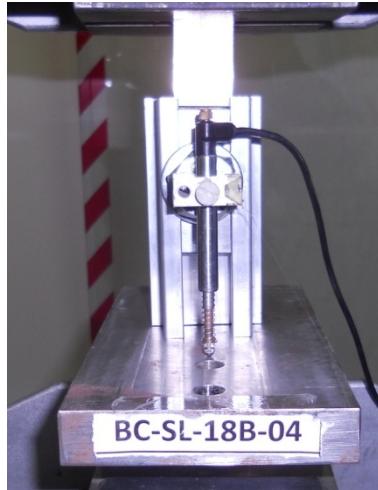
BC-SL-18B_3



Test Results

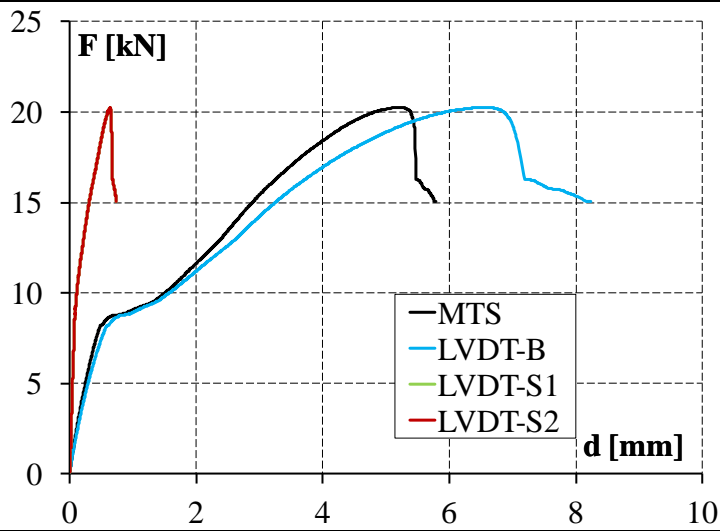
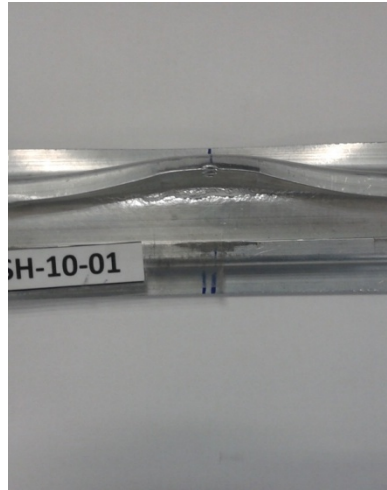
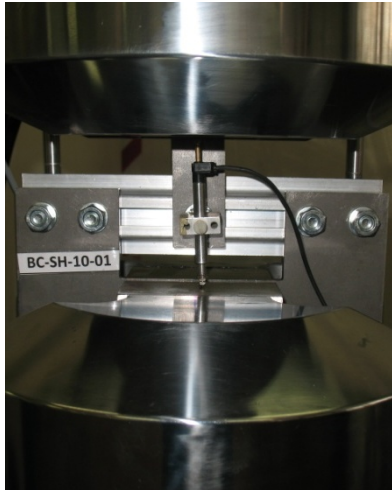
Strength F_{max} [kN/mm]	6.58
Stiffness k [kN/mm]	38.90
Failure Mechanism:	Slipping up to max possible displacement
Annotations:	

BC-SL-18B_4



Test Results	
Strength F_{max} [kN/mm]	6.13
Stiffness k [kN/mm]	27.30
Failure Mechanism:	Slipping up to max possible displacement
Annotations:	

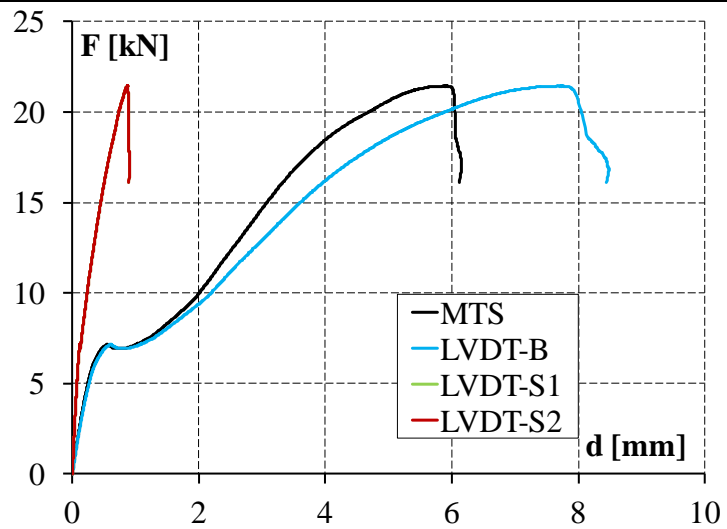
BC-SH-10_1



Test Results

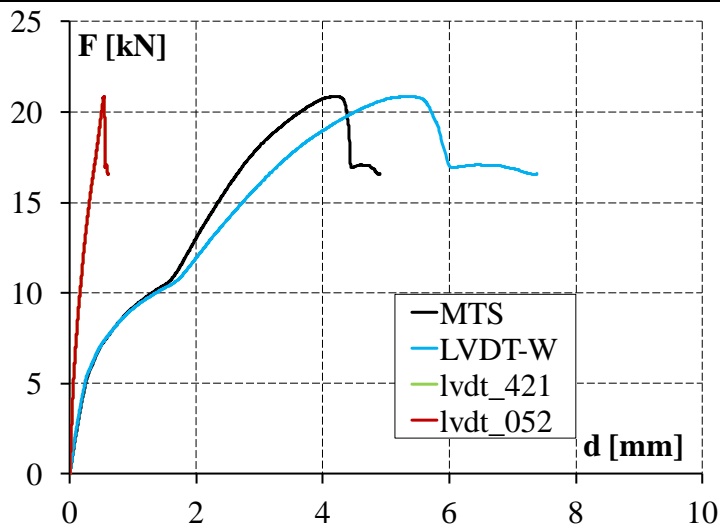
Strength F_{max} [kN/mm]	20.20
Stiffness k [kN/mm]	20.00
Failure Mechanism:	Cracking of bottom flange
Annotations:	

BC-SH-10_2



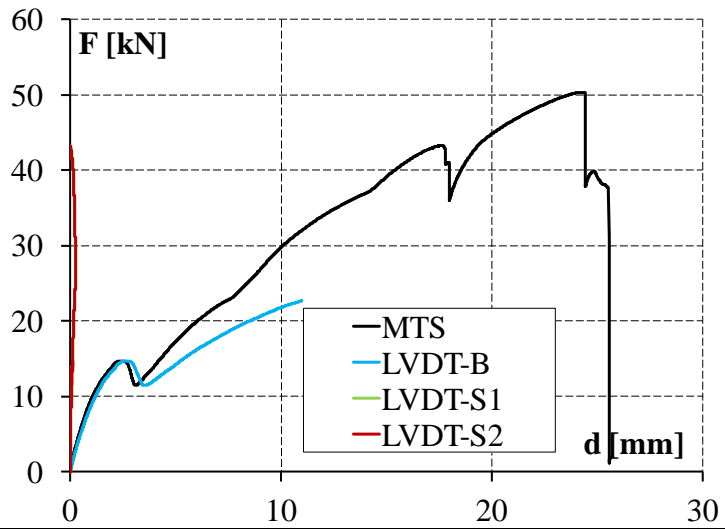
Test Results	
Strength F_{max} [kN/mm]	21.40
Stiffness k [kN/mm]	20.20
Failure Mechanism:	Cracking of bottom flange
Annotations:	

BC-SH-10_3



Test Results	
Strength F_{max} [kN/mm]	20.90
Stiffness k [kN/mm]	20.80
Failure Mechanism:	Cracking of bottom flange
Annotations:	

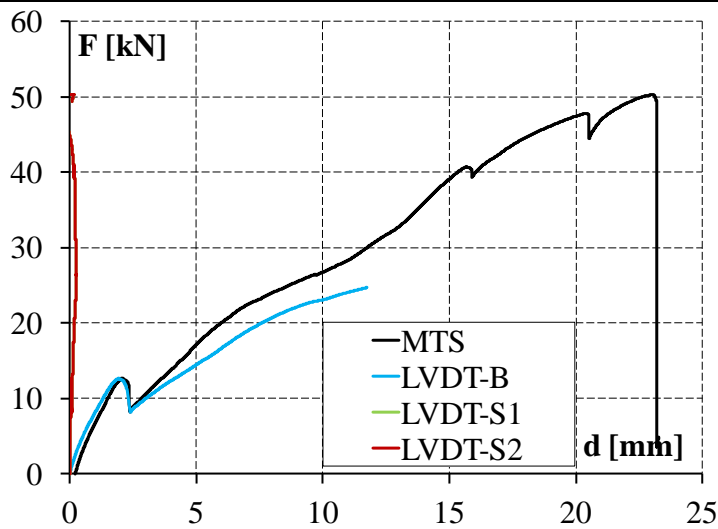
BC-SH-18_1



Test Results

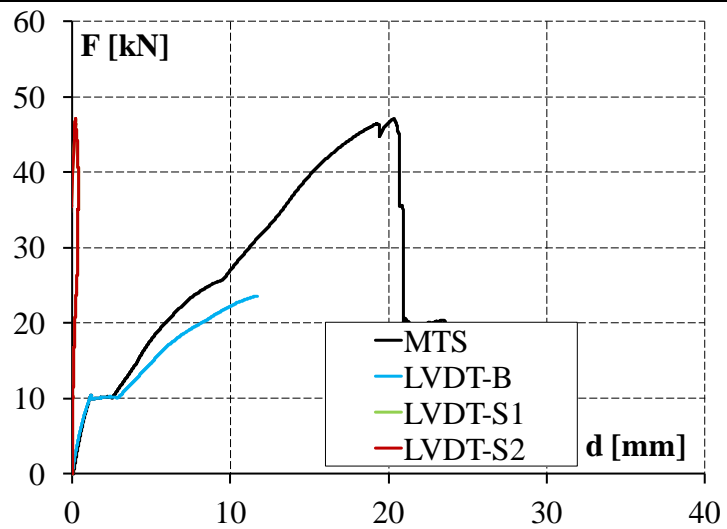
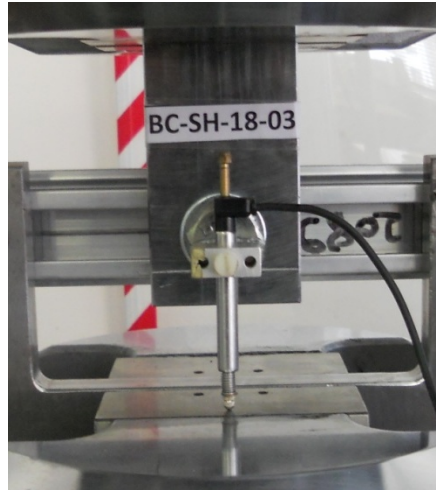
Strength F_{max} [kN/mm]	50.40
Stiffness k [kN/mm]	8.69
Failure Mechanism:	Cracking of web and top flange
Annotations:	

BC-SH-18_2



Test Results	
Strength F_{max} [kN/mm]	50.30
Stiffness k [kN/mm]	7.25
Failure Mechanism:	Cracking of web and top flange
Annotations:	

BC-SH-18_3



Test Results

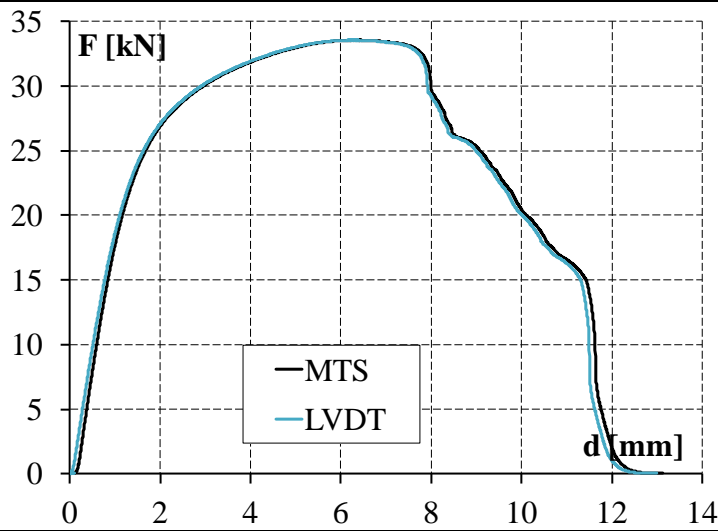
Strength F_{max} [kN/mm] 47.20

Stiffness k [kN/mm] 9.02

Failure Mechanism: Cracking of web, top and bottom flange

Annotations:

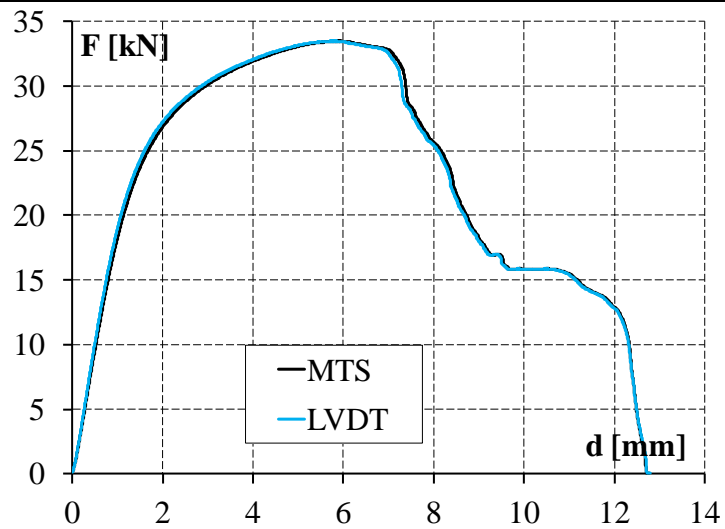
BC-PO-10_1



Test Results

Strength F_{max} [kN/mm]	33.60
Stiffness k [kN/mm]	21.70
Failure Mechanism:	Pull-out of threaded bar
Annotations:	

BC-PO-10_2

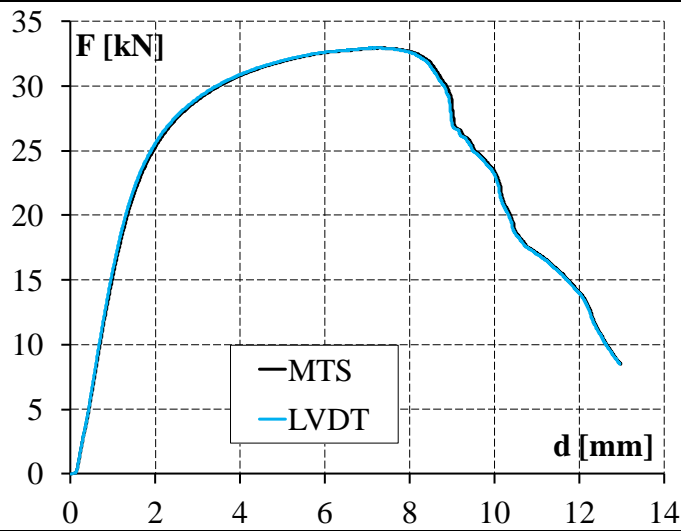


Test Results

Strength F_{max} [kN/mm]	33.50
Stiffness k [kN/mm]	21.70
Failure Mechanism:	Pull-out of threaded bar

Annotations:

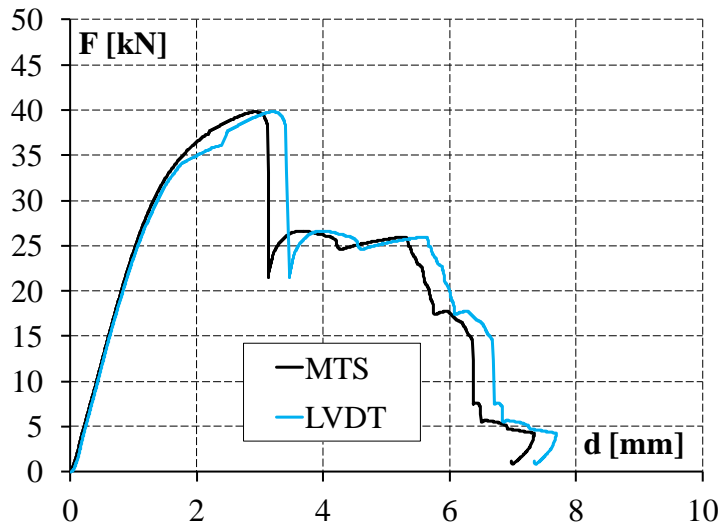
BC-PO-10_3



Test Results

Strength F_{max} [kN/mm]	33.00
Stiffness k [kN/mm]	19.90
Failure Mechanism:	Pull-out of threaded bar
Annotations:	

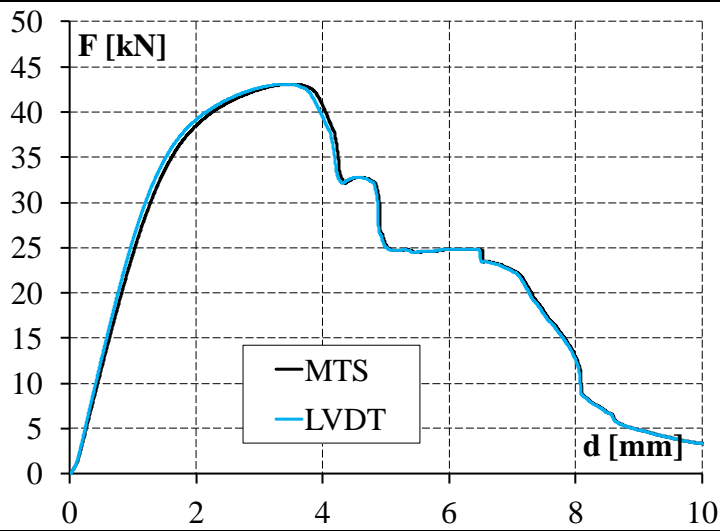
BC-PO-18_1



Test Results

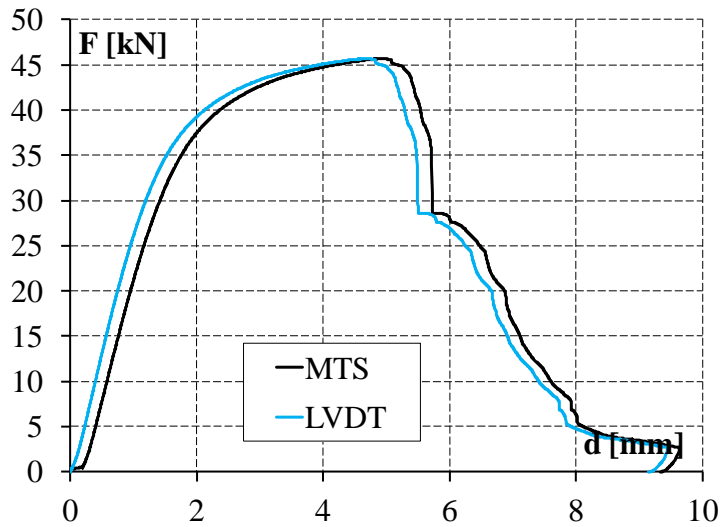
Strength F_{max} [kN/mm]	39.80
Stiffness k [kN/mm]	25.50
Failure Mechanism:	Cracking of top flange and web
Annotations:	Error in LVDT measurement at 1.83 mm displacement

BC-PO-18_2



Test Results	
Strength F_{max} [kN/mm]	43.10
Stiffness k [kN/mm]	23.90
Failure Mechanism:	Cracking of top flange and web
Annotations:	

BC-PO-18_3



Test Results

Strength F_{max} [kN/mm]	45.70
Stiffness k [kN/mm]	27.10
Failure Mechanism:	Cracking of top flange and web
Annotations:	